SUPRAMOLECULAR NANOMATERIALS FOR ENGINEERING, DRUG DELIVERY, AND MEDICAL APPLICATIONS

EDITED BY: Yohann Corvis, Hicham Fenniri, Tu Lee, Elise Lepeltier, Jianliang Shen, Nathalie Mignet and Vincent Levet

PUBLISHED IN: Frontiers in Chemistry

frontiers Research Topics

frontiers

ISSN 1664-8714
ISBN 978-2-88966-412-2
DOI 10.3389/978-2-88966-412-2

About Frontiers

Frontiers is more than just an open-access publisher of scholarly articles: it is a pioneering approach to the world of academia, radically improving the way scholarly research is managed. The grand vision of Frontiers is a world where all people have an equal opportunity to seek, share and generate knowledge. Frontiers provides immediate and permanent online open access to all its publications, but this alone is not enough to realize our grand goals.

Frontiers Journal Series

The Frontiers Journal Series is a multi-tier and interdisciplinary set of open-access, online journals, promising a paradigm shift from the current review, selection and dissemination processes in academic publishing. All Frontiers journals are driven by researchers for researchers; therefore, they constitute a service to the scholarly community. At the same time, the Frontiers Journal Series operates on a revolutionary invention, the tiered publishing system, initially addressing specific communities of scholars, and gradually climbing up to broader public understanding, thus serving the interests of the lay society, too.

Dedication to Quality

Each Frontiers article is a landmark of the highest quality, thanks to genuinely collaborative interactions between authors and review editors, who include some of the world's best academicians. Research must be certified by peers before entering a stream of knowledge that may eventually reach the public - and shape society; therefore, Frontiers only applies the most rigorous and unbiased reviews.
Frontiers revolutionizes research publishing by freely delivering the most outstanding research, evaluated with no bias from both the academic and social point of view. By applying the most advanced information technologies, Frontiers is catapulting scholarly publishing into a new generation.

What are Frontiers Research Topics?

Frontiers Research Topics are very popular trademarks of the Frontiers Journals Series: they are collections of at least ten articles, all centered on a particular subject. With their unique mix of varied contributions from Original Research to Review Articles, Frontiers Research Topics unify the most influential researchers, the latest key findings and historical advances in a hot research area! Find out more on how to host your own Frontiers Research Topic or contribute to one as an author by contacting the Frontiers Editorial Office: researchtopics@frontiersin.org

SUPRAMOLECULAR NANOMATERIALS FOR ENGINEERING, DRUG DELIVERY, AND MEDICAL APPLICATIONS

Topic Editors:
Yohann Corvis, Université de Paris, France
Hicham Fenniri, Northeastern University, United States
Tu Lee, National Central University, Taiwan
Elise Lepeltier, Université d'Angers, France
Jianliang Shen, Wenzhou Medical University, China
Nathalie Mignet, INSERM U1022 Unité de Technologies Chimiques et Biologiques Pour la Santé, France
Vincent Levet, GlaxoSmithKline (Belgium), Belgium

Citation: Corvis, Y., Fenniri, H., Lee, T., Lepeltier, E., Shen, J., Mignet, N., Levet, V., eds. (2021). Supramolecular Nanomaterials for Engineering, Drug Delivery, and Medical Applications. Lausanne: Frontiers Media SA.
doi: 10.3389/978-2-88966-412-2

Table of Contents

frontiers in Chemistry

EDITORIAL
published: 09 December 2020
doi: 10.3389/fchem.2020.626468

Editorial: Supramolecular Nanomaterials for Engineering, Drug Delivery, and Medical Applications

Elise Lepeltier[1], Vincent Levet[2], Tu Lee[3], Nathalie Mignet[4], Jianliang Shen[5], Hicham Fenniri[6] and Yohann Corvis[4]**

[1] Micro et Nanomédecines Translationnelles, MINT, UNIV Angers, Inserm 1066, CNRS, Angers, France, [2] GSK Vaccines, Rue de l'Institut 89, Rixensart, Belgium, [3] Department of Chemical and Materials Engineering, National Central University, Taoyuan City, Taiwan, [4] Université de Paris, CNRS, Inserm, UTCBS, Chemical and Biological Technologies for Health Group (utcbs.cnrs.fr), Faculté de Pharmacie, Paris, France, [5] School of Ophthalmology & Optometry, School of Biomedical Engineering, Wenzhou Medical University, Wenzhou, China, [6] Departments of Chemical Engineering, Bioengineering, Chemistry & Chemical Biology, Northeastern University, Boston, MA, United States*

Keywords: bioinspired nanomaterials, drug delivery and targeting, vaccines production and development, diagnostic agents, cancer treatment

Editorial on the Research Topic

Supramolecular Nanomaterials for Engineering, Drug Delivery, and Medical Applications

Programmed self-assembly and self-organization of carefully designed molecular monomers (Imai et al., 2018) has been widely explored to engineer stable nanostructures with the desired architecture and unique functionality (Lehn, 2015, 2017). This bottom-up approach could not only overcome design barriers associated with traditional molecular manufacturing at the nanoscale, but it could also endow the desired assemblies with adaptability, tunability, and stimuli-responsiveness due to the dynamic nature of the non-covalent interactions holding the architecture together. Hence, these supramolecular architectures may constitute the basis for novel smart nanomaterials with improved properties such as *in vitro* and *in vivo* physicochemical stability (Park et al., 2007), efficiency *via* drug loading improvement (Ahmed et al., 2019), exogenous environment adaptability (Pedersen et al., 2020), higher safety (Martin et al., 2020), manufacturability (Wren et al., 2020), and may have a broad range of applications with various interfaces, i.e., liquid/liquid (Prevot et al., 2018), solid/liquid (Couillaud et al., 2019), and gas/liquid (Manta et al., 2016; Corvis et al., 2018). Indeed, self-assembled systems (Beingessner et al., 2016; Mohamed et al., 2019) have been developed and widely explored in drug delivery (Chen et al., 2011; Song et al., 2011; Desmaële et al., 2012; Mignet et al., 2012; Al Sabbagh et al., 2020), gene delivery (Manta et al., 2017; Do et al., 2019), biomedical engineering (Sun et al., 2012; Childs et al., 2013; Meng et al., 2013; Puzan et al., 2018; Zhou et al., 2020), medicine (Journeay et al., 2008, 2009; Sun et al., 2014), and diagnostics. This body of work has led to the emergence of the field of supramolecular nanomedicine, which is the focus of this Research Topic for *Frontiers in Chemistry* (**Figure 1**).

The present Research Topic highlights nanomaterials importance in biological sciences through the supramolecular chemistry prism. Zhang et al. engineered dynamic hydrogels by cross-linking of O-carboxymethyl chitosan with reversibly connected imino-PEGylated dynamers. The double imine chitosan/dynamer and dynamer bonds were considered to provide tangled structures for controlled drug release behavior from the hydrogels. The structural and physical properties of the resulting hydrogels were examined, showing good thermal stability and optimized swelling behavior. When hydrogels with various composition ratios were further developed for the delivery of the anti-cancer drug fluorouracil (5-FU), high drug encapsulation rates up to 97% were obtained.

OPEN ACCESS

Edited and reviewed by:
Tony D. James,
University of Bath, United Kingdom

****Correspondence:***
Hicham Fenniri
h.fenniri@northeastern.edu
Yohann Corvis
yohann.corvis@u-paris.fr

Specialty section:
This article was submitted to Supramolecular Chemistry, a section of the journal Frontiers in Chemistry

Received: *05 November 2020*
Accepted: *11 November 2020*
Published: *09 December 2020*

Citation:
Lepeltier E, Levet V, Lee T, Mignet N, Shen J, Fenniri H and Corvis Y (2020) Editorial: Supramolecular Nanomaterials for Engineering, Drug Delivery, and Medical Applications. Front. Chem. 8:626468. doi: 10.3389/fchem.2020.626468

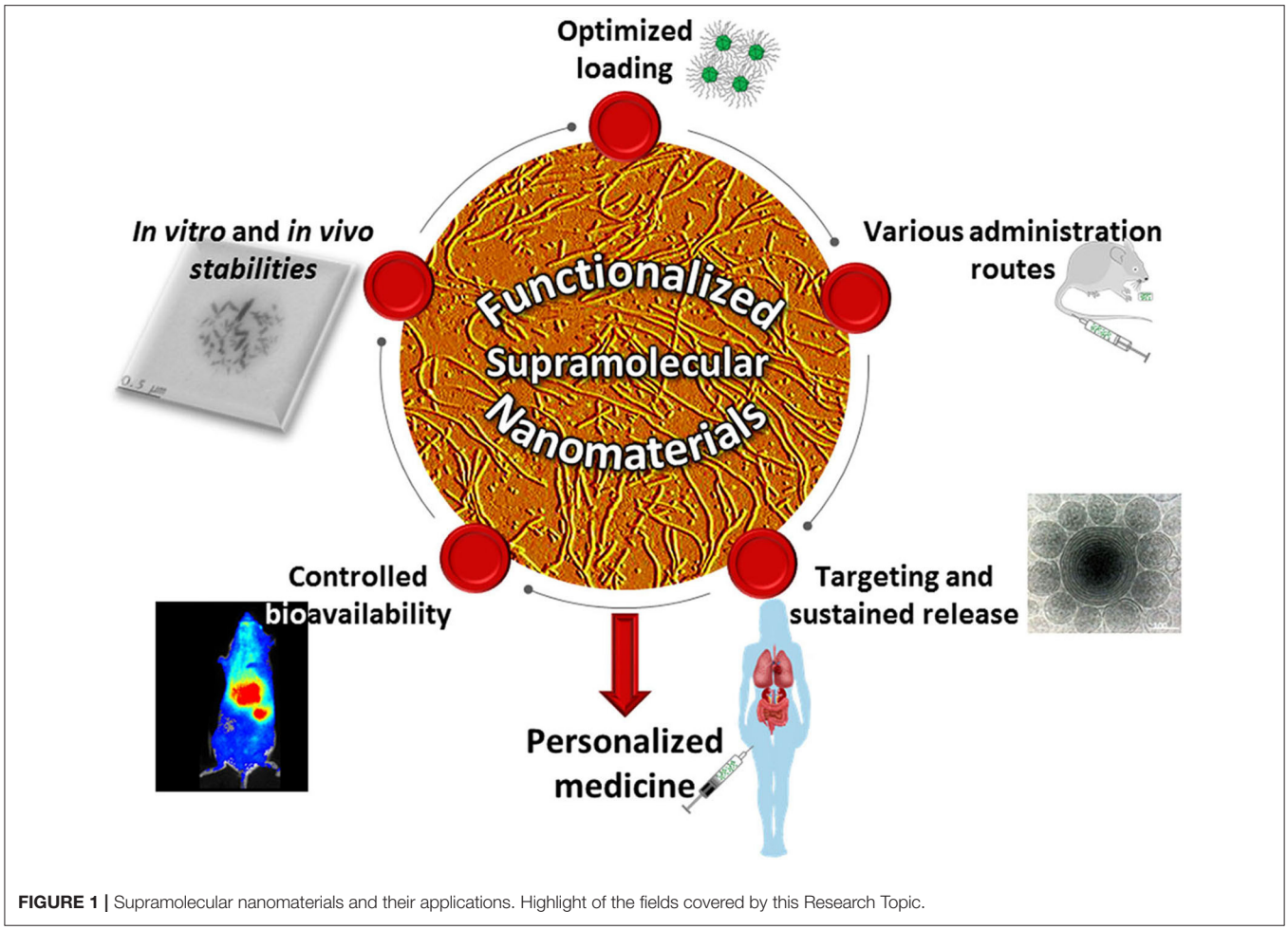

FIGURE 1 | Supramolecular nanomaterials and their applications. Highlight of the fields covered by this Research Topic.

5-FU *in-vitro* drug-release profiles from the hydrogels showed an initial burst-effect, followed by a slower increase and plateau. All reached a high total release within 12 h, which varied upon the cross-linking level that depended on drug/carrier ratios and gelation temperature, thus demonstrating the potential adjustable sustained release applications of this new type of carrier, notably for topical administration.

However, exogen compounds even at the nanoscale dimension, have the propensity to be recognized by the mononuclear phagocyte system once in the bloodstream, inducing rapid clearance of the antigen from the blood and limiting the sustained release advantage. In order to prolong systemic circulation and to prevent the therapeutic agent from aggregation, opsonization or phagocytosis, nanoparticles have been coated with hydrophilic biocompatible co-polymers since the 1990's (Klibanov et al., 1990; Tan et al., 1993; Fam et al., 2020). Liu et al. are reporting surface functionalized Persistent Luminescence NanoParticles (PLNPs) which have been proved promising nanomaterials for bioimaging applications. For that purpose, poly(N-2-hydroxypropyl)methacrylamide (pHPMA), a hydrophilic polymer widely used in nanomedicine has been intended as an alternative strategy to coat $ZnGa_2O_4$:Cr NPs for *in vivo* imaging. The results demonstrated that the newly designed ZGO NPs can circulate in mouse bloodstream much longer than non-coated ZGO-OH, i.e., at least an hour, without being trapped in the liver or spleen. The new strategy presented allowed to improve nanoparticules already developed by the same group for stability in lysosomal-like medium (Lecuyer et al., 2020) and luminescence efficiency (Maldiney et al., 2014; Teston et al., 2018).

A given nanomaterial obtained by supramolecular interactions may present various potential applications due to the intermolecular non-covalent forces. As outlined by Lu et al., supramolecular materials assembled may present interesting applications in various biomedical fields by integrating multiple interactions of polyphenols, especially tannic acid, a class of plant-derived biocompatible and biodegradable compounds consisting of two or more phenolic units in structure. Starting with the origin of supramolecular assembly, combined with the structural characteristics, biological activity of polyphenol and unique advantages of supramolecular assembly, this review systematically covers the classification of supramolecular assembly, assembly system and applications of tannic acid in, e.g., drug delivery, theranostics for cancer treatment, bone

tissue engineering, and biofunctional membrane material. Finally, current and future challenges remaining in this field were put forward. In addition, some traditional or novel assembly techniques were introduced, which also provides some inspiration for the research in this field. Moreover, from a fundamental point of view, the investigation and applications of such dynamic systems could advance our understanding of the design and function of complex chemical and biological systems.

Complex systems can be obtained when ingredients are not in their thermodynamically stable state, e.g., for pharmaceutical liquid forms when drug overall quantity impose by the loading capacity (LC) is higher than its solubility in the same continuous medium, and/or when ingredients that are normally non-miscible are associated together in the same formulation. In such "unstable" systems, excipients are added to kinetically stabilize these ingredients post self-assembly. Ho et al. described the synthesis and characterization of 4 different amphiphilic squalenyl derivatives (i.e., 1 anionic squalenyl derivative, 1 cationic squalenyl-ethanolamine derivative and 2 PEG-squalenyl derivatives of 750 and 3,000 Da, respectively), as well as the physicochemical and biopharmaceutical characterizations of their drug-loaded self-assembled NPs (113–325 nm), in aqueous solution, as drug delivery systems. Seven different model drugs, chosen to exhibit various physicochemical properties (i.e., hydrophobic, hydrophilic, charged) where used with different methods of nanoprecipitation. The best performing methods were determined for each type of formulated system (co-precipitation for hydrophobic compounds, solvent evaporation for hydrophilic compounds, dropping for small and high molecular weight hydrophilic compounds), in relation to the drug properties (molecular weight or logP values). All NP derivatives demonstrated high LC up to 45% w/w, excellent encapsulation efficiency up to 92%, appropriate biocompatibility, adequate colloidal stability in a variety of physiological environments, and sustained release properties exhibiting very low burst-effect and slow controlled-release for at least 24 h. These attributes were achieved thanks to modulated based loading method and loaded NP properties.

Sometime, natural amphiphilic stabilizing agents that are approved by FDA, like silk fibroin, may be preferred as nanocarriers for safety reasons. In their mini review, Ma et al. present the structures of silk fibroin, the controlled transformation of secondary structures, and the formation mechanism of silk fibroin-based nanoparticles and discuss the intrinsic multi-responsibility, surface functionalization, and transgenic modification of these systems for drug delivery. The silk fibroin-based NPs not only have the merits of excellent biocompatibility, but also show the features of multi-responsive systems thanks to stimuli such as pH, hyperthermia, lysosomal enzyme, light, and reactive oxygen species. The multi-responsive phenomenon is helpful for on-demand drug release, reducing systemic side toxicities of some drugs.

Through the non-covalent interactions present in self-assembled therapeutic agents, one of the advantages of smart nanomaterials is that they can be adapted to a specific pathology for personalized medicine purpose. Feng et al. synthesized a novel diblock polymer consisting of polyethylene glycol and poly(glutamic acid (3-(2-nitro-imidazolyl)-propyl)) for hypoxia-responsive polymeric micelle self-assemblies allowing biocompatibility of blank micelles, a drug loading of ∼4%, encapsulation efficiency of ∼42%, and controlled release properties when loaded with the anticancer agent doxorubicin. The cell experiments ultimately demonstrated that drug-loaded micelles had a stronger apoptosis capacity on tumor cells under hypoxic conditions. All the experiments indicated that latter hypoxia-responsive polymeric micelles have a potential for enhanced cancer treatment since both the rapid and important growth and the relatively insufficient blood supply of the tumor tissues give rise to hypoxic conditions, compared with normal tissues.

However, nanomedicines are not only useful for small organic and inorganic molecules vectorization but also for gene delivery as investigated by Gaillard et al.. They developed dual targeting agents combining the mechanisms of bioactive alkylphospholipids and gene therapies. To achieve this goal, three prodrugs series were prepared based on three cytotoxic alkylphospholipids, namely miltefosine, perifosine, and erufosine. The prodrugs were selectively hydrolyzed at physiological pH to parent cytotoxic drugs. Lipoplexes of the prodrugs with plasmid DNA could transfect cancer cells and produced some enhancement of antiproliferative activity. Therefore, the authors prove that non-classical anti-cancer systems can be also designed by supramolecular formulation of nanomedicines.

To complete the insight into self-assembled nanosystems for treatment and diagnosis applications, supramolecular self-assembled peptide-based vaccines may be considered. Indeed, vaccination is considered, especially these days more than ever due to the coronavirus pandemic, as one of the greatest contributions of science to global health, remarkably through the eradication of great illnesses like smallpox and rinderpest and through its ability to control diseases such as measles and polio (Greenwood, 2014). Since the beginning, vaccination moved from antigens based on attenuated or inactivated viruses to purified proteins and more recently to peptide sub-unit epitopes. The latter are more and more recognized as one of the safest approach relative to control over manufacturing processes, contaminations, undesirable effects and autoimmune responses but sometimes comes at the cost of insufficient biological response. As an alternative, nanovaccines including supramolecular self-assembled peptide-based vaccines may be considered but their development is currently limited by our comprehension of self-assembled nanostructures and immune cells interactions (Negahdaripour et al., 2017; Fadeel, 2019). Advanced engineering of supramolecular assembly composed for instance of cell-penetrating peptides (Bechara and Sagan, 2013; Almeida et al., 2016) as delivery vehicles may help promoting a strong cellular or humoral immune response as they favorize targeted intracellular delivery of antigens. In the present Research Topic, Abudula et al. review the span

of strategies applicable to constructing and applying such self-assembled structure as antigens themselves, going from their supramolecular architecture to their multiple application in vaccinology. The mechanisms behind the ability of these peptide-based nanovaccines to generate cell-mediated immunity or humoral response and the aspect of self-adjuvantation are highlighted. Finally, the challenges, clinical translatability and future perspectives are also discussed, considering the great potential of these innovative type of constructs for the future of vaccinology.

Self-assembled systems based on small molecules, block copolymers, dendrimers, peptides, and amphiphiles have been successfully synthesized to achieve a biological, medical, delivery, and/or sensing function(s). Some of these assemblies are designed to be responsive to stimuli such as ultrasound, light, pH, temperature, or specific reagents. Because of their design features and current applications, these supramolecular nanosystems belong to the new and very active field of supramolecular nanomedicine. We thank the 59 co-authors all around the globe which have contributed to this Research Topic. Our main objective is to provide scientists, engineers and clinicians better and newer definition of nanomedicine through the publication of original papers or timely reviews covering synthetically accessible and chemically tunable self-assembled nanosystems endowed with a pharmaceutical, medical, biological, or diagnostic function.

DEDICATIONS

This article is dedicated to Dr. Hai Doan Do, UTCBS' angel who left us too soon.

AUTHOR CONTRIBUTIONS

HF and YC have proposed the idea of this Research Topic. All authors contributed to the guest editorial board and the related manuscript has been read and revised by all the authors.

FUNDING

This work was financially supported by CNRS, Inserm, French Ministry of Higher Education Research and Innovation, National Natural Science Foundation of China (31800833 and 21977081), and Zhejiang Provincial Natural Science of Foundation of China (LZ19H180001).

ACKNOWLEDGMENTS

NM and YC would like to thank Dr. Cyrille Richard, Dr. Johanne Seguin, Dr. Thomas Lecuyer, Dr. Brice Martin, Dr. Shayan Ahmed, Jianhua Liu, Panpan Ma, Giovanni Neri, Sirine Elmousli and Amir Khaled Louaar for their valuable contribution to the nanomaterials research axis at UTCBS.

REFERENCES

Ahmed, S., Corvis, Y., Gahoual, R., Euan, A., Lai-Kuen, R., Couillaud, B. M., et al. (2019). Conception of nanosized hybrid liposome/poloxamer particles to thicken the interior core of liposomes and delay hydrophilic drug delivery. *Int. J. Pharm.* 567:118488. doi: 10.1016/j.ijpharm.2019.118488

Al Sabbagh, C., Seguin, J., Agapova, E., Kramerich, D., Boudy, V., and Mignet, N. (2020). Thermosensitive hydrogels for local delivery of 5-fluorouracil as neoadjuvant or adjuvant therapy in colorectal cancer. *Eur. J. Pharm. Biopharm.* 157, 154–164. doi: 10.1016/j.ejpb.2020.10.011

Almeida, C., Lamaziere, A., Filleau, A., Corvis, Y., Espeau, P., and Ayala-Sanmartin, J. (2016). Membrane re-arrangements and rippled phase stabilization by the cell penetrating peptide penetratin. *Biochim. Biophys. Acta Biomembr.* 1858, 2584–2591. doi: 10.1016/j.bbamem.2016.07.012

Bechara, C., and Sagan, S. (2013). Cell-penetrating peptides: 20 years later, where do we stand? *FEBS Lett.* 587, 1693–1702. doi: 10.1016/j.febslet.2013.04.031

Beingessner, R. L., Fan, Y., and Fenniri, H. (2016). Molecular and supramolecular chemistry of rosette nanotubes. *RSC Adv.* 6, 75820–75838. doi: 10.1039/c6ra16315g

Chen, Y., Song, S., Yan, Z., Fenniri, H., and Webster, T. J. (2011). Self-assembled rosette nanotubes encapsulate and slowly release dexamethasone. *Int. J. Nanomed.* 6, 1035–1044. doi: 10.2147/ijn.s18755

Childs, A., Hemraz, U. D., Castro, N. J., Fenniri, H., and Zhang, L. G. (2013). Novel biologically-inspired rosette nanotube plla scaffolds for improving human mesenchymal stem cell chondrogenic differentiation. *Biomed. Mater.* 8:065003. doi: 10.1088/1748-6041/8/6/065003

Corvis, Y., Manta, S., Thebault, C., Couture, O., Dhotel, H., Michel, J.-P., et al. (2018). Novel perfluorinated triblock amphiphilic copolymers for lipid-shelled microbubble stabilization. *Langmuir* 34, 9744–9753. doi: 10.1021/acs.langmuir.8b01668

Couillaud, B. M., Espeau, P., Mignet, N., and Corvis, Y. (2019). State of the art of pharmaceutical solid forms: from crystal property issues to nanocrystals formulation. *ChemMedChem* 14, 8–23. doi: 10.1002/cmdc.201800612

Desmaële, D., Gref, R., and Couvreur, P. (2012). Squalenoylation: a generic platform for nanoparticular drug delivery. *J. Controlled Release* 161, 609–618. doi: 10.1016/j.jconrel.2011.07.038

Do, H. D., Couillaud, B. M., Doan, B.-T., Corvis, Y., and Mignet, N. (2019). Advances on non-invasive physically triggered nucleic acid delivery from nanocarriers. *Adv. Drug Deliv. Rev.* 138, 3–17. doi: 10.1016/j.addr.2018.10.006

Fadeel, B. (2019). Hide and seek: nanomaterial interactions with the immune system. *Front. Immunol.* 10:133. doi: 10.3389/fimmu.2019.00133

Fam, S. Y., Chee, C. F., Yong, C. Y., Ho, K. L., Mariatulqabtiah, A. R., and Tan, W. S. (2020). Stealth coating of nanoparticles in drug-delivery systems. *Nanomaterials* 10:787. doi: 10.3390/nano10040787

Greenwood, B. (2014). The contribution of vaccination to global health: past, present and future. *Philos. Trans. R. Soc. Lond. B. Biol. Sci.* 369:20130433. doi: 10.1098/rstb.2013.0433

Imai, S., Hirai, Y., Nagao, C., Sawamoto, M., and Terashima, T. (2018). Programmed self-assembly systems of amphiphilic random copolymers into size-controlled and thermoresponsive micelles in water. *Macromolecules* 51, 398–409. doi: 10.1021/acs.macromol.7b01918

Journeay, W. S., Suri, S. S., Moralez, J. G., Fenniri, H., and Singh, B. (2008). Rosette nanotubes show low acute pulmonary toxicity *in vivo*. *Int. J. Nanomed.* 3, 373–383. doi: 10.2147/ijn.s3489

Journeay, W. S., Suri, S. S., Moralez, J. G., Fenniri, H., and Singh, B. (2009). Macrophage inflammatory response to self-assembling rosette nanotubes. *Small* 5, 1446–1452. doi: 10.1002/smll.200801717

Klibanov, A. L., Maruyama, K., Torchilin, V. P., and Huang, L. (1990). Amphipathic polyethyleneglycols effectively prolong the circulation time of liposomes. *FEBS Lett.* 268, 235–237. doi: 10.1016/0014-5793(90)81016-h

Lecuyer, T., Durand, M.-A., Volatron, J., Desmau, M., Lai-Kuen, R., Corvis, Y., et al. (2020). Degradation of znga2o4:Cr3+ luminescent nanoparticles in lysosomal-like medium. *Nanoscale* 12, 1967–1974. doi: 10.1039/c9nr06867h

Lehn, J.-M. (2015). Perspectives in chemistry - aspects of adaptive chemistry and materials. *Angew. Chem. Int. Ed. Engl.* 54, 3276–3289. doi: 10.1002/anie.201409399

Lehn, J.-M. (2017). Supramolecular chemistry: Where from? Where to? *Chem. Soc. Rev.* 46, 2378–2379. doi: 10.1039/c7cs00115k

Maldiney, T., Bessiere, A., Seguin, J., Teston, E., Sharma, S. K., Viana, B., et al. (2014). The *in vivo* activation of persistent nanophosphors for optical imaging of vascularization, tumours and grafted cells. *Nat. mater.* 13, 418–426. doi: 10.1038/nmat3908

Manta, S., Bessodes, M., Bureau Michel, F., Scherman, D., Delalande, A., Pichon, C., et al. (2016). Characterization of positively charged lipid shell microbubbles with tunable resistive pulse sensing (trps) method: a technical note. *Ultrasound Med. Biol.* 42, 624–630. doi: 10.1016/j.ultrasmedbio.2015.10.010

Manta, S., Renault, G., Delalande, A., Couture, O., Lagoutte, I., Seguin, J., et al. (2017). Cationic microbubbles and antibiotic-free miniplasmid for sustained ultrasound-mediated transgene expression in liver. *J. Controlled Release* 262, 170–181. doi: 10.1016/j.jconrel.2017.07.015

Martin, B., Seguin, J., Annereau, M., Fleury, T., Laï-Kuen, R., Neri, G., et al. (2020). Preparation of parenteral nanocrystal suspensions of etoposide from the excipient free dry state of the drug to enhance *in vivo* antitumoral properties. *Sci. Rep.* 10:18059. doi: 10.1038/s41598-020-74809-z

Meng, X., Stout, D. A., Sun, L., Beingessner, R. L., Fenniri, H., and Webster, T. J. (2013). Novel injectable biomimetic hydrogels with carbon nanofibers and self assembled rosette nanotubes for myocardial applications. *J. Biomed. Mater. Res. Part A* 101A, 1095–1102. doi: 10.1002/jbm.a.34400

Mignet, N., Seguin, J., Ramos Romano, M., Brulle, L., Touil, Y. S., Scherman, D., et al. (2012). Development of a liposomal formulation of the natural flavonoid fisetin. *Int. J. Pharm.* 423, 69–76. doi: 10.1016/j.ijpharm.2011.04.066

Mohamed, M. A., Fallahi, A., El-Sokkary, A. M. A., Salehi, S., Akl, M. A., Jafari, A., et al. (2019). Stimuli-responsive hydrogels for manipulation of cell microenvironment: from chemistry to biofabrication technology. *Prog. Polym. Sci.* 98:101147. doi: 10.1016/j.progpolymsci.2019.101147

Negahdaripour, M., Golkar, N., Hajighahramani, N., Kianpour, S., Nezafat, N., and Ghasemi, Y. (2017). Harnessing self-assembled peptide nanoparticles in epitope vaccine design. *Biotechnol. Adv.* 35, 575–596. doi: 10.1016/j.biotechadv.2017.05.002

Park, J.-S., Ahn, J.-Y., Lee, S.-H., Lee, H., Han, K.-Y., Seo, H.-S., et al. (2007). Enhanced stability of heterologous proteins by supramolecular self-assembly. *Appl. Microbiol. Biotechnol.* 75, 347–355. doi: 10.1007/s00253-006-0826-3

Pedersen, S. L., Huynh, T. H., Poschko, P., Fruergaard, A. S., Jarlstad Olesen, M. T., Chen, Y., et al. (2020). Remotely triggered liquefaction of hydrogel materials. *ACS Nano* 14, 9145–9155. doi: 10.1021/acsnano.0c04522

Prevot, G., Soria, F. N., Thiolat, M.-L., Daniel, J., Verlhac, J. B., Blanchard-Desce, M., et al. (2018). Harnessing lysosomal ph through plga nanoemulsion as a treatment of lysosomal-related neurodegenerative diseases. *Bioconjug. Chem.* 29, 4083–4089. doi: 10.1021/acs.bioconjchem.8b00697

Puzan, M. L., Legesse, B., Koppes, R. A., Fenniri, H., and Koppes, A. N. (2018). Bioactive organic rosette nanotubes support sensory neurite outgrowth. *ACS Biomater. Sci. Eng.* 4, 1630–1640. doi: 10.1021/acsbiomaterials.8b00326

Song, S., Chen, Y., Yan, Z., Fenniri, H., and Webster, T. J. (2011). Self-assembled rosette nanotubes for incorporating hydrophobic drugs in physiological environments. *Int. J. Nanomed.* 6, 101–107. doi: 10.2147/ijn.s11957

Sun, L., Li, D., Hemraz, U. D., Fenniri, H., and Webster, T. J. (2014). Self-assembled rosette nanotubes and poly(2-hydroxyethyl methacrylate) hydrogels promote skin cell functions. *J. Biomed. Mater. Res. Part A* 102A, 3446–3451. doi: 10.1002/jbm.a.35008

Sun, L., Zhang, L., Hemraz, U. D., Fenniri, H., and Webster, T. J. (2012). Bioactive rosette nanotube-hydroxyapatite nanocomposites improve osteoblast functions. *Tissue Eng. Part A* 18, 1741–1750. doi: 10.1089/ten.tea.2011.0456

Tan, J. S., Butterfield, D. E., Voycheck, C. L., Caldwell, K. D., and Li, J. T. (1993). Surface modification of nanoparticles by peo/ppo block copolymers to minimize interactions with blood components and prolong blood circulation in rats. *Biomaterials* 14, 823–833. doi: 10.1016/0142-9612(93)90004-l

Teston, E., Maldiney, T., Marangon, I., Volatron, J., Lalatonne, Y., Motte, L., et al. (2018). Nanohybrids with magnetic and persistent luminescence properties for cell labeling, tracking, *in vivo* real-time imaging, and magnetic vectorization. *Small* 14:1800020. doi: 10.1002/smll.201800020

Wren, S., Minelli, C., Pei, Y., and Akhtar, N. (2020). Evaluation of particle size techniques to support the development of manufacturing scale nanoparticles for application in pharmaceuticals. *J. Pharm. Sci.* 109, 2284–2293. doi: 10.1016/j.xphs.2020.04.001

Zhou, X., Tenaglio, S., Esworthy, T., Hann, S. Y., Cui, H., Webster, T. J., et al. (2020). Three-dimensional printing biologically inspired DNA-based gradient scaffolds for cartilage tissue regeneration. *ACS Appl. Mater. Interfaces* 12, 33219–33228. doi: 10.1021/acsami.0c07918

Conflict of Interest: VL was employed by the GSK group of companies.

The remaining authors declare that the research was conducted in the absence of any commercial or financial relationships that could be construed as a potential conflict of interest.

frontiers in Chemistry

ORIGINAL RESEARCH
published: 26 August 2020
doi: 10.3389/fchem.2020.00739

Dynamic Hydrogels Based on Double Imine Connections and Application for Delivery of Fluorouracil

Yan Zhang[1], *Chi-Yen Pham*[2], *Rui Yu*[3], *Eddy Petit*[3], *Suming Li*[3]* *and Mihail Barboiu*[3]*

[1] Key Laboratory of Carbohydrate Chemistry and Biotechnology, Ministry of Education, School of Pharmaceutical Sciences, Jiangnan University, Wuxi, China, [2] Department of Pharmacological, Medical and Agronomical Biotechnology, Hanoi University of Science and Technology, Hanoi, Vietnam, [3] Institut Europeen des Membranes, UMR5635, University of Montpellier, ENSCM, CNRS, Montpellier, France

Dynamic hydrogels have been prepared by cross-linking of *O*-carboxymethyl chitosan (*O*-CMCS) with reversibly connected imino-PEGylated dynamers. The double imine chitosan/dynamer and dynamer bonds and were used to provide tighter structures and adaptive drug release behaviors of the hydrogels. The structural and physical properties of the resulted hydrogels were examined, showing good thermal stability and higher swelling behaviors (up to 3,000%). When hydrogels with various composition ratios were further applied for delivery of anti-cancer drug fluorouracil (5-FU), high drug encapsulation rates were recorded, up to 97%. The release profile of 5-FU showed fast rate at the beginning, followed by slow increase to the maximum amount within 12 h, demonstrating potential as drug carriers for efficient drug delivery.

Keywords: dynamic covalent chemistry, dynamers, hydrogels, drug delivery, imine, fluorouracil

OPEN ACCESS

Edited by:
Hicham Fenniri,
Northeastern University, United States

Reviewed by:
Tangxin Xiao,
Changzhou University, China
Xingyi Li,
Affiliated Eye Hospital of Wenzhou Medical College, China

***Correspondence:**
Suming Li
suming.li@umontpellier.fr
Mihail Barboiu
mihail-dumitru.barboiu@umontpellier.fr

Specialty section:
This article was submitted to Supramolecular Chemistry, a section of the journal Frontiers in Chemistry

Received: *29 May 2020*
Accepted: *17 July 2020*
Published: *26 August 2020*

Citation:
Zhang Y, Pham C-Y, Yu R, Petit E, Li S and Barboiu M (2020) Dynamic Hydrogels Based on Double Imine Connections and Application for Delivery of Fluorouracil. Front. Chem. 8:739. doi: 10.3389/fchem.2020.00739

INTRODUCTION

With the increasing interest of dynamic covalent chemistry from various fields, dynamic polymers—dynamers have presented as a powerful tool to achieve adaptive materials (Aida et al., 2012; Roy et al., 2015; Zhang and Barboiu, 2015, 2016), and found wide applications in bio-recognition (Yao et al., 2014; Yasen et al., 2017; Zhang et al., 2020b), materials design (Goor et al., 2017; Zhang et al., 2020c), drug delivery (Bakker et al., 2016), etc. The reversibly covalent bonds, such as imine, hydrazine, and disulfide, etc. have provided dynamic features to the polymers, leading to responsivity to different stimuli, including pH (Charbonneau et al., 2011), light (Fuhrmann et al., 2016), and biological targets, for example, enzymes (Zhang et al., 2016a,b, 2018b) and DNA (Catana et al., 2015; Clima et al., 2015; Zhang et al., 2018a).

As the promising drug carriers, hydrogels have been experiencing fast development in recent years (Lai and He, 2016; Oliva et al., 2017). With the retained large amounts of water and excellent biocompatibility, hydrogels demonstrated useful tool for targeted drug delivery and controlled drug release (Li and Mooney, 2016; Lei et al., 2018; Huang et al., 2020; Zhang et al., 2020a). According to the cross-linking methods, hydrogels can be formed through non-covalent physical interactions or covalent chemical bonds (Goujon et al., 2017; Gu et al., 2018). In the former case, supramolecular interactions are usually involved for the establishment of hydrogels, including hydrogen bonding, host-guest interactions, etc. (Xiao and Wang, 2018; Xiao et al., 2019; Yu J. et al., 2020). Reversible reactions, such as imine disulfide or esther bond formation, have also been applied in hydrogel preparations (Wei et al., 2015; Yamada and Schneider, 2016). Resulting in the formation of "dynamic gels" i.e., dyna-gels (Marin et al., 2014), which are dynamic on both the molecular and

supramolecular levels, as systems reversibly exchanging their components, responding to external stimuli, such as pH and temperature (Deng et al., 2012). For example, pH-responsive polymers based on Schiff-base reaction have been designed and used for delivery and pseudo targeted release of doxorubicin (DOX) (Tao et al., 2018).

Although extensive research work has been done by the insertion of dynamic reactions into hydrogel formation, dynamer as one of the starting materials, further reversibly crosslinked with natural polymers for hydrogel construction was rarely reported. Multistate pH-sensitive *O*-carboxymethyl chitosan PEGylated hydrogels, presenting outstanding self-healing properties were synthesized by our group as cell growing cyto-compatible platforms (Yu R. et al., 2020). Thus, in the current work, we would continue to explore the PEG-ylated dynameric—*O*-carboxymethyl chitosan (*O*-CMCS) cross-linked networks (**Figure 1**) resulting in the formation of biomimetic adaptive double imine adaptive hydrogels. These hydrogels presenting good mechanical properties and excellent swelling properties, were used as a carrier for anti-cancer drug 5-fluorouracil (5-FU) which make them beneficial for further biomedical applications.

MATERIALS AND METHODS

Materials

1,3,5-benzenetrialdehyde was obtained from Manchester Organics, Great Britain. Poly(ethylene glycol) bis(3-aminopropyl) terminated (Mn ∼ 1500) and 5-FU were purchased from Sigma Aldrich, France. *O*-carboxymethyl chitosan (*O*-CMCS) with average molecular weight (Mw) of 2×10^5 was purchased from Golden-shell Biochemical Co., Ltd., China, the degree of substitution of *O*-CMCS was 80%. All organic solvents, including methanol, dichloromethane, and acetonitrile were of analytical grade, obtained from Sigma Aldrich, France.

Synthesis of the PEGylated Dynamer

1,3,5-benzenetrialdehyde, BTA (**1**, 1 mmol, 162.14 mg), Poly(ethylene glycol)bis(3-aminopropyl) terminated (PEG, **2**, Mn∼1500, 1 mmol, 1.5 g), and MeOH (30 mL) have been added in a flask, and the reaction mixture was stirred at 60°C for 3 days until equilibrium was reached (**Scheme 1**). After evaporation of the solvent, 20 mL of Milli-Q water were added, yielding a homogeneous dynamer solution of 50 mM (counted from the amount of BTA core structure). ^{1}H NMR spectroscopy was used to monitor the formation of imine bonds. The experiments were carried out with Bruker NMR spectrometer (AMX500) of 300 MHz, by using $CDCl_3$ (0.5 mL) as the solvent, while chemical shifts were recorded in ppm.

Preparation of the Hydrogels

The gels were formed by adding *O*-CMCS to dynamer in aqueous solution. *O*-CMCS solution was prepared by adding *O*-CMCS (72.2 mg, 0.29 mmol counted from repeating unit) to 2.5 mL Milli-Q water at room temperature, followed by sonication for 15 min to yield a transparent solution of 116 mM (counted from repeating unit). Subsequently, dynamer and *O*-CMCS solutions were mixed together at r.t., with different *O*-CMCS/dynamer molar ratios of 1:4, 1:2, 1:1, 2:1, 4:1, and the resulted mixtures were kept at r.t. to afford the designed hydrogels.

Characterization of the Hydrogels

To confirm the formation of imine bond during the gelation process, Fourier-Transform Infrared Spectroscopy (FTIR) was used to analyse the starting dynamer, *O*-CMCS solutions, and the resulted hydrogels. The experiments were performed with Nicolet Nexus FT-IR spectrometer, equipped with ATR Diamant Golden Gate.

Differential scanning calorimetry (DSC) and thermogravimetric analysis (TGA) were carried out using a DuPont instrument (TA instrument Inc., USA), to examine thermal properties of the hydrogels, under nitrogen atmosphere. Measurements for DSC were performed under a heating rate of 10°C min^{-1}, with temperature range from −70 to 220°C. TGA measurements were recorded from 20 to 600°C at a heating rate of 10°C min^{-1}.

Rheological Measurements

Rheological properties of hydrogels were examined with Physical MCR 301 Rheometer (Anton Paar). The tested samples were placed on a cone plate (diameter of 4 cm, apex angle of 2°, and clearance 56 m). Measurements were made in the linear viscoelastic region.

Swelling Test

The swelling test was performed by immersion of dried gels in Phosphate Buffered Saline (PBS) buffer (pH 7.4). The samples were taken out after 1, 3, 5, 6, 24, 48, and 168 h, wiped to remove surface water and weighed (W_s). They were then freeze-dried for 24 h, and weighed again (W_d). The swelling ratio was determined according to the following equation:

$$\textit{Swelling ratio}\ (\%) = (M_s - M_d)/M_d \times 100 \quad (1)$$

Where M_s and M_d are the mass of swollen hydrogel and of freeze dried gel, respectively.

In vitro Drug Release

5-FU was selected as a hydrophilic model drug to study the *in vitro* drug release profile from the hydrogels. Firstly, 5-FU was encapsulated in hydrogels by dissolution in a dynamer solution, followed by gelation process after mixing with *O*-CMCS solution. Then the release profile was studied by immersing the hydrogel in 1 mL PBS buffer (pH 7.4) at 37°C. At each preset time interval, the whole medium was collected for measurements, and replaced by 1 mL fresh PBS solution. The released amount of 5-FU was determined by HPLC measurements.

High-performance liquid chromatography-UV (HPLC-UV) was performed by using a HPLC system equipped with Waters 717 Autosampler, Waters 616 Pump, Waters 2996 Photodiode Array Detector, and a reverse phase Thermo Scientific C18 column (L ¼ 250 mm, I.D ¼ 4.6 mm, and 5 mm particles). The mobile phase was a Buffer A (HPLC grade water 0.1%

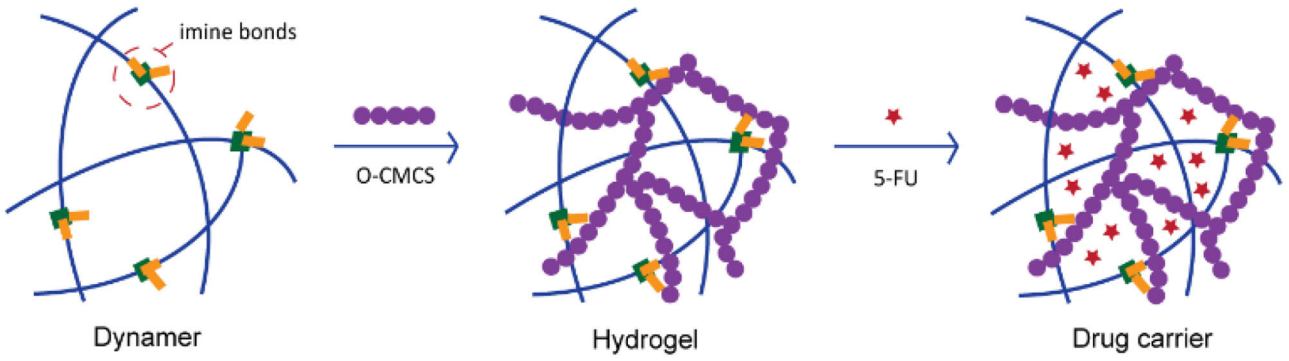

FIGURE 1 | Illustration of the concept for double-imine dynamic hydrogels and application for drug loading.

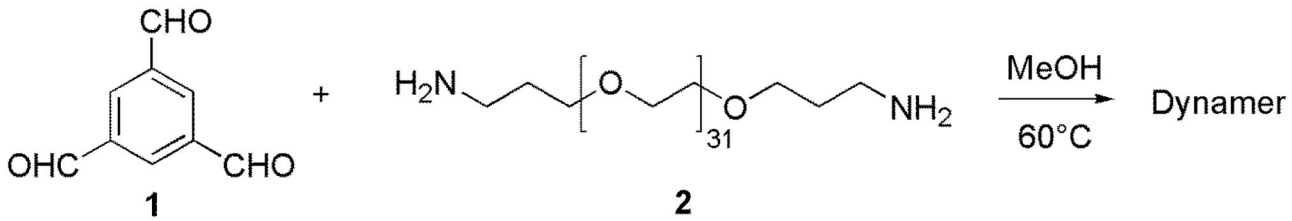

SCHEME 1 | Synthesis of the PEG dynamer.

trifluoroacetic acid) and Buffer B (HPLC grade acetonitrile 0.1% trifluoroacetic acid). The flow rate was 1 mL min^{-1}.

RESULTS AND DISCUSSIONS

Characterization of the Dynamer

The reversible imine reaction was applied to construct a dynameric network, while using 1,3,5-benzenetrialdehyde, BTA **1** as the core structure, and the bis-amine terminated PEG **2** as the water-soluble linker (**Scheme 1**). The molar ratio between the two components **1** and **2** was 1:1, thus, leaving 1/3 of total aldehyde groups free to be further cross-linked to the amine groups of *O*-CMCS. After heating at 60°C for 3 days in MeOH, the equilibrium was reached as no change of the signals was observed on the ^{1}H-NMR spectra. As can be seen in **Figure 2**, there are three aldehyde signals (10.1–10.3 ppm) which are assigned to trialdehyde **1**, mono-substituted, di-substituted aldehydes (from low to high magnetic fields). Moreover, the signals in the range of 8.0–8.7 ppm present the imine and aromatic protons. Signal at 2.0 ppm can be assigned to the methylene groups of PEG **2**.

Characterization of the Hydrogels

FTIR analysis was performed to figure out the degree of cross-linking between dynamer and *O*-CMCS after gelation process. The freeze-dried hydrogels after different time intervals were analyzed to follow the formation of imine bonds. As shown in **Figure 3**, the characteristic bands of aldehyde (signal 1) and the newly formed imine bonds (signal 2) were observed at 1700 and 1645 cm^{-1}, respectively, whereas the band at 1595 cm^{-1} belongs to carboxyl groups of *O*-CMCS. With increasing time, there is significant increase of signal 2 for the imine bonds and decrease of signal 1, demonstrating higher degree of cross-linking with time.

Differential scanning calorimetry (DSC) was performed to evaluate the thermal properties of the freeze-dried hydrogels. As can be seen in **Figure 4A**, a large endothermic peak is detected in the range of 75–110°C due to the presence of traces of water. Moreover, a small endothermic peak was found at 30.4°C with an enthalpy of 4.2 J/g, which can be attributed to the melting of PEG. Compared to the melting temperature (Tm) of PEG1500 at 50.0°C, the decreased Tm of the hydrogels could be explained by the covalent bonding of PEG to the hydrogel network which reduced its chain mobility. From literature data, we observe only a clear water evaporation peak, reminiscent with an amorphous behavior of the *O*-CMCS (Katugampola et al., 2014).

Figure 4B presents the TGA thermogram of freeze dried *O*-CMCS-PEG hydrogels. Initially about 12.3% weight loss was detected in the range of 25–80°C due to the evaporation of loosely bound water molecules from the samples. The second stage was a predominant one, where nearly 60% weight loss occurred in the temperature range from 250 to 390°C, indicating the a onset degradation of *O*-CMCS at 240°C. At the last stage from 380 to 480°C, around 10.9% of weight loss was observed, which was assigned to the thermal degradation of PEG. It is noteworthy that nearly 27% of initial weight remains till 600°C. From the literature the O-CMCS the onset degradation occurs at 166°C, much lower that crosslinked O-CMCS hydrogels (Katugampola et al., 2014).

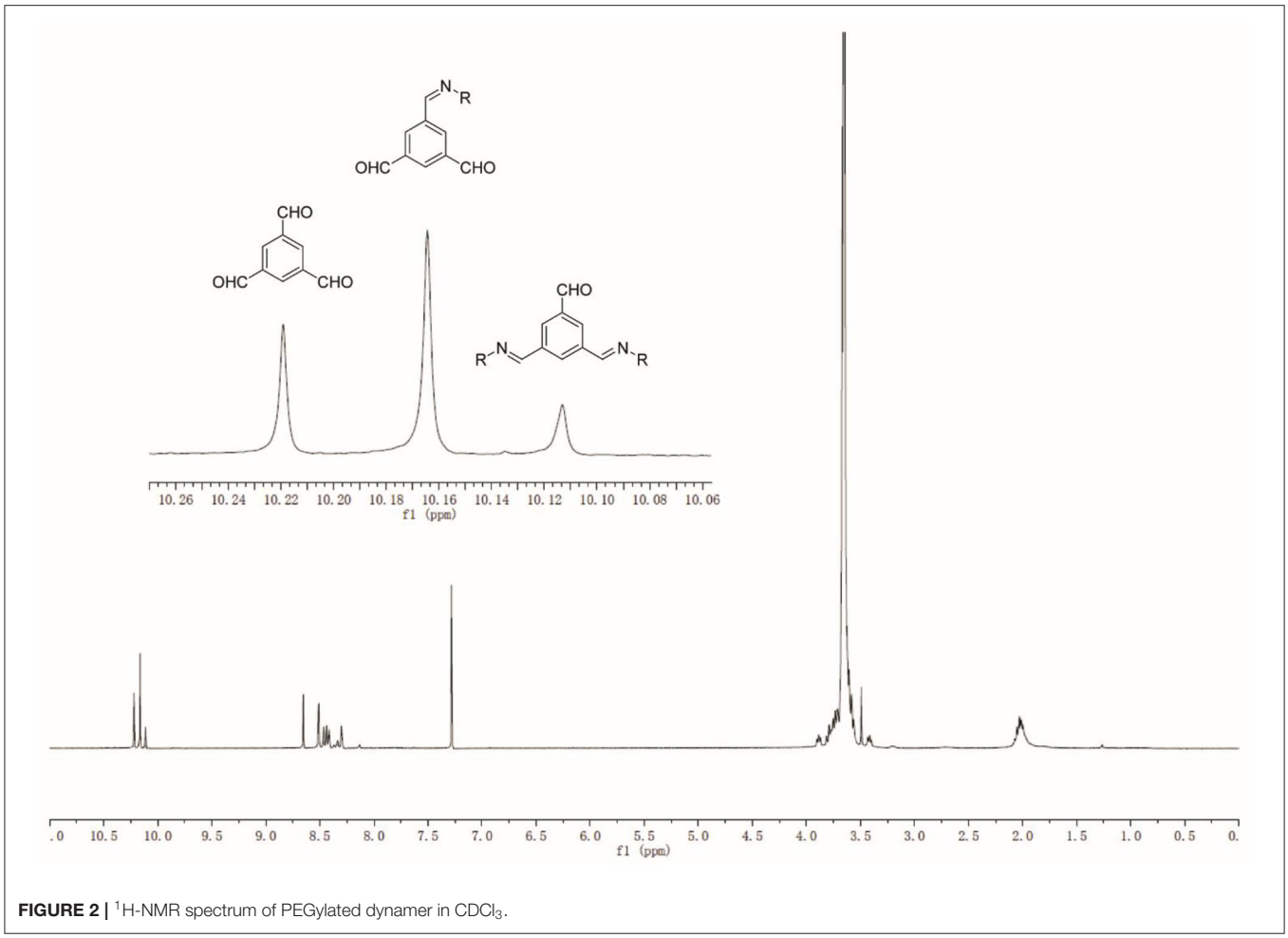

FIGURE 2 | ^{1}H-NMR spectrum of PEGylated dynamer in $CDCl_3$.

Rheological Studies

Rheological measurements were performed to elucidate the viscoelastic characteristics of the hydrogels. Thus, the gelation process with varying PEG dynamer/*O*-CMCS molar ratios of 4:1, 2:1, 1:1, 1:2, 1:4 was studied. **Figure 5** showed the changes of storage modulus (G′) and loss modulus (G″) of various hydrogels as a function of time at 25°C. For all samples, the storage modulus was lower than the loss modulus at the beginning, which illustrated a liquid-like behavior (G′ < G″) of the starting dynamer and *O*-CMCS solutions. After an induction time, both G′ and G″ began to increase, G′ increasing at a faster rate than G″. A crossover point of G′ and G″ was detected, indicating sol-gel transition or gelation. It is noteworthy that with varying the molar ratio of PEG dynamer/*O*-CMCS from 4:1 to 1:4, higher G′ and G″ moduli shorter gelation time were obtained. In fact, the modulus at gelation point increased from 0.14 to 3.36 Pa, and the gelation time was shortened from 1,850 to 250 s. These results demonstrated that higher content of *O*-CMCS leads to increased degree of cross-linking between the aldehyde groups of cross-linking PEG dynamer and the amine groups of *O*-CMCS. Furthermore, by adopting half concentrations of both PEG dynamer and *O*-CMCS solutions at the molar ratio of 1:1 (1:1 diluted), the detected modulus at gelation point became even lower, accompanied with prolonged gelation time.

Swelling Studies

The swelling properties of hydrogels with PEG dynamer to *O*-CMCS molar ratios of 2:1, 1:1, and 1:2 were studied in PBS at pH 7.4. As shown in **Figure 6A**, the swelling degree rapidly increased in the initial hours and slowly decreased thereafter. For the hydrogel formed with dynamer/*O*-CMCS molar ratio of 1:2, the highest swelling degree of 2,600% was reached after 5 h only. On the other hand, the highest swelling degrees of the hydrogels with molar ratios of 1:1 and 2:1 were reached after 24 h, with swelling degree calculated close to 3,000%. These values might be considered with a *SD*% = 8% as previously reported for similar Chitosan hydrogels (Damiri et al., 2020). These findings well agree with the less cross-linked structures of the hydrogels with molar ratios of 1:1 and 2:1 compared to the hydrogel containing more *O*-CMCS (molar ratio of 1:2). **Figure 6B** presents the mass changes of the freeze-dried hydrogels as a function of soaking time in PBS buffer. A rapid decrease of the hydrogel mass was observed for all the samples during the first 24 h, indicating the dissolution of non-cross-linked components of the hydrogels into the PBS. Among the different samples, the

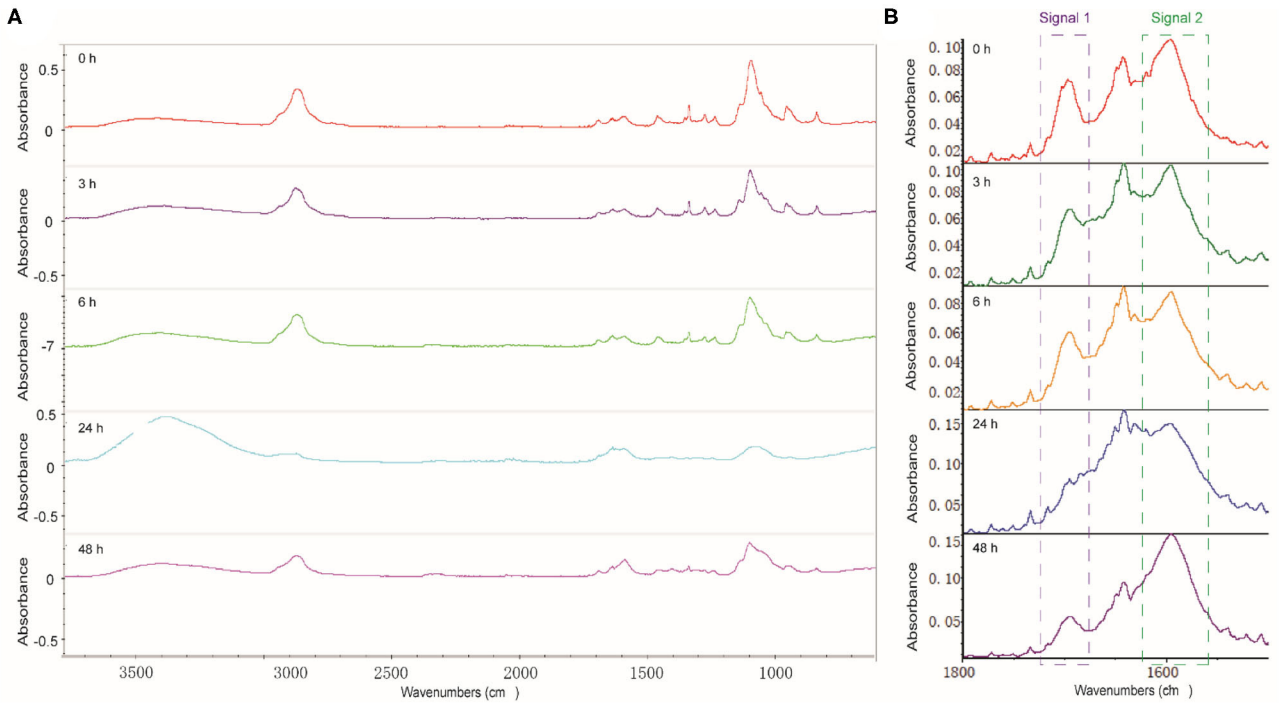

FIGURE 3 | (A) Full scale and **(B)** enlarged carbonyl region of the FTIR spectra of hydrogels with different reaction time.

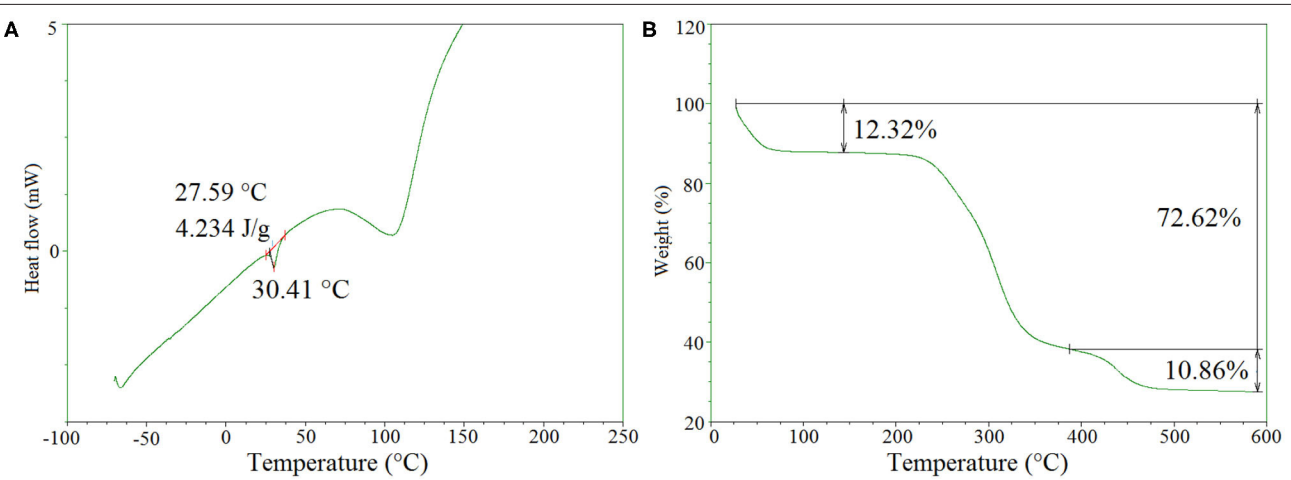

FIGURE 4 | Typical **(A)** DSC and **(B)** TGA curves of the freeze-dried hydrogels.

highest mass loss up to 65% was obtained at 48 h for the hydrogel with molar ratio of 2:1, which can be explained by the lowest degree of cross-linking compared to hydrogels with other molar ratios. Beyond 48 h, the mass of each hydrogel remained almost unchanged.

In vitro Drug Release Performance

In the current work, 5-fluorouracil 5-FU was physically encapsulated into the dynameric hydrogels, and the *in vitro* release was studied in pH 7.4 PBS at 37°C. A calibration curve of 5-FU was first established by HPLC analysis. In all cases, high encapsulation efficiencies were obtained, up to 97%.

Figure 7A presents the release profiles of 5-FU from the hydrogels prepared at 25°C with different dynamer/*O*-CMCS molar ratios. The drug release values might be considered with a *SD*% = 5% as previously reported for similar Chitosan hydrogels (Damiri et al., 2020). For the hydrogel made from molar ratio of 1:1, the release rate of 5-FU appeared very fast at the beginning, reaching 71% after 2 h, followed by slow increase with total

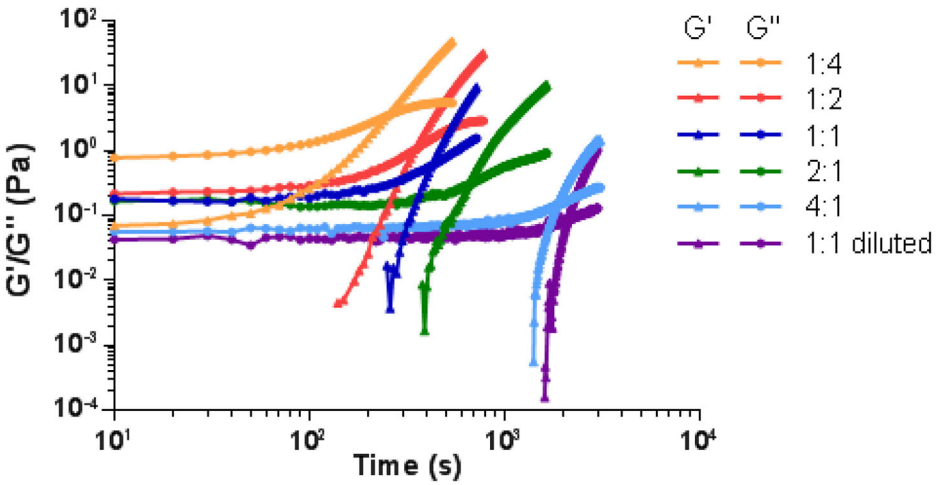

FIGURE 5 | G′ and G″ variation as a function of time of the hydrogels prepared with different dynamer/*O*-CMCS molar ratios.

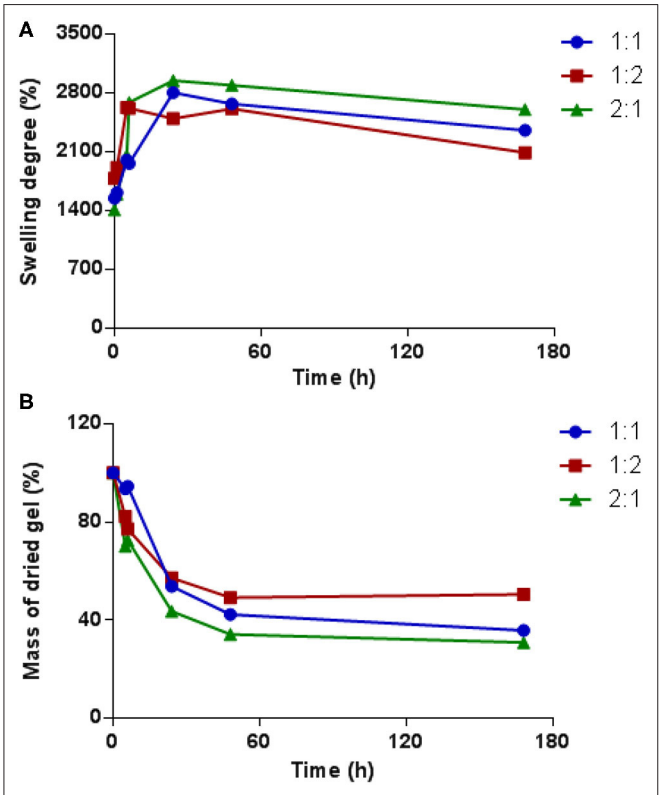

FIGURE 6 | (A) Swelling degree variations of hydrogels obtained from different dynamer/*O*-CMCS molar ratios as a function of time; **(B)** change of dried gel masses with time.

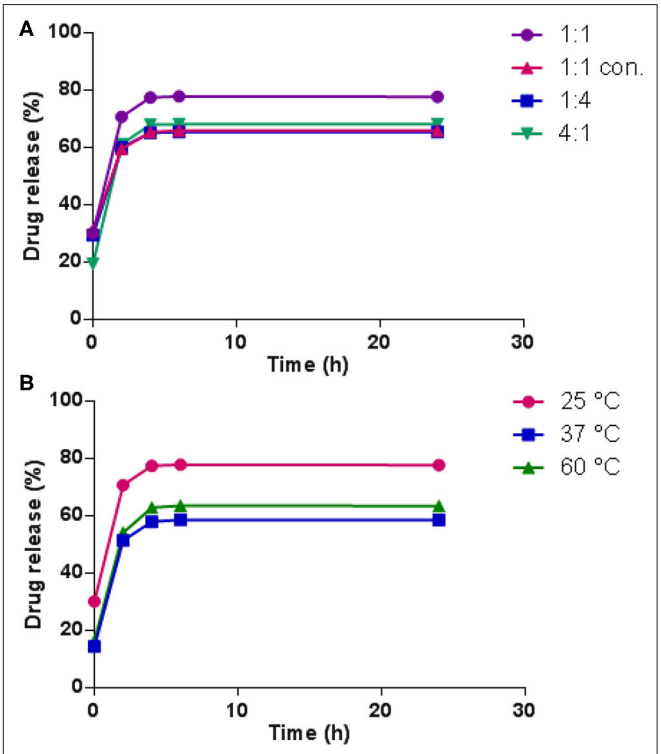

FIGURE 7 | 5-FU release profiles **(A)** from the hydrogels obtained from different dynamer/*O*-CMCS molar ratios at 25°C; **(B)** with different temperatures.

release of 77% by 24 h. Comparatively, hydrogels made from molar ratio of 1:4 and twice concentrated starting materials exhibited a total release of 5-FU below 70%, probably due to the highly cross-linked structures of the hydrogels. However, the hydrogel with molar ratio of 4:1 and thus less cross-linked structure, also showed lower total release of 5-FU compared to the hydrogel made from molar ratio of 1:1. It could be possibly explained by the high affinity between hydrophilic PEG fragments and 5-FU. On the other hand, in all cases, drug release leveled off beyond 5 h, when the volume shrinkage of

the hydrogels was observed, indicating the tighter entrapment of 5-FU inside the hydrogel structure.

To examine the effect of gelation temperature on the release profile of 5-FU from the hydrogels, hydrogels prepared at 37 and 60°C were also tested. As illustrated in **Figure 7B**, much lower initial release was observed by elevating the gelation temperature, 14% at 37°C and 16% at 60°C compared to 30% at 25°C. Meanwhile, the total release of 5-FU also decreased to a large extent at higher temperatures, which confirmed the lower drug release with highly cross-linked hydrogel structures.

CONCLUSIONS

In the current work, dynamic hydrogels were prepared cross-linking of PEG dynamers with *O*-carboxymethyl chitosan *via* amino/carbonyl-imine chemistry. The hydrogels were characterized by NMR, FT-IR spectroscopies, demonstrating the complete formation of the cross-linked imine bond networks of the hydrogel. The swelling property of the hydrogels was subsequently examined. Rheological measurements revealed that higher amount of *O*-CMCS contributes to shorter gelation time due to more cross-linking. Thereafter, they were successfully applied for delivery of anti-tumor drug 5-FU. The loading of 5-FU was efficient, with encapsulation rate up to 97%. The release profile was fast at the beginning, then gradually reached the maximum level within half a day. This is the first example of dynameric hydrogels constructed through cross-linking of imine bonds, revealing promising drug delivery properties. Further work on stimuli-responsive dynamic hydrogels for controlled drug delivery system is under study.

DATA AVAILABILITY STATEMENT

The raw data supporting the conclusions of this article will be made available by the authors, without undue reservation.

AUTHOR CONTRIBUTIONS

Conceptualization: MB and SL. Synthesis and characterization of materials: YZ, C-YP, RY, and EP. Writing—original draft preparation: YZ. Supervision: MB and SL. Funding acquisition: MB. All authors contributed to the article and approved the submitted version.

FUNDING

This work was supported by ANR DYNAFUN, ANR-15-CE29-0009-02, and ANR SmartMatter, ANR-20-MERA-0001.

REFERENCES

Aida, T., Meijer, E. W., and Stupp, S. I. (2012). Functional supramolecular polymers. *Science* 335, 813–817. doi: 10.1126/science.1205962

Bakker, M. H., Lee, C. C., Meijer, E. W., Dankers, P. Y. W., and Albertazzi, L. (2016). Multicomponent supramolecular polymers as a modular platform for intracellular delivery. *ACS Nano* 10, 1845–1852. doi: 10.1021/acsnano.5b05383

Catana, R., Barboiu, M., Moleavin, I., Clima, L., Rotaru, A., Ursu, E.-L., et al. (2015). Dynamic constitutional frameworks for DNA biomimetic recognition. *Chem. Commun.* 51, 2021–2024. doi: 10.1039/C4CC07525K

Charbonneau, C., Chassenieux, C., Colombani, O., and Nicolai, T. (2011). Controlling the dynamics of self-assembled triblock copolymer networks via the pH. *Macromolecules* 44, 4487–4495. doi: 10.1021/ma2002382

Clima, L., Peptanariu, D., Pinteala, M., Salic, A., and Barboiu, M. (2015). DyNAvectors: dynamic constitutional vectors for adaptive DNA transfection. *Chem. Commun.* 51, 17529–17531. doi: 10.1039/C5CC06715D

Damiri, F., Bachra, Y., Bounacir, C., Laaraibi, A., and Berrada, M. (2020). Synthesis and characterization of lyophilized chitosan-based hydrogels cross-linked with benzaldehyde for controlled drug release. *J. Chem.* 2020:8747639. doi: 10.1155/2020/8747639

Deng, G., Li, F., Yu, H., Liu, F., Liu, C., Sun, W., et al. (2012). Dynamic hydrogels with an environmental adaptive self-healing ability and dual responsive sol–gel transitions. *ACS Macro Lett.* 1, 275–279. doi: 10.1021/mz200195n

Fuhrmann, A., Göstl, R., Wendt, R., Kötteritzsch, J., Hager, M. D., Schubert, U. S., et al. (2016). Conditional repair by locally switching the thermal healing capability of dynamic covalent polymers with light. *Nat. Commun.* 7:13623. doi: 10.1038/ncomms13623

Goor, O. J. G. M., Hendrikse, S. I. S., Dankers, P. Y. W., and Meijer, E. W. (2017). From supramolecular polymers to multi-component biomaterials. *Chem. Soc. Rev.* 46, 6621–6637. doi: 10.1039/C7CS00564D

Goujon, A., Mariani, G., Lang, T., Moulin, E., Rawiso, M., Buhler, E., et al. (2017). Controlled sol–gel transitions by actuating molecular machine based supramolecular polymers. *J. Am. Chem. Soc.* 139, 4923–4928. doi: 10.1021/jacs.7b00983

Gu, R., Flidrova, K., and Lehn, J.-M. (2018). Dynamic covalent metathesis in the C=C/C=N exchange between Knoevenagel compounds and imines. *J. Am. Chem. Soc.* 140, 5560–5568. doi: 10.1021/jacs.8b01849

Huang, Y., Li, H., He, X., Yang, X., Li, L., Liu, S., et al. (2020). Near-infrared photothermal release of hydrogen sulfide from nanocomposite hydrogels for anti-inflammation applications. *Chin. Chem. Lett.* 31, 787–791. doi: 10.1016/j.cclet.2019.05.025

Katugampola, P., Winstead, C., and Adeleke, A. (2014). Thermal stability of cazrboxymethyl cgitosan varying the degree of substitution. *Int. J. Pharm. Sci. Invent.* 3, 42–48. Available online at: http://www.ijpsi.org/Papers/Vol3(5)/Version-2/I0352042048.pdf

Lai, W.-F., and He, Z.-D. (2016). Design and fabrication of hydrogel-based nanoparticulate systems for *in vivo* drug delivery. *J. Control. Release* 243, 269–282. doi: 10.1016/j.jconrel.2016.10.013

Lei, L., Li, X., Xiong, T., Yu, J., Yu, X., Song, Z., et al. (2018). Covalently cross-linked chitosan hydrogel sheet for topical ophthalmic delivery of levofloxacin. *J. Biomed. Nanotechnol.* 14, 371–378. doi: 10.1166/jbn.2018.2477

Li, J., and Mooney, D. J. (2016). Designing hydrogels for controlled drug delivery. *Nat. Rev. Mater.* 1:16071. doi: 10.1038/natrevmats.2016.71

Marin, L., Moraru, S., Popescu, M.-C., Nicolescu, A., Zgardan, C., Simionescu, B. C., et al. (2014). "Out of water" constitutional self-organization of chitosan-cinnamaldehyde dynagels. *Chem. Eur. J.* 20, 4814–4821. doi: 10.1002/chem.201304714

Oliva, N., Conde, J., Wang, K., and Artzi, N. (2017). Designing hydrogels for on-demand therapy. *Acc. Chem. Res.* 50, 669–679. doi: 10.1021/acs.accounts.6b00536

Roy, N., Bruchmann, B., and Lehn, J.-M. (2015). DYNAMERS: dynamic polymers as self-healing materials. *Chem. Soc. Rev.* 44, 3786–3807. doi: 10.1039/C5CS00194C

Tao, Y., Liu, S., Zhang, Y., Chi, Z., and Xu, J. (2018). A pH-responsive polymer based on dynamic imine bonds as a drug delivery material with pseudo target release behavior. *Polym. Chem.* 9, 878–884. doi: 10.1039/C7PY02108A

Wei, Z., Yang, J. H., Liu, Z. Q., Xu, F., Zhou, J. X., Zrínyi, M., et al. (2015). Novel biocompatible polysaccharide-based self-healing hydrogel. *Adv. Funct. Mater.* 25, 1352–1359. doi: 10.1002/adfm.201401502

Xiao, T., and Wang, L. (2018). Recent advances of functional gels controlled by pillar[n]arene-based host–guest interactions. *Tetrahedron Lett.* 59, 1172–1182. doi: 10.1016/j.tetlet.2018.02.028

Xiao, T., Xu, L., Zhou, L., Sun, X., Lin, C., and Wang, L. (2019). Dynamic hydrogels mediated by macrocyclic host–guest interactions. *J. Mater. Chem. B* 7, 1526–1540. doi: 10.1039/C8TB02339E

Yamada, Y., and Schneider, J. P. (2016). Fragmentation of injectable bioadhesive hydrogels affords chemotherapeutic macromolecules. *Biomacromolecules* 17, 2634–2641. doi: 10.1021/acs.biomac.6b00701

Yao, X., Ma, X., and Tian, H. (2014). Aggregation-induced emission encoding supramolecular polymers based on controllable sulfonatocalixarene recognition in aqueous solution. *J. Mater. Chem. C* 2, 5155–5160. doi: 10.1039/c4tc00503a

Yasen, W., Dong, R., Zhou, L., Wu, J., Cao, C., Aini, A., et al. (2017). Synthesis of a cationic supramolecular block copolymer with covalent and noncovalent polymer blocks for gene delivery. *ACS Appl. Mater. Interfaces* 9, 9006–9014. doi: 10.1021/acsami.6b15919

Yu, J., Chen, X., Yang, Y., Zhao, X., Chen, X., Jing, T., et al. (2020). Construction of supramolecular hydrogels using imidazolidinyl urea as hydrogen bonding reinforced factor. *J. Mater. Chem. B* 8, 3058–3063. doi: 10.1039/D0TB00331J

Yu, R., Zhang, Y., Barboiu, M., Maumus, M., Noël, D., Jorgensen, C., et al. (2020). Biobased pH-responsive and self-healing hydrogels prepared from O-carboxymethyl chitosan and a 3-dimensional dynamer as cartilage engineering scaffold. *Carbohydr. Polym.* 244:116471. doi: 10.1016/j.carbpol.2020.116471

Zhang, W., Wang, R., Sun, Z., Zhu, X., Zhao, Q., Zhang, T., et al. (2020a). Catechol-functionalized hydrogels: biomimetic design, adhesion mechanism, and biomedical applications. *Chem. Soc. Rev.* 49, 433–464. doi: 10.1039/C9CS00285E

Zhang, Y., and Barboiu, M. (2015). Dynameric asymmetric membranes for directional water transport. *Chem. Commun.* 15, 15925–15927. doi: 10.1039/c5cc06805c

Zhang, Y., and Barboiu, M. (2016). Constitutional cynamic materials—toward natural selection of function. *Chem. Rev.* 116, 809–834. doi: 10.1021/acs.chemrev.5b00168

Zhang, Y., Barboiu, M., Ramström, O., and Chen, J. (2020b). Surface-directed selection of dynamic constitutional frameworks as an optimized microenvironment for controlled enzyme activation. *ACS Catal.* 10, 1423–1427. doi: 10.1021/acscatal.9b04938

Zhang, Y., Feng, W.-X., Legrand, Y.-M., Supuran, C. T., Su, C.-Y., and Barboiu, M. (2016a). Dynameric host frameworks for the activation of lipase through H-bond and interfacial encapsulation. *Chem. Commun.* 52, 13768–13770. doi: 10.1039/C6CC08399D

Zhang, Y., Legrand, Y.-M., Petit, E., Supuran, C. T., and Barboiu, M. (2016b). Dynamic encapsulation and activation of carbonic anhydrase in multivalent dynameric host matrices. *Chem. Commun.* 52, 4053–4055. doi: 10.1039/C6CC00796A

Zhang, Y., Petit, E., and Barboiu, M. (2018a). Multivalent dendrimers and their differential recognition of short single-stranded DNAs of various length and sequence. *ChemPlusChem* 83, 354–360. doi: 10.1002/cplu.201800081

Zhang, Y., Qi, Y., Ulrich, S., Barboiu, M., and Ramström, O. (2020c). Dynamic covalent polymers for biomedical applications. *Mater. Chem. Front.* 4, 489–506. doi: 10.1039/C9QM00598F

Zhang, Y., Supuran, C. T., and Barboiu, M. (2018b). Exponential activation of carbonic anhydrase by encapsulation in dynameric host matrices with chiral discrimination. *Chem. Eur. J.* 24, 715–720. doi: 10.1002/chem.201704605

Conflict of Interest: The authors declare that the research was conducted in the absence of any commercial or financial relationships that could be construed as a potential conflict of interest.

frontiers in Chemistry

ORIGINAL RESEARCH
published: 04 September 2020
doi: 10.3389/fchem.2020.00742

Hypoxia-Responsive Polymeric Micelles for Enhancing Cancer Treatment

Huayang Feng[1,2†], Dandan Chu[1†], Fan Yang[1], Zhanrong Li[1], Bingbing Fan[2], Lin Jin[1] and Jingguo Li[1,2*]*

[1] Henan Provincial People's Hospital, Zhengzhou University People's Hospital, Zhengzhou, China, [2] School of Materials Science and Engineering, Zhengzhou University, Zhengzhou, China

Polymeric drug vectors have shown great potentials in cancer therapy. However, intelligent controlled release of drugs has become a major challenge in nanomedicine research. Hypoxia-responsive polymeric micelles have received widespread attention in recent years due to the inherent hypoxic state of tumor tissue. In this study, a novel diblock polymer consisting of polyethylene glycol and poly[glutamic acid (3-(2-nitro-imidazolyl)-propyl)] was synthesized and self-assembled into hypoxia-responsive polymeric micelles for the controlled release of doxorubicin (DOX). The cell experiments demonstrated that DOX-loaded micelles had a stronger killing capacity on tumor cells under hypoxic conditions, while the blank micelles had good biocompatibility. All the experiments indicate that our hypoxia-responsive polymeric micelles have a great potential for enhanced cancer treatment.

Keywords: hypoxia-responsive, polymeric micelles, cancer treatment, doxorubicin, drug delivery

OPEN ACCESS

Edited by:
Jianliang Shen,
Wenzhou Medical University, China

Reviewed by:
Haibo Wang,
Sichuan University, China
Ping Huang,
Shanghai Jiao Tong University, China

****Correspondence:***
Zhanrong Li
lizhanrong@zzu.edu.cn
Jingguo Li
lijingguo@zzu.edu.cn

† These authors have contributed equally to this work

Specialty section:
This article was submitted to Polymer Chemistry, a section of the journal Frontiers in Chemistry

Received: *22 May 2020*
Accepted: *17 July 2020*
Published: *04 September 2020*

Citation:
Feng H, Chu D, Yang F, Li Z, Fan B, Jin L and Li J (2020) Hypoxia-Responsive Polymeric Micelles for Enhancing Cancer Treatment. Front. Chem. 8:742. doi: 10.3389/fchem.2020.00742

INTRODUCTION

Cancer is a disease that endangers human life. About 9.6 million people died because of cancer in 2018 according to American Cancer Society (Bray et al., 2018). Therefore, the development of more effective methods for the treatment of cancer is of great significance for promoting human health. At present, the main treatments for cancer include chemotherapy, radiotherapy, and surgery. Among them, surgery and radiation therapy are local treatments, which can only kill local tumor cells. Chemotherapy is a whole-body treatment method, which can kill not only native tumor cells but also metastatic cancer cells, and has a systemic therapeutic effect (Krishnan and Rajasekaran, 2014). However, most chemotherapeutic drugs such as DOX generally have shortcomings like large toxic side effects and short drug effects, which seriously affect the clinical tumor treatment effect (Feng et al., 2018; Pugazhendhi et al., 2018).

To solve these problems, researchers have developed many nanoscale drug delivery systems to improve the anticancer efficacy of drugs (Li et al., 2014a,b; Li et al., 2016b; Chen et al., 2018; Gao et al., 2019; Guo et al., 2020; Ma et al., 2020). Among many drug delivery vehicles, polymeric micelles have attracted more and more researchers' attention because of their low biological toxicity, high stability, and high drug loading capacity (Li et al., 2016a; Huang et al., 2018; Li et al., 2020a,b). Polymer micelles are usually composed of a hydrophilic shell and a hydrophobic core, which are usually self-assembled from amphiphilic block polymers in water with a size varying from 10 to 200 nm. The above structure of the polymeric micelles gives them the following advantages: (1) it can improve the water solubility of many hydrophobic drugs; (2) it can extend the circulation

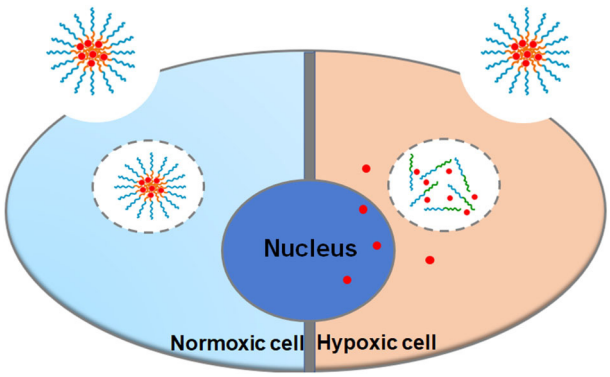

GRAPHICAL ABSTRACT | A hypoxia-responsive polymer micelle encapsulated with DOX was developed for therapy of cancer. *in vitro* studies demonstrated the enhanced anticancer effect of the nanomicelles.

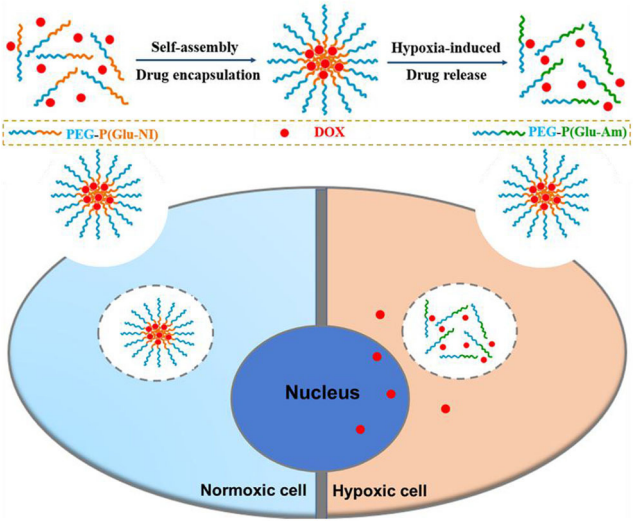

SCHEME 1 | Schematic of fabrication and hypoxia-sensitive drug release process.

time of the drugs in the body through reducing the clearance of the drug by the kidney; (3) it can increase the concentration of drugs in tumor tissues through enhanced penetration and retention effects (EPR effect), also known as passive targeting (Matsumura and Maeda, 1986; Danhier et al., 2010).

More and more researchers have concentrated on stimuli-responsive polymeric nanocarriers because of their good application prospects in drug delivery and intelligent controlled release of drugs (Dong et al., 2016; Kamaly et al., 2016; Gao and Dong, 2018; Hu et al., 2019; Song et al., 2019). Among them, hypoxia-responsive polymeric nanocarriers are a new class of stimulus-responsive carriers that have been studied recently (Liu et al., 2015; Dong et al., 2020). Due to the strong growth of the tumor tissue and the relatively insufficient blood supply, the tumor tissues are usually in a hypoxic state compared with the normal tissues. Researchers have developed a variety of hypoxia-responsive carriers based on the characteristics of tumor tissue hypoxia. The carriers can disintegrate or deform to release drugs in hypoxic tumor tissues, but will not disintegrate or deform in normal tissues, thereby improving drug efficacy and reducing toxic side effects. Among many compounds with hypoxia responsiveness, 2-nitroimidazole has been mostly studied (Thambi et al., 2014). 2-Nitroimidazole (NI) is hydrophobic, and it could be reduced to hydrophilic aminoimidazole easily by enzymes in the body under hypoxic conditions, which can be used as an important component of hypoxia-responsive carriers.

Herein, a novel diblock hypoxia-responsive polymer consisting of polyethylene glycol(PEG) and poly(glutamic acid (3-(2-nitro-imidazolyl)-propyl))(P(LGlu-NI)), abbreviated as PEGN, is synthesized and self-assembled to hypoxia-responsive micelles for the controlled release of DOX (**Scheme 1**). The PEG block served as a hydrophilic shell, and the P(LGlu-NI) block is used as a hypoxia-responsive hydrophobic core to support DOX. Under hypoxic conditions, the hydrophobic nitroimidazole could turn to the hydrophilic aminoimidazole, which could make the micelle disintegrated or deformed, thereby releasing DOX quickly. The anticancer activity of DOX-loaded micelles was examined in human breast adenocarcinoma MCF-7 cells.

EXPERIMENTAL

Materials

a-Methoxy-3-amino poly (ethylene glycol) (mPEG-NH_2, Mn = 2 kDa) was purchased from Ponsure Biotech (Shanghai, China). 1-Chloro-3-hydroxypropane (Macklin, China), DL-glutamic acid (Macklin, China), 2-nitroimidazole (Accela, China), and doxorubicin hydrochloride (Melone Pharma, China) were used as received. A dialysis bag (Mw cutoff: 3.5 kDa) was purchased from Shanghai Green Bird Technology Development Co., Ltd. (Shanghai, China). Anhydrous *N*, *N*-dimethylformamide (DMF) was purchased from JK chemical (Beijing, China). Menthol, diethyl ether, petroleum ether, and ethyl acetate were purchased from Zhengzhou Yinfeng Reagent Co., Ltd. (Zhengzhou, China). Petroleum ether and ethyl acetate were dried over CaH_2 and then distilled under ambient pressure.

MCF-7 cells were obtained from the Kunming cell library of the Chinese Academy of Sciences. MEM medium was purchased from HyClone (America). Phosphate-buffered saline (PBS) and 1% penicillin–streptomycin double antibody were purchased from Solarbio (Shanghai, China). Fetal bovine serum (FBS) was purchased from SeraPro (Germany). Trypsin–EDTA (0.25%) solution was purchased from Gibco (America). Cell Counting Kit-8 (CCK-8) was purchased from Dojindo.

Synthesis of Diblock Copolymers (PEGN)

Synthesis of Glutamic Acid (3-Chloropropyl) (LGlu-Cl)

11 g glutamic acid was dissolved in 100 mL of 3-chloro-1-propanol, and then 10 mL trimethylchlorosilane was added into

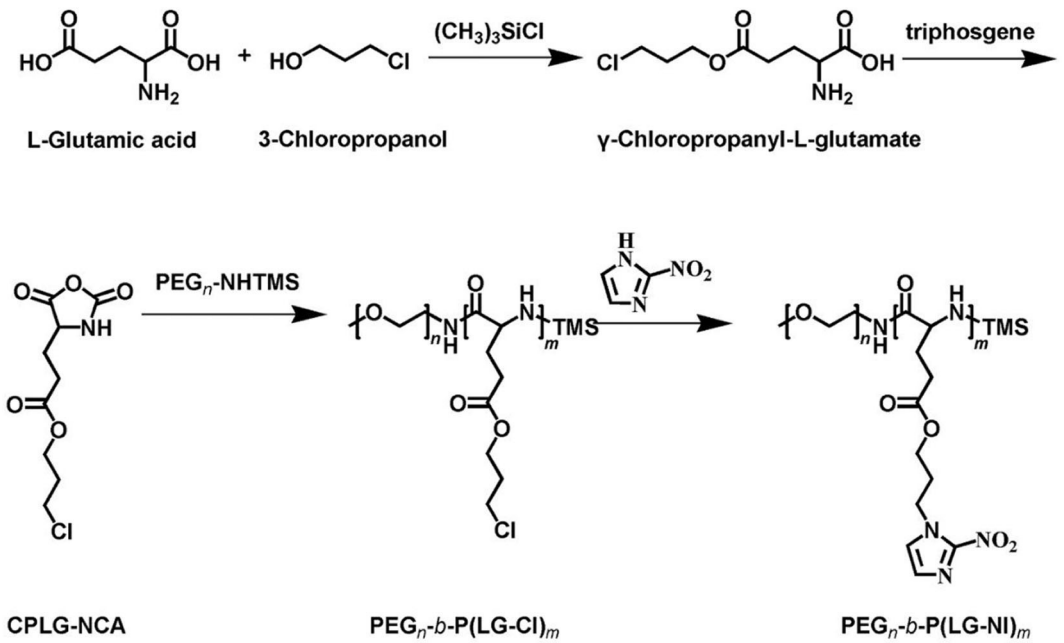

SCHEME 2 | The synthesis approach of copolymer PEGN.

the above system. The reaction was allowed to proceed at room temperature for 5 days. After being transparent, the reaction solution was precipitated into a large amount of diethyl ether, filtered, washed three times with diethyl ether, and finally dried for 24 h under vacuum.

Synthesis of N-Carboxyanhydride of Glutamic Acid (3-Chloropropyl) (LGlu-Cl-NCA)

5.8 g LGlu-Cl was dissolved in 200 mL of ethyl acetate, and then the mixture was stirred at 70°C. After the mixture started to reflux, 3.2 g of triphosgene dissolved in 20 mL of ethyl acetate was added into the above mixture slowly. The reaction was allowed to proceed at 70°C for 4 h. After being transparent, the reaction solution was cooled in a refrigerator at −20°C. The reaction solution was washed with cold saturated Na_2CO_3 and NaCl solution and then dried with anhydrous $MgSO_4$. After being concentrated using a rotary evaporator, the solution was precipitated into a large amount of petroleum ether, filtered, and recrystallized with petroleum ether and ethyl acetate for the subsequent ring-opening polymerization reaction.

Synthesis of PEG-b-P(LGlu-Cl)

0.7 g of PEG-NH_2 was dissolved into 20 mL of anhydrous DMF. Then, 2.6 g (LGlu-Cl)-NCA was added into the above solution under the protection of nitrogen, and the reaction was allowed to proceed at 40°C for 3 days. The above system was transferred to a dialysis bag (Mw cutoff: 3.5 kDa) and dialyzed against pure water for 3 d and lyophilized to obtain a white powder, which was the target product (Mn = 4.9 kDa, calculated from the 1H NMR spectrum, $mPEG_{45}$-b-P $(LGlu\text{-}Cl)_{14}$).

Synthesis of PEG-b-P(LGlu-NI) (PEGN)

294.9 mg NI and 352.7 mg K_2CO_3 were dissolved in 10 mL of DMF and stirred for 10 min at room temperature. 711 mg PEG-b-P(LGlu-Cl) and 60 mg NaI were dissolved in 10 mL of DMF and then slowly added into the above solution. The reaction was allowed to proceed for 72 h at 80°C. The above system was dialyzed against deionized water for 3 days and lyophilized to obtain PEGN.

Preparation of the Micelles

30.0 mg of PEGN and 3.0 mg DOX·HCl were dissolved in 3 mL DMSO, then 5 μL of triethylamine was added to the above mixture to turn hydrophilic DOX·HCl into hydrophobic DOX. The above solution was added dropwise to 30 mL of deionized water under ultrasonic conditions. Then, the above solution was transferred into a dialysis bag and dialyzed for 1 days in deionized water to remove DMSO and unencapsulated DOX. After the dialysis, the solution was filtered with a 450-nm filter to remove large particles, and the solution was concentrated and washed three times using an ultrafiltration tube (MWCO = 100,000 Da) with physiological saline to obtain DOX-loaded micelles (PEGN/DOX). The preparation of blank micelles (PEGN bm) is the same as that of DOX-loaded micelles, except that DOX is not added during the preparation process.

Characterization of the Polymers and Nanoparticles

^{1}H NMR spectra of the monomer and polymers were obtained on a Bruker AVANCE II 400-MHz spectrometer using DMSO-d_6 as the solvent. Fourier transform infrared (FTIR) spectral studies were carried out using an IS10 670 FTIR spectrometer, and all the samples were compressed into pellets with KBr before being tested. The hydrodynamic sizes of the micelles were determined using a Nano ZS90 dynamic light scattering (DLS) equipment. The data was collected on an auto-correlator with a detection angle of scattered light at 90°. Each sample was measured three times, and the results were obtained by the average of the collected data. UV absorption of blank micelles under normal and hypoxic conditions was detected by an ultraviolet-visible spectrophotometer.

Loading Content of DOX

A UV-Vis spectrophotometer was used to determine the drug loading content of DOX. Firstly, the DOX-loaded PEGN micelle solution was lyophilized, weighed, and dissolved in DMSO. Then, the DOX concentration was quantified by measuring the absorbance of DOX at 480 nm according to a standard curve we established in advance.

Confocal Laser Scanning Microscopy (CLSM)

The cellular uptake of micelles in MCF-7 cells for different groups was analyzed on a confocal laser scanning microscope (Nikon C1si, Japanese). For the normoxic group, MCF-7 cells were incubated overnight in 6-well plates at 37°C and then incubated with PEGN/DOX micelles for 2 h. The cells were washed with PBS twice, and the nuclei were stained with Hoechst 33342 solution for 10 min. Finally, MCF-7 cells were analyzed and observed under CLSM. The excitation and emission wavelengths of DOX and Hoechst are 488 nm and 590 nm, 350 nm, and 460 nm, respectively. Except that the MEM medium containing 100 μM $CoCl_2$ was used to simulate the *in vivo* hypoxic environment, the experimental steps for the hypoxic group were the same as the above steps.

Cell Viability Assay

MCF-7 cells were seeded in 96-well plates with MEM medium containing 100 μM $CoCl_2$ and incubated at 37°C under 5% CO_2 atmosphere for 24 h. Then, the cells were separately incubated with blank and DOX-loaded micelles at various concentrations for 48 h. After the medium in each well was replaced with 100 μL fresh medium containing 10 μL CCK-8 solutions, the cells were incubated for another 4 h.

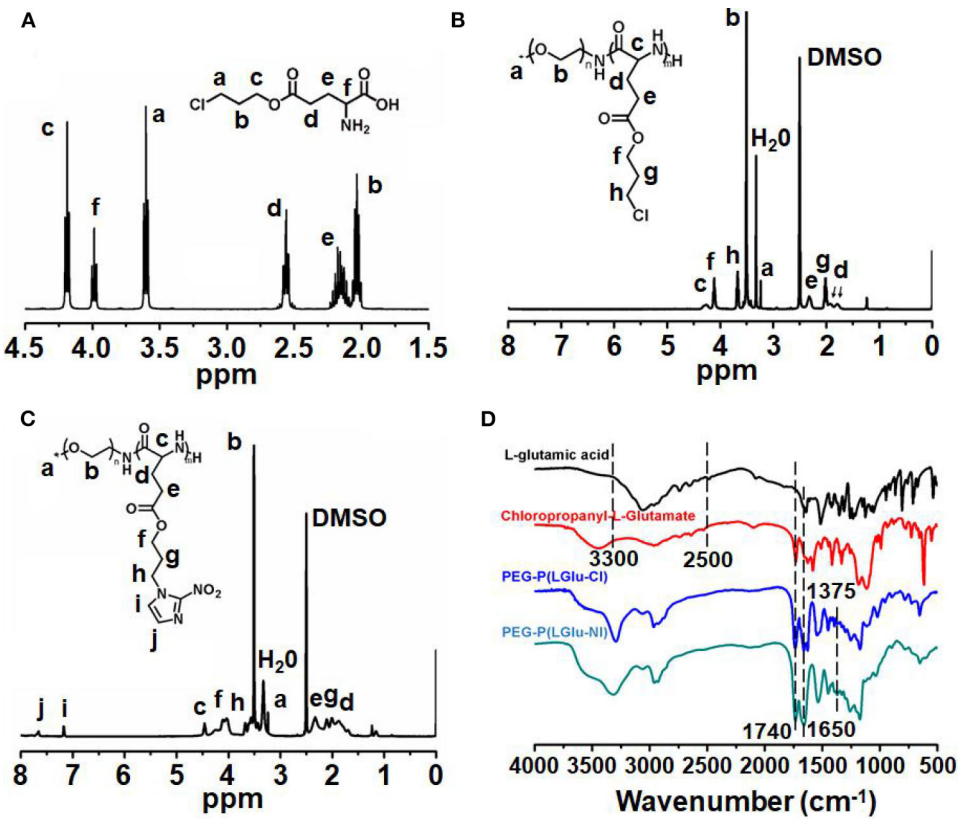

FIGURE 1 | ^{1}H-NMR spectra of **(A)** LGlu-Cl and **(B)** PEG-b-P(LGlu-Cl) and **(C)** PEGN; **(D)** FTIR spectra of PEGN and its precursors.

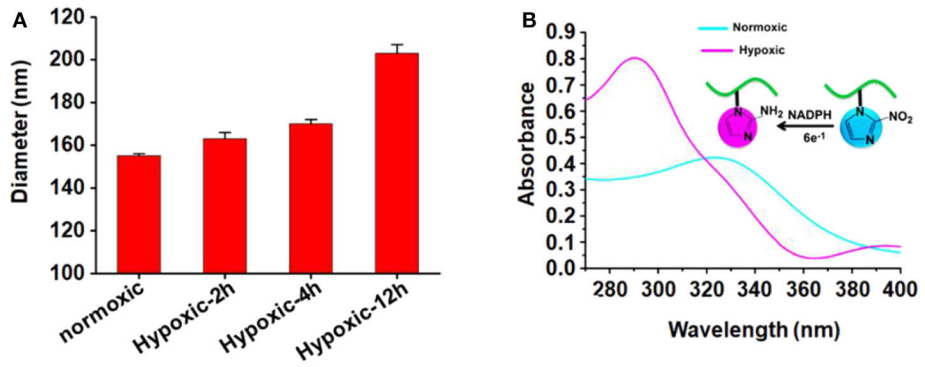

FIGURE 2 | (A) Mean particle size of blank micelles with prolonged hypoxic treatment time; **(B)** UV absorption of PEGN bm at hypoxic and normoxic conditions.

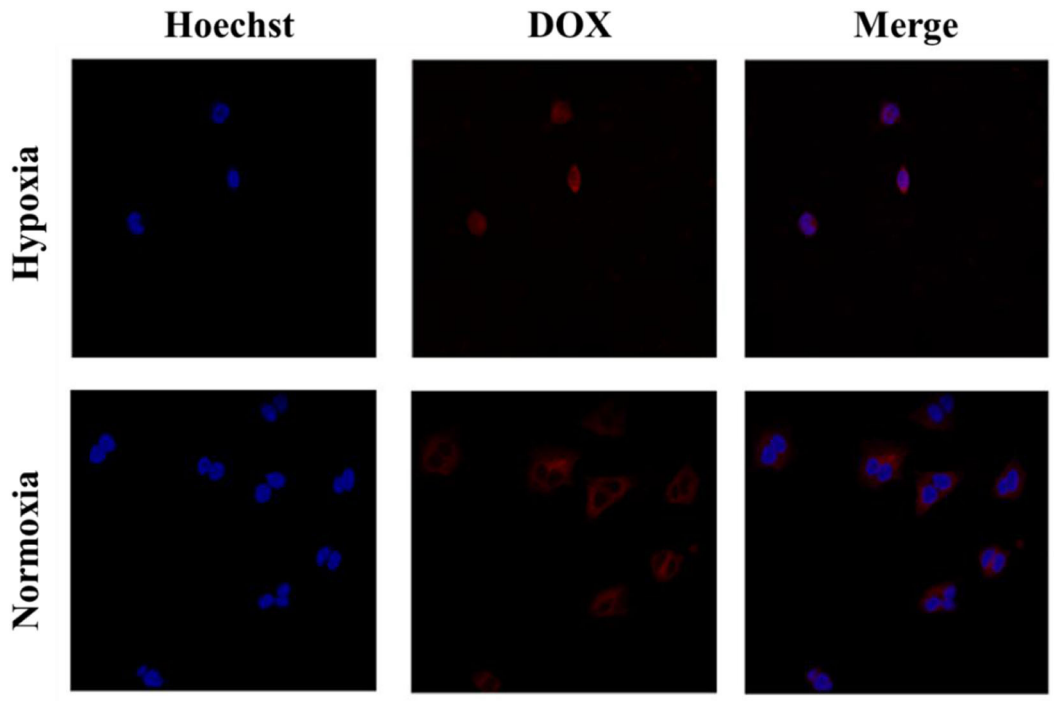

FIGURE 3 | Cellular uptake of PEGN/DOX after being cultured with MCF-7 cells for 2 h under hypoxic conditions and normoxic conditions.

After vibration for 10 min, the absorbance at 450 nm was analyzed with an Enzyme Labeler (PerkinElmer EnVision). Cell viability was calculated by comparing absorbance with the negative control. All experiments were conducted in triplicate.

Cell Apoptosis by TUNEL

The cell apoptosis rates with PEGN/DOX in normoxic and hypoxic groups were detected by TUNEL assay. For the normoxic group, MCF-7 cells were seeded into 6-well plates and cultured overnight. Then, the cells were incubated with PEGN/DOX for 24 h. Then, the cells were fixed with 4% paraformaldehyde (200 μL) for 20 min and then washed three times with PBS. Furthermore, the cells were treated with 100 μL of 1% Triton X-100 for 5 min and then washed three times with PBS. After adding 50 μL of TdT enzyme solution to each sample, the samples were washed three times with PBS. Then, the samples were treated with 50 μL of streptavidin–fluorescein solution for 30 min and washed three times with PBS. Then, the nuclei were stained with Hoechst 33342 solution for 10 min and washed with PBS for three times. At last, the samples were observed with a fluorescence microscope (Nikon ECLIPSE 80i, Japan). Except that the MEM medium containing 100 μM $CoCl_2$ was used to simulate the hypoxic environment *in vivo*, the experimental steps for the hypoxic group were the same as the above steps.

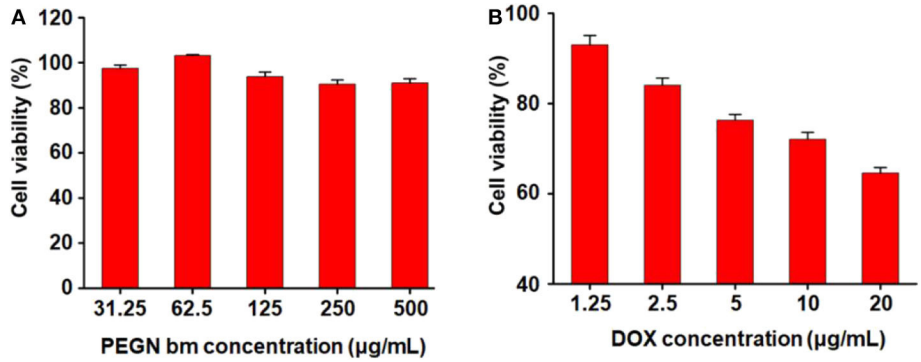

FIGURE 4 | Cytotoxicity of **(A)** PEGN bm and **(B)** PEGN/DOX.

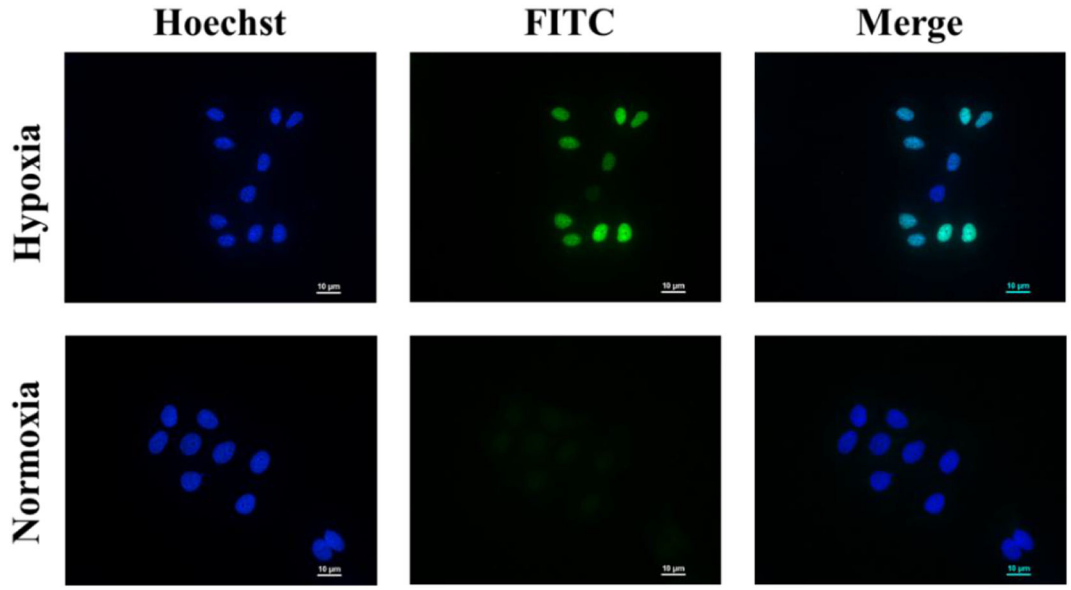

FIGURE 5 | Cell apoptosis of PEGN/DOX under normoxic and hypoxic conditions. Scale bars are all 10 μm.

RESULTS AND DISCUSSION

Polymer Synthesis and Characterization

The synthetic approach of PEG-b-P(LGlu-NI) is illustrated in **Scheme 2**. Moreover, the chemical structure of monomer and polymer was verified by ^{1}H NMR and FTIR analyses (**Figure 1**). **Figure 1A** shows the ^{1}H NMR spectra of LGlu-Cl. The peaks are assigned as follows: 4.19 ppm ($ClCH_2CH_2C\boldsymbol{H}_2O$–), 4.00 ppm ($NH_2$ (–CH_2-)$C\boldsymbol{H}$–CO–), 3.60 ppm ($ClC\boldsymbol{H}_2CH_2CH_2$-), 2.56 ppm (–$COC\boldsymbol{H}_2CH_2$-), 2.09–2.21 ppm (–$COCH_2C\boldsymbol{H}_2$-), and 2.02 ppm ($ClCH_2C\boldsymbol{H}_2CH_2$-), indicating the successful synthesis of the target product. The ^{1}H NMR spectra of PEG-b-P(LGlu-Cl) and PEG-b-P(LGlu-NI) are shown in **Figures 1B,C**. The proton chemical shifts in the ^{1}H NMR spectrum of PEG-b-P(LGlu-Cl) are 3.50 ppm (–$OC\boldsymbol{H_2}C\boldsymbol{H_2}$–), 3.28 ppm ($C\boldsymbol{H}_3$-$OCH_2CH_2$-), 4.28 ppm (–NH(–$CH_2$-)$C\boldsymbol{H}$–CO–), 4.10 ppm ($ClCH_2CH_2C\boldsymbol{H}_2O$–), 3.66 ppm ($ClC\boldsymbol{H}_2CH_2CH_2$-), 2.34 ppm (–$COC\boldsymbol{H}_2CH_2$-), 2.02 ppm ($ClCH_2C\boldsymbol{H}_2CH_2$-), and 1.75–1.91 ppm (–NH(–$C\boldsymbol{H}_2$-)CH–CO–). According to the ratio of integral values of glutamic acid block signals to the PEG block signals, the polymerization degree of LGlu-Cl moiety is 14. After the ammonolysis reaction, the appearance of the two characteristic signals of nitroimidazole at 7.65 ppm (–$NC\boldsymbol{H}CHN$–) and 7.20 ppm (–$NCHC\boldsymbol{H}N$–) indicate the successful synthesis of the final product PEGN (**Figure 1C**). **Figure 1D** shows the FTIR spectrum of products; the appearance of a characteristic peak of nitroimidazole around 1,375 cm^{-1} confirms the formation of PEGN. The presence of characteristic peaks of ester and amide bonds at 1,740 and 1,650 cm^{-1} indicates that the polymer structure is complete before and after the reaction, and there was no degradation.

Preparation and Characterization of Micelles

The size of micelles was evaluated using DLS. The mean diameter of the blank micelle and DOX-loaded micelle is 155 and 168 nm, respectively. The reason for the change of particle size may be that the loading of DOX increases the volume of the hydrophobic core, which increases the overall particle size of the micelles. **Figure 2A** shows the change of the average particle size of blank micelles with prolonged hypoxic treatment time. Under hypoxic conditions, the mean diameter of blank micelles changed from 155 to 203 nm, probably because nitroimidazole was converted to aminoimidazole under hypoxic conditions, which reduced the hydrophobicity of the hydrophobic core and led to internal aggregation force weakening, thereby increasing the volume of the micelles. By calculation with previously established calibration curves, the drug loading content of the micelles was 3.99% (encapsulation efficiency of 41.57%). **Figure 2B** is the UV absorption curve of a blank micelle under hypoxic and normal conditions. Under normal conditions, there is only very weak UV absorption at 327 nm, but a strong UV absorption peak appears at 290 nm under hypoxic conditions, indicating that the nitroimidazole group was converted into aminoimidazole under hypoxic conditions, which is consistent with the reported literature (Thambi et al., 2014).

Cell Uptake and Intracellular Distribution

Cell uptake and intracellular distribution of the DOX-loaded micelles were evaluated with CLSM. The results were obtained in MCF-7 cells. The red fluorescence indicates the position of DOX, and the blue fluorescence indicates the position of the nucleus stained with Hoechst, and the purple fluorescence is obtained by the merge of red and blue fluorescence. **Figure 3** shows the situation of DOX delivered into cancer cells under hypoxic conditions and normoxic conditions. After incubation with the micelles for 2 h under hypoxic conditions, intense purple fluorescence was observed in the nucleus, indicating that most of the DOX were delivered into the nucleus. However, after incubation with the micelles for 2 h under normoxic conditions, DOX was still mainly distributed in the cytoplasm. These results show that micelles can respond to hypoxia conditions and deliver drugs into the nucleus of tumor cells more quickly under hypoxic conditions.

Cytotoxicity

The cytotoxicity of micelles was determined in MCF-7 cells by CCK-8 assay. **Figure 4A** shows the cytotoxicity of blank micelles under hypoxic conditions. With the increase in the blank micelle concentration, the cell survival rate did not change much (all remained above 90%), indicating that the carrier has very good biological safety. **Figure 4B** shows the cytotoxicity of DOX-loaded micelles under hypoxic conditions. As the concentration of drug-loaded micelles increased, the survival rate of tumor cells decreased rapidly. When the concentration of DOX reaches 20 μg/mL, the cell survival rate under hypoxic conditions drops to 64.5 ± 0.6%. These results demonstrate that the DOX-loaded micelles have a strong killing capacity for breast cancer cells under hypoxic conditions.

Cell Apoptosis

Finally, the cell apoptosis of micelles was determined in MCF-7 cells by TUNEL assay.

As shown in **Figure 5**, the nuclei of the apoptotic cells were stained green. After being incubated with PEGN/DOX for 24 h, the apoptosis rate of MCF-7 cells at the hypoxic condition was 74.57%, and no significant apoptosis of MCF-7 cells was detected in normoxic conditions, indicating that the DOX-loaded micelles could kill cancer cells more efficiently under hypoxic conditions, which is consistent with the cell uptake experiment.

CONCLUSIONS

In conclusion, a hypoxia-responsive copolymer PEG-b-P(LGlu-NI) was successfully synthesized and self-assembled into micelles with DOX encapsulated in the hydrophobic core. The DLS results confirmed that the particle size of micelles was around 150 nm. Cell experiments show that DOX-loaded micelles have a stronger killing effect on tumor cells under hypoxic conditions, while the carriers have good biocompatibility. These results show that polymeric micelles have good potential of application in hypoxia-responsive drug release for enhancing cancer treatment.

DATA AVAILABILITY STATEMENT

The datasets presented in this study can be found in online repositories. The names of the repository/repositories and accession number(s) can be found in the article/supplementary material.

AUTHOR CONTRIBUTIONS

ZL and JL conceived and supervised the project. HF, DC, and FY performed all the experiments. BF and LJ wrote the manuscript. All authors read and approved the manuscript.

FUNDING

This research was supported by the National Natural Science Foundation of China (U1904176, 81600775, and 21504082), the Science and Technology Program of Henan Province, China (202102310072), the Medical Science and Technology Program of Henan Province, China (2018020398 and SB201902026), and the Zhongyuan Thousand Talents Plan Project.

REFERENCES

Bray, F., Ferlay, J., Soerjomataram, I., Siegel, R. L., Torre, L. A., and Jemal, A. (2018). Global cancer statistics 2018: GLOBOCAN estimates of incidence and mortality worldwide for 36 cancers in 185 countries. *CA Cancer. J. Clin.* 68, 394–424. doi: 10.3322/caac.21492

Chen, Q., Yang, Y., Lin, X., Ma, W., Chen, G., Li, W., et al. (2018). Platinum(iv) prodrugs with long lipid chains for drug delivery and overcoming

cisplatin resistance. *Chem. Commun*. 54, 5369–5372. doi: 10.1039/C8CC02791A

Danhier, F., Feron, O., and Préat, V. (2010). To exploit the tumor microenvironment: passive and active tumor targeting of nanocarriers for anti-cancer drug delivery. *J. Controlled Release*. 148, 135–146. doi: 10.1016/j.jconrel.2010.08.027

Dong, P., Zhou, Y., He, W., and Hua, D. (2016). A strategy for enhanced antibacterial activity against *Staphylococcus aureus* by the assembly of alamethicin with a thermo-sensitive polymeric carrier. *Chem. Commun*. 52, 896–899. doi: 10.1039/C5CC07054F

Dong, Z., Wang, X., Zhao, S., Qiu, H., Han, M., Li, J., et al. (2020). The influence of nanocarrier architectures on antitumor efficacy of docetaxel nanoparticles. *RSC Adv*. 10, 11074–11078. doi: 10.1039/D0RA01421D

Feng, H., Chu, D., Li, Z., Guo, Z., Jin, L., Fan, B., et al. (2018). A DOX-loaded polymer micelle for effectively inhibiting cancer cells. *RSC Adv*. 8, 25949–25954. doi: 10.1039/C8RA04089C

Gao, H., Feng, H., Bai, Y., Li, Z., Chen, L., Jin, L., et al. (2019). Multifunctional polymeric carrier for co-delivery of MRI contrast agents and siRNA to tumors. *J. Biomed. Nanotechnol*. 15, 1764–1770. doi: 10.1166/jbn.2019.2805

Gao, Y., and Dong, C. M. (2018). Quadruple thermo-photo-redox-responsive random copolypeptide nanogel and hydrogel. *Chin. Chem. Lett*. 29, 927–930. doi: 10.1016/j.cclet.2017.09.042

Guo, Z., Shi, L., Feng, H., Yang, F., Li, Z., Jin, L., et al. (2020). Reduction-sensitive nanomicelles: delivery celastrol for retinoblastoma cells effective apoptosis. *Chin. Chem. Lett*. doi: 10.1016/j.cclet.2020.03.066

Hu, J., Xu, Y., and Zhang, Y. (2019). Amphiphilic random polycarbonate self-assemble into GSH/pH dual responsive micelle-like aggregates in water. *Chin. Chem. Lett*. 30, 2039–2042. doi: 10.1016/j.cclet.2019.05.017

Huang, Y., Li, X. X., Zhang, L., Chen, X. Y., Liu, C. B., Chen, J. Q., et al. (2018). Multifunctional nanoplatform based on pH-responsive micelle coated with discontinuous gold shell for cancer photothermo-chemotherapy and photoacoustic tomography. *Chin. J. Polym. Sci*. 36, 1139–1149. doi: 10.1007/s10118-018-2141-8

Kamaly, N., Yameen, B., Wu, J., and Farokhzad, O. C. (2016). Degradable controlled-release polymers and polymeric nanoparticles: mechanisms of controlling drug release. *Chem. Rev*. 116, 2602–2663. doi: 10.1021/acs.chemrev.5b00346

Krishnan, V., and Rajasekaran, A. K. (2014). Clinical nanomedicine: a solution to the chemotherapy conundrum in pediatric leukemia therapy. *Clin. Pharmacol. Ther*. 95, 168–178. doi: 10.1038/clpt.2013.174

Li, J., Cheng, D., Yin, T., Chen, W., Lin, Y., Chen, J., et al. (2014a). Copolymer of poly (ethylene glycol) and poly (L-lysine) grafting polyethylenimine through a reducible disulfide linkage for siRNA delivery. *Nanoscale* 6, 1732–1740. doi: 10.1039/C3NR05024F

Li, J., Yu, X., Wang, Y., Yuan, Y., Xiao, H., Cheng, D., et al. (2014b). A Reduction and pH Dual-Sensitive Polymeric Vector for Long-Circulating and Tumor-Targeted siRNA Delivery. *Adv. Mater*. 26, 8217–8224. doi: 10.1002/adma.201403877

Li, J., Zhang, L., Lin, Y., Xiao, H., Zuo, M., Cheng, D., et al. (2016a). A pH-sensitive prodrug micelle self-assembled from multi-doxorubicin-tailed polyethylene glycol for cancer therapy. *RSC Adv*. 6, 9160–9163. doi: 10.1039/C5RA27293A

Li, Z., Feng, H., Jin, L., Zhang, Y., Tian, X., and Li, J. (2020a). Polymeric micelle with pH-induced variable size and doxorubicin and siRNA co-delivery for synergistic cancer therapy. *Appl. Nanosci*. 10, 1903–1913. doi: 10.1007/s13204-020-01263-8

Li, Z., Guo, Z., Chu, D., Feng, H., Zhang, J., Zhu, L., et al. (2020b). Effectively suppressed angiogenesis-mediated retinoblastoma growth using celastrol nanomicelles. *Drug Deliv*. 27, 358–366. doi: 10.1080/10717544.2020.1730522

Li, Z., Li, J., Zhu, L., Zhang, Y., Zhang, J., Yao, L., et al. (2016b). Celastrol nanomicelles attenuate cytokine secretion in macrophages and inhibit macrophage-induced corneal neovascularization in rats. *Int. J. Nanomed*. 11, 6135–6148. doi: 10.2147/IJN.S117425

Liu, Y., Liu, Y., Bu, W., Cheng, C., Zuo, C., Xiao, Q., et al. (2015). Hypoxia induced by upconversion-based photodynamic therapy: towards highly effective synergistic bioreductive therapy in tumors. *Angew. Chem. Int. Ed*. 54, 8105–8109. doi: 10.1002/anie.201500478

Ma, W., Sha, S. N., Chen, P. L., Yu, M., Chen, J. J., Huang, C. B., et al. (2020). A cell membrane-targeting self-delivery chimeric peptide for enhanced photodynamic therapy and in situ therapeutic feedback. *Adv. Healthc. Mater*. 9:1901100. doi: 10.1002/adhm.201901100

Matsumura, Y., and Maeda, H. (1986). A new concept for macromolecular therapeutics in cancer chemotherapy: mechanism of tumoritropic accumulation of proteins and the antitumor agent smancs. *Cancer Res*. 46, 6387–6392.

Pugazhendhi, A., Edison, T. N. J. I., Velmurugan, B. K., Velmurugan, B. K., Jacob, J. A., and Karuppusamy, I. (2018). Toxicity of Doxorubicin (Dox) to different experimental organ systems. *Life Sci*. 200, 26–30. doi: 10.1016/j.lfs.2018.03.023

Song, Y., Li, D., He, J., Zhang, M., and Ni, P. (2019). Facile preparation of pH-responsive PEGylated prodrugs for activated intracellular drug delivery. *Chin. Chem. Lett*. 30, 2027–2031. doi: 10.1016/j.cclet.2019.04.052

Thambi, T., Deepagan, V. G., Yoon, H. Y., Han, H. S., Kim, S. H., Son, S., et al. (2014). Hypoxia-responsive polymeric nanoparticles for tumor-targeted drug delivery. *Biomaterials* 35, 1735–1743. doi: 10.1016/j.biomaterials.2013.11.022

Conflict of Interest: The authors declare that the research was conducted in the absence of any commercial or financial relationships that could be construed as a potential conflict of interest.

frontiers in Chemistry

ORIGINAL RESEARCH
published: 24 September 2020
doi: 10.3389/fchem.2020.584114

Coating Persistent Luminescence Nanoparticles With Hydrophilic Polymers for *in vivo* Imaging

Jianhua Liu[1], *Lenka Kotrchová*[2], *Thomas Lécuyer*[1], *Yohann Corvis*[1], *Johanne Seguin*[1], *Nathalie Mignet*[1], *Tomáš Etrych*[2], *Daniel Scherman*[1], *Eva Randárová*[2]* *and Cyrille Richard*[1]*

[1] *Unité de Technologies Chimiques et Biologiques pour la Santé (UTCBS), CNRS UMR8258, Inserm U1267, Université de Paris, Paris, France,* [2] *Institute of Macromolecular Chemistry, Czech Academy of Sciences, Prague, Czechia*

Persistent luminescence nanoparticles (PLNPs) are innovative nanomaterials highly useful for bioimaging applications. Indeed, due to their particular optical properties, i.e., the ability to store the excitation energy before slowly releasing it for a prolonged period of time, they allow *in vivo* imaging without auto-fluorescence and with a high target to background ratio. However, as for most nanoparticles (NPs), without any special surface coating, they are rapidly opsonized and captured by the liver after systemic injection into small animals. To overcome this issue and prolong nanoparticle circulation in the bloodstream, a new stealth strategy was developed by covering their surface with poly(*N*-2-hydroxypropyl)methacrylamide (pHPMA), a highly hydrophilic polymer widely used in nanomedicine. Preliminary *in vivo* imaging results demonstrated the possibility of pHPMA as an alternative strategy to cover $ZnGa_2O_4$:Cr NPs to delay their capture by the liver, thereby providing a new perspective for the formulation of stealth NPs.

Keywords: persistent luminescence, nanoparticles, surface coating, HPMA polymer, imaging, *in vivo*

OPEN ACCESS

Edited by:
Tsuyoshi Minami,
University of Tokyo, Japan

Reviewed by:
Yuanli Liu,
Guilin University of Technology, China
Shunsuke Tomita,
National Institute of Advanced Industrial Science and Technology (AIST), Japan

***Correspondence:**
Eva Randárová
eva.koziolova@gmail.com
Cyrille Richard
cyrille.richard@u-paris.fr

Specialty section:
This article was submitted to Supramolecular Chemistry, a section of the journal Frontiers in Chemistry

Received: *16 July 2020*
Accepted: *24 August 2020*
Published: *24 September 2020*

Citation:
Liu J, Kotrchová L, Lécuyer T, Corvis Y, Seguin J, Mignet N, Etrych T, Scherman D, Randárová E and Richard C (2020) Coating Persistent Luminescence Nanoparticles With Hydrophilic Polymers for in vivo Imaging. Front. Chem. 8:584114. doi: 10.3389/fchem.2020.584114

INTRODUCTION

Persistent luminescence is the property of some materials which can remain luminescent for minute, sometimes hour after ceasing their excitation. This particular optical phenomenon is due to the existence of defects within the materials capable of storing excited electrons in traps before they recombine to emit photons (Brito et al., 2012). Since the first persistent luminescence phosphors (PLPs) discovered by Matsuzawa, a strontium aluminate ($SrAl_2O_4$:Eu^{2+},Dy^{3+}) emitting green light (Matsuzawa et al., 1996), several bulk (micrometric size) PLPs emitting in the visual spectrum have been prepared, some of which are now commercially used as night-vision materials for various applications such as security and traffic signs, dials or luminous paints, owing to their strong and long persistent luminescence after excitation by the sun or ambient light[1]. Recently, our lab proposed the use of this physical phenomenon to develop new probes for *in vivo* imaging (Le Masne de Chermont et al., 2007). Most real-time optical *in vivo* imaging techniques, i.e., fluorescence imaging, use fluorescent probes that need to be excited at the same time as they are detected. However, the fluorescence emitted from the probe may be contaminated by the fluorescence from endogenous chromophores also excited during this process. This phenomenon, called auto-fluorescence, has the disadvantage of hindering the detection of the probe, especially when

[1] Available online at: https://www.nemoto.co.jp/nlm

it is present in small quantities (Gao et al., 2004). We have shown that the *in vivo* application of persistent luminescence nanoparticles (PLNPs) containing appropriate luminescent ions (emitting photons in the near-infrared (NIR) range) can solve this problem (Maldiney et al., 2011a). Indeed, since PLNPs can store excitation energy before releasing it for a long time, it is possible to delay the acquisition of images, which permits *in vivo* imaging without auto-fluorescence, thus obtaining reliable information with very good sensitivity (Maldiney et al., 2014). Since this pioneering work, many research labs have utilized our approach and proposed various methods to prepare PLNPs of different sizes and compositions (Lécuyer et al., 2016) for imaging and more recently, for therapeutic applications, notably in photodynamic therapy (Liu et al., 2019; Tan et al., 2019). However, due to their size (∼100 nm), these nanoparticles (NPs) are rapidly opsonized and captured by the liver once injected into the bloodstream (Maldiney, 2015). To avoid their fast clearance, it is necessary to chemically coat their surface with hydrophilic and unfolding molecules to prevent adsorption of proteins (such as opsonins) and to postpone their capture by the reticuloendothelial system (RES), especially Kupffer cells in the liver (Aggarwal et al., 2009).

Among the hydrophilic coating molecules with stealth unfolding properties preventing protein adsorption, several polymers based on polyethylene glycol (PEG) or poly(*N*-2-hydroxypropyl)methacrylamide (pHPMA) have been successfully used to coat the surface of various nanoparticles (Amoozgar and Yeo, 2012). Also, numerous nanosized systems based on pHPMA and its copolymers have been developed for targeted therapy and diagnostics of diverse malignancies, inflammatory diseases and other pathologies since they enable passive or active accumulation and controlled drug release at the target site (Chytil et al., 2017). The hydrophilic pHPMA is biocompatible and non-immunogenic and the versatile structure of pHPMA-based systems enables conjugation of numerous drug molecules, imaging agents or targeting moieties (Randárová et al., 2020), whereas the direct conjugation to PEG structure is limited by the absence of functional groups along PEG chain and several studies have proved the appearance of anti-PEG antibodies after *in vivo* application (Zhang et al., 2016). Moreover, the novel polymerization techniques, e.g., controlled reversible addition–fragmentation chain transfer (RAFT) polymerization, enable the synthesis of highly defined polymers with very low dispersity and high chain-end functionality (Šubr et al., 2013).

This study reports a novel strategy to chemically coat PLNPs made of $ZnGa_2O_4$ doped with Cr^{3+} (Cr being the ion responsible for emission in the NIR range) with pHPMA. The nanoassembly formed by the covalent grafting of pHPMA on PLNPs has been fully physicochemically characterized using different methods and preliminary evaluation of this coating has been performed *in vivo* on healthy mice. Moreover, the pHPMA-based coating was compared with another hydrophilic polymer coating, PEG-based, often used *in vivo* to obtain stealth nanoparticles.

MATERIALS AND METHODS

Chemicals

Zinc nitrate hexahydrate (>99%) was purchased from Fluka. Gallium oxide (99.999%) and chromium (III) nitrate non-ahydrate (99.99%) were purchased from Alfa Aesar. (3-Aminopropyl)-triethoxysilane (99%) was obtained from Sigma-Aldrich. Dimethylformamide (>99.9%) was purchased from SDS. Alpha-methoxy-omega-N-hydroxysuccinimide poly(ethylene glycol) M_W 5.000 Dalton was bought from Iris Biotech GmbH. 1-Aminopropan-2-ol, methacryloyl chloride, tert-butanol (t-BuOH), dimethyl sulfoxide (DMSO), diethyl ether, ethyl acetate, acetone, methanol (MeOH), dimethylacetamide (DMA), dichloromethane (DCM), 2,2′azobis(isobutyronitrile) (AIBN), 4-cyano-4-(ethylthiocarbonothioylthio) pentanoic acid, 2-thiazoline-2-thiol, N-ethyl-N′-(3-dimethyl aminopropyl)carbodiimide hydrochloride were purchased from Merck-Sigma-Aldrich (Germany). Azo initiator V-70 was purchased from Wako Chemicals (Japan).

Synthesis of ZGO

$ZnGa_2O_4$:Cr (ZGO) nanoparticles were prepared as previously reported (Maldiney et al., 2014). In brief, 8.94 mmol of gallium oxide was dissolved in 10 ml concentrated HNO_3(35%), then the mixture sample was transferred to a Teflon-lined stainless steel autoclave and heated to 150°C overnight. After that, 0.04 mmol of $Cr(NO_3)_3.9H_2O$ and 8.97 mmol of $Zn(NO_3)_2.6H_2O$ were dissolved in 10 ml deionized water to form a transparent solution, which was mixed with the solution of $Ga(NO_3)_3$ under stirring. Then, ammonia solution was added drop by drop to adjust the pH to 7.5. The solution was stirred for 3 h at room temperature before transfer to a Teflon-lined stainless steel autoclave and heated to 120°C for 24 h. Finally, the resulting product was washed with water and ethanol several times, then dried at 60°C and sintered at 750°C for 5 h. Hydroxylation was performed by basic wet grinding of the powder (500 mg) for 15 min with a mortar and pestle in 2 mL of 5 mM HCl solution, and vigorous stirring overnight at room temperature. The hydroxylated ZGO obtained, or ZGO-OH NPs with a diameter of 40 nm were selected from the whole polydisperse colloidal suspension by centrifugation in a SANYO MSE Mistral 1,000 at 4,500 rpm for 10 min. ZGO-OH particles located in the supernatant (assessed by Dynamic Light Scattering) were collected and concentrated.

Synthesis of p(HPMA)-TT

N-(2-hydroxypropyl)methacrylamide (HPMA) and thiazolidine-2-thione (TT) functional chain transfer agent (CTA) 2-cyano-5-oxo-5-(2-thioxo-1,3-thiazolidin-3-yl)pentan-2-yl ethyl carbontrithioate (TTc-TT) were synthesized as described previously (Kostka et al., 2020). Semitelechelic pHPMA with the TT end-groups p(HPMA)-TT was prepared by RAFT polymerisation of HPMA using 2,2′-azobis(4-methoxy-2,4-dimethylvaleronitrile) (V-70) as an initiator and TTc-TT as a CTA in the molar ratio of monomer:CTA:initiator 300:2:1. An example of the synthesis for p(HPMA)-TT is as follows: HPMA

(2.0 g, 13.97 mmol) was dissolved in 17.0 mL of t-BuOH and mixed in a polymerisation ampule with TTc-TT (33.9 mg, 93.1 μmol) and initiator V-70 (14.4 mg, 46.6 μmol) dissolved in 3.0 mL of anhydrous DMA. The polymerisation mixture was bubbled with argon for 10 min and sealed. Polymerisation was conducted at 30°C for 72 h, then the polymer was precipitated in a mixture of acetone and diethyl ether (2:1), filtered and dried under a vacuum, yielding 1.5 g (75%) polymer. TTc groups from the polymer precursor were removed by the reaction with an excess of AIBN in DMA (80 °C, 3 h) (modified procedure from Perrier et al., 2005).

ZGO Coating

Nanosized ZGO-OH particles were first converted to ZGO-NH_2 NPs by adding 1 wt% of 3-aminopropyl-triethoxysilane (APTES) to a suspension of ZGO-OH NPs at 2.5 mg/mL in dimethylformamide (DMF). The reaction mixture was sonicated for the first 2 min using a Branson Ultrasonic Cleaner 1210 and vigorously stirred at room temperature for 6 h. Particles were then washed from unreacted APTES by three centrifugation and redispersion steps in DMF. ZGO-pHPMA and ZGO-PEG NPs were obtained by reacting ZGO-NH_2 either with semitelechelic p(HPMA)-TT (10 μmol) or with NHS-PEG (10 μmol) at an NP concentration of 2.5 mg/mL in DMF. Then, NPs were centrifuged and washed 2× with DMF and 2× with water.

Characterizations

Polymer Characterizations

The weight-average molecular weight M_w, number-average molecular weight M_n and dispersity Đ* of polymer precursor and conjugates were measured using SEC on an HPLC Shimadzu system equipped with a SPD-M20A photodiode array detector (Shimadzu, Japan), differential refractometer (Optilab®rEX), and multiangle light scattering (DAWN HELLEOS II) detectors (both from Wyatt Technology Co., USA). The mobile phase for the TSKgel SuperSW3000 column was a mixture of methanol:sodium acetate buffer (CH_3COONa:CH_3COOH; pH = 6.5) (80: 20; v:v) and the flow rate was 0.3 mL min^{-1}. The content of pHPMA chain end TT groups was determined spectrophotometrically in methanol using the extinction coefficient, $\varepsilon_{305} = 10\,500\ L\ mol^{-1}\ cm^{-1}$.

Nanoparticle Characterizations

Dynamic light scattering (DLS) and zeta potential measurements were performed on a Malvern Zetasizer-Nano instrument equipped with a 4 mW He-Ne laser (633 nm). DLS measurements were recorded by diluting colloidal aqueous suspensions of ZGO at a concentration of 0.1 mg/mL in water. Colloidal stability tests were performed at a NP concentration of 2 mg/ml. Zeta potential measurements were performed in 20 mM NaCl solution. Transmission electron microscopy (TEM) was

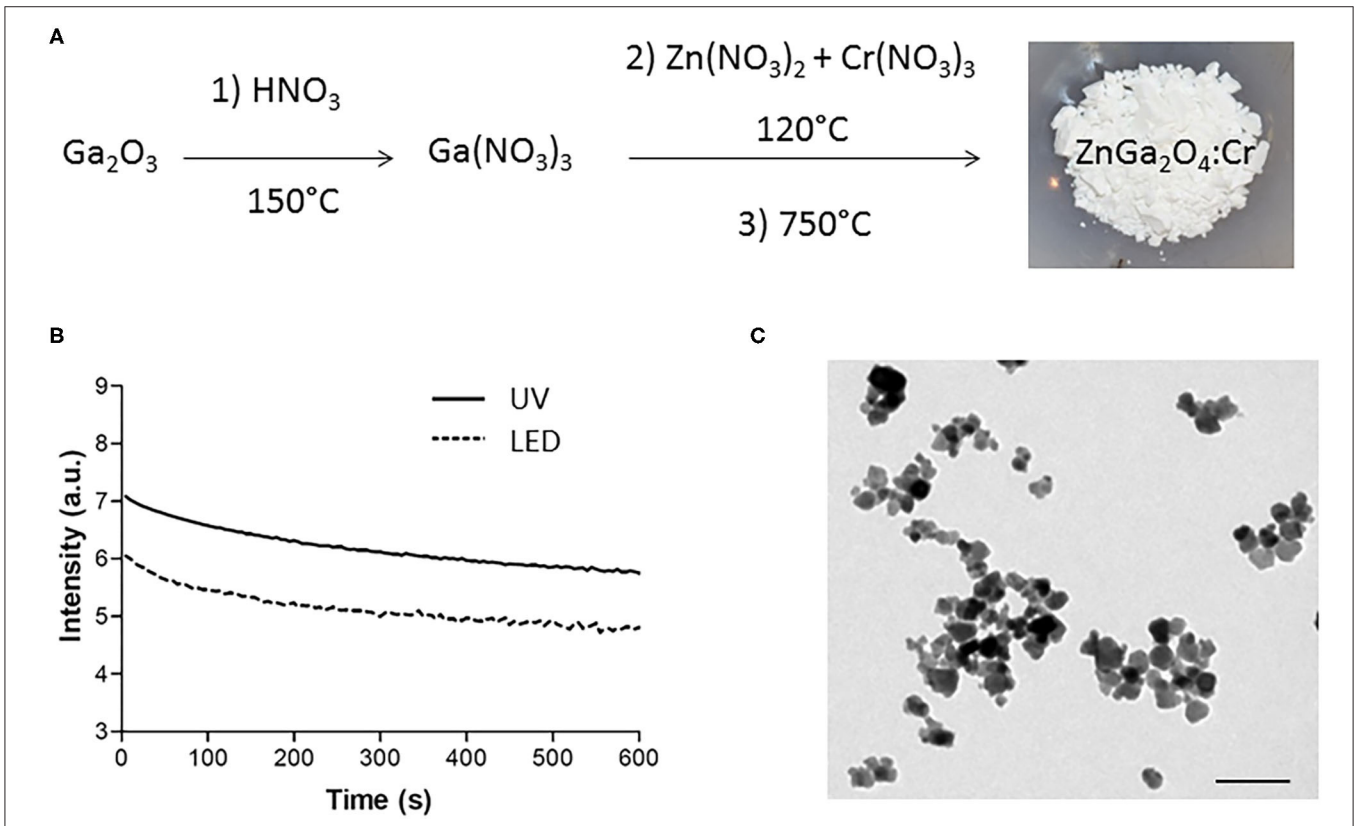

FIGURE 1 | Synthesis and characterizations of $ZnGa_2O_4$:Cr (ZGO). **(A)** Three-step synthesis of ZGO. **(B)** Optical properties of ZGO powder after UV and visible excitation. **(C)** TEM of nanosized ZGO-OH (scale bar = 80 nm).

performed at 80 kV on JEOL JEM-100S using 5 μL of suspension dropped for 1 min. Thermogravimetric analysis (TGA) was performed using a TGA/DSC 1 from Mettler-Toledo (Greifensee, Switzerland) sensitive to 1 μg and calibrated beforehand with internal standard weights. Samples of approximately 2 mg were analyzed in alumina pans with a central hole of 1 mm diameter. All the experiments were performed at a 5 K.min^{-1} heating rate and under a dry airflow of 70 mL.min^{-1}. Infrared spectra were recorded on an Affinity-1 (Shimadzu). Persistent luminescence decays were performed on an Optima camera (Biospace Lab, France). Acquisitions of the luminescence of nanoparticles were recorded for 5 min after a 2-min excitation under UV light (365 nm) or a LED lamp (5,000 ml) with a 515 nm filter.

In vivo Imaging

Eight-week-old Balb/cJRj female mice (18–22 g) were purchased from Janvier labs. *In vivo* experiments were approved by French Comité d'éthique en expérimentation animale N°034 and the French Ministry of Research (APAFIS#8519-20 16090514387844). The mice were randomly assigned to groups ($n = 3$) for experimental purposes. UV pre-excited NPs were injected retro-orbitally using insulin syringes (0.2 mL volume containing 10 mg/mL NP suspension in aqueous solution). At different time points after injection (1, 3, 7h), mice were irradiated for 2 min with LED, then imaged for 5 min with the Optima camera. Twenty-four hours after injection, animals were anesthetized with gaseous isoflurane and sacrificed by cervical dislocation. Liver, spleen, lungs, heart and kidneys were collected

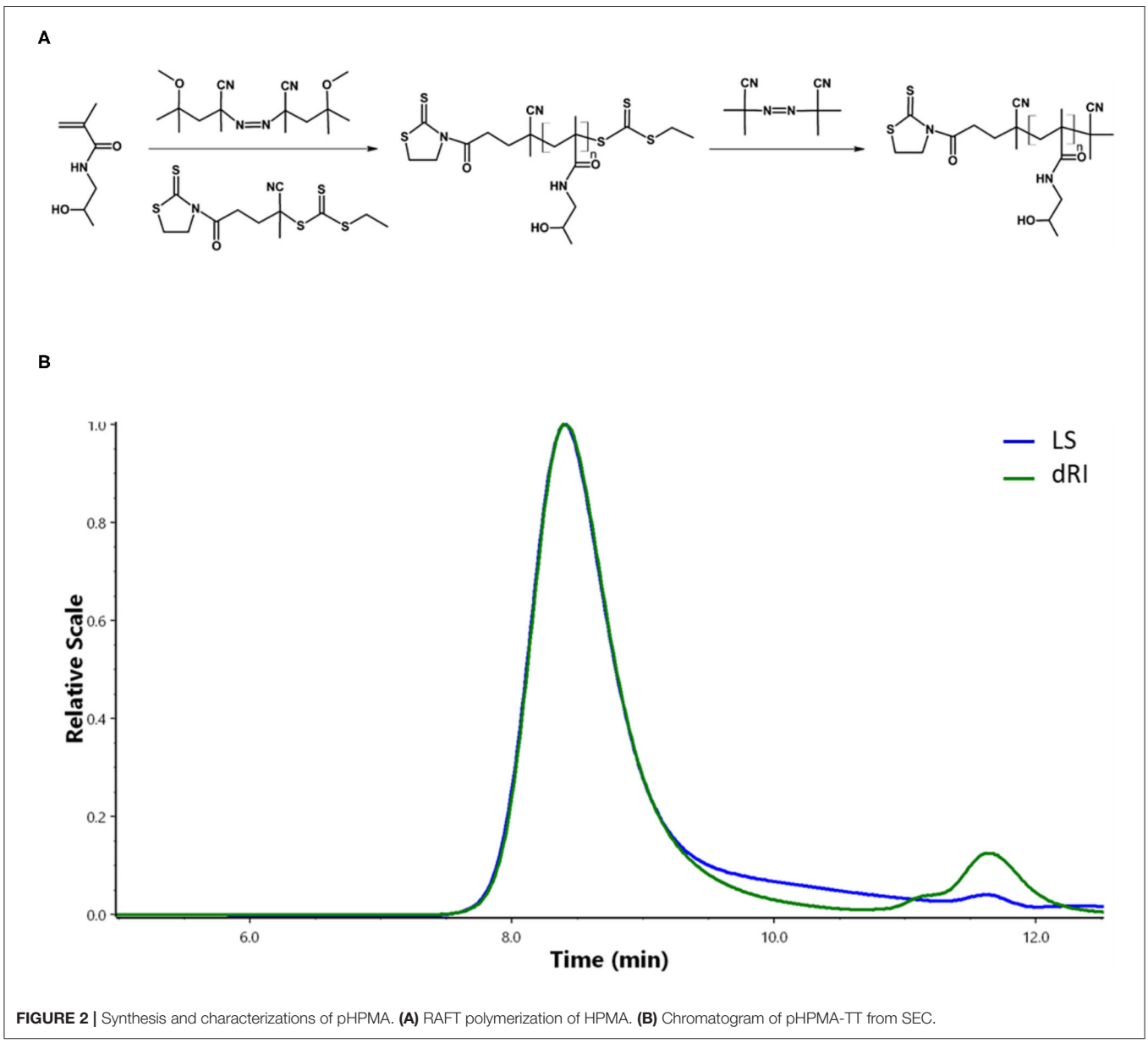

FIGURE 2 | Synthesis and characterizations of pHPMA. **(A)** RAFT polymerization of HPMA. **(B)** Chromatogram of pHPMA-TT from SEC.

and placed on a black plate, irradiated with LED and *ex vivo* luminescence measurements were recorded.

RESULTS AND DISCUSSION

The chromium-doped zinc gallate NPs ($ZnGa_{1,995}Cr_{0.005}O_4$, referred to as ZGO) were synthesized in a three-step method according to our previously published technique combining a hydrothermal treatment and 5-h calcination at 750°C (**Figure 1A**). The synthesized $ZnGa_{1,995}Cr_{0.005}O_4$ could be excited with a wide range of wavelengths to give a NIR emission band at 697 nm, which was ascribed to the 2E → 4A2 transition in the distorted trivalent chromic ions in gallate (**Supplementary Figure 1**). Indeed, in agreement with previous results (Maldiney et al., 2014), the obtained powder can emit persistent luminescence signal for several minute after excitation in UV or visible light range (**Figure 1B**). As shown later in this work, emission of light over a long time after the end of excitation is highly useful for *in vivo* optical imaging without

TABLE 1 | Physicochemical characterization of pHPMA precursor.

	M_w (g/mol)[a]	$Đ$*[a]	R_h (nm)[b]	Content of TT groups (mol%)[c]	Functionality of TT groups[d]
poly(HPMA)-TT	17 700	1.09	2.5 ± 0.3	0.65	0.70

[a]*The molecular weights and Dispersity were determined by SEC using the TSKgel SuperAW3000 column and RI and MALS detection,* [b]*the hydrodynamic radius was determined by DLS,* [c]*the content of the TT end-chain groups was determined by spectrophotometry after the removal of the TTc groups,* [d]*polymer functionality of the TT end-groups (the ratio between the M_n value determined by SEC and the M_n value calculated from the content of the TT end-chain groups determined by spectrophotometry) after the removal of the TTc groups.*

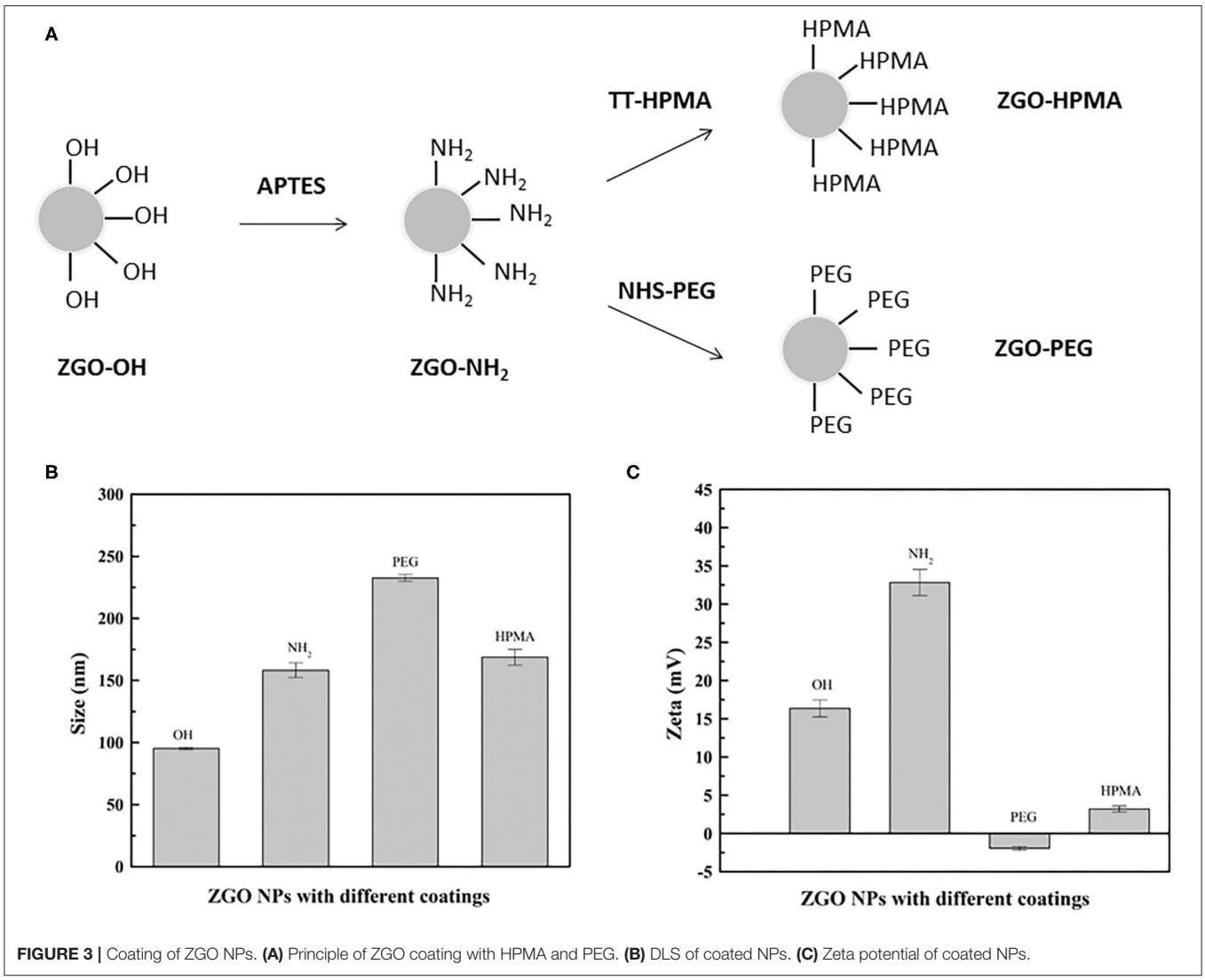

FIGURE 3 | Coating of ZGO NPs. **(A)** Principle of ZGO coating with HPMA and PEG. **(B)** DLS of coated NPs. **(C)** Zeta potential of coated NPs.

background. However, for this application, NPs should be recovered from the heterogeneous white powder. Nanosized hydroxylated ZGO (ZGO-OH) of approximately 40 nm in size were obtained by manual crushing of the powder, followed by acidic hydroxylation in HCl 5 mM overnight and extraction of nanoparticles by selective sedimentation, which was confirmed by TEM (**Figure 1C**).

Nevertheless, for *in vivo* applications, NPs surface functionalization is needed, since more than 3000 proteins can bind to the surfaces of non-functionalized NPs (Shemetov et al., 2012) in the bloodstream resulting in their rapid clearance by RES mainly present in liver and spleen, as already observed with ZGO-OH (**Supplementary Figure 2**). To overcome this issue, several strategies have been reported, such as the incorporation of PLNPs into liposomes (Chen et al., 2017) or by covalent grafting with PEG on the surface of the NPs (Maldiney et al., 2011b; Walkey et al., 2012). In this work, we propose another approach to achieve stealth NPs by coating ZGO with pHPMA, a biocompatible hydrophilic polymer already used for drug delivery in preclinical experiments (Šírová et al., 2017) and clinical trials (Kopeček and Kopečkova, 2010). This polymer (pHPMA-TT) was used to coat ZGO to evaluate the suitability of this coating for *in vivo* experiments and compared to non-functionalized ZGO-OH and PEGylated-ZGO.

Semitelechelic linear polymer precursor p(HPMA)-TT intended for NP coating was synthesized by RAFT polymerisation using CTA TTc-TT and the azo initiator V-70 at 30 C providing polymer chains with sufficient functionality of the TT α-end group and very low distribution of molecular weights (**Figure 2A**).

The ratio monomer:CTA:initiator 300:2:1 was selected to obtain the polymer chains with the molecular weight around 20,000 g/mol since these pHPMA particles exhibit a comparable hydrodynamic radius to PEG with M_w = 5,000 g/mol selected as

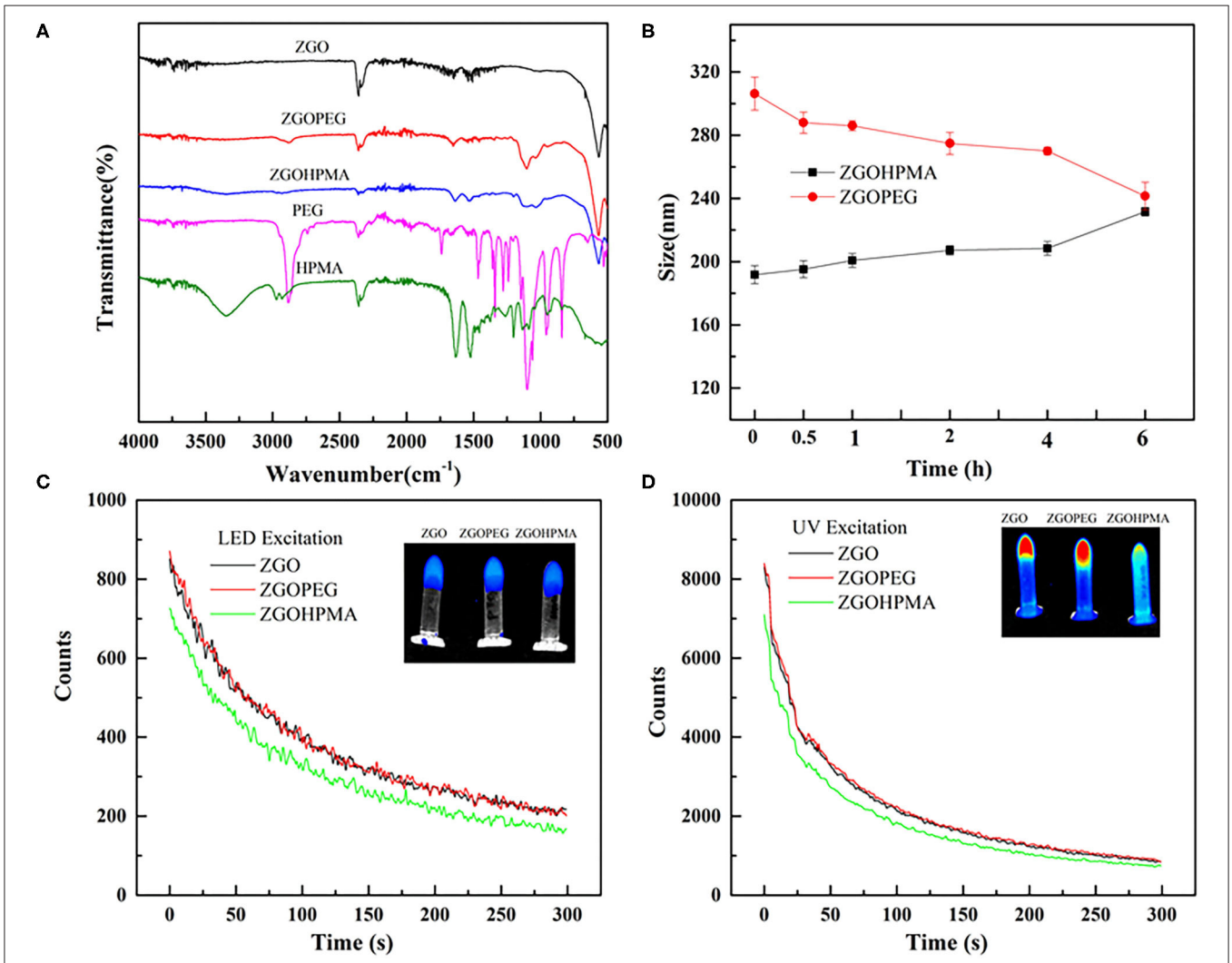

FIGURE 4 | Physico-chemical characterizations of functionalized ZGO. **(A)** FT-IR spectra of polymers and ZGO-HPMA and ZGO-PEG. **(B)** Colloidal stability of ZGO-HPMA and ZGO-PEG in glucose. **(C)** Persistent luminescence decay after visible excitation. **(D)** Persistent luminescence decay after UV excitation.

a control. The ω-TTc end-groups of p(HPMA)-TT were removed by a method (Perrier et al., 2005) that used an excess of AIBN in anhydrous DMA, thus preserving the content of the α-end TT groups in the polymers. The characteristics of p(HPMA)-TT are summarized in **Figure 2B** and **Table 1**.

Coating ZGO with both polymers was performed using a common functionalization strategy (**Figure 3A**). For this purpose, aminopropyltriethoxysilane (APTES) was first grafted on the ZGO-OH surface for 6 h in DMF (**Figure 3A**) (Maldiney, 2015). Then, after washing, the amine-covered nanoparticles (ZGO-NH_2) were split into two vials, one reacting with a solution of pHPMA to form ZGO-pHPMA NPs, while the other one reacted with NHS-PEG in DMF for 16 h to form ZGO-PEG NPs as a control.

Different physicochemical parameters were evaluated to confirm the coating of ZGO with pHPMA and PEG (**Figures 3B,C**, **4A** and **Supplementary Figure 3**). After the reaction, the hydrodynamic diameter of ZGO-pHPMA nanoparticles increased from 90 to 170 nm. Regarding ZGO-PEG, their hydrodynamic diameter almost reached 230 nm after the 2-step functionalization process. The initial zeta potential of ZGO-OH nanoparticles was around 15 mV, 35 mV for ZGO-NH_2. After functionalization with pHPMA, the zeta potential of ZGO-pHPMA was +2 mV, −1 mV after the addition of PEG (**Figure 3C**). Therefore, almost neutral NPs were obtained after coating ZGO with both neutral polymers, which is a prerequisite for the prevention of NP rapid uptake by RES. The presence of HPMA and PEG on ZGO were also confirmed by IR spectra, the characteristic peaks of each polymer being visible in **Figure 4A**. Indeed, the peaks at 2,875, 1,660, 1,075, and 925 cm^{-1} are characteristic of the PEG chain, while at 3,325, 2,950, 1,625, 1,525, and 1,100 cm^{-1} are typical of the HPMA moiety. Quantitative evaluation of the number of polymer chains grafted on ZGO was achieved by TGA. In the case of ZGO-PEG nanoparticles, the percentage weight loss stabilized at 4%, 5% for ZGO-pHPMA nanoparticles (**Supplementary Figure 3**). Starting from the molecular weight of each grafted polymer, we were able to quantify the concentration of pHPMA and PEG chains per mass unit of nanoparticles, around 4 nmol per mg of ZGO for pHPMA, close to 10 nmol/mg of nanoparticles for PEG.

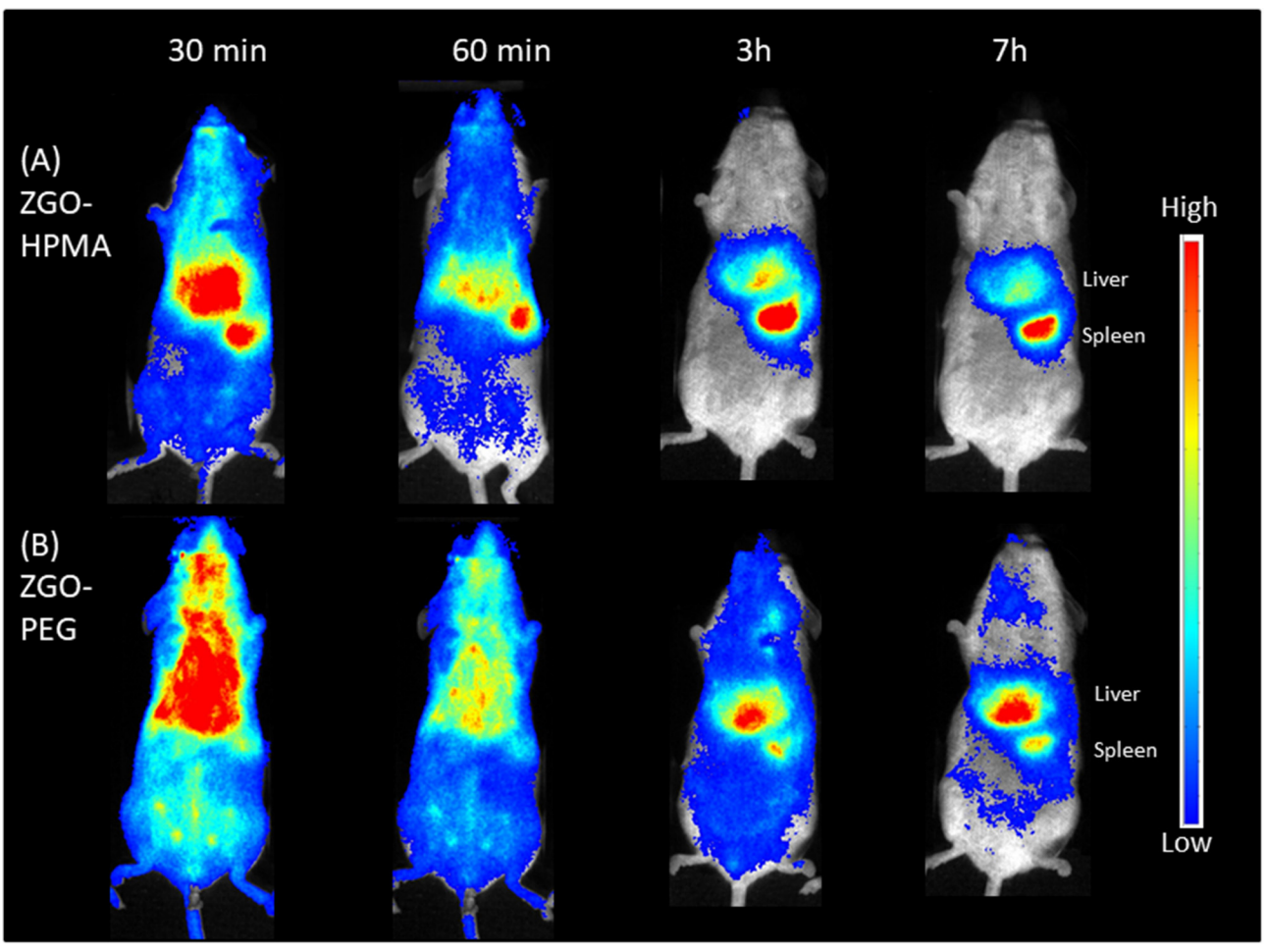

FIGURE 5 | *In vivo* biodistribution of coated ZGO in healthy mice. **(A)** ZGO-HPMA. **(B)** ZGO-PEG.

The different molecular weight and solution behavior of both polymers may play a role in the final coating density. Despite their hydrodynamic radii being comparable, the molecular weight of pHPMA was four times higher than of PEG. Also, pHPMA forms relatively expanded polymer coils in solution, while PEG chains are much more extended enabling better availability of end functional groups for the reaction with NP surface amino groups. Regarding the density of the coating, it was 0.8 molecule/nm^2 for PEG and 0.3 molecule/nm^2 for pHPMA. Indeed, a lower density coating for pHPMA explains the slightly higher zeta potential, which in this case, is influenced by the free amino groups on ZGO NPs after coating with pHPMA.

For *in vivo* use, nanoassemblies should not aggregate once dispersed into aqueous solution. The colloidal stability of both coated NPs was evaluated over 6 h after the dispersion at a concentration of 2 mg/ml in different aqueous solutions. As displayed on **Supplementary Figure 4**, when ZGO-pHPMA were dispersed in deionized water, their hydrodynamic diameter was constant during the first hour, slowly increasing to 220 nm over 6 h, whereas the ZGO-PEG NPs remained a constant size of approximately 180 nm. When dispersed in 5% glucose (**Figure 4B**), the hydrodynamic diameter of ZGO-pHPMA was stable with a Dh around 200 nm, whereas the Dh of ZGO-PEG slowly decreased from 300 nm (at T_0) to 240 nm after 6 h.

To determine if the coating can influence the optical properties of ZGO NPs, persistent luminescence decay of colloidal suspensions of ZGO-pHPMA and ZGO-PEG were measured after UV and LED excitation and compared to non-coated ZGO-OH. As shown in **Figure 4C**, after a 2-min LED excitation, the characteristic luminescence decays of ZGO was observed after the excitation was stopped, with the intensity of light slowly decreasing over a 6-min period. The effect of the coating on the luminescence intensity was negligible, with only a slight decrease in the signal for ZGO-HPMA NPs compared to those of ZGO-OH or ZGO-PEG. A similar trend was observed after UV excitation (**Figure 4D**), while the obtained persistent luminescence intensity was about 10 times more powerful than after LED excitation, in line with our previously published results (Maldiney et al., 2014).

Finally, preliminary *in vivo* imaging using ZGO coated with pHPMA was performed in healthy mice and compared to PEG-ZGO. For this purpose, suspensions of both NPs were pre-excited with a UV lamp for 2 min, then 200 µL (10 mg/mL) of each solution was injected retro-orbitally and the biodistribution of the NPs was followed over 7 h. After the injection of pHPMA-coated NPs, the luminescence signal was detectable throughout the whole animal body up to 60 min (**Figure 5**), proving the ability of pHPMA-coated NPs to circulate in the bloodstream, whereas the signal for the non-coated ZGO-OH was localized in the RES immediately after their application (**Supplementary Figure 2**), proving that the coating of ZGO with pHPMA is efficient and can successfully delay rapid NPs opsonization. For ZGO-PEG, the luminescence is also visible throughout the whole body, with less signal in the liver and spleen compared to ZGO-pHPMA. Three hours after injection, most ZGO-pHPMA resided in liver and spleen,

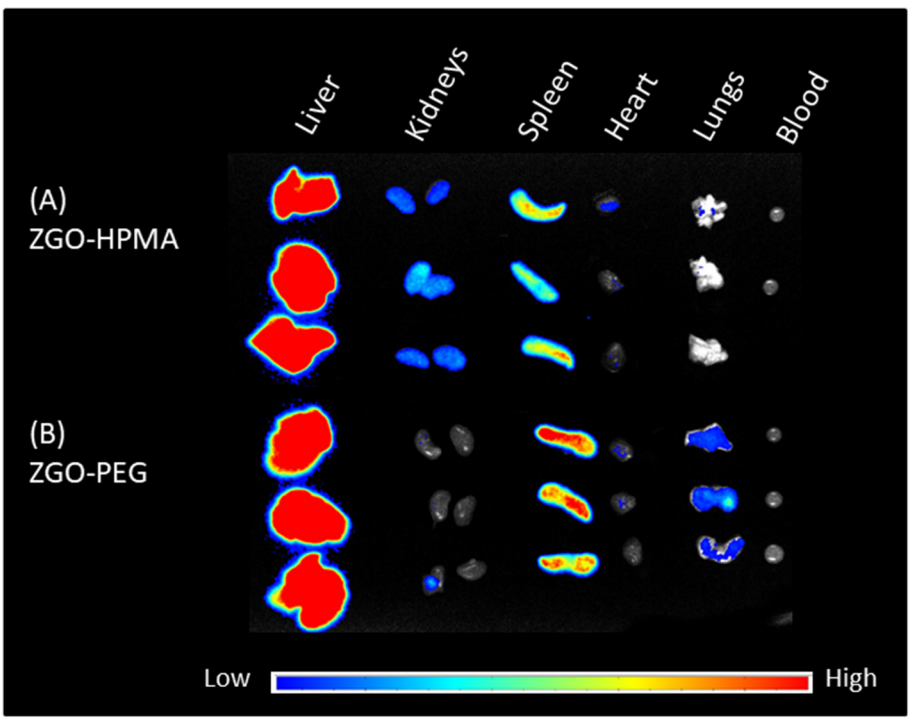

FIGURE 6 | *Ex vivo* imaging of main organs and blood 24 h after injection. **(A)** ZGO-HPMA. **(B)** ZGO-PEG.

whereas PEGylated-ZGO NPs were still circulating (**Figure 5**). The lower amount of HPMA linked to ZGO relative to PEG may be responsible for more capture by RES. In both cases, 7 h after injection, NPs were mainly localized in the liver and spleen.

Twenty-four hours after injection, mice were sacrificed, and the main organs and blood were recovered and irradiated with LED for the *ex vivo* biodistribution study. For both coatings, the luminescence signal was mostly present in the liver and spleen (**Figure 6**). Nevertheless, there was a slight difference in organ biodistribution between coatings, since the *ex vivo* luminescence signal was found in the kidneys of ZGO-pHPMA injected mice, whereas for ZGO-PEG injected mice, there was no luminescence signal in the kidneys, a slight signal in the lungs and a stronger signal in the spleen. These *ex vivo* differences, a higher signal in the kidneys and lower signal in the lungs and spleen, constitute a real difference between HPMA- and PEG-coated NPs, hence an advantage and interest of using this newly developed coating strategy.

In summary, a new approach for coating ZGO nanoparticles was developed, which prolonged the circulation of the nanoparticles in the bloodstream. Since the residence time of ZGO-pHPMA in the blood was slightly shorter than for ZGO-PEG NPs, we assume that the pHPMA chain length and structure could be optimized to obtain a higher coating density, thus longer circulation time. It is hypothesized that either the comb-like pHPMA copolymer with multiple TT groups (layer-like coating) or shorter pHPMA copolymers grafted to ZGO nanoparticles in a higher density (brush-like coating), would bring new potential to the coating ability of ZGO NPs. Applied to smaller ZGO NPs (Teston et al., 2015) could also be of interest to modify the pharmacokinetic of injected NPs.

CONCLUSION

We have reported the first use of pHPMA as an alternative strategy to coat ZGO NPs intended for *in vivo* imaging. ZGO NPs coated with the latter biocompatible polymer circulated in the bloodstream much longer than non-coated ZGO-OH. When compared to the PEG coating, it seems that the lower coating density of pHPMA chains slightly discriminate the pHPMA coating, thus the density or grafting approach should be optimized in future studies. Indeed, the pHPMA coating enabled more rapid elimination of coated NPs and decreased the long-term accumulation in organs such as spleen and lungs. Finally, the present results open new possibilities to improve ZGO coating for further applications in bioimaging and drug delivery, since the utilization of pHPMA-based coating enables the easy attachment of various drug molecules or targeting moieties.

DATA AVAILABILITY STATEMENT

The original contributions presented in the study are included in the article/**Supplementary Material**, further inquiries can be directed to the corresponding author/s.

ETHICS STATEMENT

The animal study was reviewed and approved by French Comité d'éthique en expérimentation animale N°034 and by French Ministry of Research (APAFIS#8519-20 16090514387844).

AUTHOR CONTRIBUTIONS

JL: performed the experiments. LK: synthesized HPMA. TL: performed *in vivo* experiments. JS: injected nanoparticles to mice. YC: performed TGA. DS and NM: scientific discussion. TE: corrected the manuscript. ER: designed the experiments and corrected the manuscript. CR: designed the experiments and wrote the first version of the manuscript. All authors contributed to the article and approved the submitted version.

FUNDING

This work was supported by grants from the China Scholarship Council (CSC grant N° 201706990010) and Agency of the Czech Republic (grant 19-00956Y), the Ministry of Education, Youth and Sports of CR within the Inter-excellence programme (project LTAUSA18083) and the National Sustainability Programme II, Project BIOCEV-FAR LQ1604.

SUPPLEMENTARY MATERIAL

The Supplementary Material for this article can be found online at: https://www.frontiersin.org/articles/10.3389/fchem.2020.584114/full#supplementary-material

REFERENCES

Aggarwal, P., Hall, J. B., McLeland, C. B., Dobrovolskaia, M. A., and McNeil, S. E. (2009). Nanoparticle interaction with plasma proteins as it relates to particle biodistribution,biocompatibility and therapeutic efficacy. *Adv. Drug Deliv. Rev.* 61, 428–437. doi: 10.1016/j.addr.2009.03.009

Amoozgar, Z., and Yeo, Y. (2012). Recent advances in stealth coating of nanoparticle drug delivery systems. *Wiley WIREs Nanomed. Nanobiotechnol.* 4, 219–233. doi: 10.1002/wnan.1157

Brito, H. F., Hölsä, J., Laamanen, T., Lastusaari, M., Malkamäki, M., and Rodrigues, L. C. V. (2012). Persistent luminescence mechanisms: human imagination at work. *Opt. Mater. Exp.* 2, 371–381. doi: 10.1364/OME.2.000371

Chen, L.-J., Yang, C.-X., and Yan, X.-,Ping. (2017). Liposome-coated persistent luminescence nanoparticles as luminescence trackable drug carrier for chemotherapy. *Anal. Chem.* 89, 6936–6939. doi: 10.1021/acs.analchem.7b01397

Chytil, P., Koziolová, E., Etrych, T., and Ulbrich, K. (2017). HPMA copolymer–drug conjugates with controlled tumor-specific drug release. *Macromol. Biosci.* 18:1700209. doi: 10.1002/mabi.201700209

Gao, X. H., Cui, Y. Y., Levenson, R. M., Chung, L. W. K., and Nie, S. M. (2004). *In vivo* cancer targeting and imaging with semiconductor quantum dots. *Nat. Biotechnol.* 22, 969–976. doi: 10.1038/nbt994

Kopeček, J., and Kopečkova, P. (2010). HPMA copolymers: origins, early developments, present, and future. *Adv. Drug Deliv. Rev.* 17, 122–149. doi: 10.1016/j.addr.2009.10.004

Kostka, L., Kotrchová, L., Šubr, V., Libánská, A., Ferreira, C. A., Malátová, I., et al. (2020). HPMA-based star polymer biomaterials with tuneable structure and biodegradability tailored for advanced drug delivery to solid tumours. *Biomaterials* 235:119728. doi: 10.1016/j.biomaterials.2019.119728

Le Masne de Chermont, Q., Chanéac, C., Seguin, J., Pell,é, F., Maîtrejean, S., Jolivet, J. P., et al. (2007). Nanoprobes with near-infrared persistent luminescence for in vivo imaging. *PNAS* 104, 9266–9271. doi: 10.1073/pnas.0702427104

Lécuyer, T., Teston, E., Ramirez-Garcia, G., Maldiney, T., Viana, B., Seguin, J., et al. (2016). Chemically engineered persistent luminescence nanoprobes for bioimaging. *Theranostics* 6, 2488–2524. doi: 10.7150/thno.16589

Liu, J., Lécuyer, T., Seguin, J., Mignet, N., Scherman, D., Viana, B., et al. (2019). Imaging and therapeutic applications of persistent luminescence nanomaterials. *Adv. Drug Deliv. Rev.* 138, 193–210. doi: 10.1016/j.addr.2018.10.015

Maldiney, T., et al. (2015). Controlling aminosilane layer thickness to extend the plasma half-life of stealth persistent luminescence nanoparticles in vivo. *J. Mater. Chem. B.* 3, 4009–4016. doi: 10.1039/C5TB00146C

Maldiney, T., Bessière, A., Seguin, J., Teston, E., Sharma, S. K., Viana, B., et al. (2014). The in vivo activation of persistent nanophosphors for optical imaging of vascularization, tumours and grafted cells. *Nat. Mater.* 13, 418–426. doi: 10.1038/nmat3908

Maldiney, T., Lecointre, A., Viana, B., Bessiere, A., Bessodes, M., Gourier, D., et al. (2011a). Controlling electron trap depth to enhance optical properties of persistent luminescence nanoparticles for in vivo imaging. *J. Am. Chem. Soc.* 133, 11810–11815. doi: 10.1021/ja204504w

Maldiney, T., Richard, C., Seguin, J., Wattier, N., Bessodes, M., and Scherman, D. (2011b). Effect of core diameter, surface coating, and peg chain length on the biodistribution of persistent luminescence nanoparticles in mice. *ACS Nano.* 5, 854–862. doi: 10.1021/nn101937h

Matsuzawa, T., Aoki, Y., Takeuchi, N., and Murayama, Y. (1996). A new long phosphorescent phosphor with high brightness, $SrAl_2O_4$: Eu^{2+},Dy^{3+}. *J. Electrochem. Soc.* 143, 2670–2267. doi: 10.1149/1.1837067

Perrier, S., Takolpuckdee, P., and Mars, C. A. (2005). Reversible addition-fragmentation chain transfer polymerization: end group modification for functionalized polymers and chain transfer agent recovery. *Macromolecules*. 38, 2033–2036. doi: 10.1021/ma047611m

Randárová, E., Kudláčová, J., and Etrych, T. (2020). HPMA copolymer-antibody constructs in neoplastic treatment: an overview of therapeutics, targeted diagnostics, and drug-free systems. *J. Control Rel.* 325, 304–322. doi: 10.1016/j.jconrel.2020.06.040

Shemetov, A. A., Nabiev, I., and Sukhanova, A. (2012). Molecular interaction of proteins and peptides with nanoparticles. *ACS Nano*. 6, 4585–4602. doi: 10.1021/nn300415x

Šírová, M., Strohalm, J., Chytil, P., Lidický, O., Tomala, J., Ríhová, B., et al. (2017). The structure of polymer carriers controls the efficacy of the experimental combination treatment of tumors with HPMA copolymer conjugates carrying doxorubicin and docetaxel. *J Control Rel.* 246, 1–11. doi: 10.1016/j.jconrel.2016.12.004

Šubr, V., Kostka, L., Strohalm, J., Etrych, T., and Ulbrich, K. (2013). Synthesis of well-defined semitelechelic poly[n-(2-hydroxypropyl)methacrylamide] polymers with functional group at the α-end of the polymer chain by raft polymerization. *Macromolecules*. 46:2100–2108. doi: 10.1021/ma400042u

Tan, H., Wang, T., Shao, Y., Yu, C., and Hu, L. (2019). Crucial breakthrough of functional persistent luminescence materials for biomedical and information technological applications. *Front. Chem.* 7:387. doi: 10.3389/fchem.2019.00387

Teston, E., Richard, S., Maldiney, T., Lièvre, N., Yangshu Wang, G., Motte, L., et al. (2015). Non-aqueous sol–gel synthesis of ultra small persistent luminescence nanoparticles for near-infrared in vivo imaging. *Chem. Eur. J.* 21, 7350–7354. doi: 10.1002/chem.201406599

Walkey, C. D., Olsen, J. B., Guo, H., Emili, A., and Chan, W.C.W. (2012). Nanoparticle size and surface chemistry determine serum protein adsorption and macrophage uptake. *J. Am. Chem. Soc.* 134, 2139–2147. doi: 10.1021/ja2084338

Zhang, P., Sun, F., Liu, S., and Jiang, S. (2016). Anti-PEG antibodies in the clinic: current issues and beyond PEGylation. *J. Control Rel.* 244, 184–193. doi: 10.1016/j.jconrel.2016.06.040

Conflict of Interest: The authors declare that the research was conducted in the absence of any commercial or financial relationships that could be construed as a potential conflict of interest.

frontiers in Chemistry

ORIGINAL RESEARCH
published: 02 October 2020
doi: 10.3389/fchem.2020.581260

Dual Gene Delivery Reagents From Antiproliferative Alkylphospholipids for Combined Antitumor Therapy

*Boris Gaillard, Jean-Serge Remy, Françoise Pons and Luc Lebeau**

Laboratoire de Conception et Application de Molécules Bioactives, UMR 7199 CNRS—Université de Strasbourg, Faculté de Pharmacie, Illkirch, France

Alkylphospholipids (APLs) have elicited great interest as antitumor agents due to their unique mode of action on cell membranes. However, their clinical applications have been limited so far by high hemolytic activity. Recently, cationic prodrugs of erufosine, a most promising APL, have been shown to mediate efficient intracellular gene delivery, while preserving the antiproliferative properties of the parent APL. Here, cationic prodrugs of the two APLs that are currently used in the clinic, miltefosine, and perifosine, are investigated and compared to the erufosine prodrugs. Their synthesis, stability, gene delivery and self-assembly properties, and hemolytic activity are discussed in detail. Finally, the potential of the pro-miltefosine and pro-perifosine compounds $\mathbf{M_{E12}}$ and $\mathbf{P_{E12}}$ in combined antitumor therapy is demonstrated using pUNO1-hTRAIL, a plasmid DNA encoding TRAIL, a member of the TNF superfamily. With these pro-APL compounds, we provide a proof of concept for a new promising strategy for cancer therapy combining gene therapy and APL-based chemotherapy.

Keywords: alkylphospholipid, miltefosine, perifosine, erufosine, hemolytic toxicity, prodrug, chemotherapy, gene therapy

OPEN ACCESS

Edited by:
Nathalie Mignet, INSERM U1022 Unité de Technologies Chimiques et Biologiques Pour la Santé, France

Reviewed by:
Rumiana Tzoneva, Bulgarian Academy of Sciences, Bulgaria
Ahmed H. E. Hassan, Mansoura University, Egypt

****Correspondence:***
Luc Lebeau
llebeau@unistra.fr

Specialty section:
This article was submitted to Medicinal and Pharmaceutical Chemistry, a section of the journal Frontiers in Chemistry

Received: *08 July 2020*
Accepted: *31 August 2020*
Published: *02 October 2020*

Citation:
Gaillard B, Remy J-S, Pons F and Lebeau L (2020) Dual Gene Delivery Reagents From Antiproliferative Alkylphospholipids for Combined Antitumor Therapy. Front. Chem. 8:581260. doi: 10.3389/fchem.2020.581260

INTRODUCTION

Alkylphospholipids (APLs) are metabolically stable analogs of lysophosphatidylcholines (lysoPCs) that constitute a new class of anticancer drugs with antiproliferative properties (de Almeida Pachioni et al., 2013; van Blitterswijk and Verheij, 2013; Markova et al., 2014; Jaffrès et al., 2016; Ríos-Marco et al., 2017). Due to their similarity with endogenous phospholipids, it is proposed they target the membrane lipid rafts and interfere with lipid homeostasis, thus altering lipid-linked signaling and inducing apoptosis. The unique way by which APLs can trigger cell apoptosis, through perturbation of the cell membranes, gives these compounds an advantage over conventional chemotherapeutic agents that interact with DNA. Furthermore, the action of APLs appears to be specific for tumor cells, and both cellular uptake and APL-induced apoptosis are increased in the malignant state of the cells (Kostadinova et al., 2015). Significant efforts have thus been made to synthesize metabolically stable analogs of lysoPCs with potential antineoplastic activity. Among these compounds, miltefosine and perifosine have been evaluated for their selective antitumor activity in phase I and II clinical trials against many types of advanced cancers (**Figure 1**). However, the clinical applications of these compounds still are limited, mainly due to gastrointestinal toxicity and high hemolytic activity, which are likely related to their high critical micellar concentration (CMC) that prevents their use as systemic agents. To date, the clinical use

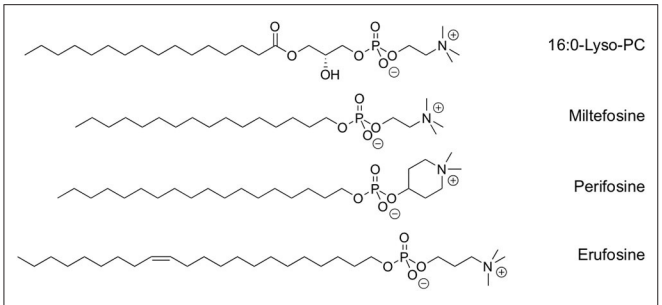

FIGURE 1 | Chemical structure of lyso-PC and clinically relevant synthetic alkylphospholipids.

of miltefosine and perifosine has been essentially limited to the treatment of metastasis in breast cancer, through topical administration. More recently, erufosine and erucylphosphocholine were developed as next-generation APLs for systemic treatment of cancers. Substitution of the alkyl chain for an unsaturated 22-carbon chain resulted in lowered surface active properties and reduced hemolytic activity as tested at clinically relevant high doses, which was not feasible with previous APLs (Georgieva et al., 2002). However, none of these two drugs has reached the clinic yet.

As APLs have mechanisms of action that target various membrane signaling pathways involved in carcinogenesis (Ríos-Marco et al., 2017), they have been extensively investigated in combination with other chemotherapeutics (Bendell et al., 2011; Richardson et al., 2011; Fu et al., 2012; Gojo et al., 2013; Guidetti et al., 2014), and radiation therapy (Belka et al., 2004; Vink et al., 2007). Indeed, the use of combined treatments to fight against cancer is well-established (Gee et al., 2005). Monotherapies involve one single agent and aim at the suspension of one single signaling pathway. In contrast, tumor cells can grow through the initial oncogenic route or activate parallel signaling pathways (Lee et al., 2014). Combined therapies can simultaneously modulate more than one signaling pathway in tumor cells, with the consequence that the therapeutic effect can be maximized and, possibly, the resistance mechanisms can be overcome. Besides, a coordinate treatment with two drugs in separated carriers is associated with complex variations in pharmacokinetics and cannot ensure a proper co-localization of the drugs for synergistic action. This issue can be addressed by covalent conjugation of the drugs into hybrid molecules (Alam et al., 2018, 2019), or through their co-delivery in one single carrier (Tsouris et al., 2014). In this respect, the recommandation of therapies combining small-molecular drugs and nucleic acids has been endorsed in recent years for cancer treatment. Furthermore, such therapies are expected to help address the issues of genetic heterogeneity and existence of complicated signaling pathways (Huang et al., 2017). Noteworthy, only very few reports have yet appeared in the literature on the combined use of nucleic acids and APLs. In 2003, Zeisig *et al.* described the use of APLs as helper lipids in dimethyldioctadecyl ammonium bromide-based liposomal formulations of a LacZ reporter gene to improve intracellular gene delivery (Zeisig et al., 2003). The authors assumed that APLs may facilitate the transport of the lipoplexes through the cell membrane due to their "detergent-like properties." In 2004, intratumoral co-injection of naked DNA with miltefosine has been reported (Settelen et al., 2004). While this non-condensing plasmid formulation failed to promote transgene expression *in vitro*, a reporter gene expression was increased by an order of magnitude *in vivo*. Another report published in 2007 describes the use of perifosine in combination with siRNA lipoplexes silencing c-FLIP, an inhibitory protein involved in the extrinsic pathway of apoptosis (Elrod et al., 2007). This is just about all that can be found in the literature on the joint use of nucleic acids and APLs.

As highly polar macromolecules, nucleic acids cannot diffuse through cell membranes and require the use of a delivery system for significant cell uptake. Various delivery strategies of nucleic acid based therapeutics have been developed, including viral (Lukashev and Zamyatnin, 2016) and non-viral (Shim et al., 2018) approaches. Although non-viral vectors can generally hardly compete with viral ones in terms of transfection efficiencies, they are superior to the latter with regard to production costs, payload size, and safety issues (Naldini, 2015). In non-viral delivery systems, convenient nucleic acid loading is usually accomplished through electrostatic interaction, and the type of non-viral vectors essentially includes cationic lipids and cationic polymers. In the course of our quest for nucleic acid carriers with improved transfection properties and safeness, we previously developed cationic derivatives of 1,2-dioleoyl-*sn*-glycero-3-phosphatidylcholine (DOPC), a major component of the cell membranes. These phosphotriester compounds proved highly efficient nucleic acid delivery reagents both *in vitro* (Pierrat et al., 2012, 2013a,b) and *in vivo* (Pierrat et al., 2016a,b,c). This inspired us to develop erufosine-based biolabile phosphotriesters (pro-APLs) as dual gene delivery reagents for combined cancer therapy (Gaillard et al., 2019). Our hypothesis was that the combination of a cationic biodegradable precursor of erufosine, as a nucleic acid carrier, and a DNA sequence encoding a pro-apoptotic protein, would diminish tumor cell survival as a result of both the expression of the transgene product and the *in situ* release of the antineoplastic APL upon carrier degradation. The results obtained indeed confirmed our hypothesis. As erufosine has not reached the clinic yet, we extended this new antitumor concept implementing gene therapy and chemotherapy to miltefosine and perifosine, the two APLs used clinically to date. We designed a series of 12 cationic prodrugs of miltefosine and perifosine which can regenerate the parent APL *in situ* under a chemical or enzyme stimulus. The properties of these APL prodrugs as gene delivery reagents have been investigated using a luciferase reporter gene assay, and the intrinsic cytotoxicity and hemolytic activity of the vectors have been determined. Finally, using a plasmid DNA encoding the tumor necrosis factor-related apoptosis-inducing ligand (TRAIL), the *in vitro* combined antiproliferative effect of TRAIL and APL prodrugs has been examined. For comparison purpose, results obtained with previously reported structure-related prodrugs of erufosine have been included and are discussed in this study.

MATERIALS AND METHODS

Detailed description of starting materials and standard procedures, and ^{1}H-, ^{13}C-, and ^{31}P-NMR spectra are given as **Supplementary Material**.

Synthesis of the Parent APLs

Dodecyl triflate, chloromethyl dodecanoate, 1-chloroethyl dodecanoate, chloromethyl dodecyl carbonate, 1-chloroethyl dodecyl carbonate, and chloromethyl oleyl carbonate were synthesized as described elsewhere (Heyes et al., 2002; Pierrat et al., 2013a).

Miltefosine Triethylamine (822 μL, 5.90 mmol) was added dropwise to phosphorus oxychloride (500 μL, 5.36 mmol) in anhydrous THF (20 mL) at 0°C under inert atmosphere. Then 1-hexadecanol (1.30 g, 5.36 mmol) in THF (10 mL) was added dropwise over a 30-min period and the reaction mixture was allowed to warm to rt. When all the alcohol had reacted (checked by TLC), temperature was brought back to 0°C and a second portion of triethylamine (3.3 mL, 21.4 mmol) was added followed by dropwise addition of 2-bromoethanol (380 μL, 5.36 mmol) in THF (10 mL). The reaction mixture was stirred at rt for 16 h before decomposition by addition of HCl 10% (10 mL) and heating at 40°C for 2 h. Solvent was removed under vacuum and the aqueous residue was extracted twice with CH_2Cl_2. The organic layer was dried over $MgSO_4$, filtered and reduced under vacuum, and the crude residue was purified by flash chromatography (CH_2Cl_2/MeOH 10:0–8:2) to yield intermediate 2-bromoethyl hexadecyl hydrogenophosphate (1.01 g, 44%). R_f: 0.43 (CH_2Cl_2/MeOH/H_2O 75:22:3). ^{1}H-NMR (400 MHz, CD_3OD/$CDCl_3$ 1:1) δ 0.85 (t, $J = 6.7$ Hz, 3H); 1.24 (m, 26H); 1.60 (tt, $J_1 = J_2 = 6.4$ Hz, 2H); 3.51 (t, $J = 6.4$ Hz; 2H); 3.86 (td, $J_1 = J_2 = 6.5$ Hz, 2H); 4.10 (t, $J_1 = J_2 = 6.5$ Hz, 2H). ^{13}C-NMR (100.7 MHz, CD_3OD/$CDCl_3$ 1:1) δ 14.3; 23.3; 26.4; 30.0; 30.3 (br); 31.3; 32.6; 66.0; 66.7. ^{31}P-NMR (162 MHz; CD_3OD/$CDCl_3$ 1:1) δ−0.56. IR ν 495; 596; 695; 733; 772; 879; 1,007; 1,218; 1,270; 1,456; 2,852; 2,921. The previous compound (1.0 g, 2.33 mmol) in $CHCl_3$/CH_3CN/*i*-PrOH 3:5:5 (13 mL) was treated with 45% (w/w) aqueous trimethylamine (5 mL, 34.3 mmol) at 70°C. When all starting material was consumed (checked by TLC), volatile was removed under vacuum and the residue was extracted twice with $CHCl_3$/MeOH 1:3. The organic layer was washed with brine, reduced under vacuum, diluted with $CHCl_3$, dried over $MgSO_4$, filtered and evaporated. The crude residue was purified by flash chromatography (CH_2Cl_2/MeOH 75:22:3–45:45:10) to yield miltefosine (0.77 g, 81%). R_f: 0.1 (CH_2Cl_2/MeOH/H_2O 75:22:3). ^{1}H-NMR (400 MHz, CD_3OD/$CDCl_3$ 1:1) δ 0.85 (t, $J =$ 6.2 Hz, 3H); 1.24 (m, 26H); 1.61 (tt, $J_1 = J_2 = 6.4$ Hz, 2H); 3.19 (s, 9H); 3.58 (m, 2H); 3.83 (td, $J_1 = J_2 = 6.5$ Hz, 2H); 4.20 (m, 2H). ^{13}C-NMR (100.7 MHz, CD_3OD/$CDCl_3$ 1:1) δ 14.3; 23.2; 26.4; 30.1 (2C); 30.3 (8C); 31.3; 32.5; 54.5; 59.7; 66.7; 67.0. ^{31}P-NMR (162 MHz, CD_3OD/$CDCl_3$ 1:1) δ−0.32. IR (ATR) ν 497; 716; 746; 853; 927; 957; 1,050; 1,126; 1,246; 1,471; 1,633; 2,849; 2,914; 3,372. HR-MS (ESI+) m/z $[M+H]^+$ calcd for $C_{21}H_{47}NO_4P^+$ 408.3237, found 408.3239.

Perifosine Phosphorus oxychloride (864 μL, 9.2 mmol) was added to 1-hexadecanol (2.50 g, 9.2 mmol) in anhydrous Et_2O (100 mL) at 0°C, followed by dropwise addition of triethylamine (1.29 mL, 9.2 mmol). The reaction mixture was stirred at rt for 16 h and filtered, and the filtrate was reduced under vacuum. The dry residue was dissolved in anhydrous $CHCl_3$ (100 mL) and *N,N*-dimethyl-4-hydroxypiperidinium tosylate (2.78 g, 9.24 mmol), triethylamine (3.00 mL, 21.5 mmol), and 4-DMAP (65 mg, 0.53 mmol) in $CHCl_3$ (100 mL) were introduced in the reaction flask and allowed to react for 2 d at rt. The reaction mixture was then reduced under vacuum, suspended in THF (100 mL) and refluxed with H_2O (2 mL) for 6 h. The crude mixture was reduced under vacuum and the residue was directly purified by flash chromatography ($CHCl_3$/MeOH/NH_4OH 10:6:1) to yield perifosine (0.70 g, 16%). R_f: 0.2 (CH_2Cl_2/MeOH/H_2O 75:22:3). ^{1}H-NMR (400 MHz, CD_3OD/$CDCl_3$ 1:1) δ 0.85 (t, $J = 6.5$ Hz, 3H); 1.24 (m, 30H); 1.59 (m, 2H); 2.10 (m, 4H); 3.09 (s, 3H); 3.16 (s, 3H); 3.25-3.53 (m, 4H); 3.82 (m, 2H); 4.40 (m, 1H). ^{13}C-NMR (100.7 MHz, CD_3OD/$CDCl_3$ 1:1) δ 14.3; 23.2; 26.4; 27.2 (2C); 29.9; 30.0; 30.2 (10C); 31.5; 32.5; 55.4 (2C); 59.2 (2C); 65.0; 66.6. ^{31}P-NMR (162 MHz, CD_3OD/$CDCl_3$ 1:1) δ−0.40. IR ν 479; 720; 846; 919; 994; 1,062; 1,124; 1,156; 1,225; 1,468; 2,848; 2,916. HR-MS (ESI+) m/z $[M+Na]^+$ calcd for $C_{25}H_{52}NNaO_4P^+$ 484.3526, found 484.3528.

Synthesis of the Pro-APLs

General Procedure The APL (0.5 mmol) and electrophilic reagent (4.0 mmol) were reacted in refluxing anhydrous $CHCl_3$ (12 mL) for 24 h with stirring under inert atmosphere. Solvent was removed *in vacuo* and the crude residue was purified by flash chromatography (CH_2Cl_2/MeOH 10:0–7:3) to yield the corresponding pro-APL.

*2-(((Dodecyloxy)(hexadecyloxy)phosphoryl)oxy)-N,N,N-trimethylethan-1-aminium triflate (**M_{12}**).* This compound (101 mg, 84%) was obtained from miltefosine (80 mg, 0.20 mmol) and dodecyl triflate (162 mg, 0.53 mmol) according to the general procedure except the reaction was conducted at rt. R_f: 0.7 (CH_2Cl_2/MeOH/H_2O 75:22:3). ^{1}H-NMR (400 MHz, $CDCl_3$) δ 0.88 (t, $J = 6.6$ Hz, 6H); 1.26 (m, 44H); 1.68 (tt, $J_1 = J_2 = 6.8$ Hz, 4H); 3.31 (s, 9H); 3.83 (m; 2H); 4.08 (m, 4H); 4.48 (m, 2H). ^{13}C-NMR (100.7 MHz, $CDCl_3$) δ 14.3 (2C); 22.9 (2C); 25.6 (2C); 29.4 (2C); 29.6 (2C); 29.7 (2C); 29.8 (4C); 29.9 (6C); 30.5 (2C); 32.1 (2C); 54.6 (3C); 61.2; 65.9; 69.2 (2C). ^{31}P-NMR (162 MHz, $CDCl_3$) δ−2.14. IR ν 517; 574; 638; 1,030; 1,161; 1,226; 1,253; 1,467; 2,852; 2,921; 3,500. HR-MS (ESI+) m/z $[M-Cl]^+$ calcd for $C_{33}H_{71}NO_4P^+$ 576.5115, found 576.5108.

*2-((((Dodecanoyloxy)methoxy)(hexadecyloxy)phosphoryl)oxy)-N,N,N-trimethylethan-1-aminium chloride (**M_{E12}**).* This compound (136 mg, 42%) was obtained from miltefosine (200 mg, 0.49 mmol) and chloromethyl dodecanoate (979 mg, 3.94 mmol) according to the general procedure. R_f: 0.5 (CH_2Cl_2/MeOH/H_2O 75:22:3). ^{1}H-NMR (400 MHz, CD_3OD/$CDCl_3$ 1:1) δ 0.85 (t, $J = 6.3$ Hz, 6H); 1.24 (m, 42H); 1.63 (tt, $J_1 = J_2 = 6.8$ Hz, 2H); 1.69 (tt, $J_1 = J_2 = 6.6$ Hz, 2H); 2.40 (t, $J = 7.5$ Hz, 2H); 3.23 (s, 9H); 3.76 (m, 2H); 4.11 (td, $J_1 = J_2 = 6.3$ Hz, 2H); 4.50 (m, 2H); 5.64 (ABX syst., $J_{AB} = 5.2$ Hz, $J_{AX} = 13.4$ Hz, $J_{BX} = 11.4$ Hz, 2H). ^{13}C-NMR (100.7 MHz, CD_3OD/$CDCl_3$ 1:1) δ 14.5 (2C); 23.3 (2C); 25.1; 25.9; 29.7; 29.8; 29.9; 30.0 (2C); 30.1 (4C); 30.2 (7C); 30.7; 32.5; 34.6; 54.7 (3C);

62.3; 66.5; 70.2; 84.2; 173.2. ^{31}P-NMR (162 MHz, $CD_3OD/CDCl_3$ 1:1) δ−3.80. IR ν 458; 490; 721; 832; 873; 965; 1,042; 1,159; 1,264; 1,468; 1,760; 2,849; 2,917; 2,956; 3,382. HR-MS (ESI+) m/z $[M\text{-}Cl]^+$ calcd for $C_{34}H_{71}NO_6P^+$ 620.5014, found 620.5004.

*2-(((1-(Dodecanoyloxy)ethoxy)(hexadecyloxy)phosphoryl)oxy)-N,N,N-trimethylethan-1-aminium chloride (**$M_{E'12}$**).* This compound (169 mg, 51%) was obtained as two separated couples of enantiomers (E1 and E2) from miltefosine (201 mg, 0.49 mmol) and 1-chloroethyl dodecanoate (1.04 g, 3.95 mmol) according to the general procedure. R_f: 0.5 (E1) and 0.4 (E2) (CH_2Cl_2/MeOH/H_2O 75:22:3). ^{1}H-NMR (400 MHz, $CD_3OD/CDCl_3$ 1:1) E1 δ 0.85 (t, J = 6.1 Hz, 6H); 1.24 (m, 42H); 1.58 (d, J = 5.3 Hz, 3H); 1.61 (tt, $J_1 = J_2$ = 6.8 Hz, 2H); 1.69 (tt, $J_1 = J_2$ = 6.6 Hz, 2H); 2.37 (t, J = 7.2 Hz, 2H); 3.24 (s, 9H); 3.76 (m, 2H); 4.09 (td, $J_1 = J_2$ = 6.7 Hz, 2H); 4.50 (m, 2H); 6.42 (qd, $J_1 = J_2$ = 5.3 Hz, 1H). ^{1}H-NMR (400 MHz, $CD_3OD/CDCl_3$ 1:1) E2 δ 0.86 (t, J = 6.2 Hz, 6H); 1.24 (m, 42H); 1.56 (d, J = 5.3 Hz, 3H); 1.61 (tt, $J_1 = J_2$ = 6.8 Hz, 2H); 1.68 (tt, $J_1 = J_2$ = 6.6 Hz, 2H); 2.37 (t, J = 7.3 Hz, 2H); 3.24 (s, 9H); 3.76 (m, 2H); 4.09 (td, $J_1 = J_2$ = 6.3 Hz, 2H); 4.50 (m, 2H); 6.42 (qd, $J_1 = J_2$ = 5.3 Hz, 2H). ^{13}C-NMR (100.7 MHz, $CD_3OD/CDCl_3$ 1:1) E1 δ 14.5 (2C); 21.7; 23.4 (2C); 25.3; 26.1; 29.6; 29.7; 29.8; 29.9; 30.0 (2C); 30.1 (2C); 30.2 (4C); 30.3 (4C); 30.7; 32.5 (2C); 34.5; 54.6 (3C); 62.3; 66.5; 70.0; 92.4; 173.3. ^{13}C-NMR (100.7 MHz, $CD_3OD/CDCl_3$ 1:1) E2 δ 14.5 (2C); 21.6; 23.4 (2C); 25.3; 26.1; 29.6; 29.7; 29.8; 29.9; 30.0 (2C); 30.1 (2C); 30.2 (4C); 30.3 (4C); 30.7; 32.5 (2C); 34.5; 54.6 (3C); 62.1; 66.5; 70.2; 92.3; 172.8. ^{31}P-NMR (162 MHz, $CD_3OD/CDCl_3$ 1:1) E1 δ−5.96. ^{31}P-NMR (162 MHz, $CD_3OD/CDCl_3$ 1:1) E2 δ−5.57. IR ν 509; 721; 934; 976; 1,050; 1,082; 1,165; 1,238; 1,267; 1,467; 1,755; 2,849; 2,916; 2,956; 3,389. HR-MS (ESI+) m/z $[M\text{-}Cl]^+$ calcd for $C_{35}H_{73}NO_6P^+$ 634.5170, found 634.5167. Note: IR absorption and HR-MS were measured on the mixture of the four diastereomers.

*3-((((((Dodecyloxy)carbonyl)oxy)methoxy)(hexadecyloxy) phosphoryl)oxy)-N,N,N-trimethylpropan-1- aminium chloride (**M_{C12}**).* This compound (86 mg, 26%) was obtained from miltefosine (200 mg, 0.49 mmol) and chloromethyl dodecyl carbonate (1.06 g, 3.78 mmol) according to the general procedure. R_f: 0.55 (CH_2Cl_2/MeOH/H_2O 75:22:3). ^{1}H-NMR (400 MHz, $CD_3OD/CDCl_3$ 1:1) δ 0.85 (t, J = 6.3 Hz, 6H); 1.24 (m, 44H); 1.69 (m, 4H); 3.23 (s, 9H); 3.77 (m, 2H); 4.13 (td, $J_1 = J_2$ = 6.9 Hz, 2H); 4.19 (t, J = 6.7 Hz, 2H); 4.52 (m, 2H); 5.66 (m, 2H). ^{13}C-NMR (100.7 MHz, $CD_3OD/CDCl_3$ 1:1) δ 14.5 (2C); 23.2 (2C); 25.9; 26.2; 29.1; 29.7; 29.8; 29.9 (2C); 30.1 (2C); 30.2 (5C); 30.3 (5C); 30.7; 32.5 (2C); 54.5 (3C); 62.2; 66.2; 70.0; 70.3; 86.6; 154.5. ^{31}P-NMR (162 MHz, $CD_3OD/CDCl_3$ 1:1) δ −3.58. IR ν 670; 771; 950; 1,042; 1,266; 1,468; 1,762; 2,850; 2,918; 3,378. HR-MS (ESI+) m/z $[M\text{-}Cl]^+$ calcd for $C_{35}H_{73}NO_7P^+$ 650.5119, found 650.5135.

*3-((((((Dodecyloxy)carbonyl)oxy)ethoxy)(hexadecyloxy) phosphoryl)oxy)-N,N,N-trimethylpropan-1-aminium chloride (**$M_{C'12}$**).* This compound (201 mg, 59%) was obtained as a mixture of diastereomers from miltefosine (200 mg, 0.49 mmol) and 1-chloroethyl dodecyl carbonate (1.16 g, 3.97 mmol) according to the general procedure. R_f: 0.5 and 0.6 (CH_2Cl_2/MeOH/H_2O 75:22:3). ^{1}H-NMR (400 MHz, $CD_3OD/CDCl_3$ 1:1) δ 0.86 (t, J = 6.3 Hz, 6H); 1.24 (m, 44H); 1.60 (d, J = 5.2 Hz, 3H); 1.68 (m, 4H); 3.23 (s, 9H); 3.75 (m, 2H); 4.17 (m, 4H); 4.49 (m, 2H); 6.29–6.38 (qd, m, 1H). ^{13}C-NMR (100.7 MHz, $CD_3OD/CDCl_3$ 1:1) δ 14.3 (2C); 21.5; 23.2 (2C); 25.9; 26.2; 29.1; 29.9; 30.0 (2C); 30.1 (2C); 30.2 (5C); 30.3 (6C); 30.7; 32.5 (2C); 54.5 (3C); 62.2; 66.3; 69.7; 70.0; 95.8; 154.0. ^{31}P-NMR (162 MHz, $CD_3OD/CDCl_3$ 1:1) δ−5.63; −5.95. IR ν 458; 490; 721; 832; 873; 965; 1,042; 1,159; 1,264; 1,468; 1,760; 2,849; 2,917; 2,956; 3,382. HR-MS (ESI+) m/z $[M\text{-}Cl]^+$ calcd for $C_{34}H_{71}NO_6P^+$ 620.5014, found 620.5004.

*3-((((((Dodecyloxy)carbonyl)oxy)methoxy)(oleyloxy) phosphoryl)oxy)-N,N,N-trimethylpropan-1-aminium chloride (**$M_{C18:1}$**).* This compound (60 mg, 16%) was obtained from miltefosine (201 mg, 0.49 mmol) and chloromethyl oleyl carbonate (1.42 g, 3.92 mmol) according to the general procedure. R_f: 0.5 (CH_2Cl_2/MeOH/H_2O 75:22:3). ^{1}H-NMR (400 MHz, $CD_3OD/CDCl_3$ 1:1) δ 0.86 (t, J = 6.1 Hz, 6H); 1.24 (m, 48H); 1.68 (m, 4H); 2.00 (m, 4H); 3.24 (s, 9H); 3.79 (m, 2H); 4.12 (td, $J_1 = J_2$ = 6.7 Hz, 2H); 4.19 (t, J = 6.5 Hz, 2H); 4.52 (m, 2H); 5.32 (m, 2H); 5.65 (m, 2H). ^{13}C-NMR (100.7 MHz, $CD_3OD/CDCl_3$ 1:1) δ 14.3 (2C); 23.2 (2C); 25.9; 26.2; 27.7 (2C); 29.1; 29.7 (2C); 29.8; 30.1 (2C); 30.2; 30.3 (3C); 30.4 (9C); 30.7; 32.5 (2C); 54.4 (3C); 62.1; 66.2; 70.0; 70.2; 86.5; 130.2; 130.5; 154.3. ^{31}P-NMR (162 MHz, $CD_3OD/CDCl_3$ 1:1) δ−3.57. IR ν 486; 721; 786; 836; 951; 977; 1,022; 1,049; 1,156; 1,258; 1,417; 1,467; 1,758; 2,850; 2,919; 2,956; 3,390. HR-MS (ESI+) m/z $[M\text{-}Cl]^+$ calcd for $C_{41}H_{83}NO_7P^+$ 732.5902, found 732.5905.

*4-(((Dodecyloxy)(octadecyloxy)phosphoryl)oxy)-1,1-dimethylpiperidin-1-ium chloride (**P_{12}**).* This compound (55 mg, 48%) was obtained from perifosine (79 mg, 0.17 mmol) and dodecyl triflate (141 mg, 0.44 mmol) according to the general procedure except the reaction was conducted at rt. R_f: 0.68 (CH_2Cl_2/MeOH/H_2O 75:22:3). ^{1}H-NMR (400 MHz, $CD_3OD/CDCl_3$ 1:1) δ 0.86 (t, J = 6.7 Hz, 6H); 1.24 (m, 48H); 1.68 (tt, $J_1 = J_2$ = 7.0 Hz, 4H); 2.10-2.32 (m, 4H); 3.14 (s, 3H); 3.20 (s, 3H); 3.41-3.55 (m, 4H); 4.06 (m, 4H); 4.70 (m, 1H). ^{13}C-NMR (100.7 MHz; $CD_3OD/CDCl_3$ 1:1) δ 14.4 (2C); 23.3 (2C); 26.1 (2C); 27.1 (2C); 29.6 (2C); 29.8 (2C); 30.0 (2C); 30.1 (5C); 30.2 (6C); 30.3; 30.6 (2C); 32.6 (2C); 54.1 (2C); 58.9 (2C); 69.3; 69.4 (2C). ^{31}P-NMR (162 MHz, $CD_3OD/CDCl_3$ 1:1) δ−2.07. IR ν 516; 573; 638; 721; 764; 923; 1,029; 1,161; 1,245; 1,467; 2,851; 2,920; 3,252. HR-MS (ESI+) m/z $[M\text{-}Cl]^+$ calcd for $C_{37}H_{77}NO_4P^+$ 630.5585, found 630.5581.

*4-((((Dodecanoyloxy)methoxy)(octadecyloxy)phosphoryl)oxy)-1,1-dimethylpiperidin-1-ium chloride (**P_{E12}**).* This compound (51 mg, 22%) was obtained from perifosine (150 mg, 0.33 mmol) and chloromethyl dodecanoate (675 mg, 2.70 mmol) according to the general procedure. R_f: 0.6 (CH_2Cl_2/MeOH/H_2O 75:22:3). ^{1}H-NMR (400 MHz, $CD_3OD/CDCl_3$ 1:1) δ 0.86 (t, J = 6.7 Hz, 6H); 1.24 (m, 46H); 1.63 (tt, $J_1 = J_2$ = 6.9 Hz, 2H); 1.68 (tt, $J_1 = J_2$ = 7.2 Hz, 2H); 2.10–2.32 (m, 4H); 2.39 (t, J = 7.6 Hz, 2H); 3.17 (s, 3H); 3.22 (s, 3H); 3.45–3.59 (m, 4H); 4.08 (td, $J_1 = J_2$ = 6.8 Hz, 2H); 4.70 (m, 1H); 5.62 (ABX syst., J_{AB} = 5.2 Hz, J_{AX} = 13.8 Hz, J_{BX} = 11.1 Hz, 2H). ^{13}C-NMR (100.7 MHz, $CD_3OD/CDCl_3$ 1:1) δ 14.5 (2C); 23.4 (2C); 25.3; 26.1; 27.1 (2C); 29.8; 29.9; 30.0; 30.1 (2C); 30.2; 30.3 (5C); 30.4 (7C); 30.9; 32.6 (2C); 34.6; 54.7 (2C); 58.9 (2C); 69.9; 70.0; 83.5; 173.1. ^{31}P-NMR (162 MHz, $CD_3OD/CDCl_3$ 1:1) δ−4.22. IR ν 531; 666; 720; 760; 802; 923;

966; 1,020; 1,148; 1,264; 1,468; 1,644; 1,764; 2,849; 2,916; 2,955; 3,378. HR-MS (ESI+) m/z $[M\text{-}Cl]^+$ calcd for $C_{38}H_{77}NO_6P^+$ 674.5483, found 674.5477.

*4-(((1-(Dodecanoyloxy)ethoxy)(octadecyloxy)phosphoryl)oxy)-1,1-dimethylpiperidin-1-ium chloride (**$P_{E'12}$**).* This compound (96 mg, 20%) was obtained as two separated couples of enantiomers (E1 and E2) from perifosine (300 mg, 0.65 mmol) and 1-chloroethyl dodecanoate (1.33 g, 5.06 mmol) according to the general procedure. R_f: 0.3 (E1) and 0.4 (E2) (CH_2Cl_2/MeOH/H_2O 75:22:3). ^{1}H-NMR (400 MHz, $CD_3OD/CDCl_3$ 1:1) D1 δ 0.86 (t, $J = 6.7$ Hz, 6H); 1.24 (m, 46H); 1.56 (d, $J = 5.2$ Hz, 3H); 1.61 (tt, $J_1 = J_2 = 6.9$ Hz, 2H); 1.68 (tt, $J_1 = J_2 = 7.2$ Hz, 2H); 2.08–2.30 (m, 4H); 2.36 (t, $J = 7.6$ Hz, 2H); 3.17 (s, 3H); 3.24 (s, 3H); 3.45–3.59 (m, 4H); 4.06 (td, $J_1 = J_2 = 6.8$ Hz, 2H); 4.70 (m, 1H); 6.46 (qd, $J_1 = J_2 = 5.2$ Hz, 1H). ^{1}H-NMR (400 MHz, $CD_3OD/CDCl_3$ 1:1) E2 δ 0.86 (t, $J = 6.7$ Hz, 6H); 1.24 (m, 46H); 1.54 (d, $J = 5.2$ Hz, 3H); 1.61 (tt, $J_1 = J_2 = 6.9$ Hz, 2H); 1.68 (tt, $J_1 = J_2 = 7.2$ Hz, 2H); 2.08–2.30 (m, 4H); 2.35 (t, $J = 7.6$ Hz, 2H); 3.18 (s, 3H); 3.24 (s, 3H); 3.45–3.59 (m, 4H); 4.08 (td, $J_1 = J_2 = 6.8$ Hz, 2H); 4.70 (m, 1H); 6.50 (qd, $J_1 = J_2 = 5.2$ Hz, 1H).^{13}C-NMR (100.7 MHz, $CD_3OD/CDCl_3$ 1:1) E1 δ 14.5 (2C); 21.7; 23.4 (2C); 25.3; 26.1; 26.8; 27.1; 29.7; 29.8; 30.0; 30.1 (2C); 30.2; 30.3 (5C); 30.4 (7C); 30.8; 32.6 (2C); 34.7; 55.2 (2C); 58.6 (2C); 69.5; 69.7; 92.1; 173.1. ^{13}C-NMR (100.7 MHz, $CD_3OD/CDCl_3$ 1:1) E2 δ 14.5 (2C); 21.7; 23.4 (2C); 25.3; 26.1; 27.0; 27.1; 29.7; 29.8; 30.0; 30.1 (2C); 30.2; 30.3 (5C); 30.4 (7C); 30.8; 32.6 (2C); 34.7; 54.8 (2C); 58.8 (2C); 69.7; 69.9; 92.3; 172.8. ^{31}P-NMR (162 MHz, $CD_3OD/CDCl_3$ 1:1) E1 δ−6.1. ^{31}P-NMR (162 MHz, $CD_3OD/CDCl_3$ 1:1) E2 δ−6.0. IR ν 553; 638; 772; 752; 974; 1,012; 1,090; 1,163; 1,263; 1,466; 1,745; 2,851; 2,920; 3,380. HR-MS (ESI+) m/z $[M\text{-}Cl]^+$ calcd for $C_{39}H_{79}NO_6P^+$ 688.5640, found 688.5627. Note: IR absorption and HR-MS were measured on the mixture of the four diastereomers.

*3-((((((Dodecyloxy)carbonyl)oxy)methoxy)(octadecyloxy) phosphoryl)oxy)-N,N,N-trimethylpropan-1-aminium chloride (**P_{C12}**).* This compound (53 mg, 22%) was obtained from perifosine (152 mg, 0.33 mmol) and chloromethyl dodecyl carbonate (738 mg, 2.65 mmol) according to the general procedure. R_f: 0.55 (CH_2Cl_2/MeOH/H_2O 75:22:3). ^{1}H-NMR (400 MHz, $CDCl_3$) δ 0.86 (t, $J = 6.8$ Hz, 6H); 1.24 (m, 48H); 1.68 (m, 4H); 2.10–2.34 (m, 4H); 3.53 (s, 3H); 3.66 (s, 3H); 3.67–3.96 (m, 4H); 4.10 (td, $J_1 = J_2 = 6.8$ Hz, 2H); 4.19 (t, $J = 6.8$ Hz, 2H); 4.80 (m, 1H); 5.65 (ABX syst., $J_{AB} = 5.6$ Hz, $J_{AX} = 11.6$ Hz, $J_{BX} = 10.4$ Hz, 2H). ^{13}C-NMR (100.7 MHz, $CD_3OD/CDCl_3$ 1:1) δ 14.4 (2C); 23.3 (2C); 26.1; 26.4; 27.1 (2C); 29.2; 29.8 (2C); 29.9 (2C); 30.2 (4C); 30.4 (10C); 30.9; 32.6 (2C); 55.7 (2C); 58.8 (2C); 69.6; 69.8; 70.1; 86.5; 154.4. ^{31}P-NMR (162 MHz, $CD_3OD/CDCl_3$ 1:1) δ−3.82. IR ν 482; 529; 665; 720; 781; 850; 922; 944; 979; 1,019; 1,165; 1,266; 1,427; 1,465; 1,761; 2,848; 2,916; 2,956; 3,492. HR-MS (ESI+) m/z $[M\text{-}Cl]^+$ calcd for $C_{39}H_{79}NO_7P^+$ 704.5589, found 704.5588.

*3-((((((Dodecyloxy)carbonyl)oxy)ethoxy)(octadecyloxy) phosphoryl)oxy)-N,N,N-trimethylpropan-1-aminium chloride (**$P_{C'12}$**).* This compound (38 mg, 16%) was obtained as two separated couples of enantiomers (E1 and E2) from perifosine (149 mg, 0.32 mmol) and 1-chloroethyl dodecyl carbonate (762 mg, 2.60 mmol) according to the general procedure. R_f: 0.4 (E1) and 0.5 (E2) (CH_2Cl_2/MeOH/H_2O 75:22:3). ^{1}H-NMR (400 MHz, $CD_3OD/CDCl_3$ 1:1) E1 δ 0.86 (t, $J = 6.8$ Hz, 6H); 1.24 (m, 48H); 1.60 (d, $J = 5.3$ Hz, 3H); 1.63 (tt, $J_1 = J_2 = 6.9$ Hz, 2H); 1.68 (tt, $J_1 = J_2 = 6.4$ Hz, 2H); 2.10–2.34 (m, 4H); 3.15 (s, 3H); 3.22 (s, 3H) 3.41–3.65 (m, 4H); 4.10 (td, $J_1 = J_2 = 6.8$ Hz, 2H); 4.19 (t, $J = 6.8$ Hz, 2H); 4.72 (m, 1H); 6.33 (m, 1H). ^{1}H-NMR (400 MHz, $CD_3OD/CDCl_3$ 1:1) E2 δ 0.86 (t, $J = 6.8$ Hz, 6H); 1.24 (m, 48H); 1.58 (d, $J = 5.3$ Hz, 3H); 1.63 (tt, $J_1 = J_2 = 6.9$ Hz, 2H); 1.68 (tt, $J_1 = J_2 = 6.4$ Hz, 2H); 2.10–2.34 (m, 4H); 3.17 (s, 3H); 3.24 (s, 3H); 3.41–3.65 (m, 4H); 4.10 (td, $J_1 = J_2 = 6.8$ Hz, 2H); 4.19(t, $J = 6.8$ Hz, 2H); 4.72 (m, 1H); 6.35 (m, 1H). ^{13}C-NMR (100.7 MHz, $CD_3OD/CDCl_3$ 1:1) E1 δ 14.6 (2C); 21.9; 23.3 (2C); 25.9; 26.2; 27.1; 29.1; 29.7; 29.8; 29.9 (2C); 30.2 (4C); 30.3 (4C); 30.4 (6C); 30.9; 32.6 (2C); 55.7 (2C); 58.3 (2C); 68.9; 69.3; 69.6; 95.1; 153.8. ^{13}C-NMR (100.7 MHz, $CD_3OD/CDCl_3$ 1:1) E2 δ 14.6 (2C); 22.0; 23.3 (2C); 25.9; 26.2; 27.1 (2C); 29.1; 29.8 (2C); 29.9 (2C); 30.2 (4C); 30.3 (5C); 30.4 (5C); 30.9; 32.6 (2C); 55.7 (2C); 58.3 (2C); 68.9; 69.3; 69.6; 95.2; 153.8. ^{31}P-NMR (162 MHz, $CD_3OD/CDCl_3$ 1:1) E1 δ−6.13. ^{31}P-NMR (162 MHz, $CD_3OD/CDCl_3$ 1:1) E2 δ−5.93. IR ν 534; 720; 772; 924; 971; 1,023; 1,152; 1,270; 1,396; 1,467; 2,849; 2,916; 2,955; 3,388. HR-MS (ESI+) m/z $[M\text{-}Cl]^+$ calcd for $C_{40}H_{81}NO_7P^+$ 718.5745, found 718.5744. Note: IR and HR-MS were measured on the mixture of the four diastereomers.

*3-((((((Dodecyloxy)carbonyl)oxy)methoxy)(oleyloxy) phosphoryl)oxy)-N,N,N-trimethylpropan-1-aminium chloride (**$P_{C18:1}$**).* This compound (40 mg, 15%) was obtained from perifosine (148 mg, 0.32 mmol) and chloromethyl oleyl carbonate (930 mg, 2.58 mmol) according to the general procedure. R_f: 0.55 (CH_2Cl_2/MeOH/H_2O 75:22:3). ^{1}H-NMR (400 MHz, $CD_3OD/CDCl_3$ 1:1) δ 0.86 (t, $J = 6.8$ Hz, 6H); 1.24 (m, 52H); 1.68 (m, 4H); 2.00 (m, 4H); 2.10–2.34 (m, 4H); 3.10 (s, 3H); 3.19 (s, 3H); 3.45–3.59 (m, 2H); 4.10 (td, $J_1 = J_2 = 6.8$ Hz, 2H); 4.19 (t, $J = 6.8$ Hz, 2H); 4.72 (m, 1H); 5.31 (m, 2H); 5.65 (m, 2H). ^{13}C-NMR (100.7 MHz, $CD_3OD/CDCl_3$ 1:1) δ 14.5 (2C); 23.3 (2C); 26.4; 26.5; 27.0 (2C); 27.8 (2C); 29.2; 30.0 (2C); 30.1; 30.2; 30.3; 30.4 (15C); 30.9; 32.6 (2C) 54.7 (2C); 58.8 (2C); 70.0; 70.1; 70.2; 86.6; 130.4 (2C); 155.2. ^{31}P-NMR (162 MHz, $CD_3OD/CDCl_3$ 1:1) δ−4.10. IR ν 516; 720; 968; 1,027; 1,251; 1,465; 1,646; 1,764; 2,851; 2,919; 3,387. HR-MS (ESI+) m/z $[M\text{-}Cl]^+$ calcd for $C_{45}H_{89}NO_7P^+$ 786.6371, found 786.6355.

RESULTS AND DISCUSSION

Synthesis

As zwitterionic phosphodiesters, APLs can be conveniently transformed into cationic lipids with potential nucleic acid condensing properties, by straightforward esterification of their phosphate group. The net positive charge generated in the resulting phosphotriester molecules can thus establish electrostatic interactions with anionic phosphates in nucleic acids. This results in the formation of complexes with a nanometric size ready for cell uptake through the endocytic route (Rehman et al., 2013). Besides, when the chemical transformation is reversible and sensitive, e.g., to a pH or enzyme stimulus as met along the endo-lysosome pathway, the zwitterionic parent APLs can be regenerated *in situ*, and this is expected to have cascading effect. Firstly, due to their membrane-active properties, the APLs

can disrupt the endosome membrane, hence facilitating escape of the genetic material into the cytosol. Secondly, as the newly unmasked negative charge on the APLs favorably competes with that of the phosphates of nucleic acids, decomplexation of the latters occurs, thus triggering decondensation of the transfection particles that favors proper processing of the transgene by the cell translation machinery. Finally, as most amphiphilic molecules enter the endocytic recycling pathway from the sorting endosomes through a highly dynamic and effective process (Mukherjee et al., 1999; Juliano, 2018), the *in situ* regenerated APL molecules are intended to traffic to the plasma membrane, where they are expected to operate their intrinsic apoptotic activity (Gaillard et al., 2020).

However, the non-selective hydrolysis of an APL-derived phosphotriester into a phosphodiester would provide a mixture of the APL together with two other phosphodiester molecules. To favor the exclusive formation of the APL, it is thus of value to mask its phosphate group by introducing a (bio)labile phosphoester that will be removed preferentially, under a chemical or enzyme stimulus. Mixed phosphoacetals have been selected for this purpose, as they may degrade through the selective cleavage of the acetal bridge (Farquhar et al., 1983). Miltefosine and perifosine were thus converted into "pro-miltefosine" and "pro-perifosine" compounds incorporating various linkers for modulating their biodegradability which will determine their effectiveness as transfection reagents and the rate of *in situ* APL release (**Figure 2**). For comparison and SAR analysis, the previously described homolog compounds in the erufosine series (Gaillard et al., 2019) have been introduced in this study. The pro-miltefosine and pro-perifosine compounds were prepared in the ester (compounds noted $\mathbf{M_{En}}$ or $\mathbf{P_{En}}$) and carbonate (compounds noted $\mathbf{M_{Cn}}$ or $\mathbf{P_{Cn}}$) mixed phosphoacetal series. The acetal bridge received a methyl substituent (compounds noted $\mathbf{M_{E'n}}$ and $\mathbf{M_{C'n}}$) to modulate the hydrolysis rate of the compounds, as was recently demonstrated in phosphotriesters (Pierrat et al., 2013b). The compounds were straightforwardly synthesized by reaction of the parent APLs with a series of dodecyl-, dodecanoyl-, and oleyl-based electrophilic reagents (**Figure 2**) The reaction yields were generally lower than those obtained in the erufosine series (Gaillard et al., 2019). They ranged from 15 to 97%, depending both on the nucleophilicity of the phosphate group in the APL and on the reactivity of the electrophilic reagent. In some cases, the stability of the reaction product also was a obstacle to higher yields. As they contain two stereogenic centers, compounds with a methyl substitution on the acetal bridge ($\mathbf{M_{E'12}}$, $\mathbf{M_{C'12}}$, $\mathbf{P_{E'12}}$, and $\mathbf{P_{C'12}}$) were obtained as a mixture of four diastereomers. The separation of the two couples of enantiomers has been realized whenever possible, for analytic purpose, but the original mixture of isomers was used in the subsequent evaluations.

Hydrolytic Stability of the Pro-APL Compounds

Aqueous formulation of the APL prodrugs produces nanosized lipid aggregates that most likely enter cells through the endocytosis pathway. To produce the expected intrinsic antineoplastic effect, APL-derived phosphotriesters need to be processed into the bioactive parent APLs. The hydrolysis of the prodrugs may be under the control of a chemical stimulus, e.g., a pH decrease as observed during the maturation of endosomes, or of degradation enzymes that massively enter the endosome compartment when continuing to lysosomes. To get some information on the transformation of pro-APLs into APLs, we monitored the hydrolysis of these compounds over time, at pH 7.4 and 4.5, conditions that mimick the extracellular milieu and the environment of the late endosome, respectively. This monitoring was realized using ^{31}P-NMR spectroscopy, according to a previously reported method (Pierrat et al., 2013b). Whatever the compound investigated, only one single ^{31}P resonance did appear during the course of the experiments, corresponding to that of the parent APL. This confirmed that hydrolysis of the pro-APLs selectively occurred at the acetal center. Consistently, phosphotriesters $\mathbf{M_{12}}$ and $\mathbf{P_{12}}$ lacking an acetal moiety revealed fully stable under both pH conditions, even after an extended incubation of 31 days at 25°C, as was previously observed for $\mathbf{E_{12}}$. All the other APL derivatives revealed sensitive to hydrolysis (**Table 1**). As a general trend, hydrolysis of the pro-APLs was quicker under neutral conditions (*i.e.,* pH 7.4) than under acidic ones (*i.e.,* pH 4.5). This revealed that the reactivity of mixed acetals of phosphoric and carboxylic or carbonic esters is completely different from that observed for dialkyl acetals that are more readily hydrolyzed under acidic conditions, and is consistent with results previously reported for other phosphoacetals (Pierrat et al., 2013a,b). Besides, substitution of one hydrogen atom with a methyl group on the acetal bridge accelerated the rate of hydrolysis of the prodrugs. This effect revealed more pronounced in the ester than in the carbonate series. With respect to the effect of the pendant arm tethered to the APLs through the acetal bridge on the rate of hydrolysis, the dodecyl and oleyl substituents did not show any significant difference. Finally, though these results allowed a comparison of the APL prodrugs with each other, it is important to consider that it could give an image of the stability of these compounds that is truncated. Indeed, in biological media, the enzyme-mediated hydrolysis of such compounds can proceed far quicker than "simple" chemical hydrolysis under pH control (Pierrat et al., 2012).

Gene Delivery Properties

The capacity of the pro-APLs to interact electrostatically with nucleic acids and form lipoplexes was checked by standard agarose gel electrophoresis. All the prodrugs tested led to full DNA complexation at a lipid/DNA phosphate ratio (N/P) > 1.3–3 (**Supplementary Figure 1**). The size (hydrodynamic diameter) and charge (zeta potential, ζ) of the lipoplexes prepared at an N/P ratio of 3 with one molar equivalent of dioleoyl-*sn*-glycero-3-phosphatidylethanolamine (DOPE), a lipid with fusogenic properties (Hui et al., 1996; Zuhorn et al., 2005), were investigated by DLS (**Supplementary Table 1**). The lipoplexes in the miltefosine series displayed a size in the range of 86–275 nm, which was similar to what was reported for DNA complexes with pro-erufosine compounds (Gaillard et al., 2019). In the perifosine series, larger complexes were formed (330–724 nm).

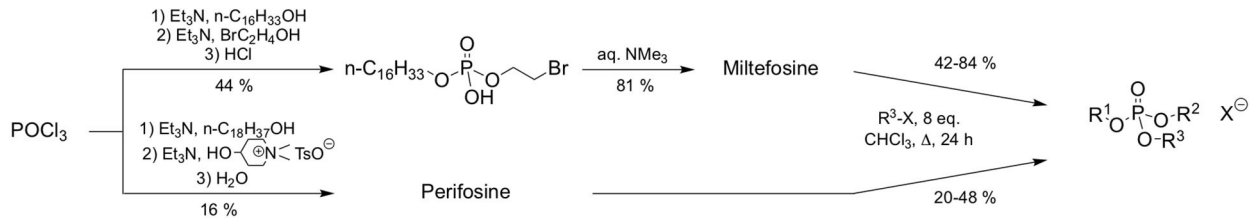

Compound	R^1	R^2	R^3	X	Yield (%)
M_{12}	$C_{16}H_{33}$	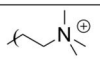		OTf	84
M_{E12}	"	"		Cl	42
$M_{E'12}$	"	"		Cl	51
M_{C12}	"	"		Cl	26
$M_{C'12}$	"	"		Cl	59
$M_{C18:1}$	"	"		Cl	16
P_{12}	$C_{18}H_{37}$			OTf	48
P_{E12}	"	"	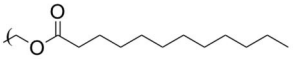	Cl	22
$P_{E'12}$	"	"	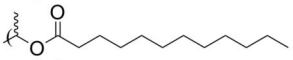	Cl	20
P_{C12}	"	"	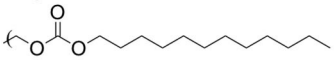	Cl	22
$P_{C'12}$	"	"	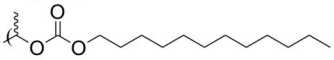	Cl	16
$P_{E18:1}$	"	"	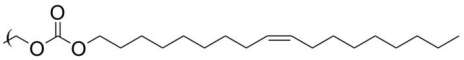	Cl	15
E_{12}	ω-9-cis-$C_{22}H_{43}$			OTf	97
E_{E12}	"	"	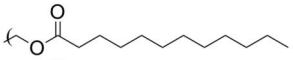	Cl	41
$E_{E'12}$	"	"	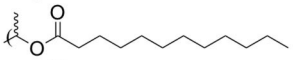	Cl	50
E_{C12}	"	"	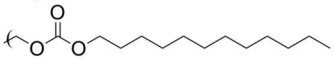	Cl	31
$E_{C'12}$	"	"		Cl	41
$E_{E18:1}$	"	"		Cl	58

FIGURE 2 | Synthetic route to APLs and pro-APLs. Data for erufosine prodrugs are reported from the literature (Gaillard et al., 2019).

This may be tentatively attributed to the expected higher main phase transition temperature of the perifosine derivatives as they display the longer saturated (stiffer) alkyl chain (Cevc, 1991). Introduction on the phosphate group of the APLs of an unsaturated chain resulted in significantly larger lipoplexes in the case of $\mathbf{M_{C18:1}}$ and $\mathbf{E_{C18:1}}$, (275 and 611 nm, resp.). Once again, results were different in the perifosine series and tethering an oleyl chain to the phosphate ($\mathbf{P_{C18:1}}$) did not translate into larger lipoplexes. With regard to the structure of the biolabile linker (ester or carbonate series, with or without substitution at the acetal bridge), no general trend could be observed. In the miltefosine series, lipoplexes prepared from acetal esters ($\mathbf{M_{E12}}$, $\mathbf{M_{E'12}}$) and acetal carbonates ($\mathbf{M_{C12}}$, $\mathbf{M_{C'12}}$) did not differ in size, but the introduction of a methyl substituent at the acetal center led to lipoplexes with half the size of those prepared from the unsubstituted compounds. In the perifosine series, acetal substitution had the opposite effect. Considering the pro-erufosine compounds, smaller lipoplexes were obtained

TABLE 1 | Hydrolytic stability of the APL prodrugs.

Compound	H_{120} (%)		$t_{1/2}$ (h)	
	pH 7.4	pH 4.5	pH 7.4	pH 4.5
$\mathbf{M_{12}}$[a]	0	0	–	–
$\mathbf{M_{E12}}$	20	3	–	–
$\mathbf{M_{E'12}}$	89	91	18	17
$\mathbf{M_{C12}}$	11	3	–	–
$\mathbf{M_{C'12}}$	14	13	–	–
$\mathbf{M_{C18:1}}$	15	2	–	–
$\mathbf{P_{12}}$[a]	0	0	–	–
$\mathbf{P_{E12}}$	16	2	–	–
$\mathbf{P_{E'12}}$	60	60	84	90
$\mathbf{P_{C12}}$	6	6	–	–
$\mathbf{E_{12}}$[a]	0	0	–	–
$\mathbf{E_{E12}}$	17	2	–	–
$\mathbf{E_{E'12}}$	56	53	96	104
$\mathbf{E_{C12}}$	8	1	–	–
$\mathbf{E_{C'12}}$	6	5	–	–
$\mathbf{E_{C18:1}}$	10	0	–	–

See ***Supplementary Material*** *for detailed experimental conditions. H_{120} corresponds to the hydrolysis rate that was measured after a 120-h incubation period. Whenever possible, time needed for 50% hydrolysis ($t_{1/2}$) was extrapolated from the experimental data. Data for erufosine prodrugs are reported from the literature (Gaillard et al., 2019).* [a]*no significant hydrolysis was measured after a 31-d incubation period.*

with the biolabile derivatives $\mathbf{E_{E12}}$, $\mathbf{E_{E'12}}$, $\mathbf{E_{C12}}$, and $\mathbf{E_{C'12}}$ as compared to phosphotriester $\mathbf{E_{12}}$ (92–140 *vs.* 194 nm), and substitution at the acetal bridge had no significant effect on the size of the lipoplexes (Gaillard et al., 2019). As could be expected considering electrophoretic behavior, all the pro-APL/DNA complexes displayed a net positive charge at N/P 3, with ζ values spreading from +16 to +54 mV.

The efficacy of the pro-APLs to mediate intracellular delivery of a plasmid DNA was examined in A549 human lung epithelial carcinoma cells using the pCMV-Gluc reporter gene encoding the luciferase of *Gaussia princeps*. This luciferase is secreted by cells and transgene expression can be conveniently assessed by standard bioluminescence measurements on aliquots of the cell culture supernatant, without need for prior cell lysis. Lipoplexes were formulated in glucose 5% at N/P ratios of 1, 3, and 5, with increasing amounts of DOPE as a helper lipid. They were deposited onto cells in the presence of 10% serum and luciferase activity was measured after 24 h (**Figure 3**). A number of general trends emerged. Firstly, lipoplexes prepared at the lower charge ratio (N/P = 1) failed to mediate any significant transgene expression. This was consistent with the results obtained in gel electrophoresis revealing that full complexation of DNA required an excess of cationic lipid (N/P > 1.3–3). Accordingly, increasing the N/P ratio to 3 or 5 allowed for obtaining high transfection rates whatever the pro-APL considered. Secondly, whatever the N/P value, DOPE-free formulations revealed only poorly efficient for mediating transgene expression. The best results were thus generally obtained with 1–2 molar equivalents of the helper lipid whereas higher proportion of DOPE appeared deleterious as evidenced by degraded transfection rates. Thirdly, with regard to the structure of the biolabile linker, pro-APLs in the ester series invariably outperformed those in the carbonate series, and allowed transfection rates that were mostly 3–10 times higher. The only differences in the size of the lipoplexes (*vide supra*), a larger size favoring particle sedimentation and cell uptake (Rejman et al., 2004), cannot explain this effect. These results thus suggest that it is the rate at which the pro-APLs are intracellularly hydrolyzed that has a major impact on the transfection efficiency. On the other hand, the introduction of a methyl substituent on the acetal bridge had mixed effects, depending on the compounds. Most of the time, this modification led to some decrease in the transfection rate. One exception however was observed in the miltefosine series, $\mathbf{M_{C'12}}$ allowing a higher transfection rate than $\mathbf{M_{C12}}$ by a *ca.* 2-fold factor. The influence of the nature of the pendant hydrophobic arm was also examined. In the miltefosine series, $\mathbf{M_{C18:1}}$ showed significantly enhanced transfection properties as compared to $\mathbf{M_{C12}}$. In the perifosine series, the opposite effect was observed and oleyl derivatives performed a little less than dodecyl derivatives. The same trend has been observed in the erufosine series (Gaillard et al., 2019). Finally, pro-APL compounds lacking a biolabile linker, *i.e.,* $\mathbf{M_{12}}$, $\mathbf{P_{12}}$, and $\mathbf{E_{12}}$, were not systematically outperformed by their more labile analogs. This revealed that enhanced biodegradability of the gene carriers did not necessarily translate into higher transgene expression. More important, likely, was where and when the degradation of the vector did occur.

Selecting $\mathbf{M_{E12}}$ and $\mathbf{P_{E12}}$ that performed the best in the previous experiments, a dose-response study was conducted. A549 epithelial cells were exposed to increasing amounts of pCMV-Gluc (from 0.1 to 0.4 μg/well) formulated into lipoplexes (pro-APL/DOPE 1/1) at the N/P ratio of 3. As a general trend, transfection rate reached a plateau at the intermediate pDNA dose of 0.2 μg/well (**Figure 4A**, left). Increasing the dose above this value did not significantly improve the transfection rate, while decreasing cell viability (**Figure 4A**, right). The same behavior was reported with $\mathbf{E_{12}}$ (Gaillard et al., 2019). Similar transfection and cytotoxicity profiles were obtained in two other pulmonary epithelial cell lines (human bronchial epithelial cells 16HBE and human lung mucoepidermoid carcinoma cells H292) (**Figures 4B,C**).

Serum Compatibility

For potential clinical applications, the interaction of positively charged lipoplexes and negatively charged proteins in the bulk medium cannot be ignored (Pouton and Seymour, 2001). Thus, a limitation of gene delivery mediated by cationic non-viral carriers is a drastic decrease of transfection efficiency in the presence of serum proteins forming the so-called "biocorona" around the transfection particles. This protein corona drastically changes the identity of the particles, may provoke their destabilization or inhibit their cell uptake and endosome escape. To investigate the effect of serum on the gene delivery properties of the APL prodrugs, cells were treated with lipoplexes in the presence of an increasing concentration of serum (**Figure 5**). Two DNA doses were considered. As might be expected, transgene expression was decreased with increasing serum concentration though at

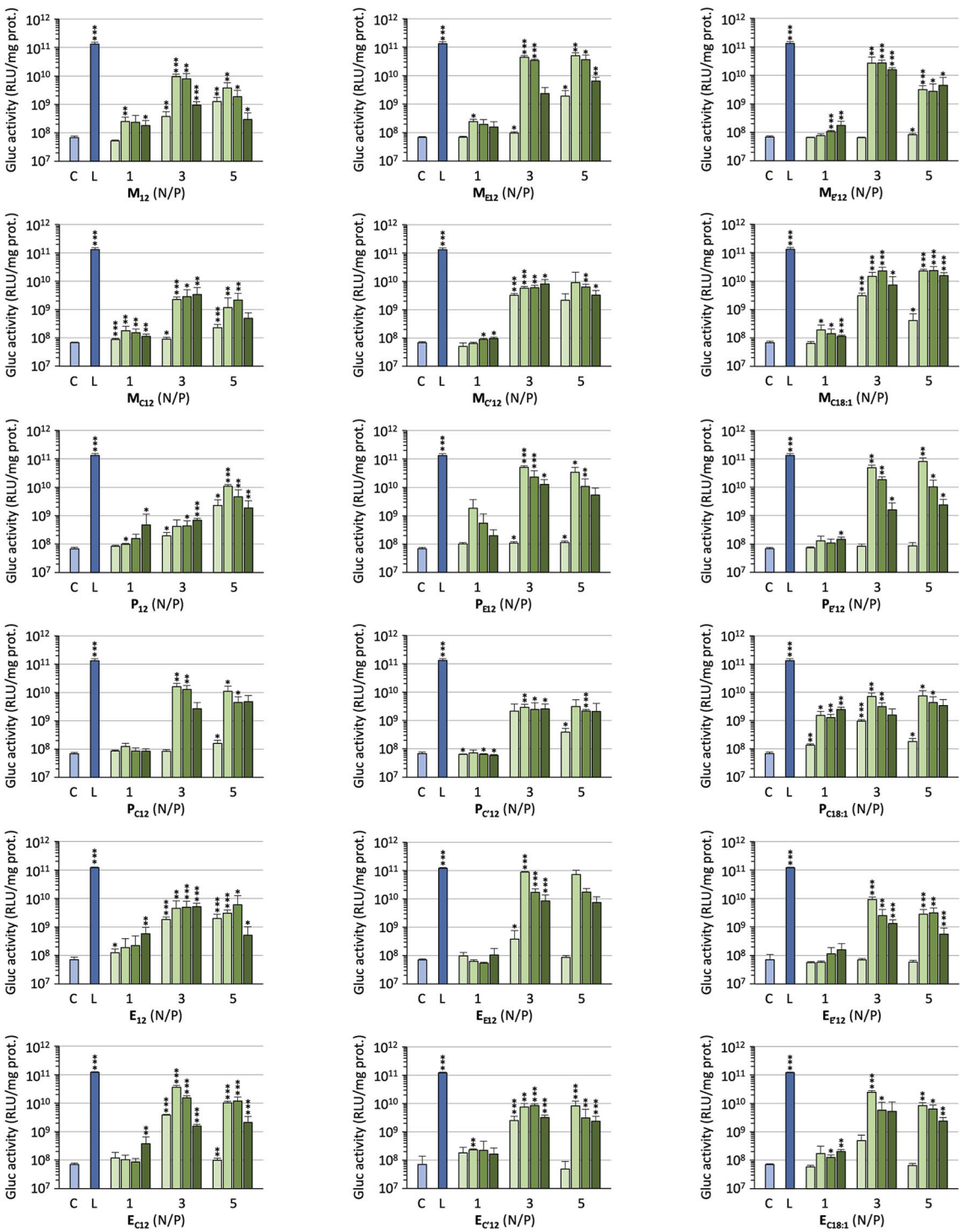

FIGURE 3 | Gene transfer efficiency of pro-APLs in A549 cells. Lipoplexes were prepared by introducing DOPE in the formulations (0, 1, 2, and 3 molar equivalents, from light to dark green, resp.) and varying the N/P ratio from 1 to 5. Control (C) refers to basal bioluminescence measured in untreated cells. Lipofectamine® 2000 (L) was used as a positive control. Data for pro-erufosine compounds are reported from our previous work (Gaillard et al., 2019). Statistical significance *vs*. control. $^{***}p < 0.001$, $^{**}p < 0.01$, $^{*}p < 0.05$.

various rates, depending on the pro-APL compound involved in the formulation. At the lower DNA dose, *i.e.,* 0.2 μg/well, $\mathbf{M_{E12}}$ and $\mathbf{P_{E12}}$ mediated significant transgene expression up to 50% serum, which is about the concentration in blood. At the higher DNA dose, 0.4 μg/well, transfection activity extended up to 75% serum. Besides, though pro-APL $\mathbf{E_{E12}}$ revealed less efficient at the

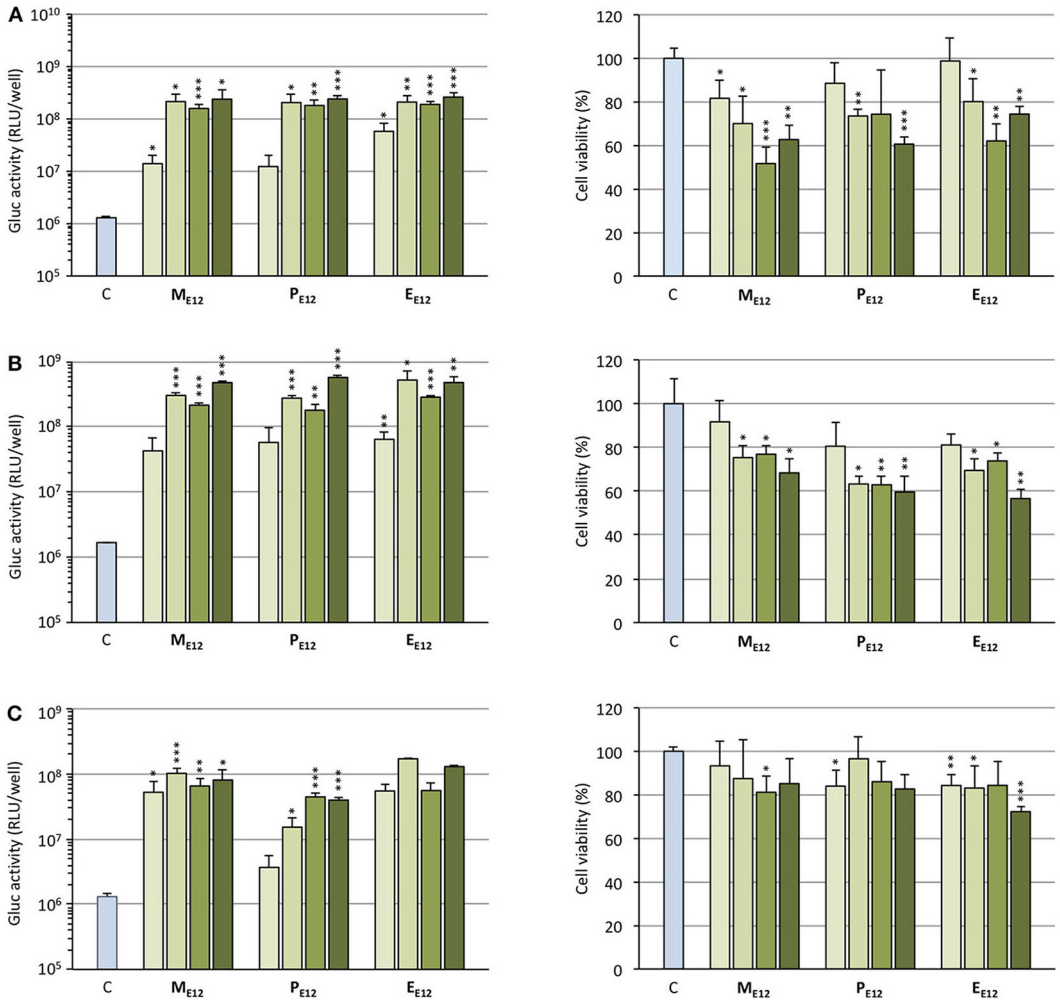

FIGURE 4 | (A) Rate of transfection (left) mediated by pro-APLs in A549 cells with increasing dose of pCMV-Gluc (0.1, 0.2, 0.3, and 0.4 μg/well, from light to dark green, resp.) and cytotoxicity of the transfection particles (right). **(B)** Rate of transfection (left) mediated by pro-APLs in H292 cells, and cytotoxicity of the transfection particles (right). **(C)** Rate of transfection (left) mediated by pro-APLs in 16HBE cells, and cytotoxicity of the transfection particles (right). Transfection experiments were carried out in the presence of 10% serum. Control refers to basal bioluminescence measured in untreated cells. Cell viability was assessed by mitochondrial activity measurements using the MTT assay. Basal mitochondrial activity measured in untreated cells is set at 100%. Data for $\mathbf{E_{E12}}$ are reported from our previous work (Gaillard et al., 2019). Statistical significance *vs.* control. $^{***}p < 0.001$, $^{**}p < 0.01$, $^{*}p < 0.05$.

low DNA dose, it provided the best transfection results at the high DNA dose in 50% serum. These results thus demonstrate that the herein described APL prodrugs are serum compatible nucleic acid carriers that can mediate efficient gene delivery at high serum content.

Self-Assembly Properties

The pro-APL molecules have been specifically engineered so they can be metabolized *in situ* under a biological stimulus to revert to the parent APL with antiproliferative activity. As membrane-active compounds, APLs can disrupt cell membranes or alter cholesterol homeostasis, and thus interfere with various membrane signaling pathways involved in carcinogenesis. It has been shown that the lytic concentration for various APLs in the absence of serum reflects their critical micellar concentration (CMC) (Fleer et al., 1992; Kötting et al., 1992). We thus aimed to determine the self-assembly properties of the APL prodrugs. For that, we applied a pyrene-based fluorescence technique that is commonly used to analyze surfactant micellization (Goddard et al., 1985; Piñeiro et al., 2015). Pyrene is a probe which fluorescence is sensitive to the polarity of the solubilizing medium. Hence, fluorescence emission can be used to detect self-assembly or aggregation of amphiphilic compounds. Due to the introduction of an "additional" hydrophobic element within the original APL structure, pro-APL compounds were expected to display a lower hydrophilic-lipophilic balance (HLB) than the parent APLs and assemble into lamellar structures in aqueous media. Therefore, the term critical aggregation concentration (CAC) is suggested instead of CMC (Parlato et al., 2011). Fluorescence measurements were carried out in ultrapure water

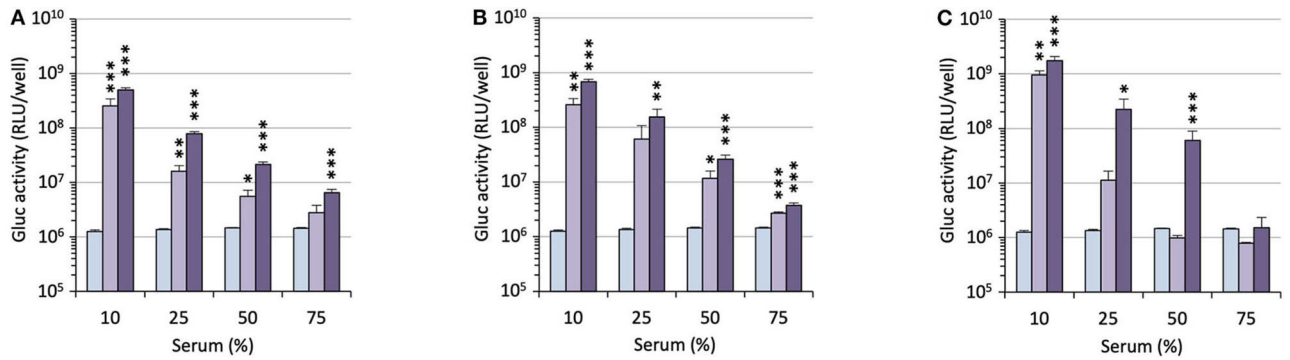

FIGURE 5 | Transfection efficiency of pro-APLs **M_{E12} (A)**, **P_{E12} (B)**, and **E_{E12} (C)** as a function of serum content. Pro-APL/DNA complexes were prepared at N/P 3, with 1 molar eq. of DOPE. A549 cells (6,000 cells/well) were seeded into 96-well plates in 100 μL of culture medium containing 10% serum. Twenty-four hours later, cell supernatant was replaced with culture medium complemented with increasing amounts of serum (from 10 to 75%) just before adding the lipoplexes (0.2 and 0.4 μg of DNA per well; light and deep purple bars, resp.). Control (light blue bar) refers to basal bioluminescence measured in untreated cells. Data for **E_{E12}** are reported from our previous work (Gaillard et al., 2019). Statistical significance *vs.* control. ***$p < 0.001$, **$p < 0.01$, *$p < 0.05$.

and data obtained for the various APLs and their prodrugs are shown in **Table 2**. The CMC measured for miltefosine, perifosine, and erufosine were 11.2, 4.4, and 1.6 μM, respectively. The value determined for miltefosine was consistent with that previously obtained by the Du Noüy ring method (12 μM) (Yaseen et al., 2005) whereas the Langmuir trough method yielded a lower one (2.5–3.0 μM) (Rakotomanga et al., 2004). For perifosine, the CMC value was similar to that determined by the Langmuir trough method (2.5 μM) (Mravljak et al., 2005).

As expected, the transformation of APLs into pro-APLs, by neutralizing the phosphate negative charge and tethering of an additional hydrophobic substituent, translated into a shift of the HLB which resulted in a decrease in the CMC/CAC values. Larger effects were observed in the pro-miltefosine series as compared to the pro-perifosine series. In the pro-erufosine series, lower variations were reported (Gaillard et al., 2019). All this was consistent with the increasing length of the "main" alkyl chain in the APL molecules (miltefosine: C_{16}; perifosine: C_{18}; erufosine: C_{22}). On the other hand, no particular trend could be identified with respect to some relationship between the nature of the labile spacer (*i.e.,* phosphoester *vs.* phosphoacetal, ester *vs.* carbonate, and non-substituted *vs.* substituted acetal) and CAC of the compounds. However, the variations measured were small and accuracy of the pyrene-based technique was limited. Thus, tentatively getting a deeper understanding of the structure-property relationships would require a more precise determination of the CAC values.

Hemolytic Activity

Hemolytic effect is systematically reported for most of the antitumor APLs that have been described so far and makes these compounds incompatible with intravenous administration (Kötting et al., 1992). APLs alter the thermotropic behavior of lipid membranes, increasing their fluidity. In red blood cells (RBC), such an alteration of the plasma membrane induces drastic morphological changes and provokes the release of hemoglobin (Petit et al., 2019). In serum-free conditions, there is a good fit between the hemolytic concentration of APLs and their CMC (Fleer et al., 1992; Kötting et al., 1992). Consequently, decreasing the CMC of APLs by turning them reversibly into derivatives with enhanced hydrophobicity should result in decreasing the hemolytic effect, thus increasing the biocompatibility of the compounds. To evaluate this hypothesis, the hemolytic activity of the APLs and pro-APLs was measured. Sheep RBC were incubated for 1 h with escalating doses of aqueous dispersion of the compounds at 37°C. At the end of the incubation period, hemoglobin leakage was determined spectrophotometrically. As expected, APLs provoked massive hemolysis in a dose-dependent manner. The concentration provoking 50% hemolysis (HC_{50}, calculated by using the best-fit regression curve method) was 43 and 46 μM for miltefosine and perifosine, respectively (**Figure 6**). The HC_{50} value found for miltefosine was consistent with those reported in the literature (41 μM Petit et al., 2019, and 34–51 μM Alonso and Alonso, 2016, depending on the hematocrit). Though other authors have reported *ca.* 30% hemolysis after a 24-h exposure to 5.4 μM perifosine (Egler and Lang, 2017), a direct correlation with our results was difficult, due to significant differences in the experimental conditions.

Under the same incubation conditions as those used for APL analysis, hemolytic effect of the APL prodrugs was substantially lower. **Table 3** displays the hemolytic activity of the compounds at 200 μM (HA_{200}) after a 1-h incubation. In most cases, < 10–20% hemolysis was measured. Thus, in order to better characterize the hemolytic effect of the pro-APLs, the incubation period has been extended and release of hemoglobin was measured after 24 h. Even under these more challenging conditions, the APL prodrugs revealed poorly harmful to RBC and significant hemolysis (> 20%) was measured only at a concentration above *ca.* 50–100 μM (**Figure 7**). The corresponding HA_{200} values are presented in **Table 3**. The direct correlation between the structure of the biolabile linker in the pro-APL molecules and their hemolytic effect (SAR analysis) is especially difficult due to the unique biodegradability profile of

TABLE 2 | CMC of APLs and CAC of pro-APLs as measured using a fluorescent probe technique.

Compound	CAC (μM)	Compound	CAC (μM)	Compound	CAC (μM)
Miltefosine	11.2 ± 2.3	Perifosine	4.4 ± 1.7	Erufosine	1.6 ± 0.5
$\mathbf{M_{12}}$	1.1 ± 0.6	$\mathbf{P_{12}}$	1.2 ± 0.4	$\mathbf{E_{12}}$	0.7 ± 0.3
$\mathbf{M_{E12}}$	4.3 ± 2.5	$\mathbf{P_{E12}}$	2.9 ± 1.0	$\mathbf{E_{E12}}$	0.6 ± 0.2
$\mathbf{M_{E'12}}$	1.3 ± 0.7	$\mathbf{P_{E'12}}$	2.3 ± 1.4	$\mathbf{E_{E'12}}$	1.1 ± 0.7
$\mathbf{M_{C12}}$	4.1 ± 2.5	$\mathbf{P_{C12}}$	4.5 ± 1.6	$\mathbf{E_{C12}}$	1.2 ± 0.2
$\mathbf{M_{C'12}}$	2.0 ± 0.7	$\mathbf{P_{C'12}}$	3.3 ± 0.7	$\mathbf{E_{C'12}}$	0.9 ± 0.2
$\mathbf{M_{C18:1}}$	0.9 ± 0.4	$\mathbf{P_{C18:1}}$	2.3 ± 1.0	$\mathbf{E_{C18:1}}$	0.8 ± 0.4

Data for erufosine and erufosine prodrugs are reported from the literature (Gaillard et al., 2019).

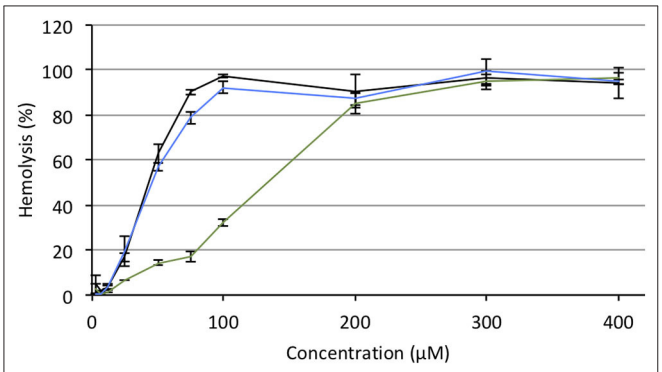

FIGURE 6 | Hemolytic effect of miltefosine (black), perifosine (blue), and erufosine (green) on sheep RBC incubated at 37°C for 1 h, as a function of the APL concentration.

TABLE 3 | Hemolytic activity of the APLs and pro-APLs (200 μM) upon incubation with sheep RBC for 24 h at 37°C.

Compound	HA_{200} (%)	
	1 h	24 h
Miltefosine	90.8 ± 1.5	n.d.
$\mathbf{M_{12}}$	13.1 ± 1.0	63.9 ± 8.1
$\mathbf{M_{E12}}$	18.0 ± 1.2	103.2 ± 3.6
$\mathbf{M_{E'12}}$	n.d.	101.7 ± 1.8
$\mathbf{M_{C12}}$	6.0 ± 1.4	59.7 ± 5.4
$\mathbf{M_{C'12}}$	21.5 ± 2.3	70.8 ± 4.4
$\mathbf{M_{C18:1}}$	1.3 ± 1.2	12.5 ± 2.8
Perifosine	85.1 ± 4.0	n.d.
$\mathbf{P_{12}}$	8.1 ± 0.9	35.7 ± 4.1
$\mathbf{P_{E12}}$	7.1 ± 0.9	20.6 ± 5.9
$\mathbf{P_{E'12}}$	n.d.	80.1 ± 0.2
$\mathbf{P_{C12}}$	< 1	60.7 ± 2.2
$\mathbf{P_{C'12}}$	< 1	24.4 ± 7.6
$\mathbf{P_{C18:1}}$	n.d.	n.d.
Erufosine	84.9 ± 4.5	n.d.
$\mathbf{E_{12}}$	1.9 ± 0.7	12.0 ± 1.9
$\mathbf{E_{E12}}$	< 1	18.6 ± 1.5
$\mathbf{E_{E'12}}$	n.d.	25.3 ± 2.6
$\mathbf{E_{C12}}$	< 1	9.6 ± 2.3
$\mathbf{E_{C'12}}$	< 1	7.3 ± 0.8
$\mathbf{E_{C18:1}}$	< 1	20.9 ± 2.5

Data for erufosine and erufosine prodrugs are reported from the literature (Gaillard et al., 2019). n.d.: not determined.

each compound, so no general trend was identified. Nevertheless, our data show that the pro-APLs display drastically reduced hemolytic effect as compared to the parent APLs. Especially, it is worth to note that hemolysis provoked by miltefosine and perifosine prodrugs after 24 h was much lower in most cases than that induced by erufosine after 1 h, and erufosine prodrugs were practically devoid of any hemolytic activity (HA_{200} < 25%, after 24 h). As erufosine is the only APL currently considered for intravenous administration (Bagley et al., 2011), it can be concluded that all the prodrugs of miltefosine and perifosine described herein could be safely qualified for this administration route.

Cytotoxicity

The cytotoxicity of APLs does not just have to do with the ability of these compounds to destabilize lipid membranes and lyse cells. There is broad agreement that, at concentrations that are pharmacologically relevant, APLs modify the cell membrane fluidity and interfere with the metabolism of phospholipids and homeostasis of cholesterol, hence provoking perturbations in various signal transduction pathways, some of which are essential for cell functioning, survival and proliferation (Ríos-Marco et al., 2017). In order to evaluate the antiproliferative potency of the pro-APL compounds, a dose-response study was conducted in the three human pulmonary epithelial cell lines considered in this study: A549 (alveolar carcinoma epithelial cells), H292 (mucoepidermoid carcinoma cells), and 16HBE (bronchial epithelial cells). The cells were exposed for a 24-h period to increasing concentration of the pro-APLs, ranging from 500 nM to 1 mM, and cell viability was assessed using the MTT colorimetric assay (Mosmann, 1983). For the three cell lines, viability decreased in a dose-dependent manner in response to APLs and pro-APLs (**Supplementary Figures 2–4**). Using the best-fit regression curve method, the IC_{50} value (concentration that provokes 50% inhibition of the cell growth) was calculated for each compound (**Table 4**). The three cell lines responded to the compounds with varying sensitivities. The IC_{50} values extended from 39 to 326 μM for A549 cells, from 46 to 295 μM for H292 cells, and from 19 to 257 μM for non-cancerous 16HBE cells. The cell toxicity of the APL prodrugs did not correlate with their hydrolytic susceptibility as determined above by the ^{31}P-NMR measurements in an "enzyme-free" model. This is attributed to enzyme-mediated hydrolysis of the pro-APL compounds in the complemented culture medium or in the intracellular compartment, competing with pure pH-controlled chemical hydrolysis. According to its structure, a pro-APL may or not be a substrate for specific lipases and, thus, may or not be hydrolyzed into the parent cytotoxic compound. Also, no direct correlation could be

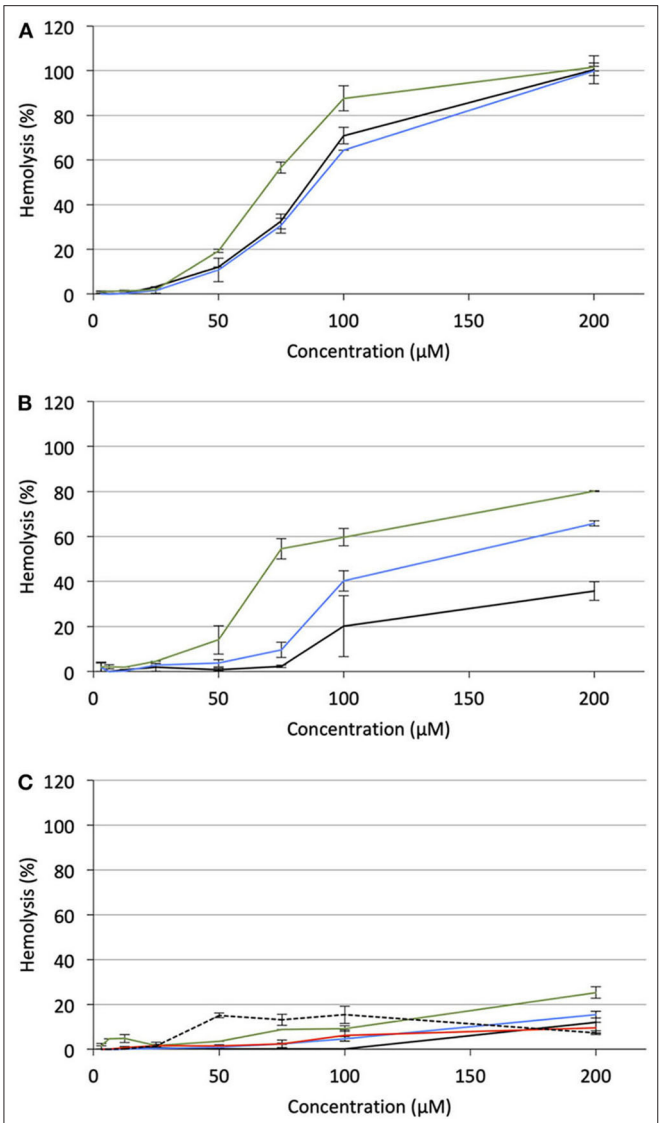

FIGURE 7 | Hemolytic effect of pro-APL compounds on sheep RBC incubated at 37°C for 24 h, as a function of the prodrug concentration. **(A)** Pro-miltefosine series ($\mathbf{M_{12}}$: black; $\mathbf{M_{E12}}$: blue; $\mathbf{M_{E'12}}$: green). **(B)** Pro-perifosine series ($\mathbf{P_{12}}$: black; $\mathbf{P_{E12}}$: blue; $\mathbf{P_{E'12}}$: green). **(C)** Pro-erufosine series ($\mathbf{E_{12}}$: black; $\mathbf{E_{E12}}$: blue; $\mathbf{E_{E'12}}$: green; $\mathbf{E_{C12}}$: red; $\mathbf{E_{C'12}}$: dashed).

found between aggregation properties (CAC) and IC_{50} values, supporting that cytotoxicity of APLs and pro-APLs did not solely express through the membrane disrupting properties of the compounds or of their hydrolysis product. Nevertheless, a marked cytotoxicity was occasioned by all the pro-APL compounds that roughly compared to that of the parent APLs, revealing that the prodrugs were productively metabolized into APLs, although not at the same rate. In the case of miltefosine and perifosine, some of the prodrugs were more potent than the parent compounds and some were less, results varying from one cell line to another. With respect to the erufosine prodrugs, although they all revealed highly cytotoxic, none of them did perform better than erufosine itself, as was previously reported (Gaillard et al., 2019).

TABLE 4 | Antitumor activity of APLs and APL prodrugs.

Compound	IC_{50} (μM)		
	A549	H292	16HBE
Miltefosine	77 ± 15	70 ± 9	73 ± 8
$\mathbf{M_{12}}$	46 ± 11	56 ± 7	107 ± 14
$\mathbf{M_{E12}}$	39 ± 7	52 ± 28	69 ± 26
$\mathbf{M_{E'12}}$	139 ± 32	59 ± 10	49 ± 6
$\mathbf{M_{C12}}$	151 ± 42	81 ± 29	62 ± 15
$\mathbf{M_{C'12}}$	48 ± 15	146 ± 37	66 ± 27
$\mathbf{M_{C18:1}}$	92 ± 22	135 ± 41	50 ± 12
Perifosine	127 ± 39	77 ± 3	116 ± 33
$\mathbf{P_{12}}$	56 ± 7	63 ± 5	72 ± 7
$\mathbf{P_{E12}}$	139 ± 4	168 ± 7	231 ± 70
$\mathbf{P_{E'12}}$	148 ± 38	116 ± 25	60 ± 5
$\mathbf{P_{C12}}$	89 ± 24	73 ± 17	82 ± 33
$\mathbf{P_{C'12}}$	189 ± 52	295 ± 33	145 ± 34
$\mathbf{P_{C18:1}}$	273 ± 69	186 ± 42	207 ± 49
Erufosine	57 ± 8	46 ± 8	19 ± 3
$\mathbf{E_{12}}$	81 ± 7	124 ± 11	225 ± 31
$\mathbf{E_{E12}}$	151 ± 42	125 ± 26	144 ± 66
$\mathbf{E_{E'12}}$	192 ± 44	73 ± 15	63 ± 7
$\mathbf{E_{C12}}$	161 ± 21	167 ± 56	252 ± 112
$\mathbf{E_{C'12}}$	179 ± 63	161 ± 25	257 ± 81
$\mathbf{E_{C18:1}}$	326 ± 36	154 ± 40	238 ± 58

The IC_{50} values were determined in various cell lines exposed to the compounds for 24 h at 37°C, using the MTT assay. Data for erufosine and erufosine prodrugs are reported from the literature (Gaillard et al., 2019).

Combined Antitumor Activity of TRAIL and APL Prodrugs

In order to investigate the potential of APL prodrugs in combined antitumor therapy, we performed gene delivery experiments with pUNO1-hTRAIL. This plasmid DNA encodes the tumor necrosis factor-related apoptosis-inducing ligand (TRAIL), a member of the tumor necrosis factor (TNF) superfamily (Shi et al., 2018). TRAIL suppresses tumor growth by a direct and specific mechanism without affecting normal tissues (Walczak et al., 1999; Nair et al., 2015). Interestingly, perifosine and edelfosine, another compound related to the APL family, have been reported to sensitize cells to TRAIL-induced apotosis (Gajate and Mollinedo, 2007; Lim et al., 2016). This, however, has not been demonstrated for other APLs so far. Expression of the TRAIL receptors in the three cell lines considered herein has been assessed elsewhere (Azijli et al., 2014; Gaillard et al., 2019). Both TRAIL death receptors, TRAIL-R1 and TRAIL-R2, were found expressed in the cell lines, in comparable amounts, except for TRAIL-R1 which expression in A549 cells is higher. Among the TRAIL decoy receptors that may impair TRAIL activity, *i.e.,* TRAIL-R3 and TRAIL-R4, TRAIL-R3 was found in H292 and 16HBE cells, but not in A549 cells, while TRAIL-R4 was missing

in the three cell lines. To sum up, the selected cells may stand as suitable models for gene delivery experiments with a pDNA encoding TRAIL for apoptosis induction.

Cells were treated with lipoplexes prepared from pro-APLs $\mathbf{M_{E12}}$, $\mathbf{P_{E12}}$, and $\mathbf{E_{E12}}$, with increasing dose of pDNA (0.1–0.4 μg per well). The gold standard gene delivery reagent Lipofectamine® 2000 was assayed in parallel for comparison purpose. In order to distinguish the intrinsic cytotoxic effect of the *in situ* generated APLs from that resulting from TRAIL expression, pCMV-Gluc was assayed in parallel to pUNO1-hTRAIL. Using pCMV-Gluc, the observed cytotoxicity was assumed to result only from the APL antiproliferative activity, whereas results obtained with pUNO1-hTRAIL are a combination of TRAIL activity and APL antiproliferative effect. Besides, monitoring of luciferase expression allowed assessing the transfection efficiency with the various carriers in the three cell lines (**Figure 4**), suggesting that replacement of the plasmid DNA coding for luciferase with pUNO1-hTRAIL should indeed result in significant TRAIL expression. As a general trend, a slow decrease in cell viability was observed with pUNO1-hTRAIL, as compared to pCMV-Gluc (**Figure 8**). Though the temptation is to take it as an indicator that functional TRAIL was produced, the difference found was not always statistically significant. The activity profile of the three pro-APLs varied according to the cell line. In A549 cells that are poorly sensitive to TRAIL (Azijli et al., 2014), no significant cytotoxic effect of the transgene expression product was evidenced, except for the pro-erufosine-based lipoplexes. Indeed, at the high pDNA doses (0.3 and 0.4 μg/well), $\mathbf{E_{E12}}$ led to 15-17% of TRAIL-induced cell death. The H292 cell line was much more sensitive to TRAIL, right from the lower dose of transgene and regardless of the pro-APL. This was consistent with previous reports in the literature describing the high sensitivity of H292 cells to TRAIL (Azijli et al., 2014). Depending on the pro-APL used to deliver the plasmid, cell death specifically induced by TRAIL could reach *ca.* 45%, and the higher score was attained with the pro-perifosine compound, $\mathbf{P_{E12}}$, in this cell line. In any case, the lipoplexes incorporating the plasmid encoding TRAIL led to a decrease in viability mostly below 50-55%, whatever the pro-APL used. On the other hand, no such effect was observed with Lipofectamine®, though only the lower DNA dose (0.1 μg/well) was assayed in this case, due to the high intrinsic cytotoxicity of the reagent that likely overwrite TRAIL activity. Finally, given their non-tumor origin, 16HBE cells were not affected by TRAIL and no specific cell toxicity was observed upon treatment with pUNO1-hTRAIL. Summing up, the combination of the APL prodrugs and pUNO1-hTRAIL revealed harmful to A549 and H292 carcinoma cells (cell death > 40–50%) while preserving normal 16HBE cells (cell death < 25%), and the two pro-miltefosine and pro-perifosine compounds, $\mathbf{M_{E12}}$ and $\mathbf{P_{E12}}$, did perform as well as or better than the previously described erufosine prodrug $\mathbf{E_{E12}}$.

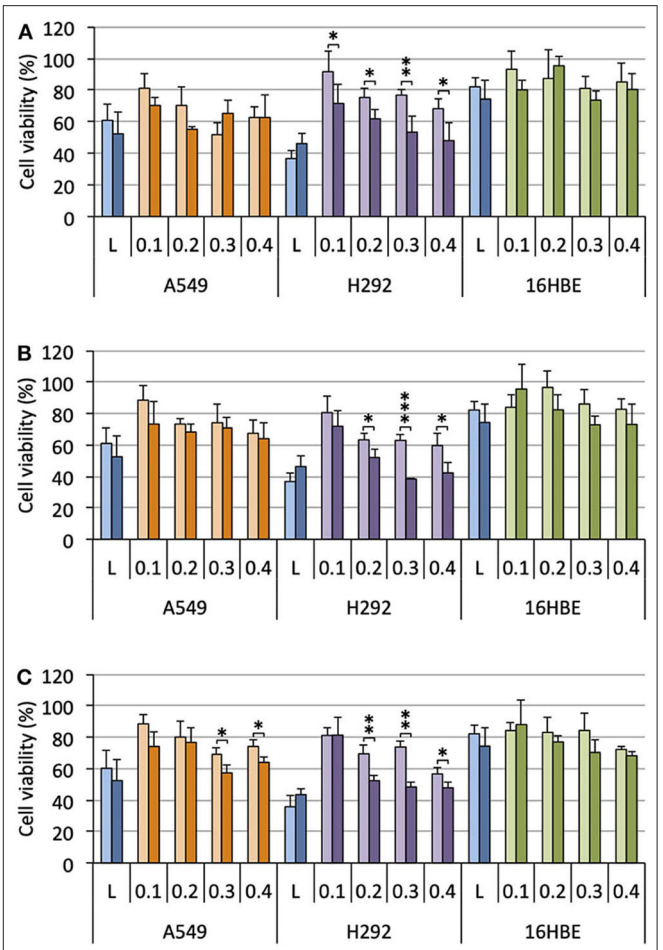

FIGURE 8 | Antiproliferative effect of lipoplexes prepared from $\mathbf{M_{E12}}$ **(A)**, $\mathbf{P_{E12}}$ **(B)**, $\mathbf{E_{E12}}$ **(C)**, and the two DNA plasmids pCMV-Gluc (light bars) and pUNO1-hTRAIL (dark bars), on the three cell lines. The lipid/pDNA complexes were formulated at N/P 3 with 1 molar eq. of DOPE, and an increasing pDNA dose (from 0.1 to 0.4 μg/well). Lipofectamine®-based lipoplexes (0.1 μg plasmid/well) were prepared according to the optimized experimental conditions determined following the supplier's instructions. Cell viability was measured by the MTT assay. Basal mitochondrial activity measured in untreated cells is set at 100%.

CONCLUSION

In this study, biolabile miltefosine- and perifosine-based cationic lipids were engineered and their properties as gene carriers and antineoplastic prodrugs were investigated in normal and carcinoma cells. Transfection efficiency was optimized varying the charge ratio of the lipoplexes and their DOPE content. Significant serum resistance of the lipoplexes was demonstrated, the pro-APLs maintaining a high transfection rate even at a serum content above 50%. Contrary to the parent compounds miltefosine and perifosine, the pro-APLs did not show any hemolytic activity which is a dose-limiting side effect of the APLs in antitumor therapy. All the pro-APLs investigated herein displayed cytotoxic effects in the same concentration range as the parent APLs, revealing that they were properly metabolized into APLs. Finally, gene delivery experiments with a DNA plasmid encoding TRAIL that can trigger apoptosis in a wide variety of cancer cells, but not in normal cells, provided a proof of concept for a new promising

strategy for cancer therapy combining gene therapy and APL-based chemotherapy.

DATA AVAILABILITY STATEMENT

All datasets generated for this study are included in the article/**Supplementary Material**.

AUTHOR CONTRIBUTIONS

LL designed the research and wrote the manuscript with editorial input from J-SR and FP. LL and BG performed the chemical synthesis experiments. BG performed the biological experiments under J-SR, FP, and LL supervision. All authors contributed to the article and approved the submitted version.

FUNDING

BG acknowledges his doctoral fellowship from the Conseil Régional d'Alsace, Labex Medalis, and Alsace contre le cancer.

ACKNOWLEDGMENTS

The authors gratefully acknowledge Alexandra Bert and Thomas Schoeps for technical support.

SUPPLEMENTARY MATERIAL

The Supplementary Material for this article can be found online at: https://www.frontiersin.org/articles/10.3389/fchem.2020.581260/full#supplementary-material

REFERENCES

Alam, M. M., Hassan, A. H. E., Kwon, Y. H., Lee, H. J., Kim, N. Y., Min, K. H., et al. (2018). Design, synthesis and evaluation of alkylphosphocholine-gefitinib conjugates as multitarget anticancer agents. *Arch. Pharm. Res.* 41, 35–45. doi: 10.1007/s12272-017-0977-z

Alam, M. M., Hassan, A. H. E., Lee, K. W., Cho, M. C., Yang, J. S., Song, J., et al. (2019). Design, synthesis and cytotoxicity of chimeric erlotinib-alkylphospholipid hybrids. *Bioorg. Chem.* 84, 51–62. doi: 10.1016/j.bioorg.2018.11.021

Alonso, L., and Alonso, A. (2016). Hemolytic potential of miltefosine is dependent on cell concentration: implications for *in vitro* cell cytotoxicity assays and pharmacokinetic data. *Biochim. Biophys. Acta* 1858, 1160–1164. doi: 10.1016/j.bbamem.2016.03.004

Azijli, K., van Roosmalen, I. A. M., Smit, J., Pillai, S., Fukushima, M., de Jong, S., et al. (2014). The novel thymidylate synthase inhibitor trifluorothymidine (TFT) and TRAIL synergistically eradicate non-small cell lung cancer cells. *Cancer Chemother. Pharmacol.* 73, 1273–1283. doi: 10.1007/s00280-014-2465-1

Bagley, R. G., Kurtzberg, L., Rouleau, C., Yao, M., and Teicher, B. A. (2011). Erufosine, an alkylphosphocholine, with differential toxicity to human cancer cells and bone marrow cells. *Cancer Chemother. Pharmacol.* 68, 1537–1546. doi: 10.1007/s00280-011-1658-0

Belka, C., Jendrossek, V., Pruschy, M., Vink, S., Verheij, M., and Budach, W. (2004). Apoptosis-modulating agents in combination with radiotherapy-current status and outlook. *Int. J. Rad. Oncol. Biol. Phys.* 58, 542–554. doi: 10.1016/j.ijrobp.2003.09.067

Bendell, J. C., Nemunaitis, J., Vukelja, S. J., Hagenstad, C., Campos, L. T., Hermann, R. C., et al. (2011). Randomized placebo-controlled phase II trial of perifosine plus capecitabine as second- or third-line therapy in patients with metastatic colorectal cancer. *J. Clin. Oncol.* 29, 4394–4400. doi: 10.1200/JCO.2011.36.1980

Cevc, G. (1991). Isothermal lipid phase transitions. *Chem. Phys. Lipids* 57, 293–307. doi: 10.1016/0009-3084(91)90082-M

de Almeida Pachioni, J., Magalhães, J. G., Lima, E. J. C., de Moura Bueno, L., Barbosa, J. F., de Sá, M. M., et al. (2013). Alkylphospholipids – A promising class of chemotherapeutic agents with a broad pharmacological spectrum. *J. Pharm. Pharm. Sci.* 16, 742–759. doi: 10.18433/J3CW23

Egler, J., and Lang, F. (2017). Triggering of eryptosis, the suicidal erythrocyte death, by perifosine. *Cell. Physiol. Biochem.* 41, 2534–2544. doi: 10.1159/000475977

Elrod, H. A., Lin, Y. D., Yue, P., Wang, X., Lonial, S., Khuri, F. R., et al. (2007). The alkylphospholipid perifosine induces apoptosis of human lung cancer cells requiring inhibition of Akt and activation of the extrinsic apoptotic pathway. *Mol. Cancer Ther.* 6, 2029–2038. doi: 10.1158/1535-7163.MCT-07-0004

Farquhar, D., Srivastva, D. N., Kuttesch, N. J., and Saunders, P. P. (1983). Biologically reversible phosphate-protective groups. *J. Pharm. Sci.* 72, 324–325. doi: 10.1002/jps.2600720332

Fleer, E. A. M., Berkovic, D., Unger, C., and Eibl, H. (1992). Cellular uptake and metabolic-fate of hexadecylphosphocholine. *Prog. Exp. Tumor Res.* 34, 33–46. doi: 10.1159/000420830

Fu, S., Hennessy, B. T., Ng, C. S., Ju, Z., Coombes, K. R., Wolf, J. K., et al. (2012). Perifosine plus docetaxel in patients with platinum and taxane resistant or refractory high-grade epithelial ovarian cancer. *Gynecol. Oncol.* 126, 47–53. doi: 10.1016/j.ygyno.2012.04.006

Gaillard, B., Remy, J. S., Pons, F., and Lebeau, L. (2019). Cationic erufosine (ErPC3) prodrugs as gene delivery reagents for antitumor combined therapy. *Chem. Eur. J.* 25, 15662–15679. doi: 10.1002/chem.201903976

Gaillard, B., Remy, J. S., Pons, F., and Lebeau, L. (2020). Synthesis and evaluation of antitumor alkylphospholipid prodrugs. *Pharm. Res.* 37:106. doi: 10.1007/s11095-020-02830-y

Gajate, C., and Mollinedo, F. (2007). Edelfosine and perifosine induce selective apoptosis in multiple myeloma by recruitment of death receptors and downstream signaling molecules into lipid rafts. *Blood* 109, 711–719. doi: 10.1182/blood-2006-04-016824

Gee, J. M. W., Howell, A., Gullick, W. J., Benz, C. C., Sutherland, R. L., Santen, R. J., et al. (2005). Consensus statement. *Endocr. Relat. Cancer* 12, S1–S7. doi: 10.1677/erc.1.01054

Georgieva, M. C., Konstantinov, S. M., Topashka-Ancheva, M., and Berger, M. R. (2002). Combination effects of alkylphosphocholines and gemcitabine in malignant and normal hematopoietic cells. *Cancer Lett.* 182, 163–174. doi: 10.1016/S0304-3835(02)00088-5

Goddard, E. D., Turro, N. J., Kuo, P. L., and Ananthapadmanabhan, K. P. (1985). Fluorescence probes for critical micelle concentration determination. *Langmuir* 1, 352–355. doi: 10.1021/la00063a015

Gojo, I., Perl, A., Luger, S., Baer, M. R., Norsworthy, K. J., Bauer, K. S., et al. (2013). Phase I study of UCN-01 and perifosine in patients with relapsed and refractory acute leukemias and high-risk myelodysplastic syndrome. *Invest. New Drugs* 31, 1217–1227. doi: 10.1007/s10637-013-9937-8

Guidetti, A., Carlo-Stella, C., Locatelli, S. L., Malorni, W., Mortarini, R., Viviani, S., et al. (2014). Phase II study of perifosine and sorafenib dual-targeted therapy in patients with relapsed or refractory lymphoproliferative diseases. *Clin. Cancer Res.* 20, 5641–5651. doi: 10.1158/1078-0432.CCR-14-0770

Heyes, J. A., Niculescu-Duvaz, D., Cooper, R. G., and Springer, C. J. (2002). Synthesis of novel cationic lipids: effect of structural modification on the efficiency of gene transfer. *J. Med. Chem.* 45, 99–114. doi: 10.1021/jm010918g

Huang, W., Chen, L. Q., Kang, L., Jin, M. J., Sun, P., Xin, X., et al. (2017). Nanomedicine-based combination anticancer therapy between nucleic acids and small-molecular drugs. *Adv. Drug Deliv. Rev.* 115, 82–97. doi: 10.1016/j.addr.2017.06.004

Hui, S. W., Langner, M., Zhao, Y. L., Ross, P., Hurley, E., and Chan, K. (1996). The role of helper lipids in cationic liposome-mediated gene transfer. *Biophys. J.* 71, 590–599. doi: 10.1016/S0006-3495(96)79309-8

Jaffrès, P. A., Gajate, C., Bouchet, A. M., Couthon-Gourvès, H., Chantôme, A., Potier-Cartereau, M., et al. (2016). Alkyl ether lipids, ion channels and lipid raft reorganization in cancer therapy. *Pharmacol. Ther.* 165, 114–131. doi: 10.1016/j.pharmthera.2016.06.003

Juliano, R. L. (2018). Intracellular trafficking and endosomal release of oligonucleotides: what we know and what we do not. *Nucl. Acid Ther.* 28, 166–177. doi: 10.1089/nat.2018.0727

Kostadinova, A., Topouzova-Hristova, T., Momchilova, A., Tzoneva, R., and Berger, M. R. (2015). Antitumor lipids - structure, functions, and medical applications. *Adv. Protein Chem. Struct. Biol.* 101, 27–66. doi: 10.1016/bs.apcsb.2015.08.001

Kötting, J., Marschner, N. W., Neumuller, W., Unger, C., and Eibl, H. (1992). Hexadecylphosphocholine and octadecyl-methyl-glycero-3-phosphocholine: a comparison of hemolytic activity, serum binding and tissue distribution. *Prog. Exp. Tumor Res.* 34, 131–142. doi: 10.1159/000420838

Lee, H. J., Zhuang, G. L., Cao, Y., Du, P., Kim, H. J., and Settleman, J. (2014). Drug resistance via feedback activation of Stat3 in oncogene-addicted cancer cells. *Cancer Cell* 26, 207–221. doi: 10.1016/j.ccr.2014.05.019

Lim, S. C., Parajuli, K. R., and Han, S. I. (2016). The alkyllysophospholipid edelfosine enhances TRAIL-mediated apoptosis in gastric cancer cells through death receptor 5 and the mitochondrial pathway. *Tumor Biol.* 37, 6205–6216. doi: 10.1007/s13277-015-4485-9

Lukashev, A. N., and Zamyatnin, A. A. (2016). Viral vectors for gene therapy: current state and clinical perspectives. *Biochem. Moscow* 81, 700–708. doi: 10.1134/S0006297916070063

Markova, A. A., Plyavnik, N. V., Morozova, N. G., Maslov, M. A., and Shtil, A. A. (2014). Antitumor phosphate-containing lipids and non-phosphorus alkyl cationic glycerolipids: chemical structures and perspectives of drug development. *Russ. Chem. Bull.* 63, 1081–1087. doi: 10.1007/s11172-014-0552-4

Mosmann, T. (1983). Rapid colorimetric assay for cellular growth and survival: application to proliferation and cytotoxicity assays. *J. Immunol. Methods* 65, 55–63. doi: 10.1016/0022-1759(83)90303-4

Mravljak, J., Reiner, Z., and Pečar, S. (2005). Synthesis and biological evaluation of spin-labeled alkylphospholipid analogs. *J. Med. Chem.* 48, 6393–6399. doi: 10.1021/jm050189v

Mukherjee, S., Soe, T. T., and Maxfield, F. R. (1999). Endocytic sorting of lipid analogues differing solely in the chemistry of their hydrophobic tails. *J. Cell Biol.* 144, 1271–1284. doi: 10.1083/jcb.144.6.1271

Nair, P. M., Flores, H., Gogineni, A., Marsters, S., Lawrence, D. A., Kelley, R. F., et al. (2015). Enhancing the antitumor efficacy of a cell-surface death ligand by covalent membrane display. *Proc. Natl. Acad. Sci. U.S.A.* 112, 5679–5684. doi: 10.1073/pnas.1418962112

Naldini, L. (2015). Gene therapy returns to centre stage. *Nature* 526, 351–360. doi: 10.1038/nature15818

Parlato, M. C., Jee, J. P., Teshite, M., and Mecozzi, S. (2011). Synthesis, characterization, and applications of hemifluorinated dibranched amphiphiles. *J. Org. Chem.* 76, 6584–6591. doi: 10.1021/jo200835y

Petit, K., Suwalsky, M., Colina, J. R., Aguilar, L. F., Jemiola-Rzeminska, M., and Strzalka, K. (2019). *In vitro* effects of the antitumor drug miltefosine on human erythrocytes and molecular models of its membrane. *Biochim. Biophys. Acta* 1861, 17–25. doi: 10.1016/j.bbamem.2018.10.009

Pierrat, P., Casset, A., Didier, P., Kereselidze, D., Lux, M., Pons, F., et al. (2016a). Cationic DOPC-detergent conjugates for safe and efficient *in vitro* and *in vivo* nucleic acid delivery. *ChemBioChem* 17, 1771–1783. doi: 10.1002/cbic.201600302

Pierrat, P., Casset, A., Kereselidze, D., Lux, M., Pons, F., and Lebeau, L. (2016b). DOPC-detergent conjugates: fusogenic carriers for improved *in vitro* and *in vivo* gene delivery. *Macromol. Biosci.* 16, 984–989. doi: 10.1002/mabi.201600012

Pierrat, P., Creusat, G., Laverny, G., Pons, F., Zuber, G., and Lebeau, L. (2012). A cationic phospholipid-detergent conjugate as a new efficient carrier for siRNA delivery. *Chem. Eur. J.* 18, 3835–3839. doi: 10.1002/chem.201103645

Pierrat, P., Kereselidze, D., Lux, M., Lebeau, L., and Pons, F. (2016c). Enhanced gene delivery to the lung using biodegradable polyunsaturated cationic phosphatidylcholine-detergent conjugates. *Int. J. Pharm.* 511, 205–218. doi: 10.1016/j.ijpharm.2016.07.012

Pierrat, P., Kereselidze, D., Wehrung, P., Zuber, G., Pons, F., and Lebeau, L. (2013a). Bioresponsive deciduous-charge amphiphiles for liposomal delivery of DNA and siRNA. *Pharm. Res.* 30, 1362–1379. doi: 10.1007/s11095-013-0976-9

Pierrat, P., Laverny, G., Creusat, G., Wehrung, P., Strub, J. M., VanDorsselaer, A., et al. (2013b). Phospholipid-detergent conjugates as novel tools for siRNA delivery. *Chem. Eur. J.* 19, 2344–2355. doi: 10.1002/chem.201203071

Piñeiro, L., Novo, M., and Al-Soufi, W. (2015). Fluorescence emission of pyrene in surfactant solutions. *Adv. Colloid Interface Sci.* 215, 1–12. doi: 10.1016/j.cis.2014.10.010

Pouton, C. W., and Seymour, L. W. (2001). Key issues in non-viral gene delivery. *Adv. Drug Deliv. Rev.* 46, 187–203. doi: 10.1016/s0169-409x(00)00133-2

Rakotomanga, M., Loiseau, P. M., and Saint-Pierre-Chazalet, M. (2004). Hexadecylphosphocholine interaction with lipid monolayers. *Biochim. Biophys. Acta* 1661, 212–218. doi: 10.1016/j.bbamem.2004.01.010

Rehman, Z. U., Zuhorn, I. S., and Hoekstra, D. (2013). How cationic lipids transfer nucleic acids into cells and across cellular membranes: recent advances. *J. Control Release* 166, 46–56. doi: 10.1016/j.jconrel.2012.12.014

Rejman, J., Oberle, V., Zuhorn, I. S., and Hoekstra, D. (2004). Size-dependent internalization of particles via the pathways of clathrin-and caveolae-mediated endocytosis. *Biochem. J.* 377, 159–169. doi: 10.1042/bj20031253

Richardson, P. G., Wolf, J., Jakubowiak, A., Zonder, J., Lonial, S., Irwin, D., et al. (2011). Perifosine plus bortezomib and dexamethasone in patients with relapsed/refractory multiple myeloma previously treated with bortezomib: results of a multicenter phase I/II trial. *J. Clin. Oncol.* 29, 4243–4249. doi: 10.1200/JCO.2010.33.9788

Ríos-Marco, P., Marco, C., Gálvez, X., Jiménez-López, J. M., and Carrasco, M. P. (2017). Alkylphospholipids: an update on molecular mechanisms and clinical relevance. *Biochim. Biophys. Acta* 1859, 1657–1667. doi: 10.1016/j.bbamem.2017.02.016

Settelen, N., Roch, O., Bock, D., Rooke, R., Braun, S., and Meyer, O. (2004). Controlled plasmid gene transfer to murine renal carcinoma by hexadecylphosphocholine. *J. Control Release* 94, 237–244. doi: 10.1016/j.jconrel.2003.10.006

Shi, Y. S., Pang, X., Wang, J. Q., and Liu, G. (2018). NanoTRAIL-oncology: a strategic approach in cancer research and therapy. *Adv. Healthc. Mater.* 7:e1800053. doi: 10.1002/adhm.201800053

Shim, G., Kim, D., Le, Q. V., Park, G. T., Kwon, T., and Oh, Y. K. (2018). Nonviral delivery systems for cancer gene therapy: strategies and challenges. *Curr. Gene Ther.* 18, 3–20. doi: 10.2174/1566523218666180119121949

Tsouris, V., Joo, M. K., Kim, S. H., Kwon, I. C., and Won, Y. Y. (2014). Nano carriers that enable co-delivery of chemotherapy and RNAi agents for treatment of drug-resistant cancers. *Biotechnol. Adv.* 32, 1037–1050. doi: 10.1016/j.biotechadv.2014.05.006

van Blitterswijk, W. J., and Verheij, M. (2013). Anticancer mechanisms and clinical application of alkylphospholipids. *Biochim. Biophys. Acta* 1831, 663–664. doi: 10.1016/j.bbalip.2012.10.008

Vink, S. R., van Blitterswijk, W. J., Schellens, J. H. M., and Verheij, M. (2007). Rationale and clinical application of alkylphospholipid analogues in combination with radiotherapy. *Cancer Treat. Rev.* 33, 191–202. doi: 10.1016/j.ctrv.2006.12.001

Walczak, H., Miller, R. E., Ariail, K., Gliniak, B., Griffith, T. S., Kubin, M., et al. (1999). Tumoricidal activity of tumor necrosis factor–related apoptosis–inducing ligand *in vivo*. *Nat. Med.* 5:157. doi: 10.1038/5517

Yaseen, M., Wang, Y., Su, T. J., and Lu, J. R. (2005). Surface adsorption of zwitterionic surfactants: n-alkyl phosphocholines characterised by surface tensiometry and neutron reflection. *J. Colloid Interface Sci.* 288, 361–370. doi: 10.1016/j.jcis.2005.03.024

Zeisig, R., Ress, A., Fichtner, I., and Walther, W. (2003). Lipoplexes with alkylphospholipid as new helper lipid for efficient *in vitro* and *in vivo* gene transfer in tumor therapy. *Cancer Gene Ther.* 10, 302–311. doi: 10.1038/sj.cgt.7700572

Zuhorn, I. S., Bakowsky, U., Polushkin, E., Visser, W. H., Stuart, M. C. A., Engberts, J., et al. (2005). Nonbilayer phase of lipoplex-membrane mixture determines endosomal escape of genetic cargo and transfection efficiency. *Mol. Ther.* 11, 801–810. doi: 10.1016/j.ymthe.2004.12.018

Conflict of Interest: The authors declare that the research was conducted in the absence of any commercial or financial relationships that could be construed as a potential conflict of interest.

frontiers in Chemistry

REVIEW
published: 06 October 2020
doi: 10.3389/fchem.2020.583484

Medical Applications Based on Supramolecular Self-Assembled Materials From Tannic Acid

Ruofei Lu[1,2], *Xiaoqiang Zhang*[1,2], *Xinxiu Cheng*[1,2], *Yagang Zhang*[1,2,3,4]*, *Xingjie Zan*[1]* and *Letao Zhang*[1]

[1] Xinjiang Technical Institute of Physics and Chemistry, Chinese Academy of Sciences, Urumqi, China, [2] University of Chinese Academy of Sciences, Beijing, China, [3] Department of Chemical and Environmental Engineering, Xinjiang Institute of Engineering, Urumqi, China, [4] School of Materials and Energy, University of Electronic Science and Technology of China, Chengdu, China

Polyphenol, characterized by various phenolic rings in the chemical structure and an abundance in nature, can be extracted from vegetables, grains, chocolates, fruits, tea, legumes, and seeds, among other sources. Tannic acid (TA), a classical polyphenol with a specific chemical structure, has been widely used in biomedicine because of its outstanding biocompatibility and antibacterial and antioxidant properties. TA has tunable interactions with various materials that are widely distributed in the body, such as proteins, polysaccharides, and glycoproteins, through multimodes including hydrogen bonding, hydrophobic interactions, and charge interactions, assisting TA as important building blocks in the supramolecular self-assembled materials. This review summarizes the recent immense progress in supramolecular self-assembled materials using TA as building blocks to generate different materials such as hydrogels, nanoparticles/microparticles, hollow capsules, and coating films, with enormous potential medical applications including drug delivery, tumor diagnosis and treatment, bone tissue engineering, biofunctional membrane material, and the treatment of certain diseases. Furthermore, we discuss the challenges and developmental prospects of supramolecular self-assembly nanomaterials based on TA.

Keywords: polyphenol, tannic acid, supramolecular, self-assembled, medical applications

OPEN ACCESS

Edited by:
Hicham Fenniri,
Northeastern University, United States

Reviewed by:
Joseph Richardson,
The University of Melbourne, Australia
Tangxin Xiao,
Changzhou University, China

***Correspondence:**
Yagang Zhang
ygzhang@uestc.edu.cn
Xingjie Zan
xjzan2000@hotmail.com

Specialty section:
This article was submitted to Supramolecular Chemistry, a section of the journal Frontiers in Chemistry

Received: *15 July 2020*
Accepted: *19 August 2020*
Published: *06 October 2020*

Citation:
Lu R, Zhang X, Cheng X, Zhang Y, Zan X and Zhang L (2020) Medical Applications Based on Supramolecular Self-Assembled Materials From Tannic Acid. Front. Chem. 8:583484. doi: 10.3389/fchem.2020.583484

INTRODUCTION

Supramolecular assembly, which originated from Lehn's groundbreaking work on host–guest self-assembly in 1987 (Lehn, 1988), is a process of spontaneous formation of unique nanostructures by dynamic covalent interactions (Wang et al., 2018a) and non-covalent intermolecular interactions (Caulder and Raymond, 1999), including hydrogen bonds, hydrophobic interactions, electrostatic interactions, van der Waals forces, and π-π stacking. It originates from biological systems and is widely applied in the biomedical field (Cui and Xu, 2017). Such assemblies are common in nature, such as the supramolecular structure of phospholipids in cellular membranes and actin in eukaryotic cytoplasm (Kim et al., 2019). In biological systems, supramolecular assembly involves a variety of functions, such as environmental demarcation, molecular transport and release, and cell–extracellular interactions and communication (Ariga et al., 2019). Inspired by the natural supramolecular assembly, scientists have developed a variety of supramolecular self-assembled biomaterials, including hydrogels, nanoparticles/microparticles, hollow capsules, and

coating films, for the diagnosis and treatment of diseases. Supramolecular materials include monodisperse molecules (proteins, polysaccharides, and other biomass materials) and complex molecular aggregates (particles, micelles) (Song et al., 2015). Supramolecular assembly can not only produce thermodynamically or dynamically stable nanostructures but also accurately control diagnostic/therapeutic components and stimulus response characteristics to physiological indicators (Wang et al., 2018b), which is very attractive in biology and medicine.

Polyphenols, including tannic acid (TA), (–)-epigallocatechin-3-gallate (EGCG), catechin, lignans, catechol, and pyrogallol, are a large class of plant-derived biocompatible and biodegradable compounds consisting of two or more phenolic units in structure (Wang X. et al., 2018). Because of their unique sources, the most important characteristics of polyphenols are their biological activities, such as anti-inflammatory, anticancer, antibacterial, and antioxidative actions, which have attracted the attention of researchers in the field of biomedicine (Galante et al., 2019; Song et al., 2019). In terms of chemical structure, polyphenol compounds also show rich chemical activity due to their multiple hydrophobic aromatic rings and hydrophilic phenolic hydroxyls groups, which provide abundant reaction sites that can interact with various groups or substances through various non-covalent interactions (Kozlovskaya et al., 2015; Patil et al., 2018) (including hydrogen bonds, hydrophobic interactions, and van der Waals interactions), dynamic covalent binding (Su et al., 2011; Ye et al., 2011; Faure et al., 2013), and metal–organic coordination interactions (Lee et al., 2011; Rahim et al., 2016; Wang Z. et al., 2017). Such prospects serve as the basis for the application of those compounds. In addition, the hydrophilicity of natural polyphenols facilitates the introduction of amphiphilic characteristics into supramolecular systems (Wang et al., 2018b). Through their significant effects on protein signal transduction and expression and cell cycle regulation implicated in the growth, transformation, and metastasis of cells, polyphenols have become a kind of promising multifunctional drug with chemopreventive and anticancer factures capable of inducing apoptosis and inhibiting the growth of cancer cells (Yang et al., 2002). Considering both the excellent structural and functional characteristics offered by natural polyphenols, materials based on polyphenols as structural units have become a hotspot of research. The addition of polyphenols to these materials endows them with some new properties, such as antioxidative, antitumor, antivirus, and bacteriostatic activities, lending to their extensive application potential in food preservation and pharmaceutical production. At present, the strategies employed for supramolecular engineering based on natural polyphenols are not only focused on building various two-dimensional functional metal–phenolic network (MPN) materials, such as capsules or membranes, but also widely used in three-dimensional supramolecular nanomedicines, including disease diagnosis and imaging, as well as drug delivery (Wang et al., 2018b). TA as a kind of polyphenolic organic compound has certain structural properties and biological activity, and it can be used as a building unit for supramolecular assembly to obtain nanomaterials with biological functions. Therefore, TA has attracted the attention of researchers in the field of biomedicine.

Supramolecular self-assembled nanomaterials, especially nanomaterials based on TA, have great potential applications in biomedical fields with respect to, for example, diagnosis, treatment, and medical devices (Zou et al., 2017). In terms of function, TA endows self-assembled nanomaterials with good biocompatibility, antibacterial, antioxidative, and antitumor characteristics; in terms of structure, supramolecular assembly can be driven by a variety of non-covalent or dynamic covalent interactions to regulate the materials on a nanometer scale and provide greater functionality to the assembled materials. The supramolecular assembly of TA combines the biological activity of polyphenols with the structural control advantages of supramolecular assembly to prepare functionalized nanobiomaterials suitable for different applications. Supramolecular materials based on TA with excellent properties, such as stimulus response, self-healing, and memory shaping capabilities, are ideal in biomedical applications (Fan et al., 2017b). Supramolecular assembly of TA can also provide a general and inexpensive platform for the design of multifunctional films (Wu et al., 2015a; Dong et al., 2017).

In this review, combined with the structural characteristics and biological activity, we introduce the principle and development process of TA supramolecular assembly. The latest progress in TA supramolecular assembly and its biomedical applications are reviewed in two different dimensions including the supramolecular assembly driving force and the assembly system. In addition, we discuss the challenges associated with TA supramolecular assembly and its developmental prospects. The comprehensive summary of the review is graphically shown in **Figure 1**.

OVERVIEW OF SUPRAMOLECULAR ASSEMBLY

With the in-depth understanding of molecular chemistry based on chemical bonds, it has been found that traditional molecules cannot perform certain specific, advanced, or complex functions but need an organized multimolecular system to work cooperatively. Therefore, it is necessary to research the interaction between molecules at the molecular level, so the concept of supramolecular chemistry has been proposed. Supramolecular chemistry works with the interaction between molecules, including ion–ion interactions, ion–dipole interactions, dipole–dipole interactions, van der Waals forces, tight packing in solids, hydrophobic effects, hydrogen bonding, π-π stacking of aromatic rings, cation–π interactions, and anion–π interactions. The study of supramolecular chemistry originated from Pedersen's report about the synthesis of crown ethers and their complexation properties of alkali metal ions in 1967 (Pedersen, 1967, 1988). Additionally, in 1978, Lehn clearly put forward the concept of supramolecular chemistry, pointing out that supramolecular chemistry concerns molecular assemblies and intermolecular bonds (Lehn, 1978). In fact, the cleavage and formation of both covalent bonds in molecular

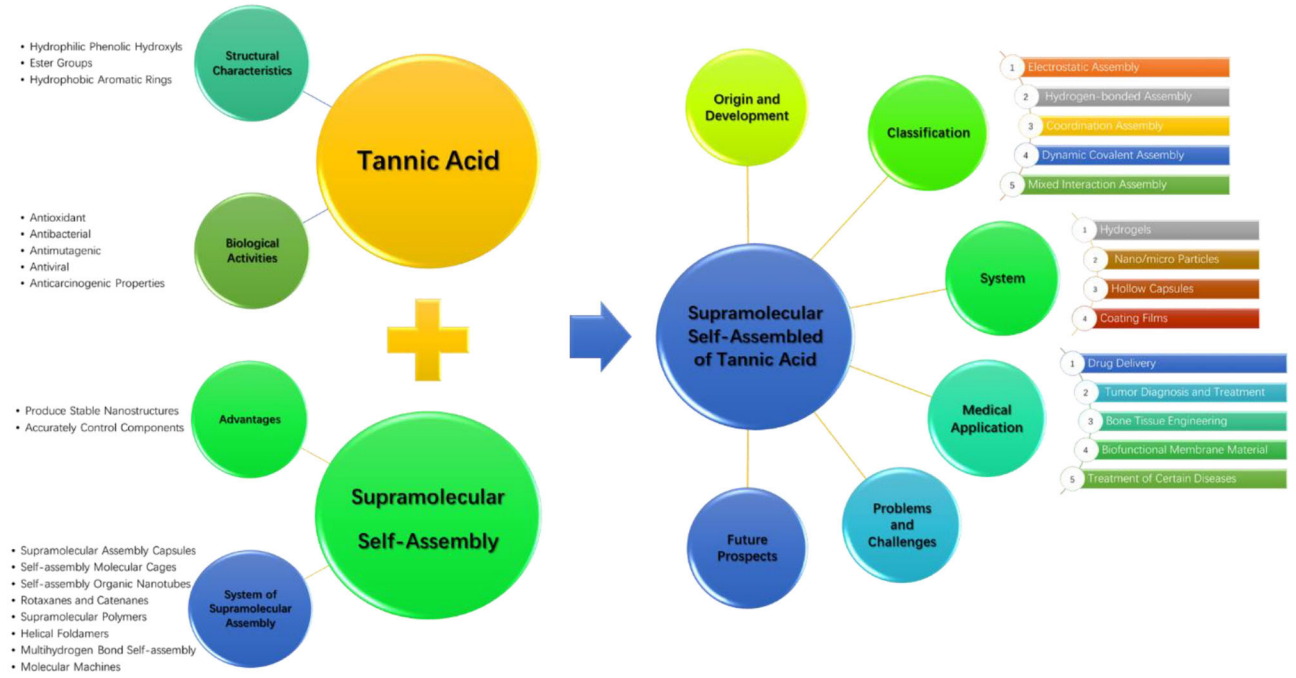

FIGURE 1 | The comprehensive summary of the review.

chemistry and non-covalent bonds in supramolecular chemistry are the flow and redistribution of electron clouds, so they are essentially the same. Molecular recognition, an important means of supramolecular chemistry, is a process by which a specific host molecule selectively binds to a guest to produce specific functions (Lehn, 1973), so its binding is purposeful. Self-assembly is an important method for the synthesis of supramolecular interactions. Based on specific molecular recognition modes, self-assembly is a process by which molecules or other assembly elements spontaneously form ordered structures via weak interactions (Philp and Stoddart, 1996; Lehn, 2002; Whitesides and Grzybowski, 2002). The emergence and application of self-assembly have greatly improved the efficiency of constructing complex host molecules. Relatively simple monomers can be synthesized by self-assembly, and the binding sites can be encoded in the monomer structure. Monomers rely on the recognition of bonding sites to achieve "procedural" self-assembly (Lehn, 2000), spontaneously forming complex, highly selective, reversible host molecules. In addition, the host molecule for self-assembly can change its structure according to the external stimulation or guest to achieve the maximum degree of bonding. In the field of supramolecular chemistry, we call it supramolecular self-assembly. Supramolecular self-assembly is a process of spontaneous molecule formation of unique nanostructures via non-covalent intermolecular interactions (Wang et al., 2018b) and dynamic covalent interactions (Caulder and Raymond, 1999).

With the deepening of research, supramolecular assembly has intersected with other disciplines, and some new research fields continue to emerge. According to basic research, a near-perfect system of supramolecular assembly has emerged. Additionally, supramolecular assembly has made some progress in the fields of supramolecular assembly capsules, self-assembly molecular cages, self-assembly organic nanotubes, rotaxanes and catenanes, supramolecular polymers, helical foldamers, multihydrogen bond self-assembly, and molecular machines, among others. The origin and development of supramolecular assembly are shown in **Figure 2**.

Early studies of molecular containers have focused on carcerands and hemicarcerands, but the synthesis of these molecules is complex, and releasing guest molecules is not easy. Therefore, scientists have gradually turned their attention to reversible supramolecular capsules, which are self-assembled by relatively simple monomer molecules via weak non-covalent interactions between molecules. The supramolecular assembly capsule originated from the first hydrogen-bonded supramolecular capsules with a tennis ball shape based on the glycoluril structure, as reported by Wyler et al. (1993). This field is still in the stage of vigorous development. However, the design and construction of supramolecular capsules require the consideration of various factors, and the selection of guests requires comprehensive consideration of various factors such as shape, size, and surface chemical properties. Thus, the kinds of capsules available are few thus far, and basic research persists; therefore, a long time is needed for its industrialization and commercial application.

The molecular cage is the assembly of molecules with a three-dimensional cage cavity structure, which usually has a complex structure. In the 1990s, Fujita reported a new nanoscale metal-bonded molecular cage based on PdL2-based building blocks

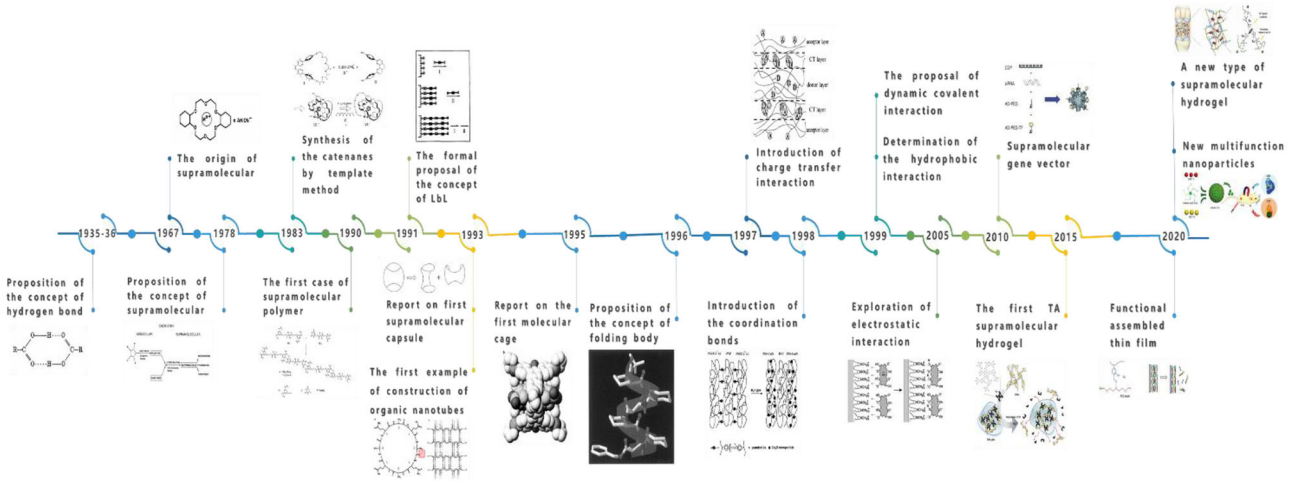

FIGURE 2 | The origin and development of supramolecular assembly.

(Fujita et al., 1995). With the development of supramolecular assembly, molecular cages have attracted interest and attention because of their unique structural characteristics and wide range of potential applications. An increasing number of metal-bonded self-assembled molecular cages, covalently bonded molecular cages, and other self-assembled molecular cages have been synthesized, which are widely used in the fields of molecular recognition, catalysis, and gas adsorption, among others.

As a kind of one-dimensional nanomaterial, carbon nanotubes have unique physical and chemical properties. Since carbon nanotubes were discovered by Iijima (1991), after nearly 30 years of development, they have been chemically modified to different degrees and endowed with different properties, although some limitations persist in the modification of carbon nanotubes with only one element, such as difficulty in controlling the size, derivation after synthesis, and responses to external stimuli. Supramolecular self-assembled organic nanotubes can overcome these shortcomings and thus facilitate the functionalization, derivatization, and reversible response to external environmental changes, leading to the wide use of supramolecular self-assembled nanotubes in the fields of molecular inclusion and separation, chemotherapy, transmembrane transport, ion channels, and drug delivery, among others. The Granja team successfully constructed the first case of self-assembled organic nanotubes using cyclic peptides, synthesizing cyclic octapeptides with an alternating arrangement of α-(D,L)-amino acid residues and thus opening a new world for the development of self-assembled organic nanotubes (Ghadiri et al., 1993).

Both rotaxanes and catenanes are very interesting compounds that link the subunits of the molecular structure by the mechanical force of non-covalent bonds. A supramolecular assembly usually appears in the construction process of rotaxanes and catenanes, the structure of which is similar to rotaxanes, but the linear molecules have no capped groups, or the capped groups are too small to block macrocyclic molecules, which are called quasi-rotaxanes. The special structures of quasi-rotaxanes, rotaxanes, and hydrocarbons endow them with great application potential in the construction of molecular devices and nanofunctional materials. The interlocking structures of rotaxanes and catenanes were initially synthesized via a statistical method. There is no mutual attraction between the subunits of the interlocking molecules, and the interlocking structure is formed because of the probability that the two randomly pierced parts cannot be separated after the reaction. In 1960, Wasserman first obtained the interlocking ring, called the catenane, with a yield of < 1% by statistical methods (Wasserman, 1960). In 1967, I. T. Harrison and S. Harrison first described the rotaxanes, which they called hooplanes (Harrison and Harrison, 1967), and the yield was only 6%. Obviously, the probability of random piecing together of subunits is small, so the yield of interlocking molecules is low. In 1983, (Dietrich-Buchecker et al., 1983) formed a stable quasi-rotaxane complex by ion coordination and then synthesized hydrocarbons with a yield of 27% by the cyclization reaction. Sauvage pioneered the method of synthesizing catenanes using univalent copper ions as templates and efficiently synthesized interlocking molecules by the template method. In this method, copper ions coordinate with organic ligands to gather two molecules together, and then the ring-closing reaction is used to connect the terminal to form the ring–ring catenane structure (Dietrich-Buchecker et al., 1983). Thus, the yield can be greatly improved by using the non-covalent weak interaction between molecules as a template to prepare interlocking structures.

The supramolecular polymer is the molecular aggregate assembled by non-covalent bond interactions between monomer structural elements (De Greef et al., 2009). They are mostly monomers with bifunctional groups formed spontaneously by molecular self-assembly in suitable solvents without any initiator. In 1990, Lehn, a famous supramolecular chemist, reported the first case of the supramolecular polymer $(1.2)_n$ based on

hydrogen bonding, which is the first case of supramolecular polymer (Claudine Fouquey and Anne-Marie, 1990). However, the non-covalent interaction in the supramolecular polymer structure lacks directionality, which can easily lead to a microphase separation structure or gelation in the process of polymer network formation. Therefore, how to incorporate sufficiently strong but still reversible interactions has become a difficult problem for researchers. Sijbesma et al. (1997) synthesized reversible self-assembling polymer systems, using units of 2-ureido-4-pyrimidone that dimerize strongly in a self-complementary array of four cooperative hydrogen bonds as an associating end group to solve the problem of polymer reversibility and high strength. They also pointed out that thermal and environmental controls on life and bonding strength can adjust the properties of polymers so that polymer networks with thermodynamically controlled structures can be formed, which has great significance in the development of reversible supramolecular polymers (Sijbesma et al., 1997). Because of the reversibility of non-covalent bonds, the polymerization and depolymerization of supramolecular polymers can easily occur; thus, as an excellent intelligent material, it has wide application prospects in sustained drug release. For example, Davis' team reported the first clinical trial using supramolecular cyclodextrin as a gene carrier, which uses cyclodextrin polymer and siRNA to form gene nanoparticles to treat patients with pigment cancer by targeting, and the effect of clinical gene therapy was achieved (Davis et al., 2010). Although supramolecular polymers have been studied for decades, they are still in the early stage of development, including the principle of monomer self-assembly, the mechanism of supramolecular polymerization, and the relationship between structure and function.

Protein is the most abundant and functional polymer in cell components, which plays the role of an executor of various life functions in life activities. To perform their biological function, proteins must be correctly folded into a specific configuration. These orderly and stable folding structures are mainly realized via the cooperation of non-covalent bond interactions. In recent years, because of the great interest in simulating the helical structure of biopolymers, the study of folded molecules has become a research hotspot in the field of supramolecular self-assembly. On the one hand, folded molecules play a vital role in simulating the structure of biopolymers, which is expected to provide theoretical and scientific bases for the synthesis of proteins; on the other hand, folded molecules can form a spiral structure with nanocavities or a new type of organic nanotubes by self-assembly. They have potential applications in molecular recognition, ion channels, molecular catalysis, and nanoreactors, among others. In recent years, various types of oligomers have been synthesized. These oligomers adopt helical secondary structures via intramolecular non-covalent interactions, and they are called foldamers together with other solid polymers with secondary structures. In 1996, (Appella et al., 1996). first proposed the term "foldamer" (Appella et al., 1996), but research on foldamers has existed for a long time. In 1998, Gellman reported the original definition of the foldamer: any polymer with a specific compact structure (Gellman, 1998). Because of the inaccurate use of the word "polymer" in this concept, what are widely studied are not polymers but oligomers with a specific molecular formula and relative molecular mass, and the term "specific compact structure" in the concept is too vague. Therefore, in 2001, (Hill et al., 2001) made necessary modifications to the definition of foldamer and defined it as an oligomer that presents an ordered and compact conformation in solution; the tight conformation is stabilized by direct non-covalent interactions of non-adjacent units (Hill et al., 2001). This definition is more accurate than the previous one, showing that the oligomer changes from disorder to order in solution; that is to say, the driving force of the "folding reaction" comes from the potential non-covalent bond interaction of the oligomer. Therefore, the oligomer that cannot undergo a "folding reaction" cannot be called a foldamer. In recent years, biomimetic folding based on small molecules has attracted the attention of researchers. For example, Xiao et al. (2019a) dimerized small organic molecules through quadruple hydrogen bonds and then formed folding dimers with the help of interaction, and they can further form one-dimensional supramolecular stacking through additional weak interactions in the solid state, which is similar to the biomimetic folding of DNA. Hydrogen bonding is a very important non-covalent interaction in supramolecular chemistry, and it is called the "omnipotent interaction in supramolecular chemistry" in the variety of non-covalent interactions. Because of the characteristics of high strength and remarkable orientation, hydrogen bonding has been widely used in the field of supramolecular assembly in recent years. In 1920, Latimer and Rodebush (1920) first described the phenomenon of the hydrogen bond clearly when they explained the association between water molecules. Bernal and Megaw (1935) and Huggins (1936) formally proposed the concept of the hydrogen bond in 1935 and 1936, respectively. Hydrogen bonding means that when H forms a covalent bond with F, O, N, and other atoms, these atoms are partially negatively charged because of their high electronegativity and attraction to electrons, while the hydrogen atom is partially positively charged, forming a state similar to that of hydrogen ions and thus attracting lone pairs of electrons of F, O, N, and other atoms adjacent to it. This concept is widely accepted because of Pauling's (1985) famous monograph on chemical bonds. Although the energy of a single hydrogen bond is weaker than that of a covalent bond, the synergistic effect of multiple hydrogen bonds can reach a comparable level. Designing and synthesizing a simple, highly stable, and easy-to-derive multihydrogen bond system will be the focuses of research in the future.

The molecular machine, an independent molecule or molecular assembly, extends the concept of a macroscopic machine to the molecular level and can perform a machine-like motion under appropriate external stimulation (Balzani et al., 2000). One of the important goals of supramolecular assembly is to create orderly, functional devices at the molecular level that can interfere with, store, process, and transmit information. There are many such exquisite machines in nature; for example, both the photocapture antennae of bacteria formed by photosynthesis and ATP synthetase are formed by a number of molecules via self-assembly and self-organization. Supramolecular self-assembly is an effective tool to construct molecular machines. A molecular machine

based on a single molecule involves changes in the molecular conformation or configuration around the covalent bond when its components move. For example, (Pollard et al., 2007) designed molecular motors via Zmure isomerization with a double-bond configuration (Pollard et al., 2007). There are essential differences between molecular machines based on supramolecular assembly and a single molecule. The motion in molecular machines based on supramolecules often involves the change in the conformation of supramolecular systems. Through the method of self-assembly, selecting the appropriate construction unit, and controlling the manner of non-covalent interactions, the ideal molecular assembly can be obtained under the drive of thermodynamics. However, regardless of structure or function, the complexity and ingenuity of biomolecule machines are far beyond synthetic molecular machines. The study of synthetic molecules is still in its infancy, and some problems must be further explored. For example, most studies on the behavior of molecular machines are carried out in solution, and it is necessary to arrange them in a certain, orderly way to function at the macrolevel similar to dynamic proteins, including tissue at the interface, deposited on the surface, and fixed on the membrane or porous materials.

The bottom-up construction of nanoscale functional materials by supramolecular self-assembly is a hotspot and challenge in current research, and it is an important means to create new materials and produce new functions. Compared with the traditional chemical reaction, the supramolecular assembly system has some typical characteristics. The first is order, wherein the structure of self-assembly is more orderly than individual components. Second, in terms of interaction forces, non-covalent bonds and dynamic covalent bonds are used as driving forces in supramolecular assembly, and these weak interactions are far smaller than traditional chemical bonds, but they determine the physical properties of liquids, the solubility of solids, and the molecular assembly of biofilms, so they play an important role in material synthesis. Finally, in terms of the construction unit, the construction unit of supramolecular assembly includes not only atoms and molecules but also nanoscale and micron structures with different chemical compositions, shapes, and functions. Supramolecular assembly usually involves a layered assembly process, which is called layer-by-layer (LbL) assembly. LbL is one of the classic supramolecular assembly techniques, with its main advantages including simplicity, low cost, ruggedness, and flexibility (Decher et al., 1992). Additionally, multifunctional supramolecular nanomaterials are obtained by accurately regulating the assembly process at the nanometer scale (Yang et al., 2019b). In the past half-century, LbL assembly has received increasing attention with the promotion of existing materials and assembly technology and characterization of technological innovation.

STRUCTURAL FEATURES OF TA CONTRIBUTING TO SELF-ASSEMBLY

TA, as shown in **Figure 3**, which is mostly distributed in various plants containing vegetables, fruits, oak, grapes, tea leaves, olives, and others, is a biodegradable, naturally existing polyphenolic compound (Wu et al., 2015b; Shin et al., 2018), and it has been affirmed as a safe potential direct food-product additive by the US Food and Drug Administration (Le et al., 2018). TA, as a well-known high-molecular-weight polyphenolic compound and hydrolyzable tannin (Shutava et al., 2005), has antidiarrheal, convergence, and hemostatic functions (You et al., 2014). As a classical polyphenol, TA often exists in solution as loosely bounded complexes due to its ability to form intramolecular and intermolecular hydrogen bonds (Shutava et al., 2005). Moreover, TA has also been revealed to exhibit high biological activities such as antioxidant, antibacterial, antimutagenic, antiviral, and anticarcinogenic properties (Costa et al., 2011; Le et al., 2018). These characteristics of high bioactivity, extensive sources, low expense, and good biocompatibility make TA widely used in the leather manufacturing, food processing, and medical and biological applications industries (Wu et al., 2015b; Abouelmagd et al., 2019). In particular, its application in biology and medicine has aroused the interest of scientists.

The peculiar properties of TA mainly depend on its unique structural characteristics. According to structural analysis, TA possesses a central glucose molecule, which is linked to 10 gallic acid units via five diacetyl ester groups (Abouelmagd et al., 2019). Abundant adjacent phenolic hydroxyls and ester groups provide TA with high chemical reactivity, providing sufficient response sites to different substances (Gao and Zharov, 2014; Xu et al., 2019), which facilitate the ideal properties of TA as a sustainable scaffold on substrate surfaces. In addition, the unique structural properties of TA, including abundant hydrophobic aromatic rings and hydrophilic phenolic hydroxyl groups, allow it to react with various substances through covalent and non-covalent interactions, such as hydrogen bonding and electrostatic, π-π stacking, and hydrophobic interactions (Song et al., 2019; Zhao et al., 2019b). For example, the interaction between TA and ammonium cations can be attributed to electrostatic interactions, hydrogen bonding, and π-π stacking (Gao and Zharov, 2014). TA also has excellent antioxidant properties due to a large number of phenol groups because it can scavenge reactive oxygen species (ROS) by converting the phenol to the quinone group in an oxidative stress environment (Chung et al., 1998b). Moreover, the weak acidity and extensive hydrogen bonds of TA are reasonable because it contains 25 hydroxyl groups (Richardson et al., 2016; Onat et al., 2018). However, the pKa of TA varies for different sources, with an average close to 8.5, and is easily affected by oxidation in basic solutions (Ringwald and Ball, 2016). In addition, TA has not only an effective adsorption performance but also immunomodulatory effects in animals (Takemoto et al., 2015).

In recent years, surface modifications and structural functional materials based on TA have become a research focus. For example, TA has been used to obtain coating by reaction with Fe^{3+} ions on various substrates within only 30 s, where a modified TA/Fe^{3+} coating sealed the microholes of a filter membrane with a geometry similar to dentinal tubules (Oh et al., 2015). TA is also conducive to enhance the antibacterial and antioxidant activities of sponges (Shukla et al., 2012). By adding weak polyelectrolytes in the film assembly, the obtained

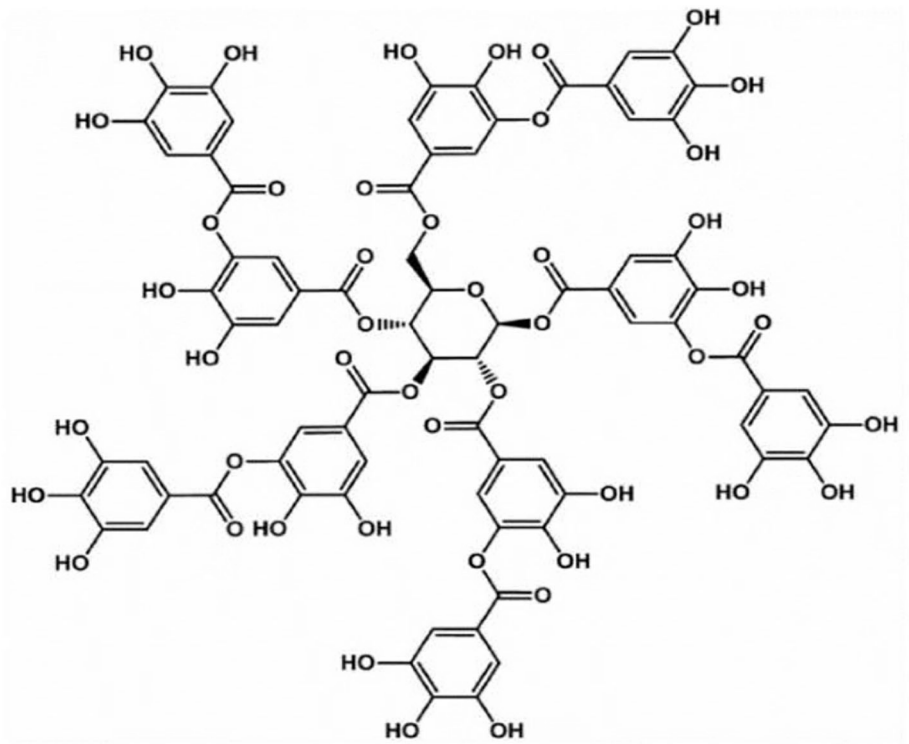

FIGURE 3 | The molecular structure of TA.

PEM film is able to preprogram adjustable retention/release properties (Zhuk et al., 2014), which can be used to regulate drug release. Previous work has demonstrated that hydrophobic interactions of TA and proteins contribute to enhancing their mechanical and thermal properties. Related reports have revealed that TA can precipitate not only various proteins, including collagen, gelatin, and albumin, but also some polysaccharides and alkaloids (Aoki et al., 1981; Shutava et al., 2005). It also interacts with certain specific and targeted amino acids (Fraga et al., 2010). The LbL films fabricated from TA and PVPON via reversible hydrogen bonding are used to controllably regulate physiological processes by gradually disassembling and releasing TA into the media (Zhou et al., 2013). The films compounded by TA and lignin are expected to enhance Col-H strength against compression force, the antibacterial effect, and mechanical stability (Velmurugan et al., 2014; Gogoi et al., 2017). TA is increasingly used in biomaterials and medicine because of its excellent biocompatibility and high reactivity.

DEVELOPMENT OF TA SELF-ASSEMBLY

Self-Assembly Principle of TA

Supramolecular assembly of TA depends on the physical and chemical properties of phenol functional groups in TA, which endows TA with a variety of reaction activities, as shown in **Figure 4**. Phenol functional groups in TA molecules can be used as hydrogen donors or hydrogen receptors to participate in various chemical reactions (Quideau et al., 2011). Because phenol is a kind of molecule with stable enol tautomerism, the weak nucleophilic property of phenol changes to a strong nucleophile when the hydroxyl on phenol is deprotonated to phenol anion (PhO^-). As a result, TA can be used as an oxygen or a carbon-based nucleophile to participate in multiple ion reactions (Quideau et al., 2011). Phenol cations (PhO^+) can be formed by two-electron transfer dehydrogenation coupling oxidation under neutral or weakly acidic conditions, and this delocalized and stable cationic intermediate is a strong carbon-based electrophilic, so it is easy to react with nucleophiles. Moreover, the amphiphilic nature of this complex structure of the TA—hydrophobic aromatic ring and hydrophilic phenolic hydroxyl group—endows TA with supramolecular assembly ability through hydrophobic interaction. The planar aromatic nuclei of phenol give TA the ability to assemble supramolecularly through π-π stacking (van der Waals force). Because polyphenol hydroxyl groups are negatively charged under physiological pH, TA is expected to achieve supramolecular assembly by electrostatic interaction with cationic compounds (Abouelmagd et al., 2019). Moreover, the oxygen atom with strong electronegativity can be used as a hydrogen acceptor, while the hydrogen atom with weak electronegativity serves as a hydrogen donor in the polar O–H bond of the polyphenol hydroxyl group. Thus, TA has the ability to undergo supramolecular assembly through hydrogen-bond interactions. In addition, the two adjacent phenolic hydroxyl groups of TA are able to coordinate with metal ions to form complex precipitates via the formation of oxygen anions. TA is

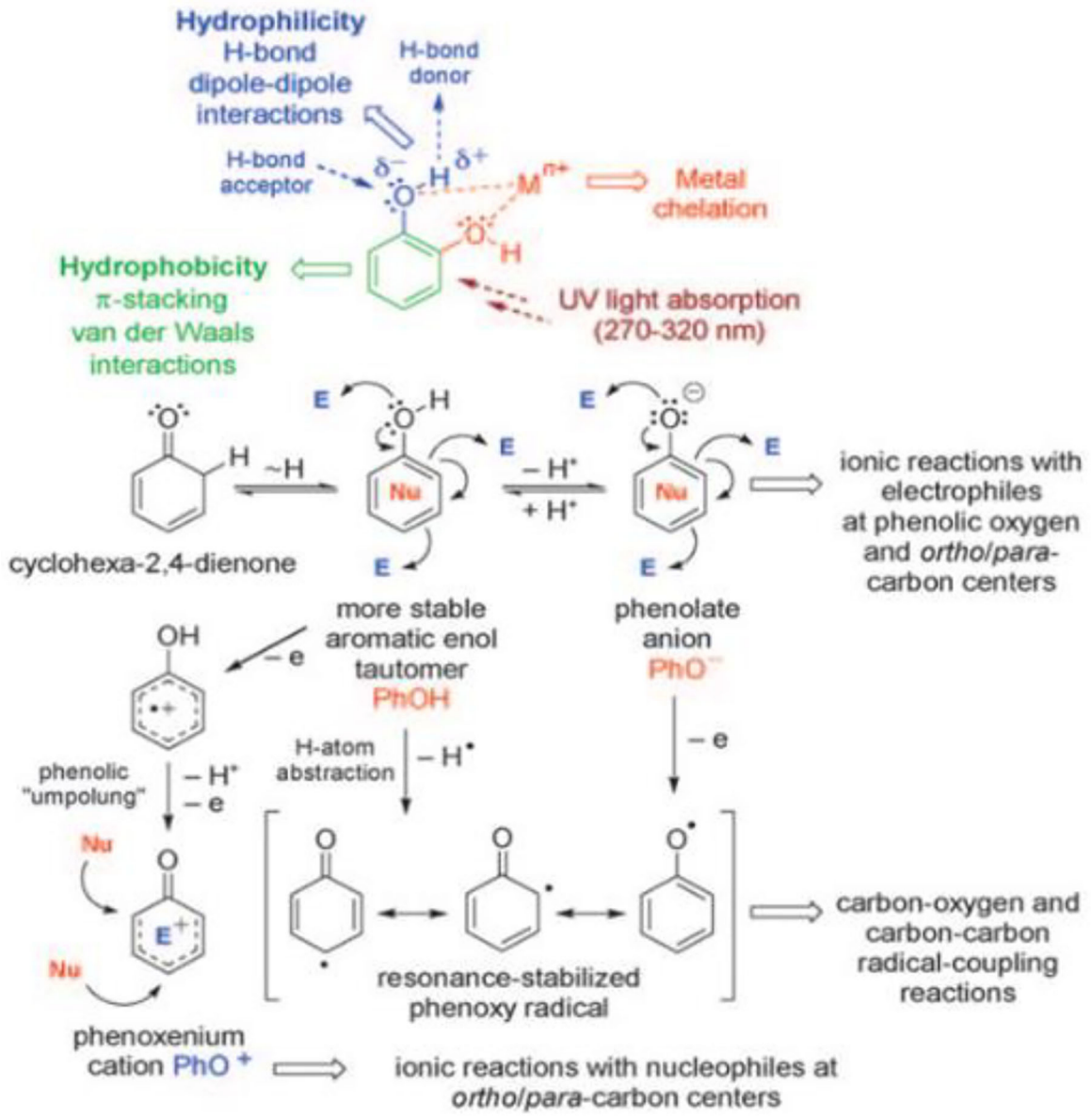

FIGURE 4 | Basic reactivity of the phenol [E = electrophile, Nu = nucleophile (Quideau et al., 2011)].

able to supramolecularly assemble through metal coordination interactions due to the abundant catechol and pyrogallol in its structure (Andjelkovic et al., 2006).

The Origin and Development of LbL Assembly of TA

The LbL assembly method plays an important role in the supramolecular assembly of TA, which is the alternating deposition of interacting materials on different substrates. The strategy of alternating deposition can be traced back to the pioneering work carried out by Iler and Kirkland in 1964–1966 (Kirkland, 1965; Iler, 1966), who prepared inorganic films by the assembly of negatively charged silica particles and positively charged alumina fibers. However, it was not until 1991 that Decher and Hong, as pioneer researchers, carried out a comprehensive characterization of LbL multilayer films (Decher and Hong, 1991), which successfully opened the door for LbL assembly. In the traditional sense, LbL assembly involves alternating deposition through electrostatic interactions driven by enthalpy and entropy (Fu and Schlenoff, 2016). However, after Cassier et al. (1998) finished their preliminary study of biotin–streptavidin interactions, the driving forces of LbL assembly were expanded to other interactions rather than simplex electrostatic interactions. For example, Stockton and Rubner (1997) first conducted a groundbreaking study on the preparation of LbL modules using hydrogen-bond interactions; coordination bonds

(Xiong et al., 1998) and charge transfer interactions (Shimazaki et al., 1997) were introduced in 1997 and 1998, respectively. Kotov (1999) and Cochin and Laschewsky (1999) identified hydrophobic interactions as the main driving forces for the buildup of LbL in 1999. In addition, host–guest interactions are also widely used in LbL assembly of multilayer films in biomimetic systems (Muller et al., 1993). In brief, supramolecular nanomaterials with different properties and functions can be obtained by different assembly interactions. In addition, the supramolecular assembly based on TA can be traced back to the electrostatic interactions involved in the zeta potential and surface charge density of nylon 6 fibers treated with acid dye solution by Ogasawara et al. (1981). It was not until 2005 that Shutava et al. (2005), formally explored the electrostatic assembly of TA and cationic polymers, which opened a new world for LbL assembly of supramolecular materials based on TA.

Classification of TA Self-Assembly

According to the assembly driven interaction, TA self-assembly can be divided into four major types: (1) electrostatic assembly, (2) hydrogen-bonded assembly, (3) coordination assembly, (4) dynamic covalent assembly, and (5) mixed interaction assembly.

Electrostatic Assembly of TA

The electrostatic assembly of TA is the supramolecular assembly process by electrostatic interaction between TA as a negatively charged assembly unit and positively charged polymer. The electrostatic assembly of TA is based on the ionization of abundant polyphenol hydroxyl groups in the TA molecule, filling its surface with a negative charge. Positively charged polymers are generally cationic polymers, which have a strong interaction with negatively charged cell membranes under physiological pH. They can adhere to the cell surface and enhance penetration, so they are attractive in the field of biomedicine. Shutava et al. (2005) performed a groundbreaking study on the electrostatic assembly of TA and cationic polymers. They alternately assembled TA with two different cationic polymers including strong poly(dimethyldiallylamide) (PDDA) and weak poly(allylamine) (PAH), as shown in **Figure 5A**, to obtain nanomembranes and capsules with a pH response. The capsules showed low permeability at pH 5–7 and high permeability at low or high pH. Combined with the antioxidant, antibacterial, and antiviral properties of TA, the pH-responsive capsules had the potential to be used as drug carriers. However, Shutava et al. (2005) did not carry out cytotoxicity experiments on the obtained materials, and the high density of positive charge on most cationic polymer functional groups may cause cytotoxicity, so it remains doubtful whether the materials can be used in drug delivery. Although non-cytotoxic cationic polymers are limited, poly(4-hydroxy-L-proline ester) (PHPE) is a non-cytotoxic cationic polymer, which is cationic under physiological pH. Its natural degradation product is hydroxyproline (Hyp), which can be safely considered for biomedical applications. Onat et al. (2018) prepared water-soluble complexes of PHPE and TA (PHPE-TA) at pH 4 and deposited the film on the surface by LbL assembly, followed by crosslinking the multilayer film with $NaIO_4$ to enhance stability under physiological conditions. Because the prepared LbL film shows good bone conduction properties, it is expected to be used for the coating of orthopedic implants, various biomaterials (such as bone screws and knobs), or special scaffolds for bone tissue engineering, as shown in **Figure 5B**. In addition, based on TA maintenance of antibiotic molecules through electrostatic interactions, the film has biological response characteristics, which can broaden the spectrum of antibacterial activity. Zhuk et al. (2014) used LbL assembly to directly assemble TA with several cationic antibiotics (tobramycin, gentamicin, and polymyxin B) to form a highly efficient, bioresponsive, controlled-release antibacterial coating, which can be used to prevent bacterial colonization in biomedical devices. In fact, because of the complexity of the antibiotic structure, there is hydrogen-bond interaction between TA and antibiotics in addition to electrostatic interactions. Recently, Abouelmagd et al. (2019) used the complex of TA and cationic antibiotics as a new pH-responsive drug carrier with high drug loading and optimal stability, indicating that TA/antibiotic self-assembly complex is a good carrier for pH-sensitive water-soluble drugs, as shown in **Figure 5C**. Although the TA self-assembly materials based on electrostatic interaction show certain advantages in the biomedical field, there are still some problems that limit the further development of TA supramolecular assembly. First, electrostatic-based assembly is sensitive to the ionization state of salts and polymers, and they are relatively unstable without covalent crosslinking (Hoogeveen et al., 1996). Second, selectable and preparable materials for electrostatic interaction are limited, which are suitable only for the preparation of charged and water-soluble multilayer materials that are sensitive to external stimuli (Xiao et al., 2016). Finally, the introduction of cationic polymers in electrostatic interaction may cause cytotoxicity.

Hydrogen-Bonded Assembly of TA

Compared with electrostatic assembly, hydrogen-bonded assembly is more attractive for biomedical applications because toxic cationic polymers are not introduced in the assembly process (Takemoto et al., 2015). However, the stability of hydrogen-bonded assembly under physiological conditions limits its practical application. The natural polyphenol TA with a multibranched chain can provide relatively stable hydrogen bonding under physiological conditions (Sundaramurthy et al., 2014), so the hydrogen-bond assembly of TA has been widely studied. Le et al. (2018) used paclitaxel (PTX) as a model drug and prepared PTX-loaded TA/poly (N-vinylpyrrolidone) nanoparticles (PTX-NP) by flash nanoprecipitation via the intermolecular hydrogen-bond interactions, and they explained the assembly mechanism of hydrogen-bonded PTX-NP by molecular dynamics simulation. Moreover, it has been confirmed that PTX-NP may be a promising oral drug formulation for chemotherapy *in vitro* and *in vivo*, as shown in **Figure 6A** (Le et al., 2018). Adatoz et al. (2018) prepared hydrogen-bonded and pH-responsive poly(2-ethyl-2-oxazoline) (PEOX) and TA multilayers by LbL deposition, which can be reassembled into H-bonded pH-responsive PEOX/TA fibers in phosphate buffer solution, pH 3, validating that pH-responsive fiber aggregates have certain application prospects in a variety of biomedical applications from controlled release to sensors. Luo et al. (2020), using silk fibroin (SF) and TA as raw materials, effectively constructed

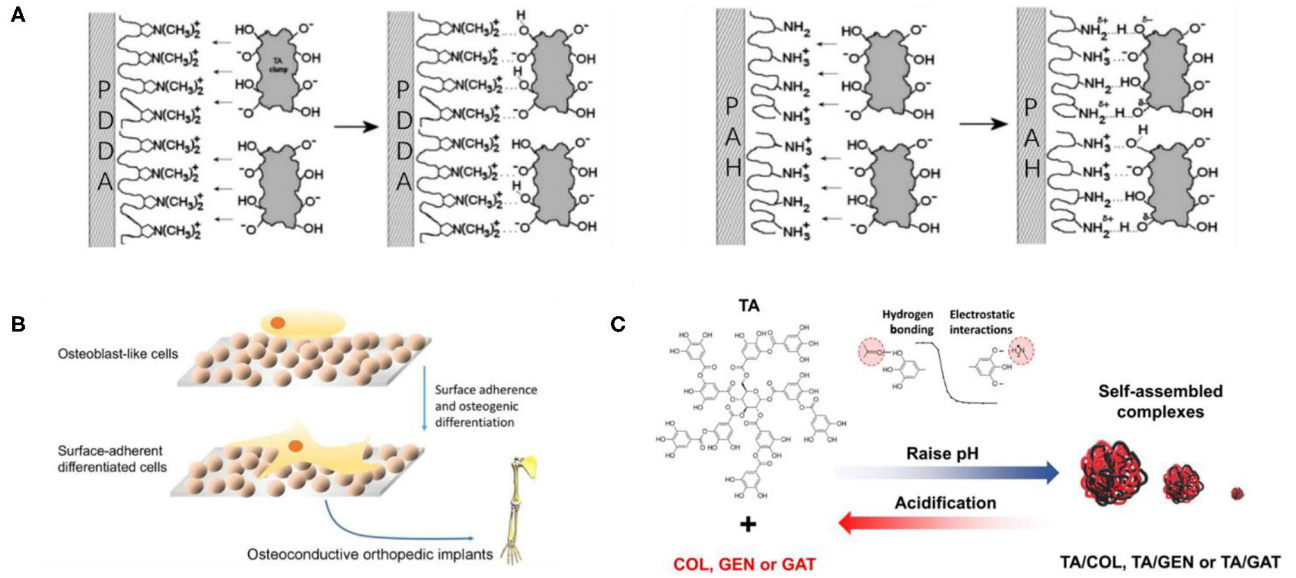

FIGURE 5 | Electrostatic assembly and application of TA. **(A)** Possible bond formation models of the interaction between TA and polyamine in LbL films for PAH and PDDA (Shutava et al., 2005). **(B)** Osteoconductive behavior of PHPE-TA multilayers (Onat et al., 2018). **(C)** The pH-dependent assembly and dissociation of TA/drug complexes driven by electrostatic interactions and hydrogen bonding (Abouelmagd et al., 2019).

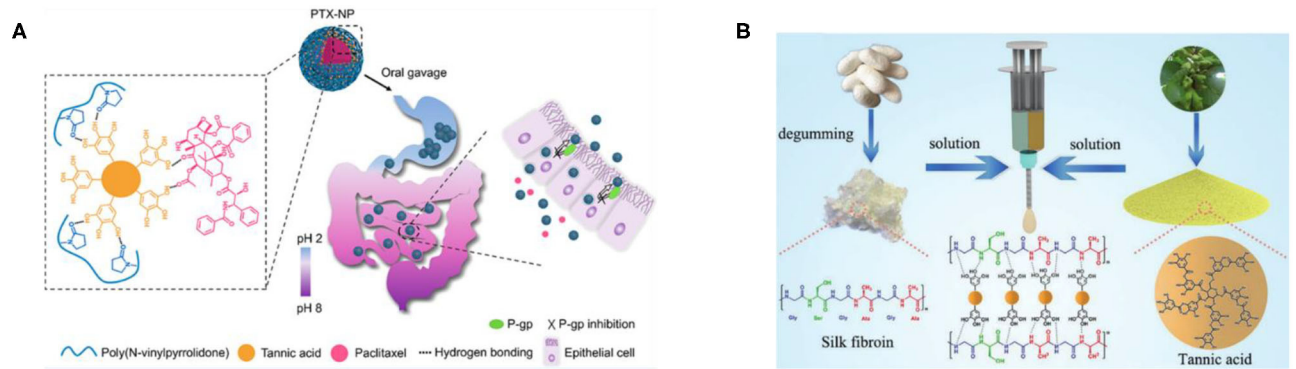

FIGURE 6 | Hydrogen-bonded assembly and application of TA. **(A)** PTX-NP assembled by intermolecular hydrogen-bonded interactions have features including P-gp inhibitory functions and pH-sensitive behavior (Le et al., 2018). **(B)** The formation schematic of the FT hydrogel adhesive (dominated by hydrogen-bond interactions) (Luo et al., 2020).

multifunctional hydrogel adhesives with high extensibility (up to 32,000%), real-time self-healing ability, underwater adhesion, sealing, biocompatibility, and antibacterial properties, through the hydrogen bonding of TA and SF chains in water, which has potential applications in medical fields such as tissue adhesives and integrated bioelectronics, as shown in **Figure 6B**. Although the polyhydroxyl structure of TA can provide relatively stable hydrogen bonds under physiological conditions due to the inherent limitations of the hydrogen-bond structure, it is greatly affected by pH, ionic strength, and other factors. As a result, the hydrogen-bond assembly of TA is unstable compared with the electrostatic interactions.

Coordination Assembly of TA

The coordination assembly of TA occurs through the MPN structure to form metal–organic supramolecular assembly materials (Richardson et al., 2016). At present, more research is focused on the assembly of TA with iron or ferrous ions, which has many applications in the field of biomedicine such as antibacterial coating (Ko and Huang, 2020), clinical diagnosis, nanoprobe treatment (Zou et al., 2018; Yan et al., 2019), tooth desensitizers (Zhou et al., 2013), separation and protection of living cells (Kim et al., 2017), self-healing and functional films (Lee et al., 2018), and antioxidant coatings (Maerten et al., 2017). Ejima et al. (2013) first proposed the synthesis of coordination complexes using natural polyphenol TA as an

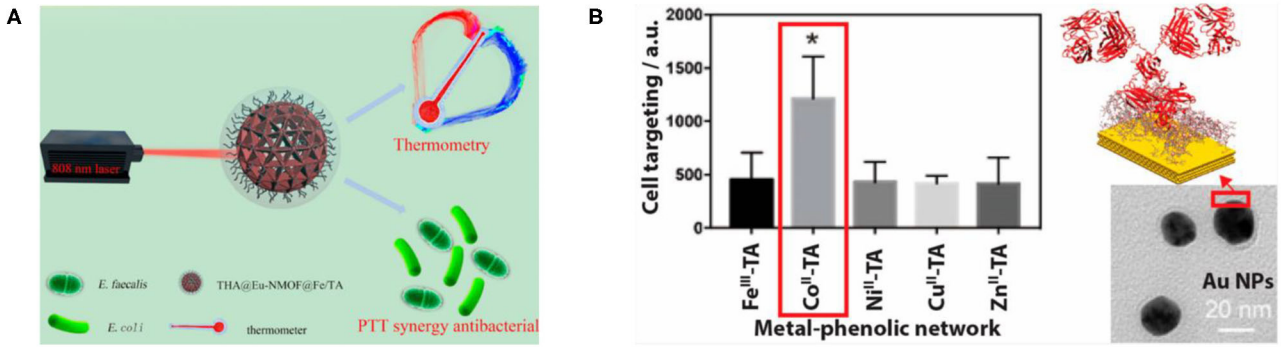

FIGURE 7 | Coordination assembly and application of TA. **(A)** The application of THA@Eu-NMOF@Fe/TA nanoprobe assembled by coordination (Yan et al., 2019). **(B)** The MPN coatings assembled by crosslinking of metal ions (FeIII, CoII, NiII, CuII, or ZnII) with TA can be used to enhance targeting (Zhang et al., 2020). *means the highest median Au intensity.

organic ligand and Fe(III) as an inorganic crosslinking agent, which can be used to prepare various films and particles on a series of substrates by one-step assembly. Because TA can be used as a molecular tool for chelating and developing iron activation, TA as a natural iron complexing agent may be a promising method for the prevention and treatment of iron-related cancer or other iron overload diseases. For example, Phiwchai et al. (2018) found that the self-assembled Fe^{3+}/TA complex formed by TA binding with extracellular iron has the characteristics of autophagy induction. Yan et al. (2019) designed and assembled an intelligent integrated nanoprobe (THA@Eu-NMOF@Fe/TA) based on the Eu(III) nanometal–organic skeleton (Eu-NMOF), in which photothermal therapy (PTT) and antimicrobial agents are carried out simultaneously by using coordinated complex Fe/TA as a photothermal and antibacterial agent. This opens the way for a new type of cancer treatment probe to achieve real-time temperature sensing feedback in the process of PTT and antibacterial effects, as shown in **Figure 7A** (Yan et al., 2019). In addition, TA can be complexed with other metals such as gold, silver (Fang et al., 2018b), zirconium (Bag et al., 2015), and stainless steel (Xu et al., 2019) to obtain supramolecular nanomaterials with different properties and biomedical functions. Zhang et al. (2020) cross-linked TA with metal ions such as [Fe(III), Co(II), Cu(II), Ni(II) or Zn(II)] to form an MPN coating, followed by coating with gold nanoparticles, and physically adsorbed antibodies on the surface, demonstrating that it could enhance the targeting of antibodies and their respective antigens, as shown in **Figure 7B**. Although the coordination complex of TA can prepare many biological functional materials, it still has some limitations. For example, the materials coordinated with TA need specific metal elements. Therefore, coordination assembly is limited by material selection (Zou et al., 2018). In addition, the assembly process is slow because of the influence of metal ligands and solvent types, and the supramolecular nanomaterials constructed may have some impurities.

Dynamic Covalent Assembly

The dynamic covalent bond integrates the characteristics of the covalent bond and non-covalent bond, endowing it with special features (Cougnon and Sanders, 2012; Lehn, 2012; Li et al., 2013). They can be formed and broken reversibly, similar to non-covalent bonds, whereas they can be as strong and durable as covalent bonds under different conditions. In recent years, because dynamic covalent interactions combine the robustness of "classical" covalent bonds with the typical flexibility of non-covalent interactions accelerating the development of complex nanostructures, increasing attention has been focused on supramolecular chemistry (Wilson et al., 2014). Five widely used dynamic covalent bonds are disulfide, hydrazone, borate esters, imines, and thioesters. The boric acid ester bond is a dynamic covalent bond formed by the coupling of boric acid with alcohols or phenols. Borate esters are unstable and are easily hydrolyzed and exchanged in the presence of o-diol and catechol (Wilson et al., 2014). Phenylboric acid (PBA) is a Lewis acid, which can form reversible borate esters with *cis*-diols such as carbohydrates and ribonucleotides (Chen et al., 2012; Kim et al., 2016b). Tumor-targeting nanoparticles mediated by PBA represent an attractive strategy for enhancing siRNA transport and treatment of metastatic cancer. However, the non-specific binding to various biofilms containing a *cis*-glycol structure limits the potential application of a drug delivery system. Fan et al. (2017a) constructed an siRNA nanodelivery system with dual functions of pH-responsiveness and tumor-targeting stemming from the reversible dynamic covalent borate bond formed by PBA and Cat based on catechol-modified polyethylene glycol (PEG-Cat) and PBA terminal polyethyleneimine (PEI-PBA), which can be used in the effective treatment of primary and metastatic tumors. Zhou et al. (2018) proposed a new reversible-covalent crosslinking strategy and prepared adenosine triphosphate (ATP)-grafted hydroxyapatite (HA) (HA-ATP) and PBA-modified PEI (PEI-PBA) to couple HA-PEI to borate bonds. By comparing the two siRNA delivery systems of physical adsorption and reversible-covalent crosslinking, the reversible-covalent crosslinking strategy is expected to turn on/off the connection between the extracellular stable state and intracellular unstable state, which can stimulate the disassembly of polymers in tumor cells and significantly improve the transport of siRNA (Zhou et al., 2018). Compared with PBA, boric acid polymers are more often used to construct reversible-covalent

borate ester bonds. Bortezomib (BTZ) is an effective and specific proteasome inhibitor for cancer treatment (Wang et al., 2015). Su et al. (2011) coupled BTZ with a polymer carrier containing catechol through a reversible dynamic covalent borate ester bond and then synthesized a new type of cell-targeted and pH-sensitive polymer carrier by modifying biotin-targeted ligands that are selectively ingested by cancer cells through the mechanism mediated by cell surface receptors, thus delivering the anticancer drug BTZ to cancer cells. However, the activity of BTZ against solid tumors is lower; systemic use will lead to a higher risk of adverse reactions, and BTZ resistance has been observed. Wang et al. (2015) reported a pH-responsive polymer based on a polyamide dendrimer, which is functionalized by the catechol group inside the dendrimer and achieves the "off-on" release of BTZ in the slightly acidic tumor microenvironment through catechol–borate dynamic covalent bonding interactions with BTZ, allowing the therapeutic effect of BTZ in cancer treatment to be maintained while reducing its adverse reactions. Recently, in view of the factors that limit the clinical application of BTZ, such as low water solubility, instability, a non-specific distribution, and poor permeability to tumors, Zhao et al. (2019a) designed a new strategy without any organic synthesis and modification. Based on the dynamic and reasonable supramolecular self-assembly of BTZ, TA, and poloxamer (F68), a new high-load, high-stability, and controlled-release nanosheet was designed. Among them, the borate ester bond has unique room temperature dynamic reversibility and a multistimulus response, which can be used as a connection. It can not only improve the efficiency of drug loading but also reduce premature leakage. This study paves a possible way to solve the dilemma between functionality and medicine, as shown in **Figure 8** (Zhao et al., 2019a). At present, some functional systems use a single type of dynamic covalent bond, but most have multiple interactions including dynamic covalent and non-covalent interactions. The application of the dynamic covalent bond in life science will focus on the coupling activation and inactivation of chemical disruptors, which may be identified by *in situ* selection (Wilson et al., 2014).

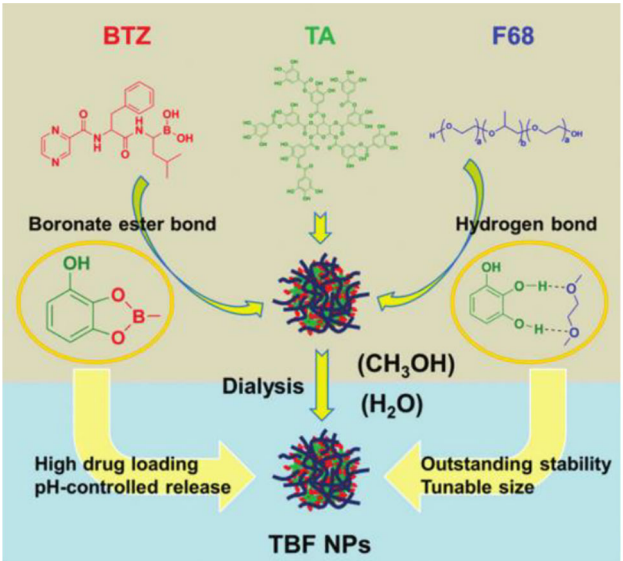

FIGURE 8 | Dynamic covalent assembly and application of TA. Construction and properties of a dynamic self-delivery system based on tannic acid (TA), bortezomib (BTZ), and poloxamer (F68) (Zhao et al., 2019a).

Mixed Interaction Assembly of TA

Despite some limitations in the stability and material selection of the supramolecular assembly process based on a single interaction, the cooperative assembly of multiple interactions can solve the above problems. The supramolecular assembly of TA with multiple interactions is carried out through dynamic covalent and non-covalent interactions such as static electricity, hydrogen bonding, hydrophobicity, and coordination, which are very common in TA and protein. Shin et al. (2018) found that TA can form multiple hydrogen bonds and hydrophobic interactions with many proteins, which is called TANNylation, and confirmed that systematic injection of TANNylated therapeutic proteins, peptides, or viruses may enhance the treatment of heart disease, as shown in **Figure 9A**. Bai et al. (2019) introduced TA into SF by electrostatic interactions and hydrogen bonding, and they developed a silk-based sealant with good moisture and instant hemostatic properties, which can be used as a promising surgical sealant for seamless sealing of ruptured tissues in wet and dynamic biological environments. Wang X. et al. (2018) prepared polyphenol–poloxamer self-assembled supramolecular nanoparticles (PPNPs), which have good biocompatibility due to multivalent hydrogen bonding between TA and PluronicF-127 combined with hydrophobic interactions on the poly(propylene oxide) chain, so PPNPs provide a good bimodal contrast agent for tumor imaging *in vivo*. Sun et al. (2020) demonstrated the possibility of developing a rapidly degradable chitosan-based multilayer film for controlled drug release and found that TA and DOX showed sustained drug release through electrostatic, hydrogen bond and hydrophobic interactions, as shown in **Figure 9B**. TA interacts strongly with proline-rich proteins, including salivary proteins, collagen, and gelatin. The PEI–gelatin–TA deposition method proposed by Ringwald and Ball (2016) can be used to prepare bioactive TA as antibacterial or antioxidant composite film materials conveniently and repeatedly. As a positively charged globular protein, lysozyme (Lys) can strongly bind to TA through hydrophobic interaction, hydrogen bonding interaction, and electrostatic interaction. Yang et al. (2019a) carried out a further study on the assembly of TA and gelatin. By taking advantage of the antioxidant properties of TA and the biocompatibility of gelatin, the TA/gelatin multilayers prepared by the LbL method showed good antioxidant properties, which are expected to improve the effect and success rate of implants. In addition, Yang et al. (2019b) used LbL to assemble and construct a multifunctional membrane (TA/Lys) with the characteristics of good oxidation resistance, rapid initial cell adhesion, enhanced osteogenesis, and broad-spectrum antibacterial, which is expected to be used in implant coating. It is worth noting that acidic lysozyme can also be assembled with graphene oxide (GO) by electrostatic, hydrophobic, π-π stacking, and van der Waals interaction.

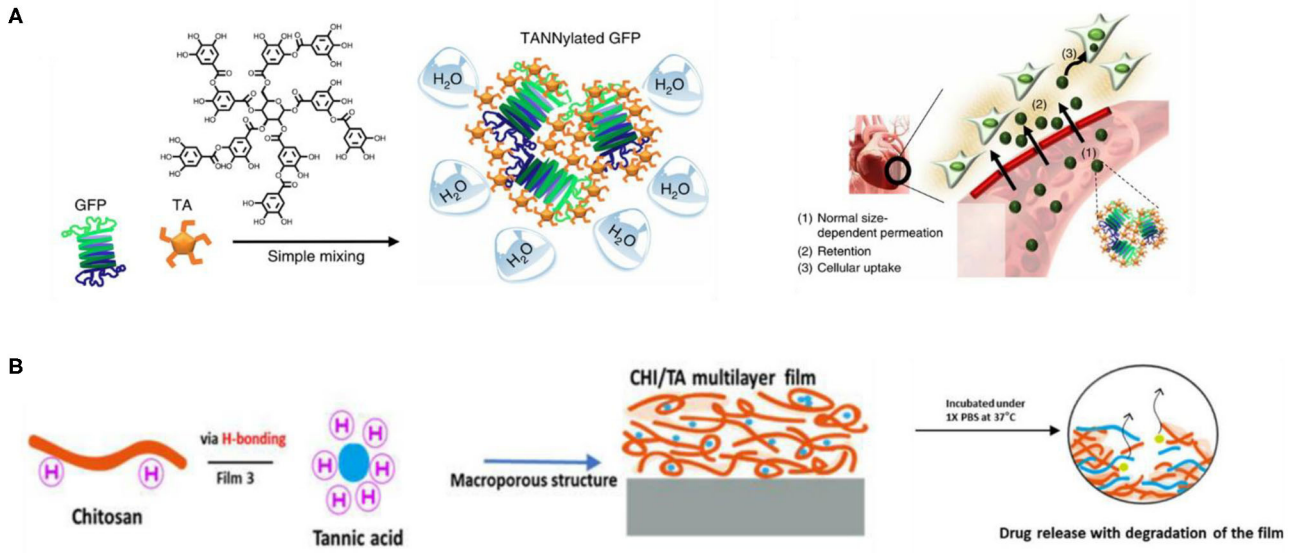

FIGURE 9 | Mixed interaction assembly and application of tannic acid. **(A)** Schematic of the preparation of nanocomplexes of TANNylated GFP resulting in heart-targeting function (Shin et al., 2018). **(B)** CHI/TA film driven by electrostatic interactions and hydrogen bonds used as a sustained drug release carrier (Sun et al., 2020).

Li et al. (2019b) prepared a 10-nm ultrathin $(GO/Lys)_8$ layer by LbL technology, which has a significant bacteriostatic effect on Gram-positive *Staphylococcus aureus* and Gram-negative *Escherichia coli* and can enhance the efficiency of osteogenic differentiation, so it has potential application in bone implant coating. The supramolecular assembly of TA based on multiple interactions has better properties than supramolecular materials assembled by a single interaction and attracts more research interest.

MEDICAL APPLICATIONS OF TA SELF-ASSEMBLY

Medical Application of Polyphenols

Polyphenols, including TA, EGCG, and catechin, are hydroxyl-rich molecules extracted from plants (Wang X. et al., 2018). The unique structure of polyphenol hydroxyl groups not only provides non-covalent bonds but also introduces dynamic covalent bonds. They have a wide range of biological characteristics, such as anti-inflammatory, anticancer, antibacterial, and antioxidation effects, resulting in their wide use in the field of biomedicine (Galante et al., 2019; Song et al., 2019). TA, as a kind of polyphenolic organic compound, has some structural properties and biological activity, and it can be used as a building unit for supramolecular assembly to obtain nanomaterials with biological functions.

EGCG, the most abundant and active polyphenol of green tea (Sundaramurthy et al., 2014), has strong binding affinity with some polymers via non-covalent bond interactions (Guillerm et al., 2012). Ren et al. (2020) used the coordination of metal–polyphenols to prepare a high-loading-capacity organic therapeutic nanodrug (PTCG-NPs) by using EGCG, Pt-OH, and PEG-b-PPOH as building blocks. The powerful metal polyphenol synergistic effect endowed PTCG-NPs with excellent stability in a physiological environment to achieve effective drug release, while activated cisplatin helped improve the level of hydrogen peroxide in cells. Through a cascade reaction, PTCG-NPs specifically opened the gates of cancer cells, releasing oxygen species and anticancer drugs to achieve the combination of chemo/chemodynamic treatment. By using Gd-doped PTCG-NPs, the imaging function was successfully introduced to monitor drug release and release behavior, providing nanodrug diagnostic ability. The translational potential of PTCG-NPs was discovered in *in vivo* studies, because they had excellent biocompatibility and synergistic antitumor effects (Ren et al., 2020). Compared with most traditional drug delivery systems, the hybrid technology of metal and polyphenol ligand improves the anticancer effect of nanodrugs, avoids the systemic toxicity of platinum drugs, and enriches the therapeutic function of nanodrugs. Their pioneering work not only provided a new strategy for the development of nanotherapeutic drugs but also expanded the application in the field of cancer treatment (Mathivanan et al., 2019). For the challenging problem of targeted therapy of metastatic melanoma, the assembly of EGCG and metal shows good results. Using green tea polyphenols, EGCG, and lanthanide metal ions (Sm^{3+}) as building blocks, Li et al. (2019a) designed self-assembled Sm-III-EGCG nanocomplexes with synergistic antitumor properties. The systemic toxic effects of these nanocomposites on healthy cells are negligible, but the activity of melanoma cells is significantly reduced by effectively regulating their metabolic pathway. Green tea–based self-assembled nanocomposites have all the key features of promising clinical candidates and can address the challenges

associated with the treatment of advanced metastatic melanoma (Li et al., 2019a).

BTZ is a first-class inhibitor of boric acid proteasome for cancer treatment. However, because of its complexation with dietary polyphenols, its therapeutic effect is severely inhibited. Inspired by this dynamic covalent chemistry, Wang et al. (2018b) proposed a polyphenol-mediated BTZ assembly strategy for a new type of supramolecular nanodrug for cancer treatment, which transformed natural polyphenols from enemies to friends. First, BTZ can simply combine with natural polyphenols containing catechol through borate bonds, and then it can conveniently form dynamic amphiphilic drugs, which possess pH-dependent assembly/disassembly behavior under special physiological conditions. Ferric ion was also incorporated into the supramolecular system via metal–phenolic coordination interactions to both introduce bioimaging functions and facilitate stability of the supramolecular nanomedicines. Second, Fe(III) ions were introduced into the supramolecular system through metal–phenol coordination, which not only endowed the biological imaging function but also promoted the stability of supramolecular nanodrugs. In addition, they chose to use four natural polyphenols with good biocompatibility and bioavailability, including catechin, EGCG, procyanidin, and TA, to confirm the versatility and modularity of the material design strategy. This unique theoretical system of supramolecular design has many advantages, such as high and precise control of drug loading, excellent biodegradation and biocompatibility, ease of operation and setup, and no requirement for presynthesis. The acquired supramolecular nanodrugs have a variety of biological functions, adjustable shapes and sizes, and limited side effects and can be used for a variety of diseases. Their work not only achieved a small drug assembly strategy based on natural polyphenols, which enables supramolecular nanodrugs to effectively release and control BTZ at targeted tumor sites, but also was very effective in treating cancer through significantly inducing tumor cell apoptosis and inhibiting tumor growth. In addition, their work promoted the further development of more kinds of natural polyphenol nanodrugs (Wang et al., 2018b).

Advantages of TA Self-Assembly in Medical Applications

Because TA has a variety of biological activities, self-assembled supramolecular nanomaterials based on TA have unique advantages in the field of biomedicine. First, TA interacts with biomolecules and metal ions in bacteria to increase the cell membrane permeability, destroy the cell membrane stability, and change the protein-to-lipid ratio (Chung et al., 1998a), so that the assembled materials have good antibacterial properties. The phenol group in TA has good antioxidant activity, in which ROS can be eliminated by converting the phenol to a quinone group to consume ROS under oxidative stress, providing the assembled material with good antioxidant activity (Liu et al., 2018). TA combines with calcium ions, one of the six most important metal ions in the process of osteogenesis, so that the assembly material has a strong osteogenic effect (Xu et al., 2018). TA, which is easily metabolized by hydrolysis of the ester bond, can be biodegraded to gallic acid and glucose without cytotoxicity to the surface (Onat et al., 2018). Therefore, it provides the assembly material with good biocompatibility and safety. TA can form precipitable complexes with proteins in a non-specific manner (Franz et al., 2011), endowing the assembly materials with hemostatic properties. TA can inhibit membrane lipid peroxidation (Mathivanan et al., 2019), resulting in assembly materials with antiviral and antitumor activity. In addition, TA endows assembly materials with medical properties such as immunomodulatory effects (Chung et al., 1998b) and targeting of heart tissue (Shin et al., 2018), so self-assembled nanomaterials based on TA have attracted attention in medical applications.

In particular, the antioxidant activity of TA itself makes it a green natural reducing agent, which can reduce many kinds of metal ions such as Au^{+}, Ag^{+}, Fe^{3+}, and Pd^{2+}, and the use of natural plant polyphenol TA as a reducing agent is in line with the principles of sustainable and eco-friendly development. Fang et al. (2018a) synthesized AuNPs@TA core-shell nanocomposites using TA as the reducing agent, and it can be utilized as a sensor for Fe^{3+} and H_2O_2. Wang et al. developed a strategy for the preparation of antibacterial nanoparticle magnetic nanocomposites by alternately depositing Lys and TA. The reducibility of TA can reduce Ag^{+} to Ag nanoparticles *in situ*, which has a synergistic antibacterial effect with TA. Because TA can be oxidized to quinone by itself to achieve the purpose of reducing Ag^{+}, the deposition of Ag nanoparticles does not require the addition of an additional reducing agent. Antibacterial experiments have shown that this nanocomposite has a good inhibitory effect on Gram-negative *E. coli* and Gram-positive *S. aureus*. In addition, because of the excellent magnetic response properties of IONPs (Fe_3O_4 nanoparticles), they are conducive to the recycling of nanocomposites, so this nanocomposite is an ideal material with green environmental protection and good antibacterial properties (Wang X. et al., 2017). In addition to metal ions, TA can reduce GO and supply material functionality. Lei et al. (2011) prepared TA-RGO (reduced GO) materials through the reduction of GO by TA and surface functional modification of GO. TA-RGO materials have good dispersibility in water and organic solvents. Therefore, we can consider the preparation of materials and functional polymers into composites. Kim et al. (2016a) prepared a polyamide reverse osmosis nanocomposite membrane with a TA-RGO active layer by polymerizing triformyl chloride, m-phenylenediamine, and TA-RGO on a polysulfone carrier. The experimental result showed that the polyamide film embedded in TA-RGO had better antibacterial properties than the polyamide film embedded in TA or GO alone.

Of course, as a biomaterial, TA has some limitations. For example, the ability of TA to inactivate protein (Ninan et al., 2016; Wang et al., 2016) and change the structure and stability of the cell membrane may harm human cells. Second, because of the chelating effect of TA on metal ions, overuse may cause diseases such as iron deficiency anemia and calcium deficiency. In addition, the use of TA on large wounds may lead to absorptive poisoning (Song et al., 2019). Supramolecular assembly can functionalize TA or assemble TA into nanostructured composites through assembly regulation, and the concentration of assembly

materials can be greatly reduced by LbL assembly, thus reducing the limitations of TA materials.

Self-Assembly System and Application of TA

Supramolecular self-assembly using TA as building blocks can generate different materials, such as hydrogels, nanoparticles/microparticles, hollow capsules, and coating films, resulting in enormous potential medical applications including drug delivery, tumor diagnosis and treatment, bone tissue engineering, biofunctional membrane materials, and the treatment of certain diseases.

Hydrogels

Natural hydrogels, such as extracellular matrix or mucus, have the ability to regulate a series of biological properties of macromolecules and cells (Crouzier et al., 2012). Therefore, biomimetic supramolecular hydrogels with biological functions have been studied. Supramolecular hydrogel is a three-dimensional polymer network with high water content formed by connecting small molecules in a non-covalent way, which has many properties, such as biocompatibility (Calo and Khutoryanskiy, 2015), excellent cell adhesion (Jen et al., 1996), biodegradability (Kamath and Park, 1993), and ease of molecular transport (Hoffman, 2012), leading to a variety of biomedical applications. TA, as a kind of economical and effective natural polyphenol compound, has a polyphenol-arm structure, which can grasp the polymer chain through a hydrogen bond, ion bond, and coordination bond. Synthetic hydrogels were first discovered by Wichterle and Lim (1960). Self-assembled hydrogels based on TA first appeared in 2015. DNA-TA film hydrogels based on hydrogen bonds were synthesized by Shin et al. (2015) via LbL assembly technology, who found that DNA/TA hybrid hydrogels have biodegradability, ductility, tissue adhesion, and hemostatic abilities. Fan et al. (2017b) developed a new strategy for crosslinking available polymers with -N- or -O- units into supramolecular hydrogels via acid interactions based on TA, a classical multifunctional material with rapid self-healing, mechanical durability, pH-responsive, and free radical–scavenging activities. The construction of supramolecular hydrogels consisted of two programs. (1) TA assembled the dynamic part via a hydrogen bond or ionic bond with a polymer chain. (2) These polymer chains were cross-connected to networks by coordination bonds with Fe(III). By adjusting the weight ratio of polymer/TA and TA/Fe^{3+}, these two interactions could be well-balanced, which is the key to constructing supramolecular hydrogels. In addition, the mechanical properties of the obtained hydrogels are regulated by the interaction balance. When the optimal proportion of TA/Fe(III) is maintained at 3:5, the component density—that is, the ratio of TA/polymer—increases, the moduli are enhanced, and the mechanical strength can be adjusted from 10 Pa to 10 kPa. Their work confirmed that TA provides a simple and feasible approach for the construction of multifunctional hydrogels, as a multifunctional and versatile catechol group modifier, which has advantages including simple processing, low cost, and a large preparation scale (Fan et al., 2017b). Considering the hydrogels prepared *in vivo* with features including minimal invasiveness, ease of use, and high translational potential, Bjornmalm et al. (2019) successfully prepared a metal–phenol supramolecular hydrogel by TA and Ti(IV) *in vivo*. Subsequently, they provided an essential characterization of the prepared hydrogel by optical and electron microscopy, Raman spectroscopy, and rheology and evaluated the permeability and porosity of the hydrogels by glucose permeability and particle tracking analysis, respectively. The results showed that the TA-Ti(IV) hydrogel not only was stable and well-tolerated but also triggered a faint and persistent foreign body reaction. In addition, the biological distribution of titanium was studied by mass spectrometry. Although 14 weeks had passed, titanium in the samples basically remained at the basic level, indicating that the accumulation of titanium in the distal tissue was very low and even negligible. Compared with the poloxamer hydrogel, the prepared TA-Ti(IV) hydrogel showed a more sustained release (from $<$1 days to $>$10 days) when the corticosteroid dexamethasone was used clinically. Apparently, their research provided a solid foundation for further development of the titanium-containing hydrogel in biomedical fields, such as drug delivery and regenerative medicine, as shown in **Figure 10A** (Bjornmalm et al., 2019). Although hydrogel-based bone adhesives are expected to revolutionize the clinical treatment of bone repair, they still have serious deficiencies, such as inappropriate mechanical strength, cytotoxicity, and poor fixation performance. Based on the unique role of gum molecules in bone strength and flexural strength, Bai et al. (2020) introduced natural polyphenol as a powerful synthetic tool for the preparation of high-performance biocompatible bone adhesives, which can avoid the defects of traditional hydrogels, enhance water-resistant fixation, and guide bone regeneration. They used TA, SF, and HA to prepare SF@TA@HA hydrogel by self-assembly, which has good biocompatibility, controllable biodegradation, strong wet adhesion ability, and broad-spectrum antibacterial activity. The synergistic effect between the strong affinity of SF and TA and the coordination bond of TA and HA resulted in excellent immobilization properties of the hydrogel. Their work proposed a biomimetic bone adhesive that can provide stable fracture fixation and accelerate bone regeneration during bone reconstruction, as shown in **Figure 10B**. In clinical applications, it is very important but challenging to prevent scarring and accelerate wound healing, especially infection. Ma et al. (2020) prepared a new thermosensitive and pH-responsive composite hydrogel (HPCH/TA/Fe) based on the simple assembly of HPCH, TA and Fe^{3+}. As a structural unit, TA can not only dynamically associate with HPCH and Fe^{3+} via non-covalent bonding but also be used as a pH-dependent and sustained-release antibacterial agent. It was found that the prepared hydrogel had good biocompatibility and long-lasting antibacterial activity. It could also effectively inhibit bacterial infection and accelerate wound healing without scarring. The hydrogel synthesized by their group is expected to have good application prospects in the treatment of infected wounds, as shown in **Figure 10C**. Inspired by natural biological protein materials, Lin et al. (2020) used TA as a molecular coupling bridge between cellulose nanocrystal (CNC) and the polyvinyl alcohol (PVA) chain to prepare a biobased advanced physical hydrogel

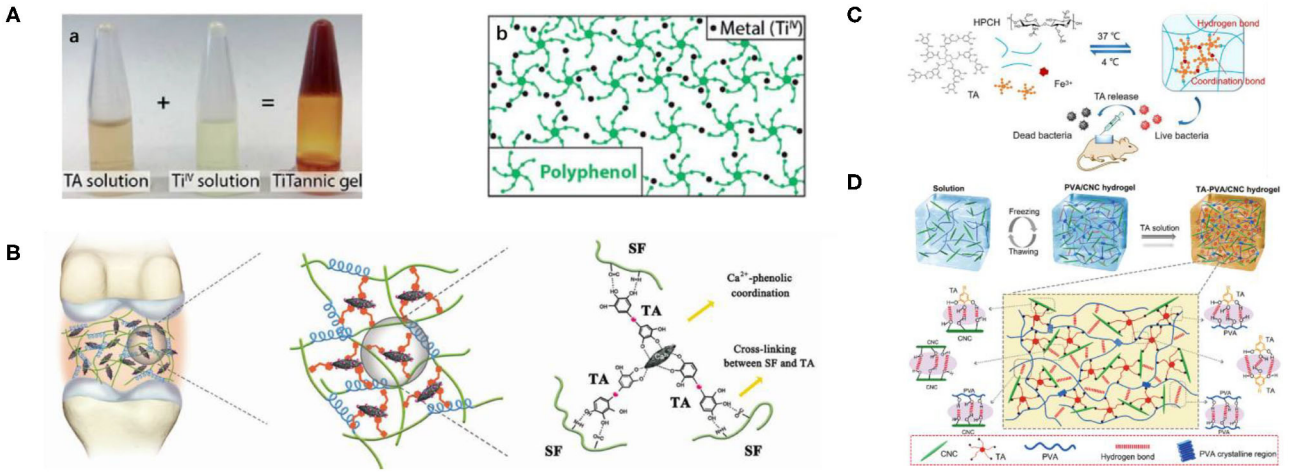

FIGURE 10 | Hydrogel based on TA and its application. **(A)** Supramolecular gelation based on TA and metal. (a) The formation process of the TA-Ti hydrogel. (b) Schematic illustration of the gel stabilized by the coordination between the metal ion and polyphenol (Bjornmalm et al., 2019). **(B)** The proposed mechanism schematic for the high toughness of SF@TA@HA (Bai et al., 2020). **(C)** The synthesis and possible schematic of the HPC H/TA/Fe hydrogel (Ma et al., 2020). **(D)** The fabrication and possible mechanism of TA–PVA/CNC hydrogels (Lin et al., 2020).

through strong hydrogen bonds. These biomimetic hydrogels have remarkable toughness, ultrahigh strength, high elongation, good self-recovery, extensive adhesion, and good antibacterial properties, resulting in broad application prospects in the field of tissue engineering and biomedicine, as shown in **Figure 10D**. In recent years, dynamic hydrogels based on macrocyclic host–guest interaction have attracted the attention of researchers. Different supramolecular hosts are introduced into hydrogels, and dynamic hydrogels with different properties can be obtained by physical or chemical crosslinking. These hydrogels have great application potential in the fields of biomedical materials, self-repairing materials, and intelligent materials. However, the formation mechanism of dynamic hydrogel still must be further studied, and as a biomedical application, hydrogel needs more extensive research in biocompatibility and cytotoxicity testing (Xiao et al., 2019b). In addition, the poor mechanical stability (Hoffman, 2012) and rapid drug release of hydrogels (Brandl et al., 2010) limit their development.

Nanoparticles/Microparticles

Polymer nanoparticles/microparticles based on non-covalent interaction are a kind of soft material that can be used as effective delivery systems with properties of a stimulus response, self-healing, and controlled release, and they are very attractive in biomedical and related applications (Wang et al., 2018a). Nanoparticles/microparticles based on hydrogen bonding have been widely studied as a delivery system in recent years. By using the intermolecular hydrogen bond and electrostatic interaction between neutral poly(2-methyl-2-oxazoline) (PMeOx), TA, and adriamycin hydrochloride (Dox), Liu et al. (2020) developed a direct coassembly strategy for the preparation of PMeOx-TA-Dox nanoparticles. The prepared spherical nanoparticles possessed advantages of good water dispersion, stability, and biocompatibility. In addition, PMeOx-TA-Dox nanoparticles had pH-dependent drug loading and release behavior and cell uptake characteristics, as Dox and PMeOx-TA can be separated rapidly in fetal serum, which can promote Dox release and entry into the nucleus. Their work was expected to reveal a new therapeutic drug carrier, as shown in **Figure 11A** (Liu et al., 2020). In addition, researchers have studied nanoparticles/microparticles based on coordination. He et al. (2020) developed Lira/TA/Al^{3+}ternary nanoparticles based on the formation of a hydrogen bond between Lilaru peptide and TA and the stability of the complexation of TA with Al^{3+}, which can be used to treat T_2D by frequent administration of lira peptide, to overcome the shortcomings of low bioavailability and lira with a short half-life. The high stability and controllable size of nanoparticles are mainly determined by the hydrogen bond between lira and TA as the main driving force and the coordination of Al^{3+} and TA as an additional crosslinking effect. This nanoparticle system shows better therapeutic potential because of its long-term blood glucose control, improved cardiovascular function, and reduced tissue toxicity of multiple organs, as shown in **Figure 11B** (He et al., 2020). Xiong et al. (2019) used doxorubicin as a chemotherapeutic drug, ferric trichloride ($FeCl_3$) as an iron prolapse inducer, and TA as an intracellular superoxide dismutase–like reaction activator to construct a drug-organic-inorganic self-assembly nanosystem (DFTA) for the combined treatment of ER^+ breast cancer. The assembled nanosystem is based on coordination and π-π interactions. The authors found that the oxidative stress disorders were antagonized by intracellular oxidation–reduction cascade reactions, ferroptosis, and PT, thus endowing the $DFTA^+$ laser system with the effect of accurately attacking ER^+ breast cancer, which has obvious antitumor effects and low toxicity. Their highly effective nanosystem based on chemotherapy, iron decline, and platinum is expected to be a new approach for

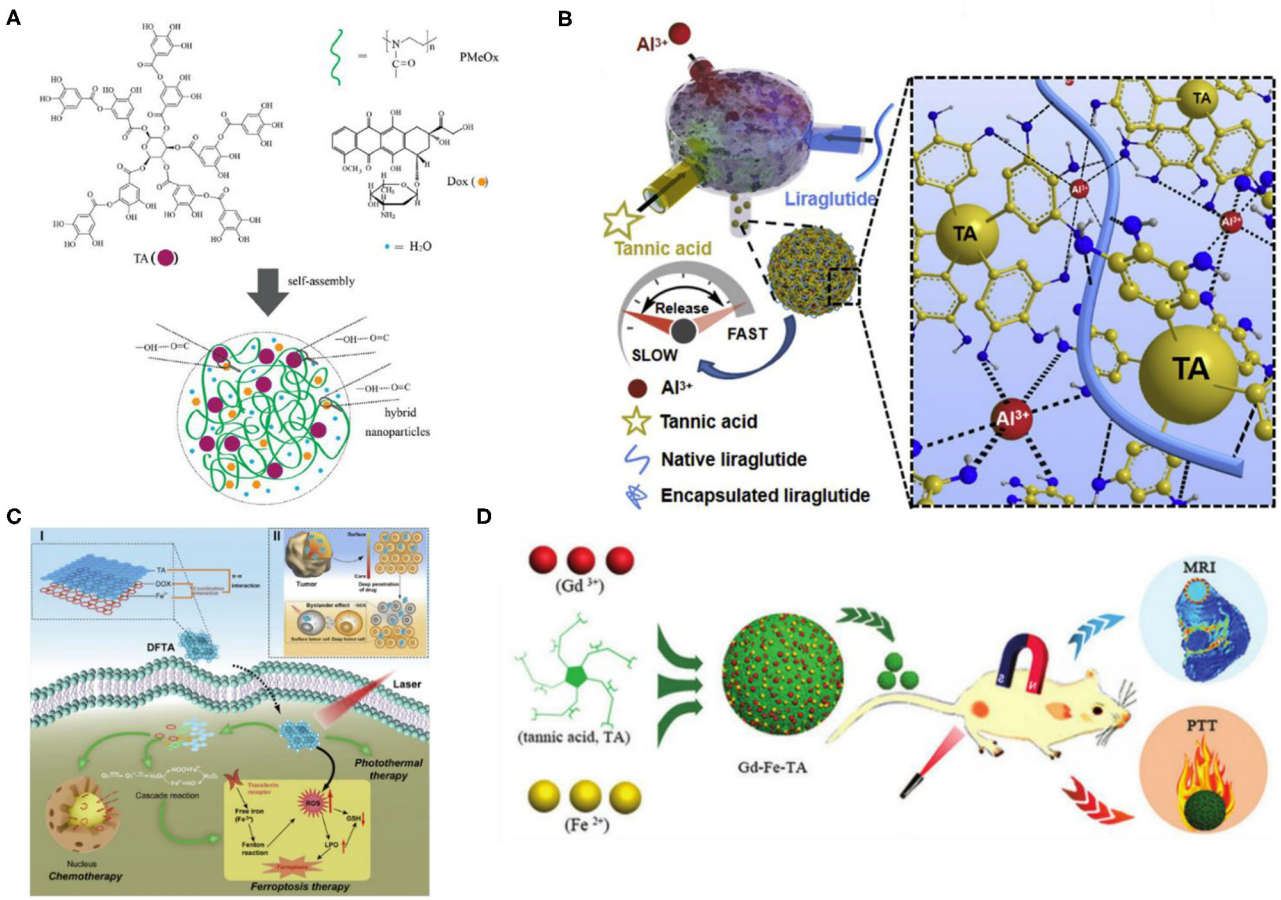

FIGURE 11 | Nano/microparticles based on TA and its application. **(A)** Chemical structures of TA, PMeOx, and Dox and a schematic of nanoparticles based on them (Liu et al., 2020). **(B)** Schematic illustration of the ternary nanoparticle assembly based on TA and Al^{3+} (He et al., 2020). **(C)** The assembly of DFTA driven by π-π interactions and coordination reactions, as well as triple combination therapy mechanisms of DFTA after targeted uptake by tumor cells (Xiong et al., 2019). **(D)** The synthesis and applications of polymer nanoparticles based on bimetal–TA (Qin et al., 2020).

the effective treatment of ER^+ breast cancer, as shown in **Figure 11C**. Qin et al. (2020) used gadolinium nitrate and ferrous sulfate as metal sources and plant polyphenols (TA) as organic ligands to synthesize bimetallic–phenolic coordination polymer nanoparticles by the metal–catechol coordination assembly process, which can not only effectively enhance tumor signals as contrast agents but also effectively inhibit tumor growth by photothermotherapy. This work provides a new idea for the synthesis of multifunctional coordination polymer nanoparticles and expands their potential applications in the field of acoustics, as shown in **Figure 11D**. Although the preparation of nanoparticles has been widely studied in recent years, the low efficiency of preparation technology, tedious steps, and other factors limit their wider application, so how to obtain stable nanoparticles more simply and efficiently may be a future research direction.

Hollow Capsules

Hollow capsules fabricated via LbL assembly of polymers comprise an ultrathin permeable shell (<50 nm) that participates in various types of interactions (Mathivanan et al., 2019; Wang et al., 2020) and microsized or nanosized cavities that deposit drugs or active molecules. The shells are able to trigger the release of loaded molecules to protect the load from external stress and thus extend the time of release. The initial related research has mainly focused on the assembly of metal coordination capsules, and the engineering of metal-specific functions for capsule design is rarely explored. Guo et al. (2014) reported that a multifunctional capsule assembled by an MPN is prepared by a phenolic ligand (TA) and a series of metals. The film thickness, disassembly characteristics, and fluorescence behavior of MPN capsules can be controlled by coordination metals. In addition, the functional properties of MPN capsules are customized for drug delivery, positron emission tomography, magnetic resonance imaging (MRI), and catalysis (Guo et al., 2014). An excellent feature of LbL capsules is that they are capable of accurately controlling the transport and release of drug or biologically active molecules by inherent responsiveness against environmental and external triggers (Mathivanan et al., 2019). The risk of instability in the chemical and physical

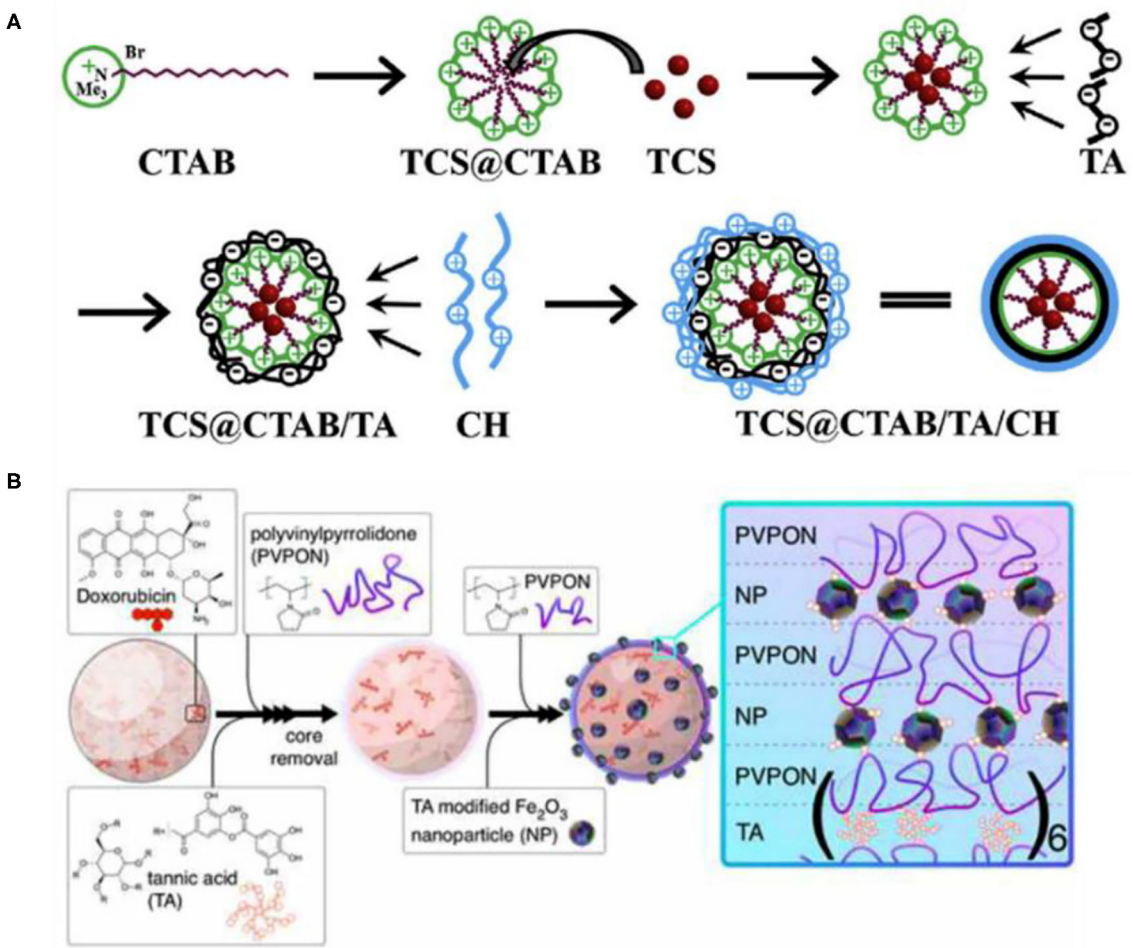

FIGURE 12 | Hollow capsules based on TA and their application. **(A)** The preparation of nanocapsules via electrostatic assembly (Cai et al., 2019). **(B)** The assembly of hollow $(TA/PVPON)_n$ capsules (n denotes the number of bilayers) on doxorubicin-loaded porous 3-μm SiO_2 microparticles. The final shell composition $[(TA/PVPON)_6(Fe_2O_3/PVPON)_2]$ was obtained by depositing Fe_2O_3 nanoparticles (NPs) modified by TA in alternating layers with PVPON (Alford et al., 2018).

properties of capsules can be minimized by changing the layer number and polymer species in the shell (Alford et al., 2018). The unique properties of hollow capsules have resulted in their wide attention in various fields, such as nanoreactors, sensors for nanomedicine, and drug delivery for disease diagnosis and treatment (Wang P. et al., 2018). Mathivanan et al. (2019) prepared a capsule and coating (TA/PnPropOx) based on the LbL assembly technology of TA and PnPropOx, where natural polyphenol TA was used for the hydrogen-bond donor. They found that the temperature and pH of the assembly process had an apparent influence on the physical properties of the capsule, including growth, morphology, and stability. The capsule also showed good stability at pH 2–9, which might be attributed to the dehydration of TA/PnPropOx during LbL assembly. Because the side chain controls the hydrophilic and hydrophobic balance in the capsule, it is necessary to study the influence of the two-position side chain in poly(2-oxazoline) on the encapsulation performance and permeability of the capsule in the future. In conclusion, the capsules they prepared showed considerable potential for drug release (Mathivanan et al., 2019). Cai et al. (2019) first prepared novel nanocapsules (TCS@CTAB/TA/CH) using an electrostatic LbL assembly method with the alternative imine bond as an assembly driving force, which can be used for drug introduction and controlled release. When the pH changed from 8 to 4, the release efficiency of TCS increased by 61.8%, which was mainly because the TA/CH could be used as a pH bacterial-triggered valve to control TCS release, indicating that the prepared nanocapsules had good pH-responsive activity. Subsequently, the nanocapsules and dextran aldehyde (DA) could be assembled into pH-responsive $(DA\text{-}TCS@CTAB/TA/CH)_n$ multifilms with good antibacterial and adhesion resistance through the imine bond. The controllable release function of the films positions them as a new antibacterial material for surface modification of antibacterial materials, as shown in **Figure 12A** (Cai et al., 2019). Alford et al. (2018) introduced a novel 3-μm-diameter biocompatible microcapsule composed of TA and poly(N-vinylpyrrolidone) and 4-nm iron oxide nanoparticles via LbL deposition in 2018, which can

be used as a contrast agent to achieve targeted drug delivery and real-time tracking by combining MRI and ultrasound-triggered drug release technology. The characteristics of these materials include a long cycle; active contrast; a customizable shape, size, and composition; and precise high payload delivery, which provide a safe and powerful platform as efficient contrast-enhanced imaging agents to facilitate real-time tracking and targeted delivery of encapsulated drugs, showing great value in biomedical imaging, as shown in **Figure 12B** (Alford et al., 2018). Future research on the supramolecular assembly of nanocapsules should focus on the following points: (1) to find assembly materials with reasonable rates and biosafety of biodegradation, (2) to improve the loading and release efficiency of hollow capsules, (3) to accurately achieve the release of hollow capsules at the determined site through environmental response or an external trigger, and (4) to achieve the multifunctional integration of hollow capsules for biomedical applications.

Coating Films

Self-assembled coatings for surface modification and medical potential have become a hot research topic. The assembled coating has a good adjustable structure and reproducibility, so it is widely used in many medical fields, including dental implants and bone coatings. Ejima et al. (2013) first proposed synthesis of coordination complexes using natural polyphenol TA as an organic ligand and Fe(III) as an inorganic crosslinking agent, which can be used to prepare various films and particles on a series of substrates by one-step assembly. This coordination complex assembly based on metal–polyphenols is a milestone for the development of a simple and general strategy for thin film and particle engineering (Ejima et al., 2013). The one-step assembly of coordination complexes for versatile film and particle engineering not only gives assembly the advantages of a simple process, mild manufacturing conditions, varied materials, and low equipment cost but also allows the coating of a variety of substrates with different complex shapes and the precise control of coating thickness up to the nanometer scale. To achieve a persistent, flat, and stable insulin supply, a new drug carrier was designed. Wang et al. (2020) assembled PEG–insulin and TA into a film, which can release PEG–insulin into the medium through a reversible, dynamic hydrogen bond. In addition, the unique release mechanism of the films explained the unique release kinetics of PEG–insulin, which had zero-order kinetics. The composite films can help reduce fasting blood glucose level that are close to normal for an extended period. Of note, the thickness of the film is closely related to the reaction time. Their work was promising in the treatment of diabetes, as shown in **Figure 13A** (Wang et al., 2020). Zhu et al. (2019) constructed a novel multifunctional thin-film nanofibrous composite membrane based on TA and polyvinyl alcohol (PSBMA) on TFNC membrane surfaces by LbL assembly, expecting to achieve the filtration of dye and protein. The composite membranes had not only excellent blood compatibility, such as a great reduction of platelet adhesion, reduction of the hemolysis rate, and significant prolongation of the clotting time, but also good antibiological pollution performance, including lower bovine serum albumin (BSA) adsorption, better hydrophilicity, less *E. coli* and *S. aureus* bacterial attachment and higher water flux recovery. Their zwitterionic multilayers demonstrated broad application prospects in the fields of water treatment and blood contact biomedicine and provided a useful idea for the preparation of biocompatible coatings on various substrates (Zhu et al., 2019). By chelating TA and Fe^{3+} ions, Song et al. (2019) assembled the TA coating on medical gauze as a hemostatic dressing to solve the problem of potential absorption poisoning with large-area wound TA. The study found that the TA coating possessed excellent adsorption on proteins including BSA, immunoglobulin G, and fibrinogen. In addition, it had a good hemostatic performance in the process of animal wound coagulation due to erythrolysis and protein adsorption, especially the fibrinogen associated with blood clotting. Their coating with features, including economical, environmentally friendly and flexibility characteristics, demonstrated the potential to become a new type of hemostatic material in the medical field, as shown in **Figure 13B** (Song et al., 2019). Kumorek et al. (2020) prepared LbL films based on TA as cationic modifiers and pristine chitosan, which was modified with N-(2-hydroxypropyl)-3-trimethylammonium chloride. The films showed excellent antibacterial properties and an obvious pH dependence. They found that electrostatic interactions mainly drove the formation of the complex, while hydrogen bonding accompanied the process. The pH triggered the decomposable LbL membrane for use as a degradable coating, allowing the release of therapeutic drugs in biomedical applications and preventing bacterial adhesion (Kumorek et al., 2020). Because the preparation process of TA supramolecular assembled nanofilm coating is simple, the structure is controllable, and it can be coated on almost all substrates, endowing it with great prospects in bone tissue engineering and the functionalization of biomaterials. The antibacterial application of medical devices has great prospects, and the assembled film coating can be assembled by hydrogels, microparticles/nanoparticles and capsules, thus enriching the structure and function of the assembly materials.

Although various functional nanomaterials based on TA self-assembly have attracted increasing attention, some problems related to TA or the histidine complex should not be overlooked. For example, the practical use of antioxidants and chelating agents based on TA in the gastrointestinal tract is limited by the ability of tannins to bind to proteins in foods in non-specific ways, forming insoluble sediments and aggregates. TA has also been reported to inhibit the activity of digestive enzymes (Zhao et al., 2013). Similar to the self-assembled membrane of TA, on the one hand, the pH value has great prospects for the performance of membrane (Shutava et al., 2005; Zhou et al., 2013), because the dissociation of the phenolic hydroxyl group and direct breaking of the hydrogen bond cause the rapid destruction of the film in high pH solution. On the other hand, the stability of the membrane under physiological conditions has a negative impact on the reactivity of the capsule shell (Richert et al., 2004). In addition, when the polymer and TA are mixed in aqueous solution, hydrogels are often not obtained because of the dependence on hydrogen bonds or ionic interactions rather than covalent grafting but show homogeneous solutions or agglomerations. However, with the addition of Fe^{3+} and the

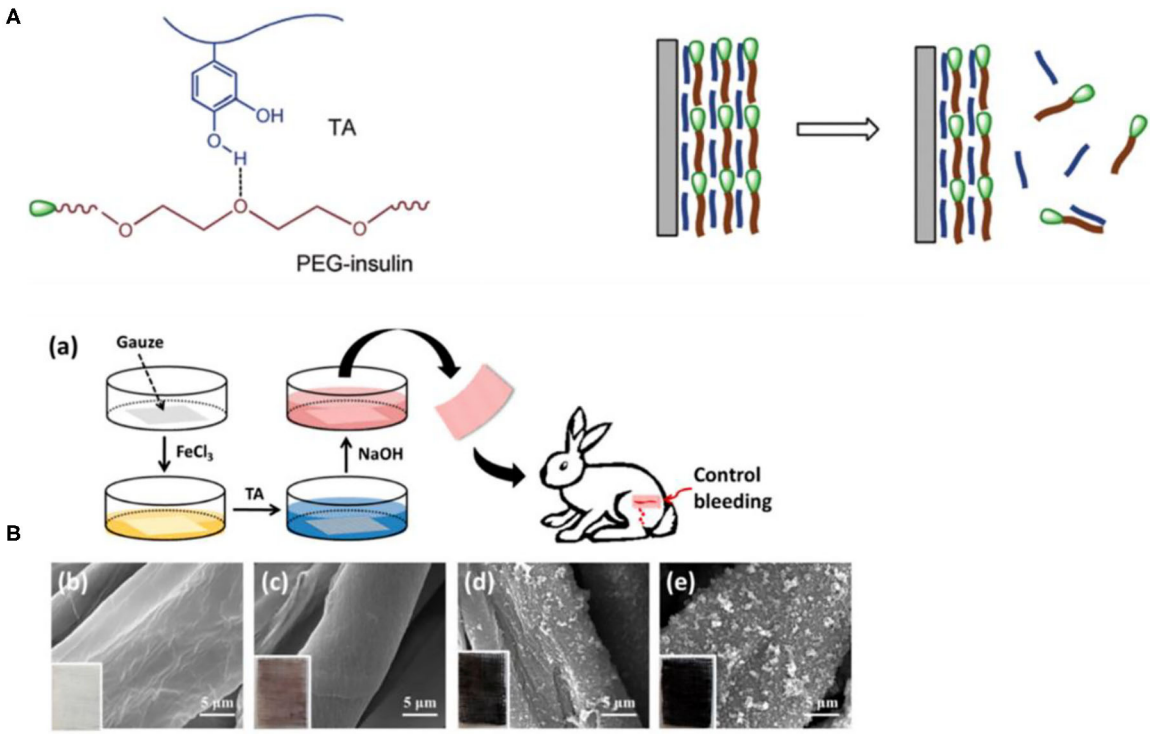

FIGURE 13 | Coating films based on TA and their application. **(A)** The interaction of PEG–insulin and TA was driven by hydrogen bonding, and gradual disintegration of the PEG–insulin/TA LbL film led to the release of PEG–insulin (Wang et al., 2020). **(B)** (a) The preparation and application of the TA-coated gauze in bleeding control [SEM images of the gauze deposited with 0 (b), 1 (c), 3 (d), and 5 (e) TA deposition cycles] (Song et al., 2019).

pH adjustable coordination interaction between TA and Fe^{3+}, an ideal hydrogel is obtained (Fan et al., 2017b).

CONCLUSION AND FUTURE PERSPECTIVES

In the past decades, supramolecular assembly technology has been greatly enriched and developed, from traditional dip-coating assembly, spin-coating assembly, spray assembly, jet assembly, and electromagnetic assembly to the current lithography technology, three-dimensional printing and DPN (DPN is the technology of transferring alkyl mercaptan to a gold surface using an atomic force microscope cantilever tip), as well as dynamic film, coordination drive assembly and stereo complex assembly technology (Richardson et al., 2016). The regulation of supramolecular assembly is more accurate, which gives more functions to materials. Thus, supramolecular assembly based on TA has achieved great development in a short time. Although the existing supramolecular assembly technology is not applied in its entirety to the assembly of TA, the development of cutting-edge technologies such as lithography and DPN may push the supramolecular assembly of TA to a new level.

TA has special structural properties and biological activity. The polyhydroxyl structure of TA endows it with the ability to assemble supramolecular nanomaterials through a variety of non-covalent and covalent interactions. Additionally, the biocompatibility and antibacterial and antioxidant activities of TA allow supramolecular assembly materials to possess a variety of biomedical applications. The precise regulation of the structure by supramolecular assembly, combined with the structure and biological activity of TA, gives the supramolecular assembly nanomaterials of TA unique advantages in the fields of drug delivery, bone tissue engineering, and functional membrane coating, among others.

Although supramolecular assembly based on TA has many advantages, some challenges remain. From the dimension of the driving force of TA supramolecular assembly, the cationic polymer as a construction unit in assembly materials by electrostatic interactions may cause problems of cytotoxicity. Thus, the search for a low charge density, safe profile after biodegradation, and non-cytotoxic cationic polymers as construction units can solve the problem of cytotoxicity of electrostatic assembly. Although the assembly materials based on hydrogen bonding do not introduce cationic polymers, the assembled materials are unstable relative to electrostatic assembly due to the influence of pH, ionic strength, and other factors. However, the assembly process based on coordination is slow and can easily introduce impurities. In addition, other interactions, such as hydrophobic, charge transfer interaction, and host–guest interactions, as well as π-π stacking, are generally not used as the driving force of assembly alone but function together with other interactions to drive the assembly of TA supramolecular materials. Generally, supramolecular assembly

with a single non-covalent interaction is relatively unstable, and the selection of assembly materials is few, so the development of mixed interaction assembly of TA may assemble more stable nanomaterials, and it may also be a good strategy to expand the variety of assembly materials. From the dimension of the TA assembly system, hydrogel supramolecules have limitations of poor mechanical stability (Hoffman, 2012) and rapid drug release (Brandl et al., 2010). The low efficiency and tedious steps of the preparation of microparticles/nanoparticles limit their wide application. For the hollow capsule system, how to improve the loading efficiency of the hollow capsule, accurately control the release, and achieve the multifunctional integration of hollow capsule biomedical devices remains as a challenge. In addition, the membrane coating system can be assembled by hydrogels, microparticles/nanoparticles and capsules to enrich the structure and function of the assembly materials, which may be an ideal strategy to change the TA assembly defects.

Supramolecular assembly materials of TA have been applied in the fields of drug delivery, tumor diagnosis and treatment, bone tissue engineering, biological functional membrane materials, and the treatment of certain diseases. It is believed that with the gradual deepening of the study of plant polyphenols and the development of supramolecular assembly technology, the application value of supramolecular nanomaterials based on TA will be better developed, and it will be more widely used in the field of medicine.

AUTHOR CONTRIBUTIONS

RL collected the literature involved in the review, wrote the draft of the review, and revised its format. XZh supplemented the content of the review. XC and LZ put forward suggestions for revision of the content of the review. XZa and YZ put forward constructive suggestions for review writing and revision. All authors contributed to the article and approved the submitted version.

FUNDING

This work was financially supported by the National Natural Science Foundation of China (21464015 and 21472235), Xinjiang Tianshan Talents Program (2018xgytsyc 2-3), UESTC Talent Startup Funds (A1098 5310 2360 1208), and One Thousand Talents Program.

REFERENCES

Abouelmagd, S. A., Abd Ellah, N. H., Amen, O., Abdelmoez, A., and Mohamed, N. G. (2019). Self-assembled tannic acid complexes for pH-responsive delivery of antibiotics: role of drug-carrier interactions. *Int. J. Pharm.* 562, 76–85. doi: 10.1016/j.ijpharm.2019.03.009

Adatoz, E. B., Hendessi, S., Ow-Yang, C. W., and Demirel, A. L. (2018). Restructuring of poly(2-ethyl-2-oxazoline)/tannic acid multilayers into fibers. *Soft Matter* 14, 3849–3857. doi: 10.1039/C8SM00381E

Alford, A., Rich, M., Kozlovskaya, V., Chen, J., Sherwood, J., Bolding, M., et al. (2018). Ultrasound-triggered delivery of anticancer therapeutics from MRI-visible multilayer microcapsules. *Adv. Therap.* 1:1800051. doi: 10.1002/adtp.201800051

Andjelkovic, M., Van Camp, J., De Meulenaer, B., Depaemelaere, G., Socaciu, C., Verloo, M., et al. (2006). Iron-chelation properties of phenolic acids bearing catechol and galloyl groups. *Food Chem.* 98, 23–31. doi: 10.1016/j.foodchem.2005.05.044

Aoki, K., Shinke, R., and Nishira, H. (1981). Formation of tannic acid–protein complex on polyacrylamide gels and its application to electrophoretic technique. *Agric. Biol. Chem.* 45, 121–127. doi: 10.1271/bbb1961.45.121

Appella, D. H., Christianson, L. A., Karle, I. L., Powell, D. R., and Gellman, S. H. (1996). beta-peptide foldamers: Robust Helix formation in a new family of beta-amino acid oligomers. *J. Am. Chem. Soc.* 118, 13071–13072. doi: 10.1021/ja963290l

Ariga, K., Ahn, E., Park, M., and Kim, B. S. (2019). Layer-by-layer assembly: recent progress from layered assemblies to layered nanoarchitectonics. *Chem. Asian J.* 14, 2553–2566. doi: 10.1002/asia.201900627

Bag, E., Begik, O., Yusan, P., and Erel-Goktepe, I. (2015). Hydrogen-bonded multilayers with controllable pH-induced disintegration kinetics for controlled release applications from surfaces. *J. Macromol. Sci. A Pure Appl. Chem.* 52, 286–298. doi: 10.1080/10601325.2015.1007274

Bai, S., Zhang, X., Cai, P., Huang, X., Huang, Y., Liu, R., et al. (2019). A silk-based sealant with tough adhesion for instant hemostasis of bleeding tissues. *Nanoscale Horizon.* 4, 1333–1341. doi: 10.1039/C9NH00317G

Bai, S., Zhang, X., Lv, X., Zhang, M., Huang, X., Shi, Y., et al. (2020). Bioinspired mineral-organic bone adhesives for stable fracture fixation and accelerated bone regeneration. *Adv. Funct. Mater.* 30:1908381. doi: 10.1002/adfm.201908381

Balzani, V., Credi, A., Raymo, F. M., and Stoddart, J. F. (2000). Artificial molecular machines. *Angew. Chem. Int. Ed. Engl.* 39, 3348–3391. doi: 10.1002/1521-3773(20001002)39:19<3348::AID-ANIE3348>3.0.CO;2-X

Bernal, J. D., and Megaw, H. D. (1935). The function of hydrogen in intermolecular forces. *Proc. R. Soc. Lond. A Math. Phys. Sci.* 151, 0384–0420. doi: 10.1098/rspa.1935.0157

Bjornmalm, M., Wong, L. M., Wojciechowski, J. P., Penders, J., Horgan, C. C., Booth, M. A., et al. (2019). *In vivo* biocompatibility and immunogenicity of metal-phenolic gelation. *Chem. Sci.* 10, 10179–10194. doi: 10.1039/C9SC03325D

Brandl, F., Kastner, F., Gschwind, R. M., Blunk, T., Tessmar, J., and Goepferich, A. (2010). Hydrogel-based drug delivery systems: comparison of drug diffusivity and release kinetics. *J. Control. Release* 142, 221–228. doi: 10.1016/j.jconrel.2009.10.030

Cai, H., Wang, P., and Zhang, D. (2019). pH-responsive linkages-enabled layer-by-layer assembled antibacterial and antiadhesive multilayer films with polyelectrolyte nanocapsules as biocide delivery vehicles. *J. Drug Deliv. Sci. Technol.* 54:101251. doi: 10.1016/j.jddst.2019.101251

Calo, E., and Khutoryanskiy, V. V. (2015). Biomedical applications of hydrogels: A review of patents and commercial products. *Eur. Polym. J.* 65, 252–267. doi: 10.1016/j.eurpolymj.2014.11.024

Cassier, T., Lowack, K., and Decher, G. (1998). Layer-by-layer assembled protein/polymer hybrid films: nanoconstruction via specific recognition. *Supramol. Sci.* 5, 309–315. doi: 10.1016/S0968-5677(98)00024-8

Caulder, D. L., and Raymond, K. N. (1999). Supermolecules by design. *Acc. Chem. Res.* 32, 975–982. doi: 10.1021/ar970224v

Chen, W. X., Cheng, Y. F., and Wang, B. H. (2012). Dual-responsive boronate crosslinked micelles for targeted drug delivery. *Angew. Chem. Int. Ed. Engl.* 51, 5293–5295. doi: 10.1002/anie.201201179

Chung, K. T., Lu, Z., and Chou, M. W. (1998a). Mechanism of inhibition of tannic acid and related compounds on the growth of intestinal bacteria. *Food Chem. Toxicol.* 36, 1053–1060. doi: 10.1016/S0278-6915(98)00086-6

Chung, K. T., Wong, T. Y., Wei, C. I., Huang, Y. W., and Lin, Y. (1998b). Tannins and human health: a review. *Crit. Rev. Food Sci. Nutr.* 38, 421–464. doi: 10.1080/10408699891274273

Claudine Fouquey, J. M. L., and Anne-Marie, L. (1990). Molecular recognition directed self-assembly of supramolecular liquid crystalline polymers

from complementary chiral components. *Adv. Mater.* 5, 254–257. doi: 10.1002/adma.19900020506

Cochin, D., and Laschewsky, A. (1999). Layer-by-layer self-assembly of hydrophobically modified polyelectrolytes. *Macromol. Chem. Phys.* 200, 609–615. doi: 10.1002/(SICI)1521-3935(19990301)200:3<609::AID-MACP609>3.0.CO;2-X

Costa, E., Coelho, M., Ilharco, L. M., Aguiar-Ricardo, A., and Hammond, P. T. (2011). Tannic acid mediated suppression of PNIPAAM microgels thermoresponsive behavior. *Macromolecules* 44, 612–621. doi: 10.1021/ma1025016

Cougnon, F. B. L., and Sanders, J. K. M. (2012). Evolution of dynamic combinatorial chemistry. *Acc. Chem. Res.* 45, 2211–2221. doi: 10.1021/ar200240m

Crouzier, T., Beckwitt, C. H., and Ribbeck, K. (2012). Mucin multilayers assembled through sugar-lectin interactions. *Biomacromolecules* 13, 3401–3408. doi: 10.1021/bm301222f

Cui, H. G., and Xu, B. (2017). Supramolecular medicine. *Chem. Soc. Rev.* 46, 6430–6432. doi: 10.1039/C7CS90102J

Davis, M. E., Zuckerman, J. E., Choi, C. H. J., Seligson, D., Tolcher, A., Alabi, C. A., et al. (2010). Evidence of RNAi in humans from systemically administered siRNA via targeted nanoparticles. *Nature* 464, 1067–U1140. doi: 10.1038/nature08956

De Greef, T. F. A., Smulders, M. M. J., Wolffs, M., Schenning, A., Sijbesma, R. P., and Meijer, E. W. (2009). Supramolecular polymerization. *Chem. Rev.* 109, 5687–5754. doi: 10.1021/cr900181u

Decher, G., and Hong, J. D. (1991). Buildup of ultrathin multilayer films by a self-assembly process.1. consecutive adsorption of anionic and cationic bipolar amphiphiles on charged surfaces. *Makromol. Chem. Macromol. Symp.* 46, 321–327. doi: 10.1002/masy.19910460145

Decher, G., Hong, J. D., and Schmitt, J. (1992). Buildup of ultrathin multilayer films by a self-assembly process.3. consecutively alternating adsorption of anionic and cationic polyelectrolytes on charged surfaces. *Thin Solid Films* 210, 831–835. doi: 10.1016/0040-6090(92)90417-A

Dietrich-Buchecker, C. O., Sauvage, J. P., and Kintzingi, J. P. (1983). Une nouvelle famille de molecules : les metallo-catenanes. *Tetrahedron Lett.* 24, 5095–5098. doi: 10.1016/S0040-4039(00)94050-4

Dong, C., Wang, Z., Wu, J., Wang, Y., Wang, J., and Wang, S. (2017). A green strategy to immobilize silver nanoparticles onto reverse osmosis membrane for enhanced anti-biofouling property. *Desalination* 401, 32–41. doi: 10.1016/j.desal.2016.06.034

Ejima, H., Richardson, J. J., Liang, K., Best, J. P., van Koeverden, M. P., Such, G. K., et al. (2013). One-step assembly of coordination complexes for versatile film and particle engineering. *Science* 341, 154–157. doi: 10.1126/science.1237265

Fan, B., Kang, L., Chen, L., Sun, P., Jin, M., Wang, Q., et al. (2017a). Systemic siRNA delivery with a dual pH-responsive and tumor-targeted nanovector for inhibiting tumor growth and spontaneous metastasis in orthotopic murine model of breast carcinoma. *Theranostics* 7, 357–376. doi: 10.7150/thno.16855

Fan, H., Wang, L., Feng, X., Bu, Y., Wu, D., and Jin, Z. (2017b). Supramolecular hydrogel formation based on tannic acid. *Macromolecules* 50, 666–676. doi: 10.1021/acs.macromol.6b02106

Fang, Y., Tan, J., Lan, T., Foo, S. G. F., Pyun, D. G., Lim, S., et al. (2018b). Universal one-pot, one-step synthesis of core-shell nanocomposites with self-assembled tannic acid shell and their antibacterial and catalytic activities. *J. Appl. Polym. Sci.* 135:45829. doi: 10.1002/app.45829

Fang, Y., Tan, J. J., Choi, H., Lim, S., and Kim, D. H. (2018a). Highly sensitive naked eye detection of Iron (III) and H2O2 using poly-(tannic acid) (PTA) coated Au nanocomposite. *Sens. Actuator B Chem.* 259, 155–161. doi: 10.1016/j.snb.2017.12.031

Faure, E., Falentin-Daudre, C., Jerome, C., Lyskawa, J., Fournier, D., Woisel, P., et al. (2013). Catechols as versatile platforms in polymer chemistry. *Prog. Polym. Sci.* 38, 236–270. doi: 10.1016/j.progpolymsci.2012.06.004

Fraga, C. G., Galleano, M., Verstraeten, S. V., and Oteiza, P. I. (2010). Basic biochemical mechanisms behind the health benefits of polyphenols. *Mol. Aspects Med.* 31, 435–445. doi: 10.1016/j.mam.2010.09.006

Franz, S., Rammelt, S., Scharnweber, D., and Simon, J. C. (2011). Immune responses to implants - A review of the implications for the design of immunomodulatory biomaterials. *Biomaterials* 32, 6692–6709. doi: 10.1016/j.biomaterials.2011.05.078

Fu, J., and Schlenoff, J. B. (2016). Driving forces for oppositely charged polyion association in aqueous solutions: enthalpic, entropic, but not electrostatic. *J. Am. Chem. Soc.* 138, 980–990. doi: 10.1021/jacs.5b11878

Fujita, M., Oguro, D., Miyazawa, M., Oka, H., Yamaguchi, K., and Ogura, K. (1995). Self-assembly of 10 molecules into nanometer-sized organic host frameworks. *Nature* 378, 469–471. doi: 10.1038/378469a0

Galante, D., Banfi, L., Baruzzo, G., Basso, A., D'Arrigo, C., Lunaccio, D., et al. (2019). Multicomponent synthesis of polyphenols and their *in vitro* evaluation as potential β-Amyloid aggregation inhibitors. *Molecules* 24:2636. doi: 10.3390/molecules24142636

Gao, Z., and Zharov, I. (2014). Large pore mesoporous silica nanoparticles by templating with a nonsurfactant molecule, tannic acid. *Chem. Mater.* 26, 2030–2037. doi: 10.1021/cm4039945

Gellman, S. H. (1998). Foldamers: a manifesto. *Acc. Chem. Res.* 31, 173–180. doi: 10.1021/ar960298r

Ghadiri, M. R., Granja, J. R., Milligan, R. A., Mcree, D. E., and Khazanovich, N. (1993). Self-assembling organic nanotubes based on a cyclic peptide architecture. *Nature* 366, 324–327. doi: 10.1038/366324a0

Gogoi, S., Maji, S., Mishra, D., Devi, K. S. P., Maiti, T. K., and Karak, N. (2017). Nano-bio engineered carbon dot-peptide functionalized water dispersible hyperbranched polyurethane for bone tissue regeneration. *Macromol. Biosci.* 17:15. doi: 10.1002/mabi.201600271

Guillerm, B., Monge, S., Lapinte, V., and Robin, J. J. (2012). How to modulate the chemical structure of polyoxazolines by appropriate functionalization. *Macromol. Rapid Commun.* 33, 1600–1612. doi: 10.1002/marc.201200266

Guo, J., Ping, Y., Ejima, H., Alt, K., Meissner, M., Richardson, J. J., et al. (2014). Engineering multifunctional capsules through the assembly of metal-phenolic networks. *Angew. Chem. Int. Ed. Engl.* 53, 5546–5551. doi: 10.1002/anie.201311136

Harrison, I. T., and Harrison, S. (1967). Synthesis of a stable complex of a macrocycle and a threaded chain. *J. Am. Chem. Soc.* 89, 5723–5724. doi: 10.1021/ja00998a052

He, Z., Nie, T., Hu, Y., Zhou, Y., Zhu, J., Liu, Z., et al. (2020). A polyphenol-metal nanoparticle platform for tunable release of liraglutide to improve blood glycemic control and reduce cardiovascular complications in a mouse model of type II diabetes. *J. Control. Release* 318, 86–97. doi: 10.1016/j.jconrel.2019.12.014

Hill, D. J., Mio, M. J., Prince, R. B., Hughes, T. S., and Moore, J. S. (2001). A field guide to foldamers. *Chem. Rev.* 101, 3893–4011. doi: 10.1021/cr990120t

Hoffman, A. S. (2012). Hydrogels for biomedical applications. *Adv. Drug Deliv. Rev.* 64, 18–23. doi: 10.1016/j.addr.2012.09.010

Hoogeveen, N. G., Stuart, M. A. C., Fleer, G. J., and Bohmer, M. R. (1996). Formation and stability of multilayers of polyelectrolytes. *Langmuir* 12, 3675–3681. doi: 10.1021/la951574y

Huggins, M. L. (1936). Hydrogen bridges in organic compounds. *J. Org. Chem.* 1, 407–456. doi: 10.1021/jo01234a001

Iijima, S. (1991). Helical microtubules of graphitic carbon. *Nature* 354, 56–58. doi: 10.1038/354056a0

Iler, R. K. (1966). Multilayers of colloidal particles. *J. Colloid Interf. Sci.* 21, 569–594. doi: 10.1016/0095-8522(66)90018-3

Jen, A. C., Wake, M. C., and Mikos, A. G. (1996). Review: hydrogels for cell immobilization. *Biotechnol. Bioeng.* 50, 357–364. doi: 10.1002/(SICI)1097-0290(19960520)50:4<357::AID-BIT2>3.0.CO;2-K

Kamath, K. R., and Park, K. (1993). Biodegradable hydrogels in drug-delivery. *Adv. Drug Deliv. Rev.* 11, 59–84. doi: 10.1016/0169-409X(93)90027-2

Kim, B. J., Han, S., Lee, K. B., and Choi, I. S. (2017). Biphasic supramolecular self-assembly of ferric ions and tannic acid across interfaces for nanofilm formation. *Adv. Mater.* 29:7. doi: 10.1002/adma.201700784

Kim, H. J., Choi, Y. S., Lim, M. Y., Jung, K. H., Kim, D. G., Kim, J. J., et al. (2016a). Reverse osmosis nanocomposite membranes containing graphene oxides coated by tannic acid with chlorine-tolerant and antimicrobial properties. *J. Memb. Sci.* 514, 25–34. doi: 10.1016/j.memsci.2016.04.026

Kim, J., Lee, Y. M., Kim, H., Park, D., Kim, J., and Kim, W. J. (2016b). Phenylboronic acid-sugar grafted polymer architecture as a dual stimuli-responsive gene carrier for targeted anti-angiogenic tumor therapy. *Biomaterials* 75, 102–111. doi: 10.1016/j.biomaterials.2015.10.022

Kim, J., Narayana, A., Patel, S., and Sahay, G. (2019). Advances in intracellular delivery through supramolecular self-assembly of

oligonucleotides and peptides. *Theranostics* 9, 3191–3212. doi: 10.7150/thno.33921

Kirkland, J. J. (1965). Porous thin-layer modified glass bead supports for gas liquid chromatography. *Analy. Chem.* 37, 1458–1461. doi: 10.1021/ac60231a004

Ko, M. P., and Huang, C. J. (2020). A versatile approach to antimicrobial coatings via metal-phenolic networks. *Colloids Surf. B Biointerfaces* 187:110771. doi: 10.1016/j.colsurfb.2020.110771

Kotov, N. A. (1999). Layer-by-layer self-assembly: The contribution of hydrophobic interactions. *Nanostruct. Mater.* 12, 789–796. doi: 10.1016/S0965-9773(99)00237-8

Kozlovskaya, V., Xue, B., Lei, W. Q., Padgett, L. E., Tse, H. M., and Kharlampieva, E. (2015). Hydrogen-bonded multilayers of tannic acid as mediators of T-cell immunity. *Adv. Healthc. Mater.* 4, 686–694. doi: 10.1002/adhm.201400657

Kumorek, M., Minisy, I. M., Krunclova, T., Vorsilakova, M., Venclikova, K., Chanova, E. M., et al. (2020). pH-responsive and antibacterial properties of self-assembled multilayer films based on chitosan and tannic acid. *Mater. Sci. Eng. C Mater. Biol. Appl.* 109:110493. doi: 10.1016/j.msec.2019.110493

Latimer, W. M., and Rodebush, W. H. (1920). Polarity and ionization from the standpoint of the Lewis theory of valence. *J. Am. Chem. Soc.* 42, 1419–1433. doi: 10.1021/ja01452a015

Le, Z., Chen, Y., Han, H., Tian, H., Zhao, P., Yang, C., et al. (2018). Hydrogen-bonded tannic acid-based anticancer nanoparticle for enhancement of oral chemotherapy. *ACS Appl. Mater. Interfaces* 10, 42186–42197. doi: 10.1021/acsami.8b18979

Lee, B. P., Messersmith, P. B., Israelachvili, J. N., Waite, J. H. (2011). Mussel-inspired adhesives and coatings. *Annu. Rev. Mater. Res.* 41, 99–132. doi: 10.1146/annurev-matsci-062910-100429

Lee, H., Kim, W. I., Youn, W., Park, T., Lee, S., Kim, T. S., et al. (2018). Iron gall ink revisited: *in situ* oxidation of Fe(II)-tannin complex for fluidic-interface engineering. *Adv. Mater.* 30:8. doi: 10.1002/adma.201805091

Lehn, J.M. (1973). Design of organic complexing agents. strategies towards properties. *Springer-Verlag* 16, 1–69. doi: 10.1007/BFb0004364

Lehn, J. M. (1978). Cryptates - inclusion complexes of macropolycyclic receptor molecules. *Pure Appl. Chem.* 50, 871–892. doi: 10.1351/pac197850090871

Lehn, J. M. (1988). Supramolecular chemistry - scope and perspectives molecules, supermolecules, and molecular devices. *Angew. Chem. Int. Edn.* 27, 89–112. doi: 10.1002/anie.198800891

Lehn, J. M. (2000). Programmed chemical systems: Multiple subprograms and multiple processing/expression of molecular information. *Chem. Eur. J.* 6, 2097–2102. doi: 10.1002/1521-3765(20000616)6:12<2097::AID-CHEM20973.0.CO;2-T

Lehn, J. M. (2002). Toward self-organization and complex matter. *Science* 295, 2400–2403. doi: 10.1126/science.1071063

Lehn, J. M. (2012). "Constitutional dynamic chemistry: bridge from supramolecular chemistry to adaptive chemistry," in *Constitutional Dynamic Chemistry*, ed M. Barboiu (Berlin: Springer-Verlag Berlin), 1–32.

Lei, Y. D., Tang, Z. H., Liao, R. J., and Guo, B. C. (2011). Hydrolysable tannin as environmentally friendly reducer and stabilizer for graphene oxide. *Green Chem.* 13, 1655–1658. doi: 10.1039/c1gc15081b

Li, J. W., Nowak, P., and Otto, S. (2013). Dynamic combinatorial libraries: from exploring molecular recognition to systems chemistry. *J. Am. Chem. Soc.* 135, 9222–9239. doi: 10.1021/ja402586c

Li, K., Xiao, G., Richardson, J. J., Tardy, B. L., Ejima, H., Huang, W., et al. (2019a). Targeted therapy against metastatic melanoma based on self-assembled metal-phenolic nanocomplexes comprised of green tea catechin. *Adv. Sci.* 6:1801688. doi: 10.1002/advs.201801688

Li, M., Li, H., Pan, Q., Gao, C., Wang, Y., Yang, S., et al. (2019b). Graphene oxide and lysozyme ultrathin films with strong antibacterial and enhanced osteogenesis. *Langmuir* 35, 6752–6761. doi: 10.1021/acs.langmuir.9b00035

Lin, F., Wang, Z., Chen, J., Lu, B., Tang, L., Chen, X., et al. (2020). A bioinspired hydrogen bond crosslink strategy toward toughening ultrastrong and multifunctional nanocomposite hydrogels. *J. Mater. Chem. B* 8, 4002–4015. doi: 10.1039/D0TB00424C

Liu, H., Qu, X., Kim, E., Lei, M., Dai, K., Tan, X. L., et al. (2018). Bio-inspired redox-cycling antimicrobial film for sustained generation of reactive oxygen species. *Biomaterials* 162, 109–122. doi: 10.1016/j.biomaterials.2017.12.027

Liu, L., Yin, L., Bian, H., and Zhang, N. (2020). Polymeric nanoparticles of poly(2-oxazoline), tannic acid and doxorubicin for controlled release and cancer treatment. *Chin. Chem. Lett.* 31, 501–504. doi: 10.1016/j.cclet.2019.04.041

Luo, J., Yang, J., Zheng, X., Ke, X., Chen, Y., Tan, H., et al. (2020). A highly stretchable, real-time self-healable hydrogel adhesive matrix for tissue patches and flexible electronics. *Adv. Healthc. Mater.* 9:e1901423. doi: 10.1002/adhm.201901423

Ma, M., Zhong, Y., and Jiang, X. (2020). Thermosensitive and pH-responsive tannin-containing hydroxypropyl chitin hydrogel with long-lasting antibacterial activity for wound healing. *Carbohydr. Polym.* 236:116096. doi: 10.1016/j.carbpol.2020.116096

Maerten, C., Lopez, L., Lupattelli, P., Rydzek, G., Pronkin, S., Schaaf, P., et al. (2017). Electrotriggered confined self-assembly of metal-polyphenol nanocoatings using a morphogenic approach. *Chem. Mater.* 29, 9668–9679. doi: 10.1021/acs.chemmater.7b03349

Mathivanan, N., Paramasivam, G., Vergaelen, M., Rajendran, J., Hoogenboom, R., and Sundaramurthy, A. (2019). Hydrogen-bonded multilayer thin films and capsules based on poly(2-n-propyl-2-oxazoline) and tannic acid: investigation on intermolecular forces, stability, and permeability. *Langmuir* 35, 14712–14724. doi: 10.1021/acs.langmuir.9b02938

Muller, W., Ringsdorf, H., Rump, E., Wildburg, G., Zhang, X., Angermaier, L., et al. (1993). Attempts to mimic docking processes of the immune-system - recognition-induced formation of protein multilayers. *Science* 262, 1706–1708. doi: 10.1126/science.8259513

Ninan, N., Forget, A., Shastri, V. P., Voelcker, N. H., and Blencowe, A. (2016). Antibacterial and anti-inflammatory ph-responsive tannic acid-carboxylated agarose composite hydrogels for wound healing. *ACS Appl. Mater. Interfaces* 8, 28511–28521. doi: 10.1021/acsami.6b10491

Ogasawara, S., et al. (1981). Zeta-potential and surface charge density of tannic acid-treated nylon 6 fibers in acid dye solutions. *Sen'i Gakkaishi* 37, T241–T246. doi: 10.2115/fiber.37.6_T241

Oh, D. X., Prajatelistia, E., Ju, S. W., Kim, H. J., Baek, S. J., Cha, H. J., et al. (2015). A rapid, efficient, and facile solution for dental hypersensitivity: the tannin-iron complex. *Sci. Rep.* 5:10884. doi: 10.1038/srep10884

Onat, B., Ozcubukcu, S., Banerjee, S., and Erel-Goktepe, I. (2018). Osteoconductive layer-by-layer films of Poly(4-hydroxy-L-proline ester) (PHPE) and Tannic acid. *Eur. Polym. J.* 103, 101–115. doi: 10.1016/j.eurpolymj.2018.03.034

Patil, N., Jerome, C., and Detrembleur, C. (2018). Recent advances in the synthesis of catechol-derived (bio)polymers for applications in energy storage and environment. *Prog. Polym. Sci.* 82, 34–91. doi: 10.1016/j.progpolymsci.2018.04.002

Pauling, L. (1985). Citation classic - the nature of the chemical-bond and the structure of molecules and crystals - an introduction to modern structural chemistry. *Curr. Cont. Eng. Technol. Appl. Sci.* 16.

Pedersen, C. J. (1967). Cyclic polyethers and their complexes with metal salts. *J. Am. Chem. Soc.* 89, 2495–2496. doi: 10.1021/ja00986a052

Pedersen, C. J. (1988). The discovery of crown ethers. *Chem. Scr* 28, 229–235.

Philp, D., and Stoddart, J. F. (1996). Self-assembly in natural and unnatural systems. *Angew. Chem. Int. Edn.* 35, 1154–1196. doi: 10.1002/anie.199611541

Phiwchai, I., Yuensook, W., Sawaengsiriphon, N., Krungchanuchat, S., and Pilapong, C. (2018). Tannic acid (TA): A molecular tool for chelating and imaging labile iron. *Eur. J. Pharm. Sci.* 114, 64–73. doi: 10.1016/j.ejps.2017.12.004

Pollard, M. M., Klok, M., Pijper, D., and Feringa, B. L. (2007). Rate acceleration of light-driven rotary molecular motors. *Adv. Funct. Mater.* 17, 718–729. doi: 10.1002/adfm.200601025

Qin, J., Liang, G., Feng, Y., Feng, B., Wang, G., Wu, N., et al. (2020). Synthesis of gadolinium/iron-bimetal-phenolic coordination polymer nanoparticles for theranostic applications. *Nanoscale* 12, 6096–6103. doi: 10.1039/C9NR10020B

Quideau, S., Deffieux, D., Douat-Casassus, C., and Pouysegu, L. (2011). Plant polyphenols: chemical properties, biological activities, and synthesis. *Angew. Chem. Int. Ed. Engl.* 50, 586–621. doi: 10.1002/anie.201000044

Rahim, M. A., Bjornmalm, M., Suma, T., Faria, M., Ju, Y., Kempe, K., et al. (2016). Metal-phenolic supramolecular gelation. *Angew. Chem. Int. Edn.* 55, 13803–13807. doi: 10.1002/anie.201608413

Ren, Z., Sun, S., Sun, R., Cui, G., Hong, L., Rao, B., et al. (2020). A metal-polyphenol-coordinated nanomedicine for synergistic cascade cancer

chemotherapy and chemodynamic therapy. *Adv. Mater. Weinheim* 32:e1906024. doi: 10.1002/adma.201906024

Richardson, J. J., Cui, J., Bjornmalm, M., Braunger, J. A., Ejima, H., and Caruso, F. (2016). Innovation in layer-by-layer assembly. *Chem. Rev.* 116, 14828–14867. doi: 10.1021/acs.chemrev.6b00627

Richert, L., Boulmedais, F., Lavalle, P., Mutterer, J., Ferreux, E., Decher, G., et al. (2004). Improvement of stability and cell adhesion properties of polyelectrolyte multilayer films by chemical cross-linking. *Biomacromolecules* 5, 284–294. doi: 10.1021/bm0342281

Ringwald, C., and Ball, V. (2016). Step-by-step deposition of type B gelatin and tannic acid displays a peculiar ionic strength dependence at pH 5. *RSC Adv.* 6, 4730–4738. doi: 10.1039/C5RA24337H

Shimazaki, Y., Mitsuishi, M., Ito, S., and Yamamoto, M. (1997). Preparation of the layer-by-layer deposited ultrathin film based on the charge-transfer interaction. *Langmuir* 13, 1385–1387. doi: 10.1021/la9609579

Shin, M., Lee, H. A., Lee, M., Shin, Y., Song, J. J., Kang, S. W., et al. (2018). Targeting protein and peptide therapeutics to the heart via tannic acid modification. *Nat. Biomed. Eng.* 2, 304–317. doi: 10.1038/s41551-018-0227-9

Shin, M., Ryu, J. H., Park, J. P., Kim, K., Yang, J. W., and Lee, H. (2015). DNA/tannic acid hybrid gel exhibiting biodegradability, extensibility, tissue adhesiveness, and hemostatic ability. *Adv. Funct. Mater.* 25, 1270–1278. doi: 10.1002/adfm.201403992

Shukla, A., Fang, J. C., Puranam, S., Jensen, F. R., and Hammond, P. T. (2012). Hemostatic multilayer coatings. *Adv. Mater.* 24, 492–496. doi: 10.1002/adma.201103794

Shutava, T., Prouty, M., Kommireddy, D., and Lvov, Y. (2005). pH responsive decomposable layer-by-layer nanofilms and capsules on the basis of tannic acid. *Macromolecules* 38, 2850–2858. doi: 10.1021/ma047629x

Sijbesma, R. P., Beijer, F. H., Brunsveld, L., Folmer, B. J. B., Hirschberg, J., Lange, R. F. M., et al. (1997). Reversible polymers formed from self-complementary monomers using quadruple hydrogen bonding. *Science* 278, 1601–1604. doi: 10.1126/science.278.5343.1601

Song, B., Yang, L., Han, L., and Jia, L. (2019). Metal ion-chelated tannic acid coating for hemostatic dressing. *Materials* 12:1803. doi: 10.3390/ma12111803

Song, G. B., Xu, J., Zheng, H., Feng, Y., Zhang, W. W., Li, K., et al. (2015). Novel soluble dietary fiber-tannin self-assembled film: a promising protein protective material. *J. Agric. Food Chem.* 63, 5813–5820. doi: 10.1021/acs.jafc.5b00192

Stockton, W. B., and Rubner, M. F. (1997). Molecular-level processing of conjugated polymers. 4. layer-by-layer manipulation of polyaniline via hydrogen-bonding interactions. *Macromolecules* 30, 2717–2725. doi: 10.1021/ma9700486

Su, J., Chen, F., Cryns, V. L., and Messersmith, P. B. (2011). Catechol polymers for pH-responsive, targeted drug delivery to cancer cells. *J. Am. Chem. Soc.* 133, 11850–11853. doi: 10.1021/ja203077x

Sun, H., Choi, D., Heo, J., Jung, S. Y., and Hong, J. (2020). Studies on the drug loading and release profiles of degradable chitosan-based multilayer films for anticancer treatment. *Cancers* 12:593. doi: 10.3390/cancers12030593

Sundaramurthy, A., Vergaelen, M., Maji, S., Auzely-Velty, R., Zhang, Z., De Geest, B. G., et al. (2014). Hydrogen bonded multilayer films based on poly(2-oxazoline)s and tannic acid. *Adv. Healthc. Mater.* 3, 2040–2047. doi: 10.1002/adhm.201400377

Takemoto, Y., Ajiro, H., and Akashi, M. (2015). Hydrogen-bonded multilayer films based on poly(N-vinylamide) derivatives and tannic acid. *Langmuir* 31, 6863–6869. doi: 10.1021/acs.langmuir.5b00767

Velmurugan, P., Singam, E. R. A., Rao, J. R., and Subramanian, V. (2014). Investigation on interaction of tannic acid with type i collagen and its effect on thermal, enzymatic, and conformational stability for tissue engineering applications. *Biopolymers* 101, 471–483. doi: 10.1002/bip.22405

Wang, C., Li, Y., Ma, Y., Gao, Y., Dong, D., Fang, J., et al. (2018a). Thermoresponsive polymeric nanoparticles based on poly(2-oxazoline)s and tannic acid. *J. Polym. Sci. A Polym. Chem.* 56, 1520–1527. doi: 10.1002/pola.29033

Wang, C., Sang, H., Wang, Y., Zhu, F., Hu, X., Wang, X., et al. (2018b). Foe to friend: supramolecular nanomedicines consisting of natural polyphenols and bortezomib. *Nano Lett.* 18, 7045–7051. doi: 10.1021/acs.nanolett.8b03015

Wang, M., Wang, Y., Hu, K., Shao, N., and Cheng, Y. (2015). Tumor extracellular acidity activated "off-on" release of bortezomib from a biocompatible dendrimer. *Biomater. Sci.* 3, 480–489. doi: 10.1039/C4BM00365A

Wang, P., Kankala, R. K., Fan, J., Long, R., Liu, Y., and Wang, S. (2018). Poly-L-ornithine/fucoidan-coated calcium carbonate microparticles by layer-by-layer self-assembly technique for cancer theranostics. *J. Mater. Sci. Mater. Med.* 29:68. doi: 10.1007/s10856-018-6075-z

Wang, X., Cao, W., Xiang, Q., Jin, F., Peng, X., Li, Q., et al. (2017). Silver nanoparticle and lysozyme/tannic acid layer-by-layer assembly antimicrobial multilayer on magnetic nanoparticle by an eco-friendly route. *Mater. Sci. Eng. C Mater. Biol. Appl.* 76, 886–896. doi: 10.1016/j.msec.2017.03.192

Wang, X., Yan, J., Pan, D., Yang, R., Wang, L., Xu, Y., et al. (2018). Polyphenol-poloxamer self-assembled supramolecular nanoparticles for tumor NIRF/PET imaging. *Adv. Healthc. Mater.* 7:e1701505. doi: 10.1002/adhm.201701505

Wang, Y., Fu, M., Wang, Z., Zhu, X. X., Guan, Y., and Zhang, Y. (2020). A sustained zero-order release carrier for long-acting, peakless basal insulin therapy. *J. Mater. Chem. B* 8, 1952–1959. doi: 10.1039/C9TB02728A

Wang, Y. T., Li, J., and Li, B. (2016). Nature-inspired one-step green procedure for enhancing the antibacterial and antioxidant behavior of a chitin film: controlled interfacial assembly of tannic acid onto a chitin film. *J. Agric. Food Chem.* 64, 5736–5741. doi: 10.1021/acs.jafc.6b01859

Wang, Z., Xie, Y. J., Li, Y. W., Huang, Y. R., Parent, L. R., Ditri, T., et al. (2017). Tunable, metal-loaded polydopamine nanoparticles analyzed by magnetometry. *Chem. Mater.* 29, 8195–8201. doi: 10.1021/acs.chemmater.7b02262

Wasserman, E. (1960). The preparation of interlocking rings - a catenane. *J. Am. Chem. Soc.* 82, 4433–4434. doi: 10.1021/ja01501a082

Whitesides, G. M., and Grzybowski, B. (2002). Self-assembly at all scales. *Science* 295, 2418–2421. doi: 10.1126/science.1070821

Wichterle, O., and Lim, D. (1960). Hydrophilic gels for biological use. *Nature* 185, 117–118. doi: 10.1038/185117a0

Wilson, A., Gasparini, G., and Matile, S. (2014). Functional systems with orthogonal dynamic covalent bonds. *Chem. Soc. Rev.* 43, 1948–1962. doi: 10.1039/C3CS60342C

Wu, J., Wang, Z., Yan, W., Wang, Y., Wang, J., and Wang, S. (2015a). Improving the hydrophilicity and fouling resistance of RO membranes by surface immobilization of PVP based on a metal-polyphenol precursor layer. *J. Memb. Sci.* 496, 58–69. doi: 10.1016/j.memsci.2015.08.044

Wu, S. J., Ho, Y. C., Jiang, S. Z., and Mi, F. L. (2015b). Effect of tannic acid-fish scale gelatin hydrolysate hybrid nanoparticles on intestinal barrier function and alpha-amylase activity. *Food Funct.* 6, 2283–2292. doi: 10.1039/C4FO01015A

Wyler, R., Demendoza, J., and Rebek, J. (1993). A synthetic cavity assembles through self-complementary hydrogen-bonds. *Angew. Chem. Int. Edn. Engl.* 32, 1699–1701. doi: 10.1002/anie.199316991

Xiao, F. X., Pagliaro, M., Xu, Y. J., and Liu, B. (2016). Layer-by-layer assembly of versatile nanoarchitectures with diverse dimensionality: a new perspective for rational construction of multilayer assemblies. *Chem. Soc. Rev.* 45, 3088–3121. doi: 10.1039/C5CS00781J

Xiao, T. X., Xu, L. X., Wang, J., Li, Z. Y., Sun, X. Q., and Wang, L. Y. (2019a). Biomimetic folding of small organic molecules driven by multiple non-covalent interactions. *Org. Chem. Front.* 6, 936–941. doi: 10.1039/C9QO00089E

Xiao, T. X., Xu, L. X., Zhou, L., Sun, X. Q., Lin, C., and Wang, L. Y. (2019b). Dynamic hydrogels mediated by macrocyclic host-guest interactions. *J. Mater. Chem. B* 7, 1526–1540. doi: 10.1039/C8TB02339E

Xiong, H., Wang, C., Wang, Z., Jiang, Z., Zhou, J., and Yao, J. (2019). Intracellular cascade activated nanosystem for improving ER plus breast cancer therapy through attacking GSH-mediated metabolic vulnerability. *J. Control. Release* 309, 145–157. doi: 10.1016/j.jconrel.2019.07.029

Xiong, H. M., Cheng, M. H., Zhou, Z., Zhang, X., and Shen, J. C. (1998). A nem approach to the fabrication of a self-organizing film of heterostructured polymer/Cu2S nanoparticles. *Adv. Mater.* 10, 529–532. doi: 10.1002/(SICI)1521-4095(199805)10:7<529::AID-ADMA529>3.0.CO;2-E

Xu, G., Liu, P., Pranantyo, D., Neoh, K. G., Kang, E. T., and Teo, S. L. M. (2019). One-step anchoring of tannic acid-scaffolded bifunctional coatings of antifouling and antimicrobial polymer brushes. *ACS Sus. Chem. Eng.* 7, 1786–1795. doi: 10.1021/acssuschemeng.8b05789

Xu, L. Q., Neoh, K. G., and Kang, E. T. (2018). Natural polyphenols as versatile platforms for material engineering and surface functionalization. *Prog. Polym. Sci.* 87, 165–196. doi: 10.1016/j.progpolymsci.2018.08.005

Yan, H., Ni, H., Jia, J., Shan, C., Zhang, T., Gong, Y., et al. (2019). Smart all-in-one thermometer-heater nanoprobe based on postsynthetical functionalization of a Eu(III)-metal organic framework. *Anal. Chem.* 91, 5225–5234. doi: 10.1021/acs.analchem.8b05960

Yang, C. S., Maliakal, P., and Meng, X. F. (2002). Inhibition of carcinogenesis by tea. *Annu. Rev. Pharmacol. Toxicol.* 42, 25–54. doi: 10.1146/annurev.pharmtox.42.082101.154309

Yang, S., Wang, Y., Luo, S., Shan, C., Geng, Y., Zhang, T., et al. (2019a). Building polyphenol and gelatin films as implant coating, evaluating from *in vitro* and *in vivo* performances. *Colloids Surf. B Biointerfaces* 181, 549–560. doi: 10.1016/j.colsurfb.2019.05.058

Yang, S., Wang, Y., Wu, X., Sheng, S., Wang, T., and Zan, X. (2019b). Multifunctional Tannic Acid (TA) and Lysozyme (Lys) films built layer by layer for potential application on implant coating. *ACS Biomater. Sci. Eng.* 5, 3582–3594. doi: 10.1021/acsbiomaterials.9b00717

Ye, Q., Zhou, F., and Liu, W. M. (2011). Bioinspired catecholic chemistry for surface modification. *Chem. Soc. Rev*. 40, 4244–4258. doi: 10.1039/c1cs15026j

You, J., Luo, Y., and Wu, J. (2014). Conjugation of ovotransferrin with catechin shows improved antioxidant activity. *J. Agric. Food Chem.* 62, 2581–2587. doi: 10.1021/jf405635q

Zhang, W., Besford, Q. A., Christofferson, A. J., Charchar, P., Richardson, J. J., Elbourne, A., et al. (2020). Cobalt-directed assembly of antibodies onto metal-phenolic networks for enhanced particle targeting. *Nano Lett.* 20, 2660–2666. doi: 10.1021/acs.nanolett.0c00295

Zhao, F., Liu, X., Dong, A., Deng, L., Wang, W., and Zhang, J. (2019a). Self-assembly and self-delivery nanodrug of bortezomib: a simple approach to achieve the trade-off between functionality and druggability. *J. Mater. Chem. B* 7, 7490–7493. doi: 10.1039/C9TB02174D

Zhao, L., Liu, Y., Chang, R., Xing, R., and Yan, X. (2019b). Supramolecular photothermal nanomaterials as an emerging paradigm toward precision cancer therapy. *Adv. Funct. Mater* 29:12. doi: 10.1002/adfm.201806877

Zhao, W., Iyer, V., Flores, F. P., Donhowe, E., and Kong, F. B. (2013). Microencapsulation of tannic acid for oral administration to inhibit carbohydrate digestion in the gastrointestinal tract. *Food Funct.* 4, 899–905. doi: 10.1039/c3fo30374h

Zhou, L., Chen, M., Tian, L., Guan, Y., and Zhang, Y. (2013). Release of polyphenolic drugs from dynamically bonded layer-by-layer films. *ACS Appl. Mater. Interfaces* 5, 3541–3548. doi: 10.1021/am4008787

Zhou, Z., Zhang, M., Liu, Y., Li, C., Zhang, Q., Oupicky, D., et al. (2018). Reversible covalent cross-linked polycations with enhanced stability and atp-responsive behavior for improved siRNA delivery. *Biomacromolecules* 19, 3776–3787. doi: 10.1021/acs.biomac.8b00922

Zhu, Y., Yu, X., Zhang, T., and Wang, X. (2019). Constructing zwitterionic coatings on thin-film nanofibrous composite membrane substrate for multifunctionality. *Appl. Surf. Sci.* 483, 979–990. doi: 10.1016/j.apsusc.2019.04.063

Zhuk, I., Jariwala, F., Attygalle, A. B., Wu, Y., Libera, M. R., and Sukhishvili, S. A. (2014). Self-Defensive Layer-by-Layer Films with Bacteria-Triggered Antibiotic Release. *ACS Nano* 8, 7733–7745. doi: 10.1021/nn500674g

Zou, Q., Abbas, M., Zhao, L., Li, S., Shen, G., and Yan, X. (2017). Biological photothermal nanodots based on self-assembly of peptide-porphyrin conjugates for antitumor therapy. *J. Am. Chem. Soc.* 139, 1921–1927. doi: 10.1021/jacs.6b11382

Zou, Y., Wang, Z., Zhang, H., and Liu, Y. (2018). A novel electrogenerated chemiluminescence biosensor for histone acetyltransferases activity analysis and inhibition based on mimetic superoxide dismutase of tannic acid assembled nanoprobes. *Biosens. Bioelectron.* 122, 205–210. doi: 10.1016/j.bios.2018.09.048

Conflict of Interest: The authors declare that the research was conducted in the absence of any commercial or financial relationships that could be construed as a potential conflict of interest.

frontiers in Chemistry

ORIGINAL RESEARCH
published: 19 October 2020
doi: 10.3389/fchem.2020.584242

Synthesis and Biopharmaceutical Characterization of Amphiphilic Squalenyl Derivative Based Versatile Drug Delivery Platform

Duy-Khiet Ho[1,2†‡], Rebekka Christmann[1,2†], Xabier Murgia[1,2‡], Chiara De Rossi[1], Sarah Frisch[1,2], Marcus Koch[3], Ulrich F. Schaefer[2], Brigitta Loretz[1], Didier Desmaele[4]*, Patrick Couvreur[4] and Claus-Michael Lehr[1,2]**

[1] Helmholtz Institute for Pharmaceutical Research Saarland, Helmholtz Centre for Infection Research, Saarbrücken, Germany, [2] Department of Pharmacy, Saarland University, Saarbrücken, Germany, [3] INM-Leibniz Institute for New Materials, Saarbrücken, Germany, [4] Faculté de Pharmacie, Institut Galien Paris Sud, Université Paris-Saclay, Chatenay-Malabry, France

Limited drug loading capacity (LC), mostly below 5% w/w, is a significant drawback of nanoparticulate drug delivery systems (DDS). Squalenoylation technology, which employs bioconjugation of squalenyl moiety and drug, allows self-assemble of nanoparticles (NPs) in aqueous media with significantly high LC (>30% w/w). The synthesis and particle preparation of squalenoylated prodrugs are, however, not facile for molecules with multiple reactive groups. Taking a different approach, we describe the synthesis of amphiphilic squalenyl derivatives (SqDs) as well as the physicochemical and biopharmaceutical characterizations of their self-assembled NPs as DDSs. The SqDs included in this study are (i) cationic squalenyl diethanolamine (ii) PEGylated SqD (PEG 750 Da), (iii) PEGylated SqD (PEG 3,000 Da), and (iv) anionic squalenyl hydrogen sulfate. All four SqDs self-assemble into NPs in a size range from 100 to 200 nm in an aqueous solution. Furthermore, all NP derivatives demonstrate appropriate biocompatibility and adequate colloidal stability in physiological relevant pH environments. The mucoprotein binding of PEGylated NPs is reduced compared to the charged NPs. Most importantly, this technology allows excellent LC (at maximum of 45% w/w) of a wide range of multifunctional compounds, varying in physicochemical properties and molecular weight. Interestingly, the drug release profile can be tuned by different loading methods. In summary, the SqD-based NPs appear as versatile drug delivery platforms.

Keywords: drug delivery, self-assembly, pegylated, squalenyl derivatives, squalene, nanoparticles, protein-interaction

OPEN ACCESS

Edited by:
Jianliang Shen,
Wenzhou Medical University, China

Reviewed by:
Haihua Xiao,
Chinese Academy of Sciences, China
Qian Cao,
SYSU, China

***Correspondence:**
Brigitta Loretz
brigitta.loretz@helmholtz-hips.de
Didier Desmaele
didier.desmaele@u-psud.fr
Claus-Michael Lehr
claus-michael.lehr@helmholtz-hips.de

†These authors have contributed equally to this work and share first authorship

‡Present address:
Duy-Khiet Ho,
Department of Bioengineering, School of Medicine, University of Washington, Seattle, WA, United States
Xabier Murgia,
Kusudama Therapeutics, Parque Científico y Tecnológico de Gipuzkoa, Donostia-San Sebastián, Spain

Specialty section:
This article was submitted to Supramolecular Chemistry, a section of the journal Frontiers in Chemistry

Received: *16 July 2020*
Accepted: *08 September 2020*
Published: *19 October 2020*

Citation:
Ho D-K, Christmann R, Murgia X, De Rossi C, Frisch S, Koch M, Schaefer UF, Loretz B, Desmaele D, Couvreur P and Lehr C-M (2020) Synthesis and Biopharmaceutical Characterization of Amphiphilic Squalenyl Derivative Based Versatile Drug Delivery Platform. Front. Chem. 8:584242. doi: 10.3389/fchem.2020.584242

INTRODUCTION

Nano-sized drug delivery systems (DDS) having the size range from 10 to 1,000 nm have been investigated intensively to improve the treatment efficacy of severe diseases (Bobo et al., 2016; Ho et al., 2019). DDS protect drugs from biodegradation, improve drug solubility, enhance the delivery of drugs specifically to their target sites and reduce adverse effects (Danhier et al., 2012; Sanna et al., 2012; Kalepu and Nekkanti, 2015; Kim et al., 2017). The major challenge in DDS formulation is to improve the drug loading capacity (LC), which have been mostly

reported as lower than 5% w/w while using pharmaceutically accepted excipients (Couvreur, 2013; Ho et al., 2019). With the aim to formulate nanomedicines having a maximized LC, Couvreur et al. (2006) invented the squalenoylation approach. This unique technique creates a prodrug by bioconjugation of a drug molecule and a hydrophobic squalenyl moiety. The squalenoylated prodrug could self-assemble into uniform and stable nanoparticles (NPs) in aqueous solution without using additional surfactants (Desmaële et al., 2012), which cannot be achieved by other lipid prodrugs, e.g., employing stearyl moiety (Couvreur et al., 2006). Importantly, the squalenyl drug bioconjugates, e.g., squalenyl gemcitabine, squalenyl penicillin G, as well as squalenyl dideoxycytidine or didanosine, have not only shown a high LC (>30% w/w) but also improved pharmacological profile and efficacy compared to the parent drugs (Couvreur et al., 2006; Desmaële et al., 2012; Sémiramoth et al., 2012; Hillaireau et al., 2013; Maksimenko et al., 2013; Buchy et al., 2015). Moreover, squalene is a natural lipid, which is also found in humans as a precursor of the cholesterol biosynthesis (Schroepfer, 1981). Hence, using squalenyl derivatives in developing DDS is favorable (Reddy and Couvreur, 2009).

However, it is challenging to bio-conjugate squalene and drug molecules with multiple functional groups or without functional groups (Ralay-Ranaivo et al., 2014). Furthermore, if possible, the chemical synthesis would not be facile and easily scaled-up, and poor solubility of the resulting prodrugs in common solvents could be an additional issue. Taking advantage of squalenoylation approach and extending its use in versatile DDS preparation, Lepeltier et al. (2015) proposed the core-shell structured squalenoylated chitosan NPs allowing the loading of both hydrophilic and hydrophobic compounds. However, the LC in such a system was not as high as expected, and the particles size could not be tuned easily due to the poor solubility of squalenoylated chitosan in common solvents (Lepeltier et al., 2015). Taking a different approach, without employing bioconjugation Ho et al. (2020) reported self-assembled NPs based on an anionic squalenyl derivative (aSq)—squalenyl hydrogen sulfate—which showed excellent simultaneous LC of both hydrophobic alkyl quinolone (∼10% w/w) and hydrophilic tobramycin (∼30% w/w). Importantly, this DDS also demonstrated an improved penetration through biological barriers, such as biofilms, and enhanced synergistic therapeutic effects of both actives (Ho et al., 2020). Hence, we aimed to expand such a promising DDS platform to further applications, like drug loading of anionic hydrophilic drugs and the minimization of interactions between the NPs and proteins. For these purposes, we here propose, in addition to the synthesis of aSq, the preparation of other squalenyl derivatives (SqDs), namely, (i) cationic squalenyl diethanolamine (cSq), (ii) PEGylated squalenyl derivative (PEG 750 Da, PEG750Sq), and (iii) PEGylated squalenyl derivative (PEG 3,000 Da, PEG3000Sq). Especially, the low molecular weight of SqDs in comparison to excipients used in conventional carrier systems [e.g., from biodegradable polymers like poly (lactic-co-glycolic acid)] promises to lead to a higher LC in these DDS. We studied their ability to self-assemble into NPs in aqueous solution, their morphology, as well as their colloidal stability in biophysically relevant pH milieus and cytotoxicity as surrogate for their biocompatibility. At their first contact with the human body, NPs are mostly confronted with proteins. By adsorption on the NP surface (formation of a "protein-corona"), the proteins can change the characteristics of NPs dramatically (Raesch et al., 2015; Kokkinopoulou et al., 2017). These protein–NP interactions not only play a role for systemic applications but also for non-invasive drug delivery, where the first main challenge is to overcome a protective mucus barrier (e.g., vaginal, pulmonary, gastrointestinal delivery) (Ruge et al., 2013; Murgia et al., 2018). Mucus is a hydrogel consisting mainly of water and mucins, which are high molecular weight glycoproteins with a negative net charge at physiological pH (Bansil and Turner, 2006; Lock et al., 2018; Murgia et al., 2018). One of the main defense mechanisms of mucus against xenobiotics is the physicochemical interaction with mucin glycoproteins (Lai et al., 2007; Lieleg and Ribbeck, 2011; Murgia et al., 2016). In this study, these possible interactions were investigated using nanoparticle tracking analysis (NTA), to evaluate the mucoadhesive and mucoinert characteristics of the charged and PEGylated SqDs, respectively. To assess the LC of SqDs for a broad range of molecules, a representative set of compounds, varying in physiochemical properties and molecular weight (Mw), was chosen. Depending on the drug properties, the loading procedure has been optimized using different methods, namely, (i) coprecipitation, (ii) solvent evaporation, or (iii) dropping. Subsequently, the tuning possibility of drug release by different preparation methods was studied by *in vitro* release profiles of the drug from SqD–NPs, at pH 7.4 (PBS), and 37°C.

Abbreviations: LC, drug loading capacity; SqD, squalenyl derivative; aSq, anionic squalenyl derivative; cSq, cationic squalenyl derivative; PEG750Sq, PEG750 squalenyl derivative; PEG3000Sq, PEG3000 squalenyl derivative; NP, nanoparticle; NTA, nanoparticle tracking analysis; DLS, dynamic light scattering; ELS, electrophoretic light scattering; cryo-TEM, cryogenic transmission electron microscopy; MS, mass spectrometry; PDI, polydispersity index; HPLC, high performance liquid chromatography; SD, standard deviation; SE, standard error.

MATERIALS AND METHODS

Materials

All chemicals were purchased from Sigma-Aldrich unless otherwise specified. Tetrahydrofuran (HPLC grade) (THF), ethanol, absolute (HPLC grade) (EtOH), ethyl acetate (analytical grade reagent), and Formic Acid Optima LCMS were purchased from Fisher Scientific. Acetonitrile and methanol (MeOH) were obtained from VWR Chemicals. Yeast extract was obtained from Fluka. Bacto™ Tryptone was obtained from BD Biosciences. Luria Bertani (LB) agar was obtained from Carl Roth. Gibco® HBSS (1x) Hanks' Balanced Salt Solution and Gibco® PBS was obtained from Life Technologies. Purified water was prepared by a Milli-Q water purification system (Merck Millipore, Billerica, MA, USA) (called water in the manuscript).

Synthesis and Characterization of SqDs

The preparation of 1,1′,2-trisnorsqualenic aldehyde (compound 2) and 1,1′,2-trisnorsqualenol (compound 6) (**Figure 1**) from squalene (compound 1) was performed as reported in previous

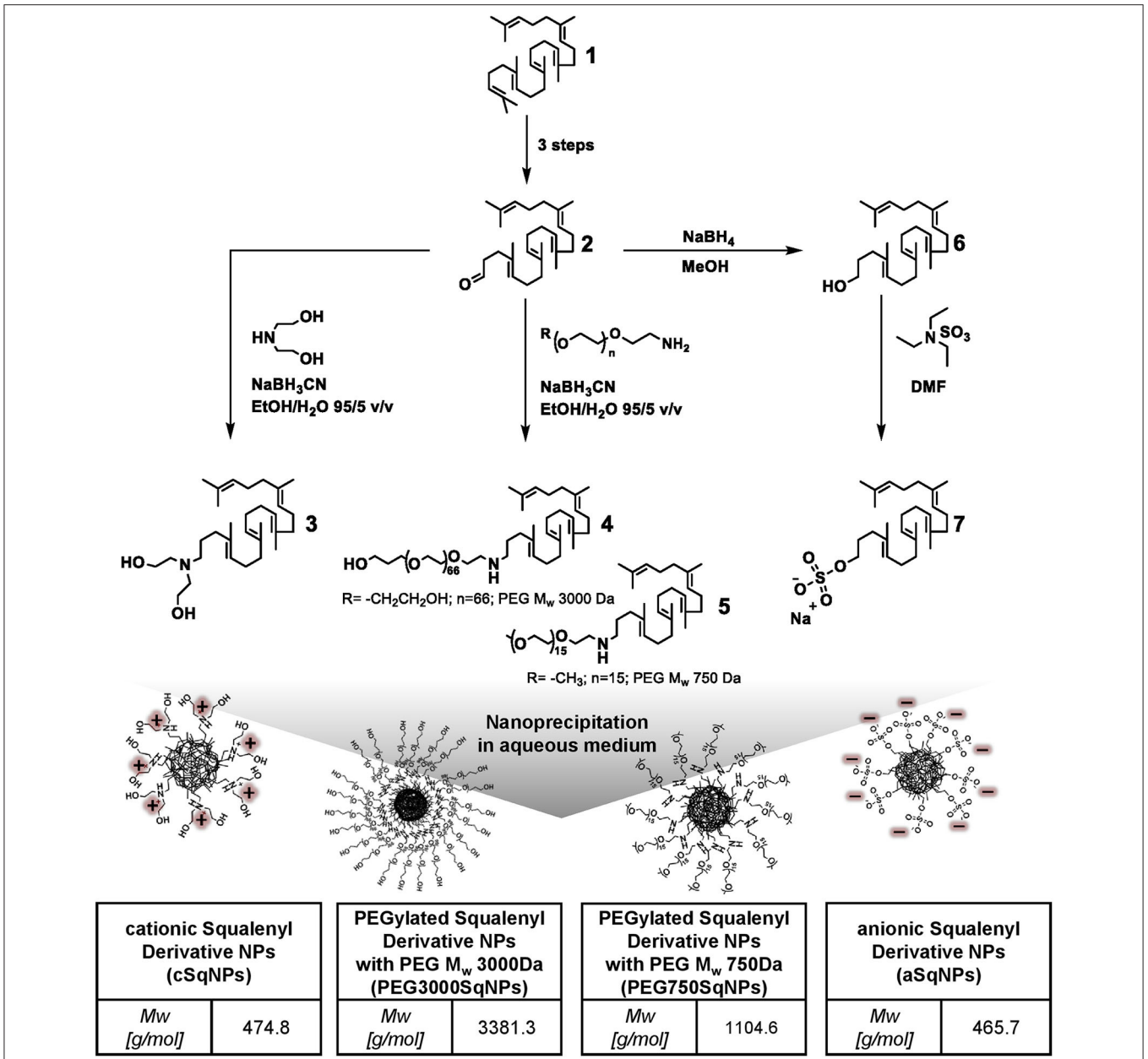

FIGURE 1 | Synthetic scheme of squalenyl derivatives (SqDs) [cationic squalenyl diethanolamine (cSq) (compound 3), PEG3000Sq (compound 4), PEG750Sq (compound 5), squalenyl derivative (aSq) (compound 7)], and schematic sketches of nanoparticles (NPs) upon nanoprecipitation in aqueous solution. The insert tables indicate abbreviation and molecular weight of the corresponding SqD.

studies (van Tamelen and Curphey, 1962; Ceruti et al., 1987; Skarbek et al., 2015).

Synthesis and Characterization of PEGylated SqDs and cSq

cSq (compound 3), PEG3000Sq (compound 4), and PEG750Sq (compound 5) were synthesized using the same procedure from 1,1′,2-trisnorsqualenic aldehyde (compound 2) (**Figure 1**). The conjugation was achieved *via* reductive amination reaction between amine and aldehyde groups, using sodium cyanoborohydride ($NaBH_3CN$) as reducing agent. Briefly, 1 molar equivalent of 1,1′,2-trisnorsqualenic aldehyde (compound 2) was solubilized in a mixed solvent of EtOH:water (95:5 v/v) at a concentration of 10% w/w. Following the addition of 1.2 molar equivalent of amine—methoxyl-PEG750-NH_2 (methoxypolyethylene glycol amine, Mw 750 Da), PEG3000-NH_2 [O-(2-aminoethyl) polyethylene glycol, Mw 3,000 Da], or diethanolamine—the reaction was carried out at room temperature for 3 h. $NaBH_3CN$, 1.2 molar equivalent, was subsequently added, and the reaction was kept for an additional

20 h allowing imine reduction. EtOH was then removed under reduced pressure, and water was added, allowing precipitation of the resulted SqD. The product was then collected by centrifugation and washed three times with water. The isolated yield was >90% in all reactions. The cSq product (compound 3) was characterized by ^{1}H-NMR (**Supplementary Figure 3**), ^{13}C-NMR (**Supplementary Figure 4**), and MS (mass spectroscopy), while the PEG750Sq product (compound 5) and PEG3000Sq product (compound 4) were characterized by ^{1}H-NMR (**Supplementary Figures 5, 7**, respectively) and ^{13}C-NMR (**Supplementary Figures 6, 8**, respectively) before further use.

Synthesis and Characterization of aSq (Compound 7)

aSq was synthesized from 1,1′,2-trisnorsqualenol as described by Ho et al. (2020) (**Figure 1**). Briefly, 1 molar equivalent of 1,1′,2-trisnorsqualenol (compound 6) was prepared in DMF (dimethylformamide) at a concentration of 10% w/w. The solution was degassed using N_2, and 1.1 molar equivalent of TEA. SO_3 (sulfur trioxide triethylamine complex) was slowly dropped into the solution at room temperature. The temperature was then increased to 60°C. Following 16 h of reaction, the resulting system was quenched with an appropriate amount of water. The solvent mixture, DMF and water, was partly removed under reduced pressure. After being diluted in an excess amount of MeOH, NaOH 1 N was added under stirring. MeOH was subsequently removed under reduced pressure, and water was added allowing precipitation of aSq. The aSq product was extracted using ethyl acetate and dried over $MgSO_4$. The solvents were completely removed under reduced pressure at 40°C. The isolated yield was 95%. The aSq product was characterized by ^{1}H-NMR (**Supplementary Figure 1**), ^{13}C-NMR (**Supplementary Figure 2**), and MS (mass spectroscopy) before further use.

Preparation of Drug-Free SqD–NPs

All drug-free self-assembled SqD–NPs in this study were prepared by nanoprecipitation in aqueous solution as described previously (Fessi et al., 1989; Ho et al., 2020). In brief, a SqD was solubilized in THF and dropped into the water at a speed of 12 drops/min under constant stirring (1,000 rpm). Afterward, THF was evaporated at 40°C, 40 mbar, and 280 rpm using a rotary evaporator (Rotavapor, Büchi, Essen, Germany) resulting in a drug-free SqD–NPs suspension in water, which was further stored at 4°C.

Figure 1 presents the schemes of the optimal representatives of SqD–NPs, including:

(i) cSq–NPs, which was prepared as follows: 0.15 ml of cSq solution in THF at a concentration of ∼7 mg/ml was dropped into 1 ml of water under stirring. THF was then removed under reduced pressure resulting in a cSq–NPs suspension in water at a concentration of 1 mg/ml.

(ii) PEG750Sq–NPs and PEG3000Sq–NPs, which were prepared using the same protocol as follows: 0.5 ml PEGylated SqD in THF:water (1:1 v/v) mixture at a concentration of 1 mg/ml was dropped into 0.75 ml of water. THF was then removed under reduced pressure resulting in the PEGylated SqD–NPs in water at a concentration of 0.5 mg/ml.

(iii) aSq–NPs, which were prepared as follows: 0.1 ml of aSq solution in THF at a concentration of 10 mg/ml was dropped into 1 ml of water under stirring. THF was then removed under reduced pressure resulting in an aSq–NPs suspension in water at a concentration of 1 mg/ml.

The NP characteristics, especially size and polydispersity index (PDI), of the drug-free cSq–NPs and aSq–NPs were studied by varying the initial SqD concentration in THF and the final NP concentration in water. The detailed information is reported in the supplementary information (**Supplementary Table 1**).

Physicochemical Characterization of Drug-Free SqD–NPs

Size, PDI, Zeta-Potential

The intensity-based hydrodynamic size (reported as *z*-average), PDI, and zeta-potential of the SqD–NPs were determined at 25°C by dynamic and electrophoretic light scattering (DLS, ELS) using a Zetasizer (Zetasizer Nano ZSP, ZEN5600, Malvern, Software 7.02) equipped with a He–Ne Laser at a 633 nm wavelength, backscattering angle of 173° for DLS. For the measurements, 20 μl of SqD–NPs suspension was diluted into 800 μl of water.

Morphology

The morphology of each drug-free SqD–NPs was investigated by cryogenic transmission electron microscopy (cryo-TEM). In brief, after plotting 3 μl of SqD–NPs suspension on a holey carbon grid (S147-4, Plano Wetzlar, Germany) for 2 s, the sample was frozen by plunging into −165°C liquid ethane, then transferred to the sample holder under liquid nitrogen conditions. All samples were examined using a JEOL (Akishima, Tokio, Japan) JEM-2100 LaB6 TEM equipped with a Gatan model 914 cryo-TEM sample holder (Pleasonton, CA, USA) and a Gatan Orius SC1000 CCD camera to gain bright-field images. Sample analysis was done at −170°C, under low-dose conditions, meaning conservative settings of ∼10 μa/cm² radiation level to avoid sample destruction.

Colloidal Stability

The colloidal stability of the drug-free SqD–NPs was studied in physiological relevant pH milieus, including pH 2, pH 5 (acetate buffer solution), and pH 7.4 (HBSS buffer solution). The tested samples were prepared by adding 25 μl of SqD–NPs suspension into 975 μl of buffer solution. NP characteristics, including size, PDI, and zeta-potential, were determined by DLS and ELS using a Zetasizer after 1, 3, and 24 h at 25°C.

Interaction of SqD–NPs With Biological Systems

Biocompatibility

As surrogate for biocompatibility, the determination of cytotoxicity by MTT assay on A549 cells was chosen. Briefly, prior to the assays, 10^4 cells were seeded in each well of the 96-well plates and grown until reaching 80% cell confluence. The SqD–NPs were suspended in HBSS at concentrations ranging

from 0.0652 to 1 mg/ml and incubated with cells for 4 h at 37°C and 5% CO_2. After the incubation time, cells were washed twice with PBS, and MTT reagent (0.5 mg/ml in HBSS) was added. The cells were then incubated for an additional 4 h, at 37°C, and 5% CO_2 allowing the formation of formazan crystals intracellularly (Mosmann, 1983). Following the removal of the supernatant, cells and formed formazan crystals were dissolved in DMSO for 30 min, and the absorbance was measured at 550 nm using a Tecan microplate reader Infinite M200Pro (Tecan, Crailsheim, Germany). Cells incubated with 1% Triton TM X-100 in HBSS served as positive controls (0% cell viability), while cells incubated with plain HBSS served as negative controls (100% cell viability), respectively. The percentage of cell viability was calculated relating to the negative controls (Ho et al., 2020).

Protein–SqD–NPs Interactions

The interaction between fluorescent SqD–NPs and mucin glycoproteins was studied *via* NTA by NanoSight (LM-10, Laser 532 nm) (Malvern, UK). NTA is able to determine the hydrodynamic diameter of NPs. Under random Brownian motions, NPs scatter light from a laser beam. The scattered light can be visualized by the NTA and captured by a video camera, to enable the software to track the movement of the NPs individually. Using the Stoke–Einstein equation, the hydrodynamic diameter of the particles can be determined.

To study the protein–SqD–NP interaction, the Brownian motion of fluorescent NPs in water was compared to their movement in water containing non-fluorescent 0.1% mucin solution (mucin from porcine stomach, type II, Sigma). For the measurements, used dilutions of the NPs, either in 0.1% mucin solution or water, were 1:100 (aSq–NPs), 1:200 (cSq–NPs), and 1:50 (PEG750Sq–NPs). To detect only the movement of the SqD–NPs, the particles were fluorescently labeled, and the fluorescence mode of the NTA was used. Therefore, SqD–NPs were loaded with 0.5% Nile red by coprecipitation; a detailed description of the method is in the Preparation of Drug-Loaded SqD–NPs section. As a vehicle control sample, the 0.1% aqueous mucin solution was studied with and without the fluorescence filter, to show the ability of the filter to exclude optical interferences of the proteins (**Supplementary Figure 9**, green line: with filter, gray line: without filter). Videos with a duration of 20–30 s were taken and analyzed by NanoSight Software NTA 3.3. The results of the particle concentration as a function of particle size are reported as mean ± standard error (SE).

Carrier Properties of SqD–NPs

Preparation of Drug-Loaded SqD–NPs

The LC of the synthesized SqDs was investigated using compounds representing different physicochemical properties, namely:

(i) hydrophobic compounds: cholesteryl BODIPY, Nile red, and dexamethasone,
(ii) hydrophilic and charged compounds: isoniazid, colistin, tigecycline, and FITC-albumin.

With the aim to maximize the LC while maintaining the NP stability, appropriate preparation methods for generating drug-loaded NPs were chosen depending on the drug properties. In brief, we explored three NP preparation methods as follows:

(i) *Co-precipitation method:* In this study, we found that this method worked best for loading hydrophobic compounds (cholesteryl BODIPY, Nile red, and dexamethasone). Briefly, hydrophobic compound and SqD were dissolved in THF. Upon NP self-assembling in water by nanoprecipitation, the hydrophobic compound localized in the core of the SqD–NPs by hydrophobic interaction.
(ii) *Solvent evaporation method:* In this study, we found that this method worked best for loading hydrophilic compounds having multiple functional groups, especially for small Mw hydrophilic compounds (e.g., isoniazid) and amphiphilic compounds (e.g., colistin). Briefly, the SqD and drug were dissolved completely in the mixture of THF:water (1:1 v/v) at desired concentrations (0.25–0.125 mg NPs/ml of NP suspension). The solution was then stirred for 24 h at room temperature allowing charge interaction of SqD and drug molecules, while the hydrophobic interaction between SqD and drug could be induced upon removal of THF using a rotary evaporator (Rotavapor, Büchi, Essen, Germany) at 40 mbar, 40°C and 65 rpm.
(iii) *Dropping method:* In this study, we found that this method worked best for loading both small (e.g., tigecycline) and high Mw hydrophilic compounds (FITC-albumin) having multiple functional groups. Briefly, the charged drug-free SqD–NPs were prepared in water as described in the Preparation of Drug-Free SqD–NPs section and diluted to a concentration of 0.25 mg/ml. SqD–NPs suspension (1 ml) was then dropped into 1 ml of the prepared drug solution in water under stirring at 200 rpm. The resulting drug-loaded SqD–NPs were further stirred for 1 day at room temperature.

The "solvent evaporation method" and "dropping method," which allowed the loading of drugs in both compartments, core and shell, of the NPs could be used in multiple drug-loading purposes. As an example, Nile red and FITC-albumin co-loaded cSq–NPs are presented in **Supplementary Material** Part 4. Briefly, the Nile red-loaded cSq–NPs were prepared by "coprecipitation method" and then dropped into an aqueous solution of FITC-albumin ("dropping method") allowing the dual-loading of both compounds.

Figure 2 summarizes an overview of the preparation methods for drug-loaded SqD–NPs, listing all the model cargos with corresponding Mw and clog *P*-values (estimated by ChemDraw Professional 16.0).

Quantification of loading capacity and encapsulation efficiency

The loading capacity (LC) and encapsulation efficiency (EE) of the drugs loaded to SqD–NPs were determined indirectly using the amount of non-loaded drug in the supernatant of the SqD–NPs suspension. The hydrophobic compound (dexamethasone, cholesteryl BODIPY, or Nile red) was extracted

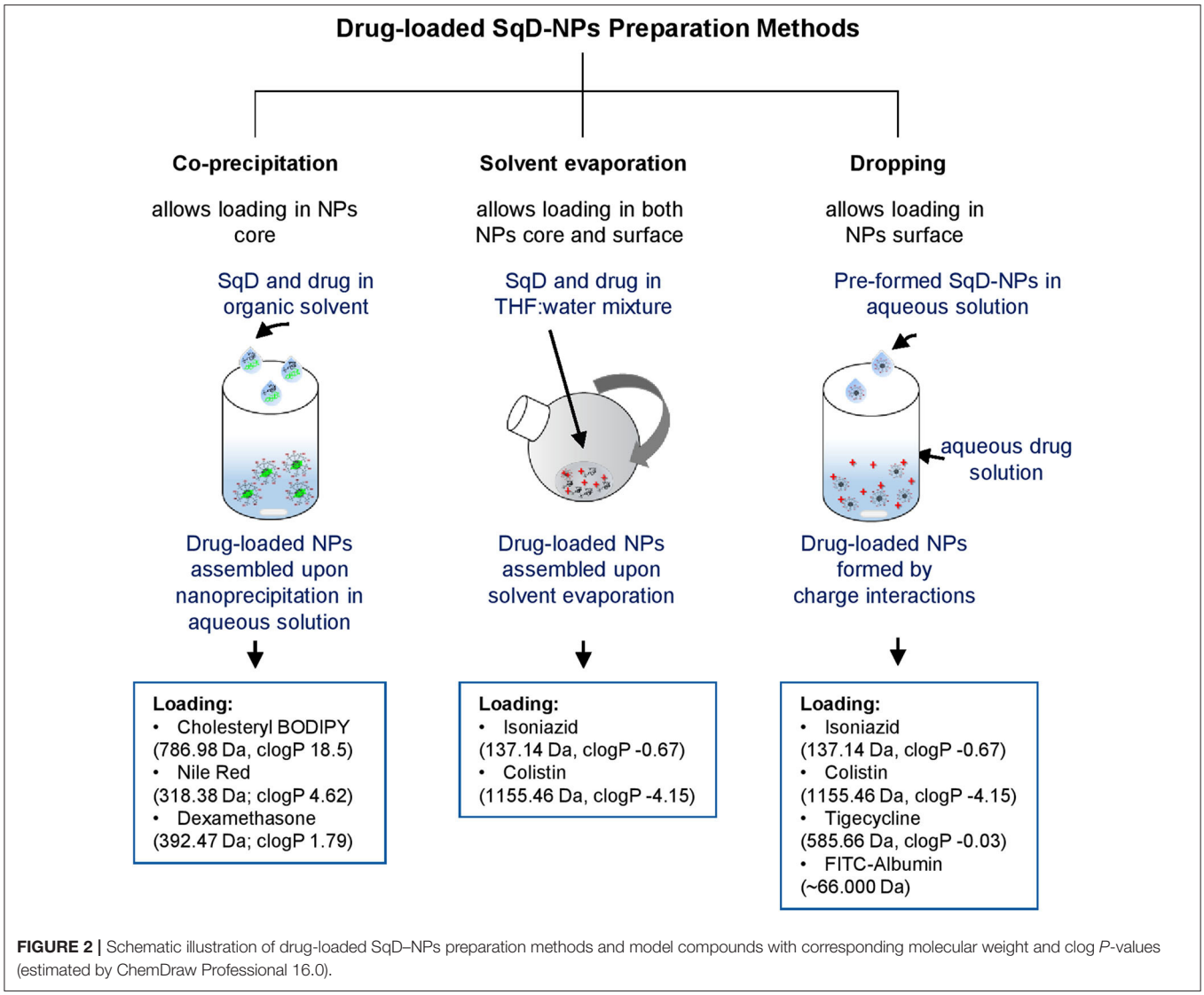

FIGURE 2 | Schematic illustration of drug-loaded SqD–NPs preparation methods and model compounds with corresponding molecular weight and clog *P*-values (estimated by ChemDraw Professional 16.0).

from the supernatant using ethyl acetate (Ho et al., 2018). The hydrophilic compound was analyzed in the supernatant after centrifugation of the SqD–NPs suspension. Isoniazid was collected by loading the NPs in a Centrisart filter (MWCO 10.000 Da) (Sartorius, Göttingen, Germany) and centrifuging at 2,000 *g* for 30 min. Colistin, tigecycline, or FITC-albumin was collected by centrifuging the drug-loaded NPs at 24.400 *g* for 30 min. The amount of cholesteryl BODIPY, Nile red, tigecycline, or FITC-albumin in the supernatant, respectively, was analyzed by a plate reader (details described in **Supplementary Material** Part 6), while dexamethasone, isoniazid, or colistin were quantified by high-performance liquid chromatography (HPLC) (details described in **Supplementary Material** Part 6).

$$EE\ [\%] = \frac{drug\ amount\ loaded\ in\ NPs\ [mg]}{initial\ drug\ amount\ [mg]} * 100 \quad (1)$$

$$LC\ [\%] = \frac{drug\ amount\ loaded\ in\ NPs\ [mg]}{total\ amount\ of\ NPs\ [mg]} * 100 \quad (2)$$

The drug amount loaded in NPs is calculated by subtraction of the non-loaded drug amount from the initial one. The total amount of NPs equals the sum of the amount of SqD and the amount of drug, which is loaded to the NPs.

Release Studies

The release studies of selected drug-loaded SqD–NPs were performed using the same procedure in PBS (pH 7.4) at 37°C and constant shaking at 250 rpm. Briefly, the optimal LC sample of the drug-loaded SqD–NPs was concentrated and then diluted in PBS to have a final concentration of the corresponding drug at 10% w/w. The cumulative drug release in percent was evaluated over a 24 h period. Samples were collected after 1, 2, 4, 6, 8, 16, and 24 h, while the release acceptor volume was always kept constant. The drug amount in the acceptor fluid was analyzed. The hydrophobic drugs were extracted using ethyl acetate before further analysis. The drug quantification was done by plate reader or HPLC (**Supplementary Material** Part 6).

Statistics

If not stated otherwise, all procedures were conducted at least in three independent experiments and measured in technical triplicate. Results are presented as mean ± standard deviation (SD). Calculations were done using either Excel, Microsoft 2016 and 2019, or GraphPad Prism 8.0. Physicochemical information of molecules was predicted by ChemDraw Professional 16.0.

RESULTS AND DISCUSSION

Synthesis and Characterization of SqDs

The cSq and PEGylated SqDs were straightforwardly obtained by simple reductive amination reaction from 1,1′,2-trisnorsqualenic aldehyde. The successful synthesis and purification of all SqDs were confirmed by ^{1}H-NMR and ^{13}C-NMR (**Supplementary Figures 1–8**). These results were confirmed by MS for aSq [(ESI-) *m/z(%)* 465.3 (100) $(M\text{-}H)^{-}$] and cSq [(ESI-) *m/z(%)* 474.4 (100) $(M\text{-}H)^{+}$], respectively. The synthetic schemes are facile and allowed isolating the final products in high yields (>90%), which, moreover, could be scaled-up easily. Notably, the synthesis of cSq with a diethanolamino polar head was further optimized with one step less compared to that of the previously reported squalene-amine derivative (van Tamelen and Curphey, 1962; Ralay-Ranaivo et al., 2014).

Preparation and Physicochemical Characterization of Drug-Free SqD–NPs

Size, PDI, Zeta-Potential, and Morphology

Overall, the introduction of anionic, cationic, or PEG moiety into squalene enhanced the amphiphilic properties of the synthesized SqDs and enabled the facile self-assembly into uniform and stable NPs in aqueous solution. Regardless of the SqD, the drug-free NPs had mean sizes ranging from 100 to 200 nm and a narrow size distribution (PDI < 0.25) (**Figure 3B**, **Supplementary Table 1**). The zeta-potential of aSq–NPs and cSq–NPs were around −40 and +40 mV, respectively, indicating the presence of their corresponding charged groups on the NP surface (**Figure 3B**, **Supplementary Table 1**). Such strong charges facilitate the further drug loading on the surface *via* electrostatic interaction and enable NP stability (Bhattacharjee, 2016).

We prepared two PEGylated SqDs having PEG with different chain length and terminal groups. The PEG750Sq terminates with a methyl group, while the PEG3000Sq terminates with a hydroxyl group. The self-assembling of these PEGylated SqDs allowed the formation of NPs with a dense surface layer of PEG. Regardless of the recorded zeta-potential, this PEG layer is expected to stabilize the NPs and minimize surface interactions between NPs and other molecules (Suk et al., 2016).

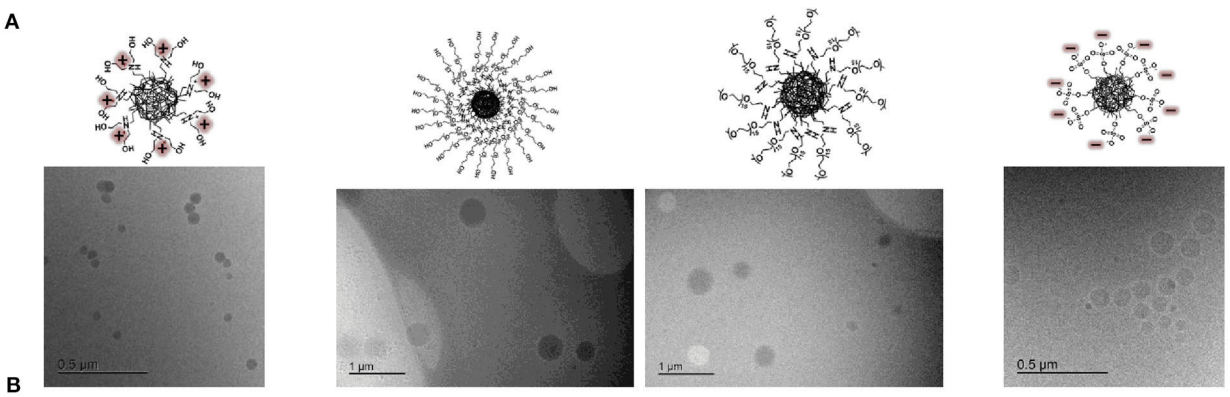

B

cationic Squalenyl Derivative NPs (cSqNPs)		PEGylated Squalenyl Derivative NPs with PEG M_w 3000Da (PEG3000SqNPs)		PEGylated Squalenyl Derivative NPs with PEG M_w 750Da (PEG750SqNPs)		anionic Squalenyl Derivative NPs (aSqNPs)	
size [nm]	156.9±7.5	*size [nm]*	135.9±3.78	*size [nm]*	128.6±16.8	*size [nm]*	123.8±6.7
PdI	0.131±0.014	*PdI*	0.134±0.033	*PdI*	0.236±0.022	*PdI*	0.168±0.013
Zeta-potential [mV]	41.4±4.3	*Zeta-potential [mV]*	-52.5±5.3	*Zeta-potential [mV]*	-9.1±1.9	*Zeta-potential [mV]*	-41.7±7.5

FIGURE 3 | Characterization of SqD–NPs, from left to right: cSq–NPs, PEG3000Sq–NPs, PEG750Sq–NPs, aSq–NPs. **(A)** Cryo-TEM images of SqD–NPs. **(B)** Hydrodynamic size, polydispersity index (PDI), zeta-potential determination by dynamic light scattering (DLS), and electrophoretic light scattering (ELS). Results presented as mean ± SD.

Different initial concentrations of aSq in THF could slightly tune the size of aSq–NPs that were prepared by nanoprecipitation in water at a final concentration of 1 mg/ml (**Supplementary Table 1**). By increasing the aSq concentration in THF from 2.5 to 25 mg/ml, the aSq-NPs had the size raised from 90 to 160 nm. This phenomenon could be explained by the assembly of more squalenyl moieties in the core compartment at higher concentrations (Ho et al., 2018). In contrast, varying the final aSq-NPs concentration in water and using the same initial aSq concentration in THF did not influence the NP size (**Supplementary Table 1**). A similar observation was reported previously for squalenoylated chitosan NPs, which showed an increase rather in NP count than in NP size (Lepeltier et al., 2015). The drug-free cSq–NPs, in turn, could be only formed in the size range of 200 nm regardless of the variation of either initial cSq concentration in organic solvent or final NP concentration in water. The cryo-TEM images of the drug-free SqD–NPs are presented in **Figure 3A** illustrating the amorphous and spherical-shaped NPs. No differences in morphology between the SqD–NPs were observed.

Colloidal Stability

The colloidal stability of drug-free SqD–NPs was investigated in different pH values representing gastric acid (pH 1–3), skin (pH ∼5), and common physiological pH environments at 7.4 (Schmid-Wendtner and Korting, 2006; Koziolek et al., 2015). The colloidal stability in the corresponding pH was evaluated based on the changes of NP size, PDI, and zeta-potential at 1, 3, and 24 h post-incubation. Overall, the aSq–NPs and PEG750Sq–NPs were stable after 24 h of incubation in all studied pH milieus, while the stability of cSq–NPs could only be maintained at pH 5 or lower. In contrast, the incubation of PEG3000Sq–NPs in all tested buffers resulted in colloidal aggregation over time (**Figure 4**).

The hydrogen sulfate groups on aSq-NPs surface were strongly acidic and deprotonated at all tested pH values resulting in a low zeta-potential (around −50 and −25 mV in pH 2/5 and 7.4, respectively), which helped stabilizing the NP suspension (Bhattacharjee, 2016). At 24 h post-incubation in all conditions, the aSq–NPs hydrodynamic diameter was always around 120 nm, while the PDI was lower than 0.2.

The cSq–NPs, in turn, exposing the diethanolamine moiety on its surface, in which pK_a-value is estimated at 8.44 (ChemDraw

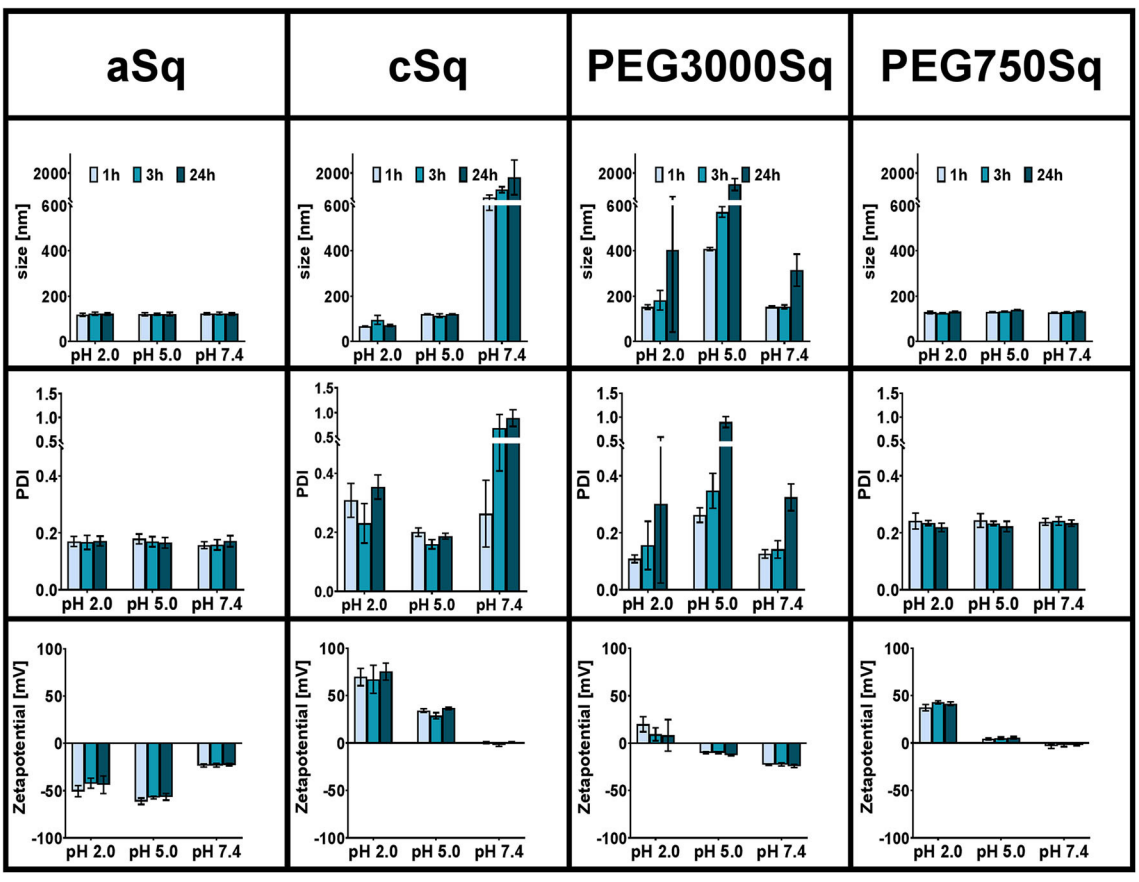

FIGURE 4 | Colloidal stability of SqD–NPs in different physiological relevant pH milieus (pH 2, 5, 7.4) at room temperature studied by DLS and ELS. Hydrodynamic size, PDI, and zeta-potential are reported as mean ± SD. Measurements were taken at three different time points: 1 h (light blue bars), 3 h (blue bars), 24 h (dark blue bars).

Professional 16.0), showed positive zeta-potential of 71 ± 11 and 33 ± 4 mV at pH 2 and 5, respectively, reflecting the protonation of the amine groups. The size and PDI of stable cSq–NPs after 24 h of incubation at pH 5 were 120.5 ± 1.5 nm and 0.19 ± 0.01 nm, respectively. Interestingly, a slightly smaller particle size (76.9 ± 17.1 nm) and a larger PDI (0.30 ± 0.07) were recorded when dispersing cSq–NPs at pH 2. The cSq–NPs could be fully charged at pH 2, which enhanced the amphiphilicity of cSq molecules. Consequently, this induced intermolecular forces and hydrophobic interactions between the squalenyl moieties leading to a denser particle packing (Ho et al., 2018). The same phenomenon was also observed before in farnesylated glycol chitosan NPs (Ho et al., 2018). At neutral pH 7.4, amine functional groups might become partly uncharged causing a decrease in zeta-potential from ∼70 mV at pH 2 to around zero, and the aggregation of cSq–NPs was observed. The colloidal instability of cSq–NPs at pH 7.4 makes these DDS rather unfavorable for systemic drug delivery. However, cSq–NPs demonstrate a good colloidal stability at pH 5, which represents the pH milieu of the skin barrier (Schmid-Wendtner and Korting, 2006). Topical application of NPs to the skin surface are known to enhance the follicular drug delivery. cSq-NPs could be especially further explored to be used for follicular vaccination (Mittal et al., 2015). In addition to the possible complexation of DNA, squalene was already used in adjuvants, boosting an immune response against vaccine antigens. Even the *in vitro* and *in vivo* transfection efficiency of a DNA complex emulsion was improved in the presence of squalene compared to the control complexes (Kwon et al., 2008; Reddy and Couvreur, 2009).

PEGylation offers plenty of advantages to nano-sized drug carriers especially to improve the *in vivo* stability and therapeutic efficacy (Suk et al., 2016; Thomas and Weber, 2019). Previously, PEGylated SqD with a Mw of 1,955 Da was incorporated into squalenoylated gemcitabine prodrug NPs in order to enhance their stability at pH 7.4 and gemcitabine performance (Bekkara-Aounallah et al., 2008). In this study, we aim to investigate the potential of PEGylated SqDs as a platform for drug delivery. Hence, the stability of NPs assembled from PEG3000Sq or PEG750Sq was studied individually. As shown in **Figure 4**, PEG3000Sq–NPs were unstable in all tested buffer media making it unfavorable for use as DDS. Although the small molecule squalene ($Mw = 410$ Da) holds excellent assembling properties, the monoconjugation with PEG having a Mw of 3,000 Da might result in a better water solubility. Thus, the hydrophobic interaction of squalenyl moieties would not be strong enough to stabilize the PEG3000Sq–NPs. On the complete opposite, SqPEG750–NPs demonstrated excellent colloidal stability in all pH milieus at all time points. The hydrodynamic diameter and PDI were always around 129.7 ± 4.5 nm and lower than 0.23 ± 0.02, respectively. The zeta-potential of SqPEG750–NPs was nearly neutral at pH 5 and 7.4; however, it increased to 40 ± 3 mV at pH 2 due to the protonation of the amino conjugation.

The particles holding appropriate colloidal stability in physiological relevant pH milieus were used in further investigations, including aSq–NPs, cSq–NPs, and PEG750Sq–NPs.

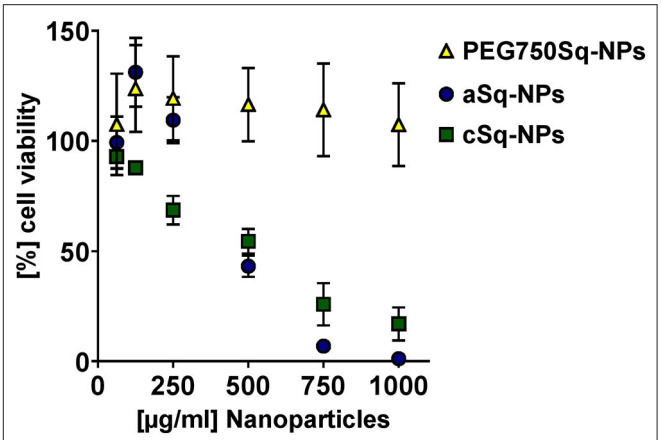

FIGURE 5 | Biocompatibility study *via* MTT assay at different concentrations of PEG750Sq–NPs (yellow triangle), aSq–NPs (dark blue circles), and cSq–NPs (green squares) diluted in HBSS on A549 cells over 4 h at 37°C and 5% CO_2. Results are presented as (%) cell viability relating to negative control in plain HBSS at different NP concentrations and reported as mean ± SD.

Interaction of SqD–NPs With Biological Systems

Biocompatibility

The biocompatibility of the SqD–NPs was tested on A549 cells *via* MTT assay (**Figure 5**). In good agreement with Ho et al. (2020) aSq–NPs demonstrated 100% viability for up to 250 µg/ml (blue circles in **Figure 5**). The cSq–NPs (green squares in **Figure 5**) showed slightly lower tolerability than aSq-NPs, which might have an explanation in the instability of cSq–NPs in HBSS buffer causing large aggregates on cells. Moreover, the nature of a cationic lipid can enhance the toxicity due to its potential interaction with anionic biological molecules like proteins and nucleic acids (Knudsen et al., 2015). Thus, only 70% cell viability was found when incubating cSq–NPs at a concentration of 250 µg/ml. Similar findings were previously described: the incubation of 250 µg/ml of positively charged squalenoylated chitosan NPs and farnesylated glycol chitosan NPs resulting in ∼80 and >70% A549 cell viability, respectively (Lepeltier et al., 2015; Ho et al., 2018). The PEG750Sq–NPs (yellow squares in **Figure 5**) were highly biocompatible demonstrating 100% cell viability at the highest tested concentration of 1 mg/ml.

Protein–SqD–NPs Interactions

Exemplary for a protein interaction study, the physicochemical interactions between fluorescent SqD–NPs and mucin glycoproteins were studied using NTA. The hydrodynamic size of the SqD–NP suspension was compared either in (i) water (blue line in **Figure 6**) or in (ii) 0.1% mucin glycoprotein aqueous solution (green line in **Figure 6**). It was hypothesized that non-interacting, fluorescent SqD–NPs would display the same particle size distribution irrespective of dispersion in water or in the low-viscosity mucin glycoprotein-containing solution. Conversely, the fluorescence signal of SqD–NPs interacting

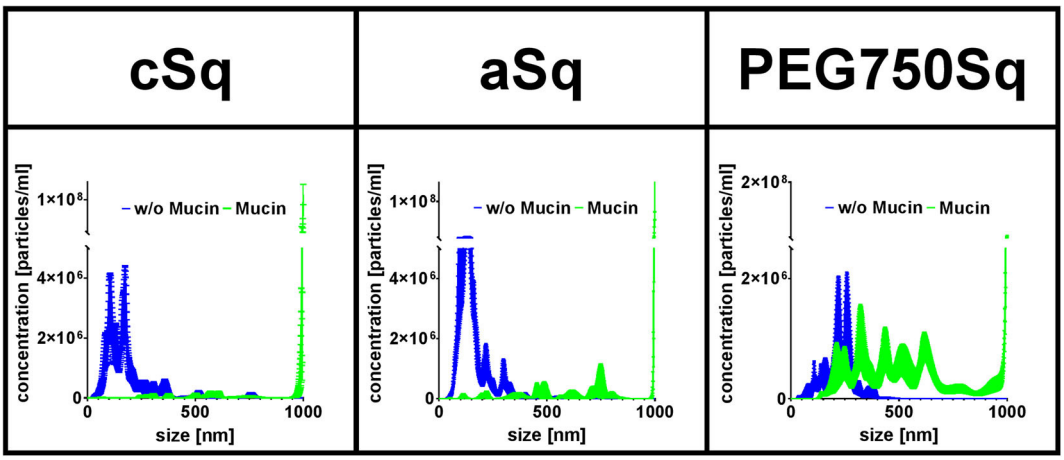

FIGURE 6 | Fluorescent SqD–NPs interaction study with mucin glycoproteins. Interactions detected by size shift determined by nanoparticle tracking analysis (NTA) measurements. Blue lines: measurement of fluorescent SqD–NPs in water. Green lines: measurement of fluorescent SqD–NPs in non-fluorescent 0.1% mucin glycoprotein aqueous solution. Results are presented as mean ± SE.

with non-fluorescent mucin glycoproteins would display a different Brownian motion, indicative of a movement hindrance, and resulting in a particle size distribution shifted toward larger particle diameters. By comparing the results of the measurements of SqD–NPs in both aqueous solution (**Figure 6**) on this basis, the interaction between the mucin glycoproteins and NPs can be ranked from high to low as follows: cSq–NPs > aSq–NPs >> PEG750Sq–NPs.

In detail, cSq–NPs were found to present a highly positive surface net charge enabling interaction with the negatively charged mucin glycoproteins. These strong interactions are demonstrated by a size shift to a larger size from ∼180 to ∼960 nm (mean of number–weighted distribution) (blue and green lines in **Figure 6**, respectively). Further, the negatively charged aSq–NPs showed interactions with the mucin glycoproteins, shifting the mean particle size from ∼160 to ∼930 nm (blue and green lines in **Figure 6**, respectively), which is less pronounced than for cSq–NPs. We assumed that those interactions are mainly caused by the hydrophobic squalenyl moiety (Murgia et al., 2018). As expected, PEG750Sq–NPs demonstrated only minor interactions with mucin glycoproteins (mean size shift from ∼230 to ∼575 nm, blue and green lines in **Figure 6**, respectively). Still PEG750Sq–NPs resulted in partial mucin adsorption, which can be explained by hydrophobic interactions between mucin glycoproteins and the NP core.

Our results, showing that interactions between mucin glycoproteins and charged NPs, cSq–NPs, and aSq–NPs are more pronounced than interactions with neutral PEG750Sq–NPs, are in good concordance with previous findings (Crater and Carrier, 2010). PEGylated NPs, with a sufficiently high PEG density on the NP surface, are widely known to be mucus penetrating because they are inert to hydrophobic interactions and hydrogen bonding (Wang et al., 2008; Xu et al., 2015; Maisel et al., 2016).

Carrier Properties of SqD–NPs

Optimal Loading Capacities of SqD–NPs

We investigated the LC of the SqD–NPs using a variety of compounds owning multiple functional groups as well as representing different physicochemical characteristics and Mw. The suitable SqD and drug-loading method to obtain optimal LC for each model compound are reported in **Table 1**, while detailed guidance for choosing appropriate SqD and preparation method is shown in **Figure 2**. Generally, the SqD–NPs are composed of two compartments—a hydrophilic shell and a hydrophobic core. The hydrophobic drugs were loaded in the core by hydrophobic interactions *via* the coprecipitation method or the solvent evaporation method. For the hydrophobic compounds, e.g., Nile red, cholesteryl BODIPY, or dexamethasone, the coprecipitation method offers more facile loading procedure and better LC. The hydrophilic drugs, in turn, could be loaded onto the NP shell by charge interactions and hydrogen bonding *via* the dropping method or the solvent evaporation method. Interestingly, by allowing the drug to distribute in both the lipophilic and hydrophilic domains of the squalenyl nanoassemblies, the solvent evaporation method is a good loading technique for amphiphilic compounds, e.g., colistin.

In this study, the model compounds dexamethasone, cholesteryl BODIPY, and Nile red—representing different Mw and hydrophobicity—could be loaded in the core of any SqD–NPs. The drug-loaded NPs had a size range of 130–250 nm and a narrow size distribution (PDI < 0.3). Notably, the optimal LC of dexamethasone was ∼33, ∼32, and ∼24% in aSq–NPs, cSq–NPs, and PEG750Sq–NPs, respectively, while the EE values in all cases were ∼90% (**Table 1**). The optimal LC and EE of cholesteryl BODIPY in aSq–NPs were 10.35 ± 0.66% and 87.6 ± 8.2%, respectively. The optimal LC and EE of Nile red in cSq–NPs were 9.03 ± 0.91% and 60.2 ± 6.7%, respectively. The lower EE recorded in loading Nile red could be explained by its low Mw

TABLE 1 | Summary of preparation methods used to load model compounds to squalenyl derivative–nanoparticles (SqD-NPs).

Squalenyl-derivative	Drug	Preparation method	Size (nm)	PDI	Zeta-potential (mV)	EE (%)	LC (%)
aSq	Cholesteryl BODIPY	Coprecipitation	254.3 ± 2.4	0.094 ± 0.011	−18.6 ± 0.1	87.6 ± 8.2	10.35 ± 0.66
	Dexamethasone	Coprecipitation	140.2 ± 25.7	0.203 ± 0.061	−40.0 ± 7.1	90.6 ± 1.2	32.75 ± 0.33
	Isoniazid	Solvent evaporation	198.9 ± 8.6	0.249 ± 0.029	−29.5 ± 1.0	42.6 ± 1.7	27.43 ± 0.79
		Dropping	112.9 ± 2.0	0.125 ± 0.017	−35.6 ± 2.3	07.4 ± 1.2	06.17 ± 0.97
	Colistin	Solvent evaporation	325.0 ± 7.1	0.152 ± 0.041	22.9 ± 1.1	90.1 ± 2.3	45.31 ± 0.73
		Dropping	195.6 ± 2.6	0.184 ± 0.002	25.1 ± 1.0	83.6 ± 4.1	35.83 ± 0.51
	Tigecycline	Dropping	198.6 ± 4.8	0.014 ± 0.010	28.6 ± 1.3	85.3 ± 6.7	44.26 ± 2.03
cSq	Nile Red	Coprecipitation	208.0 ± 3.2	0.185 ± 0.069	38.6 ± 3.7	60.2 ± 6.7	09.03 ± 0.91
	Dexamethasone	Coprecipitation	146.9 ± 8.9	0.183 ± 0.027	44.1 ± 5.7	87.9 ± 6.6	32.09 ± 1.64
	Fluorescent Albumin	Dropping	205.6 ± 2.8	0.174 ± 0.010	17.4 ± 1.7	92.1 ± 3.8	03.52 ± 0.33
PEG750Sq	Dexamethasone	Coprecipitation	162.95 ± 59.45	0.255 ± 0.075	00.1 ± 9.2	92.4 ± 2.5	23.49 ± 0.48

The characteristics of optimal drug-loaded SqD–NPs, including hydrodynamic size, polydispersity index (PDI), zeta-potential, encapsulation efficiency (EE), and loading capacity (LC) are reported. Results are presented as mean ± SD.

and less interaction with the squalenyl core. Squalene is known as a precursor in the endogenous cholesterol biosynthesis, which implies its strong interaction with dexamethasone—a derivative of cholesterol—thereof enhancing the LC and EE (Reddy and Couvreur, 2009; Ghimire et al., 2016). The same holds true for cholesteryl BODIPY, which has a high clog *P*-value and contains a cholesteryl moiety.

Isoniazid, colistin, tigecycline, and FITC-albumin, representing different Mw and hydrophilicity, were loaded in either aSq–NPs or cSq–NPs. Accordingly, the loading of these compounds was investigated using solvent evaporation method and/or dropping method (**Figure 2**), while the optimal LC and EE for each compound and the corresponding loading method are reported in **Table 1**.

Isoniazid—a positively charged and small molecule (Mw 137.14 Da)—was loaded in aSq–NPs. The solvent evaporation method resulted in a significantly higher LC of isoniazid at 27.43 ± 0.79% compared to that of the dropping method at 6.17 ± 0.97%. Using the solvent evaporation method, the preparation of isoniazid and aSq in the solvent mixture (THF:water 1:1 v/v) allowed the maximum charged interaction between the two reagents, thus, increased the EE and LC. In contrast, the preformed aSq–NPs and dropping method limited the interaction with isoniazid molecules. The optimal isoniazid-loaded aSq–NPs had the size of 198.9 ± 8.6 nm and PDI below 0.25.

The molecules with multiple functional groups—tigecycline (Mw 585.66 Da), colistin (Mw 1,155.46 Da), and FITC-albumin (Mw ∼60,000 Da)—could be loaded in NPs using the dropping method. The optimal LC and EE of stable tigecycline-loaded aSq–NPs (198.6 ± 4.8 nm, PDI 0.014 ± 0.010) were 44.26 ± 2.03 and 85.3 ± 6.7%, respectively. The LC and EE of colistin in aSq–NPs were significantly high at 35.83 ± 0.51 and 83.6 ± 4.1%, respectively, which also produced a stable DDS having the size of 195.6 ± 2.6 nm and PDI lower than 0.2. The reasonable LC and EE of FITC-albumin—a representative of negatively charged protein molecules—in cSq–NPs were 3.52 ± 0.33 and 92.1 ± 3.8%, respectively. The stable protein-loaded cSq–NPs had the size of 205.6 ± 2.8 nm and PDI below 0.2. As shown in **Table 1**, the zeta-potential values of these drug-loaded NPs changed significantly compared to the corresponding drug-free NPs reflecting the loading *via* charged interactions.

The positively charged colistin contains a lipophilic moiety and could interact with aSq molecules *via* both charged and hydrophobic interactions (Yasar et al., 2018; Menina et al., 2019). We, thus, hypothesized that the solvent evaporation method could enhance the LC and EE of colistin in aSq–NPs. In fact, colistin LC and EE obtained by using such an approach were 45.31 ± 0.73 and 90.1 ± 2.3%, respectively, which were higher than the ones obtained by the dropping method. The integration of the lipophilic moiety of colistin into aSq–NPs increased the NP size from 195.6 ± 2.6 to 325.0 ± 7.1 nm, while the positive zeta-potential (22.9 ± 1.1 mV) of the drug-loaded aSq–NPs indicated also the presence of colistin on the NP surface.

The dual loading capacity of the SqD–NPs was illustrated by loading both hydrophobic Nile red and hydrophilic FTIC-albumin in cSq-NPs. The Nile red-loaded cSq–NPs (LC ∼0.5%) were prepared by the coprecipitation, and then further loaded with hydrophilic FTIC-albumin (LC∼0.5%) by the dropping method. The colocalization of both fluorescent compounds in NPs was confirmed by confocal laser scanning microscopy images (**Supplementary Figure 10**). Such simultaneous drug loadings could benefit the delivery of actives with synergistic effects (Ho et al., 2020).

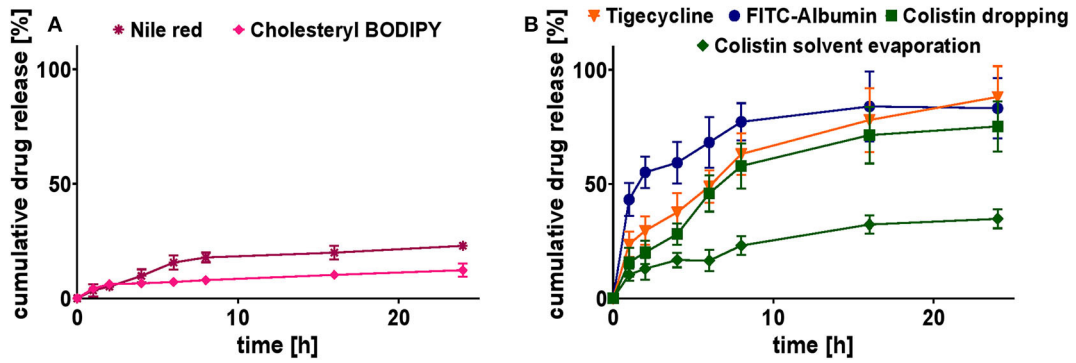

FIGURE 7 | Cumulative release study of selected model drug-loaded SqD–NPs at pH 7.4 and 37°C for 24 h in PBS. **(A)** Cumulative release profiles of hydrophobic compounds: Nile red (purple star), cholesteryl-BODIPY (pink rhomb). **(B)** Cumulative release profiles of hydrophilic compounds: FITC-albumin (blue circles), tigecycline (orange triangle), colistin (dropping: green square; solvent evaporation: green rhomb). Results are presented as mean ± SD.

In short, the SqD–NPs are capable of loading a broad range of drug molecules differing in physicochemical characteristics, thus, are versatile drug delivery platforms.

Release Studies

In vitro release profiles were conducted under the same conditions at physiological pH 7.4 (PBS), 37°C, and over 24 h (**Figures 7A,B**).

The release profiles of hydrophobic compounds were determined for the ones with the highest and lowest Mw, cholesteryl BODIPY, and Nile red, respectively. The release profiles for both compounds are shown in **Figure 7A**. They clearly demonstrate their affection by the strength of hydrophobic interactions. Compared to cholesteryl BODIPY, Nile red released twice the cumulative percentage after 24 h. Nevertheless, the release of both compounds was sustained for the period over at least 24 h.

The release profiles of hydrophilic compounds were conducted for tigecycline (highest achieved LC), FITC-albumin (protein representative) and colistin (comparison of two preparation methods), respectively. The association of hydrophilic drugs loaded onto the NP surface by the dropping method is not as strong as a covalent conjugation, leading to the assumption of a complete drug release. Cumulative release of tigecycline, colistin, and FITC-albumin reached 88 ± 13, 75 ± 11, and 83 ± 13%, respectively, after 24 h in PBS at 37°C (**Figure 7B**). The burst release at the early time points were avoided suggesting the strong charged interactions between the SqD and drug molecules. In comparison to that, the tight interaction of colistin to aSq–NPs by using the solvent evaporation method resulted in a sustained release for colistin. Only 35 ± 4% of colistin was released from aSq–NPs after 24 h in PBS at 37°C (**Figure 7B**).

Furthermore, IC90 values of tigecycline and colistin-loaded aSq–NPs were determined by the minimum inhibitory concentration (MIC) assay performed on *Pseudomonas aeruginosa* strain PA14 wild type and *Staphylococcus aureus* strain Newman. As shown in **Supplementary Table 3**, the antimicrobial effect of both antibiotic-loaded NPs was similar to that of the drug alone, even though drug release after 24 h from the NPs is not completed.

CONCLUSION

In this study, we explored the use of self-assembling amphiphilic SqDs as DDS, which had started with the aSq. We have further described the straightforward synthesis of cSq and PEGylated SqDs. In addition to the ability of self-assembling to supramolecular colloids, the latter demonstrated that SqD–NPs showed excellent stability in physiological relevant media and biocompatibility. The application of different methods for the preparation of drug-loaded SqD–NPs allowed to modulate not only the LC but also the release rate, as desired. In further studies of carrier properties, the SqD–NPs showed significantly high LC of various cargos. Our findings postulate the self-assembled SqD–NPs as versatile drug delivery platforms.

DATA AVAILABILITY STATEMENT

The raw data supporting the conclusions of this article will be made available by the authors, without undue reservation.

AUTHOR CONTRIBUTIONS

D-KH, BL, DD, PC, and C-ML conceptualized and initiated the study. PC and C-ML acquired funding and provided resources. XM, US, BL, DD, PC, and C-ML were supervisors. D-KH did chemical synthesis and characterization. D-KH and RC investigated NP self-assembly and drug-loading capacities. CDR, RC, and D-KH validated the drug quantification methods. D-KH conducted *in vitro* assays and drug release. CDR and MK visualized the NPs. XM conceptualized and validated the mucin–NPs interaction studies. RC and SF performed NP

stability and mucin–NPs interaction studies. RC and D-KH analyzed the data, prepared the figures, and wrote the original draft. RC reviewed and edited the final draft. All authors read and revised the manuscript.

FUNDING

This project received funding from the European Union's Framework Programme for Research and Innovation Horizon 2020 (2014–2020) under the Marie Sklodowska-Curie Grant Agreement No. 642028. We acknowledged the support by the Deutsche Forschungsgemeinschaft (DFG; German Research Foundation) and Saarland University within the funding program Open Access Publishing. RC was supported by Dr. Rolf M. Schwiete Stiftung, Mannheim, Germany.

ACKNOWLEDGMENTS

The authors would like to thank the kind support from Dr. Sangeun Lee, Petra König, Jana Westhues, Dr. Arnaud Peramo, and Sandrine Gouazou.

SUPPLEMENTARY MATERIAL

The Supplementary Material for this article can be found online at: https://www.frontiersin.org/articles/10.3389/fchem.2020.584242/full#supplementary-material

REFERENCES

Bansil, R., and Turner, B. S. (2006). Mucin structure, aggregation, physiological functions and biomedical applications. *Curr. Opin. Colloid Interface Sci*. 11, 164–170. doi: 10.1016/j.cocis.2005.11.001

Bekkara-Aounallah, F., Gref, R., Othman, M., Reddy, L. H., Pili, B., Allain, V., et al. (2008). Novel PEGylated nanoassemblies made of self-assembled squalenoyl nucleoside analogues. *Adv. Funct. Mater*. 18, 3718–3725. doi: 10.1002/adfm.200800705

Bhattacharjee, S. (2016). DLS and zeta potential - What they are and what they are not? *J. Control. Release*. 235, 337–351. doi: 10.1016/j.jconrel.2016.06.017

Bobo, D., Robinson, K. J., Islam, J., Thurecht, K. J., and Corrie, S. R. (2016). Nanoparticle-based medicines: a review of FDA-approved materials and clinical trials to date. *Pharm. Res*. 33, 2373–2387. doi: 10.1007/s11095-016-1958-5

Buchy, E., Valetti, S., Mura, S., Mougin, J., Troufflard, C., Couvreur, P., et al. (2015). Synthesis and cytotoxic activity of self-assembling squalene conjugates of 3-[(Pyrrol-2-yl)methylidene]-2,3-dihydro-1 H -indol-2-one anticancer agents. *Eur. J. Org. Chem*. 2015, 202–212. doi: 10.1002/ejoc.201403088

Ceruti, M., Balliano, G., Viola, F., Cattel, L., Gerst, N., and Schuber, F. (1987). Synthesis and biological activity of azasqualenes, bis-azasqualenes and derivatives. *Eur. J. Med. Chem*. 22, 199–208. doi: 10.1016/0223-5234(87)90050-X

Couvreur, P. (2013). Nanoparticles in drug delivery: past, present and future. *Adv. Drug Deliv. Rev*. 65, 21–23. doi: 10.1016/j.addr.2012.04.010

Couvreur, P., Stella, B., Reddy, L. H., Hillaireau, H., Dubernet, C., Desmaële, D., et al. (2006). Squalenoyl nanomedicines as potential therapeutics. *Nano Lett*. 6, 2544–2548. doi: 10.1021/nl061942q

Crater, J. S., and Carrier, R. L. (2010). Barrier properties of gastrointestinal mucus to nanoparticle transport. *Macromol. Biosci*. 10, 1473–1483. doi: 10.1002/mabi.201000137

Danhier, F., Ansorena, E., Silva, J. M., Coco, R., Le Breton, A., and Préat, V. (2012). PLGA-based nanoparticles: an overview of biomedical applications. *J. Control. Release* 161, 505–522. doi: 10.1016/j.jconrel.2012.01.043

Desmaële, D., Gref, R., and Couvreur, P. (2012). Squalenoylation: a generic platform for nanoparticular drug delivery. *J. Control. Release* 161, 609–618. doi: 10.1016/j.jconrel.2011.07.038

Fessi, H., Puisieux, F., Devissaguet, J. Ph, Ammoury, N., and Benita, S. (1989). Nanocapsule formation by interfacial polymer disposition following solvent displacement. *Int. J. Pharm*. 55, 1–4. doi: 10.1016/0378-5173(89)90281-0

Ghimire, G. P., Thuan, N. H., Koirala, N., and Sohng, J. K. (2016). Advances in biochemistry and microbial production of squalene and its derivatives. *J. Microbiol. Biotechnol*. 26, 441–451. doi: 10.4014/jmb.1510.10039

Hillaireau, H., Dereuddre-Bosquet, N., Skanji, R., Bekkara-Aounallah, F., Caron, J., Lepêtre, S., et al. (2013). Anti-HIV efficacy and biodistribution of nucleoside reverse transcriptase inhibitors delivered as squalenoylated prodrug nanoassemblies. *Biomaterials* 34, 4831–4838. doi: 10.1016/j.biomaterials.2013.03.022

Ho, D.-K., Frisch, S., Biehl, A., Terriac, E., Rossi, C. de, Schwarzkopf, K., et al. (2018). Farnesylated glycol chitosan as a platform for drug delivery: synthesis, characterization, and investigation of mucus-particle interactions. *Biomacromolecules* 19, 3489–3501. doi: 10.1021/acs.biomac.8b00795

Ho, D.-K., Murgia, X., Rossi, C. de, Christmann, R., Hüfner de Mello Martins, A. G., Koch, M., et al. (2020). Squalenyl hydrogen sulfate nanoparticles for simultaneous delivery of tobramycin and an alkylquinolone quorum sensing inhibitor enable the eradication of *P. aeruginosa* biofilm infections. *Angew. Chem. Int. Ed. Engl*. 59:10296. doi: 10.1002/anie.202001407

Ho, D.-K., Nichols, B. L. B., Edgar, K. J., Murgia, X., Loretz, B., and Lehr, C.-M. (2019). Challenges and strategies in drug delivery systems for treatment of pulmonary infections. *Eur. J. Pharm. Biopharm*. 144, 110–124. doi: 10.1016/j.ejpb.2019.09.002

Kalepu, S., and Nekkanti, V. (2015). Insoluble drug delivery strategies: review of recent advances and business prospects. *Acta Pharm. Sin. B* 5, 442–453. doi: 10.1016/j.apsb.2015.07.003

Kim, S. M., Faix, P. H., and Schnitzer, J. E. (2017). Overcoming key biological barriers to cancer drug delivery and efficacy. *J. Control. Release* 267, 15–30. doi: 10.1016/j.jconrel.2017.09.016

Knudsen, K. B., Northeved, H., Kumar, P. E. K., Permin, A., Gjetting, T., Andresen, T. L., et al. (2015). *In vivo* toxicity of cationic micelles and liposomes. *Nanomedicine* 11, 467–477. doi: 10.1016/j.nano.2014.08.004

Kokkinopoulou, M., Simon, J., Landfester, K., Mailänder, V., and Lieberwirth, I. (2017). Visualization of the protein corona: towards a biomolecular understanding of nanoparticle-cell-interactions. *Nanoscale* 9, 8858–8870. doi: 10.1039/C7NR02977B

Koziolek, M., Grimm, M., Becker, D., Iordanov, V., Zou, H., Shimizu, J., et al. (2015). Investigation of pH and temperature profiles in the GI tract of fasted human subjects using the Intellicap® system. *J. Pharm. Sci*. 104, 2855–2863. doi: 10.1002/jps.24274

Kwon, S. M., Nam, H. Y., Nam, T., Park, K., Lee, S., Kim, K., et al. (2008). *In vivo* time-dependent gene expression of cationic lipid-based emulsion as a stable and biocompatible non-viral gene carrier. *J. Control. Release* 128, 89–97. doi: 10.1016/j.jconrel.2008.02.004

Lai, S. K., O'Hanlon d, E., Harrold, S., Man, S. T., Wang, Y.-Y., Cone, R., et al. (2007). Rapid transport of large polymeric nanoparticles in fresh undiluted human mucus. *PNAS* 104, 1482–1487. doi: 10.1073/pnas.0608611104

Lepeltier, E., Loretz, B., Desmaële, D., Zapp, J., Herrmann, J., Couvreur, P., et al. (2015). Squalenoylation of chitosan: a platform for drug delivery? *Biomacromolecules* 16, 2930–2939. doi: 10.1021/acs.biomac.5b00840

Lieleg, O., and Ribbeck, K. (2011). Biological hydrogels as selective diffusion barriers. *Trends Cell Biol*. 21, 543–551. doi: 10.1016/j.tcb.2011.06.002

Lock, J. Y., Carlson, T. L., and Carrier, R. L. (2018). Mucus models to evaluate the diffusion of drugs and particles. *Adv. Drug Deliv. Rev*. 124, 34–49. doi: 10.1016/j.addr.2017.11.001

Maisel, K., Reddy, M., Xu, Q., Chattopadhyay, S., Cone, R., Ensign, L. M., et al. (2016). Nanoparticles coated with high molecular weight PEG penetrate mucus

and provide uniform vaginal and colorectal distribution *in vivo*. *Nanomedicine* 11, 1337–1343. doi: 10.2217/nnm-2016-0047

Maksimenko, A., Mougin, J., Mura, S., Sliwinski, E., Lepeltier, E., Bourgaux, C., et al. (2013). Polyisoprenoyl gemcitabine conjugates self assemble as nanoparticles, useful for cancer therapy. *Cancer Lett*. 334, 346–353. doi: 10.1016/j.canlet.2012.08.023

Menina, S., Eisenbeis, J., Kamal, M. A. M., Koch, M., Bischoff, M., Gordon, S., et al. (2019). Bioinspired liposomes for oral delivery of colistin to combat intracellular infections by *Salmonella enterica*. *Adv. Healthc. Mater*. 8:e1900564. doi: 10.1002/adhm.201900564

Mittal, A., Schulze, K., Ebensen, T., Weißmann, S., Hansen, S., Lehr, C. M., et al. (2015). Efficient nanoparticle-mediated needle-free transcutaneous vaccination *via* hair follicles requires adjuvantation. *Nanomedicine* 11, 147–154. doi: 10.1016/j.nano.2014.08.009

Mosmann, T. (1983). Rapid colorimetric assay for cellular growth and survival: application to prolifaration and cytotoxicity assays. *J. Immunol. Methods* 65, 55–63. doi: 10.1016/0022-1759(83)90303-4

Murgia, X., Loretz, B., Hartwig, O., Hittinger, M., and Lehr, C.-M. (2018). The role of mucus on drug transport and its potential to affect therapeutic outcomes. *Adv. Drug Deliv. Rev*. 124, 82–97. doi: 10.1016/j.addr.2017.10.009

Murgia, X., Pawelzyk, P., Schaefer, U. F., Wagner, C., Willenbacher, N., and Lehr, C.-M. (2016). Size-limited penetration of nanoparticles into porcine respiratory mucus after aerosol deposition. *Biomacromolecules* 17, 1536–1542. doi: 10.1021/acs.biomac.6b00164

Raesch, S. S., Tenzer, S., Storck, W., Rurainski, A., Selzer, D., Ruge, C. A., et al. (2015). Proteomic and lipidomic analysis of nanoparticle corona upon contact with lung surfactant reveals differences in protein, but not lipid composition. *ACS Nano* 9, 11872–11885. doi: 10.1021/acsnano.5b04215

Ralay-Ranaivo, B., Desmaële, D., Bianchini, E. P., Lepeltier, E., Bourgaux, C., Borgel, D., et al. (2014). Novel self assembling nanoparticles for the oral administration of fondaparinux: synthesis, characterization and *in vivo* evaluation. *J. Control. Release* 194, 323–331. doi: 10.1016/j.jconrel.2014.07.060

Reddy, L. H., and Couvreur, P. (2009). Squalene: a natural triterpene for use in disease management and therapy. *Adv. Drug Deliv. Rev*. 61, 1412–1426. doi: 10.1016/j.addr.2009.09.005

Ruge, C. A., Kirch, J., and Lehr, C.-M. (2013). Pulmonary drug delivery: from generating aerosols to overcoming biological barriers—therapeutic possibilities and technological challenges. *Lancet Respir. Med*. 1, 402–413. doi: 10.1016/S2213-2600(13)70072-9

Sanna, V., Roggio, A. M., Siliani, S., Piccinini, M., Marceddu, S., Mariani, A., et al. (2012). Development of novel cationic chitosan-and anionic alginate-coated poly(D,L-lactide-co-glycolide) nanoparticles for controlled release and light protection of resveratrol. *Int. J. Nanomed*. 7, 5501–5516. doi: 10.2147/IJN.S36684

Schmid-Wendtner, M.-H., and Korting, H. C. (2006). The pH of the skin surface and its impact on the barrier function. *Skin Pharmacol. Physiol*. 19, 296–302. doi: 10.1159/000094670

Schroepfer, G. J. (1981). Sterol biosynthesis. *Annu. Rev. Biochem*. 50, 585–621. doi: 10.1146/annurev.bi.50.070181.003101

Sémiramoth, N., Di Meo, C., Zouhiri, F., Saïd-Hassane, F., Valetti, S., Gorges, R., et al. (2012). Self-assembled squalenoylated penicillin bioconjugates: an original approach for the treatment of intracellular infections. *ACS Nano* 6, 3820–3831. doi: 10.1021/nn204928v

Skarbek, C., Lesueur, L. L., Chapuis, H., Deroussent, A., Pioche-Durieu, C., Daville, A., et al. (2015). Preactivated oxazaphosphorines designed for isophosphoramide mustard delivery as bulk form or nanoassemblies: synthesis and proof of concept. *J. Med. Chem*. 58, 705–717. doi: 10.1021/jm501224x

Suk, J. S., Xu, Q., Kim, N., Hanes, J., and Ensign, L. M. (2016). PEGylation as a strategy for improving nanoparticle-based drug and gene delivery. *Adv. Drug Deliv. Rev*. 99, 28–51. doi: 10.1016/j.addr.2015.09.012

Thomas, O. S., and Weber, W. (2019). Overcoming physiological barriers to nanoparticle delivery-are we there yet? *Front. Bioeng. Biotechnol*. 7:415. doi: 10.3389/fbioe.2019.00415

van Tamelen, E. E., and Curphey, T. J. (1962). The selective *in vitro* oxidation of the terminal double bonds in squalene. *Tetrahedron Lett*. 3, 121–124. doi: 10.1016/S0040-4039(00)71112-9

Wang, Y.-Y., Lai, S. K., Suk, J. S., Pace, A., Cone, R., and Hanes, J. (2008). Addressing the PEG mucoadhesivity paradox to engineer nanoparticles that "slip" through the human mucus barrier. *Angew. Chem. Int. Ed. Engl*. 47, 9726–9729. doi: 10.1002/anie.200803526

Xu, Q., Ensign, L. M., Boylan, N. J., Schön, A., Gong, X., Yang, J.-C., et al. (2015). Impact of surface polyethylene glycol (PEG) density on biodegradable nanoparticle transport in mucus *ex vivo* and distribution *in vivo*. *ACS Nano* 9, 9217–9227. doi: 10.1021/acsnano.5b03876

Yasar, H., Ho, D.-K., Rossi, C. de, Herrmann, J., Gordon, S., Loretz, B., et al. (2018). Starch-chitosan polyplexes: a versatile carrier system for anti-infectives and gene delivery. *Polymers*. 10:252. doi: 10.3390/polym10030252

Conflict of Interest: The authors declare that the research was conducted in the absence of any commercial or financial relationships that could be construed as a potential conflict of interest.

frontiers in Chemistry

MINI REVIEW
published: 30 October 2020
doi: 10.3389/fchem.2020.598160

Supramolecular Self-Assembled Peptide-Based Vaccines: Current State and Future Perspectives

Tuerdimaimaiti Abudula[1†], Khushbu Bhatt[2†], Loek J. Eggermont[3†], Nick O'Hare[3], Adnan Memic[1] and Sidi A. Bencherif[3,4,5,6*]*

[1] Center of Nanotechnology, King Abdulaziz University, Jeddah, Saudi Arabia, [2] Department of Pharmaceutical Sciences, Northeastern University, Boston, MA, United States, [3] Department of Chemical Engineering, Northeastern University, Boston, MA, United States, [4] Department of Bioengineering, Northeastern University, Boston, MA, United States, [5] Harvard John A. Paulson School of Engineering and Applied Sciences, Harvard University, Cambridge, MA, United States, [6] Sorbonne University, UTC CNRS UMR 7338, Biomechanics and Bioengineering (BMBI), University of Technology of Compiègne, Compiègne, France

Despite the undeniable success of vaccination programs in preventing diseases, effective vaccines against several life-threatening infectious pathogens such as human immunodeficiency virus are still unavailable. Vaccines are designed to boost the body's natural ability to protect itself against foreign pathogens. To enhance vaccine-based immunotherapies to combat infections, cancer, and other conditions, biomaterials have been harnessed to improve vaccine safety and efficacy. Recently, peptides engineered to self-assemble into specific nanoarchitectures have shown great potential as advanced biomaterials for vaccine development. These supramolecular nanostructures (i.e., composed of many peptides) can be programmed to organize into various forms, including nanofibers, nanotubes, nanoribbons, and hydrogels. Additionally, they have been designed to be responsive upon exposure to various external stimuli, providing new innovations in the development of smart materials for vaccine delivery and immunostimulation. Specifically, self-assembled peptides can provide cell adhesion sites, epitope recognition, and antigen presentation, depending on their biochemical and structural characteristics. Furthermore, they have been tailored to form exquisite nanostructures that provide improved enzymatic stability and biocompatibility, in addition to the controlled release and targeted delivery of immunomodulatory factors (e.g., adjuvants). In this mini review, we first describe the different types of self-assembled peptides and resulting nanostructures that have recently been investigated. Then, we discuss the recent progress and development trends of self-assembled peptide-based vaccines, their challenges, and clinical translatability, as well as their future perspectives.

Keywords: supramolecular, peptides, self-assembly, vaccine, delivery

OPEN ACCESS

Edited by:
Elise Lepeltier, Université d'Angers, France

Reviewed by:
Tangxin Xiao, Changzhou University, China
Xiao-Yu Hu, Nanjing University of Aeronautics and Astronautics, China

***Correspondence:**
Adnan Memic
amemic@kau.edu.sa
Sidi A. Bencherif
s.bencherif@northeastern.edu

[†]These authors have contributed equally to this work

Specialty section:
This article was submitted to Supramolecular Chemistry, a section of the journal Frontiers in Chemistry

Received: *25 August 2020*
Accepted: *05 October 2020*
Published: *30 October 2020*

Citation:
Abudula T, Bhatt K, Eggermont LJ, O'Hare N, Memic A and Bencherif SA (2020) Supramolecular Self-Assembled Peptide-Based Vaccines: Current State and Future Perspectives. Front. Chem. 8:598160. doi: 10.3389/fchem.2020.598160

INTRODUCTION

Vaccination has been considered as one of the crowning achievements of humankind, and gained remarkable triumph in treating many life-threatening and epidemic diseases, such as influenza, tuberculosis, and smallpox (Malonis et al., 2019; Piot et al., 2019). Vaccines can greatly reduce the burden of preventable infectious diseases by working with the body's natural defenses to

safely develop immunity to diseases (Piot et al., 2019; Parvizpour et al., 2020). For instance, to respond to the new and unprecedented coronavirus disease 2019 (COVID-19) crisis, vaccination is considered to be the best strategy to end this pandemic (Graham, 2020; Lurie et al., 2020). Conventional vaccination methods are based on pathogens (e.g., attenuated, inactivated, toxins, subunits) that can provoke immunity against antigens and provide long-lasting protection against the diseases (Chiang et al., 2010; Cockburn and Seder, 2018). Despite these advantages, this approach is suffering from a number of drawbacks, including low immunogenicity, high cost, manufacturing challenges, vaccine instability in the cold chain, and potential contaminations during manufacturing which could alter vaccine efficacy and cause a strong allergic shock (Skwarczynski and Toth, 2016).

Although great advances have been made in the development of vaccines and immunotherapies, there is an increasing demand for enhanced control over the immune responses induced against infectious diseases and cancer. Biomaterials can be leveraged for modulating the immune system and subsequently controlling immune responses (Bookstaver et al., 2018). For instance, recent immunization strategies have centered on biomaterial-based vaccines in which specific cellular components were used as antigens to stimulate the immune response against cancer (Bencherif et al., 2015; Malonis et al., 2019). Within these biomaterial-based vaccines, full-length proteins, and peptides have been extensively studied as antigens, but they can also be used as structural biomaterials (Skwarczynski and Toth, 2016). Peptides are biomolecules that generally consist of sequences of 2-50 amino acids and that have a molecular structure that is generally much simpler than that of proteins (Malonis et al., 2019). Using peptides has become a widespread trend in vaccine development since they are easily processed and presented by antigen-presenting cells, leading to potent T-cell-mediated immune responses (Purcell et al., 2007). Furthermore, current challenges associated with cell-based or protein-based vaccination, such as manufacturing complexity, biological contamination, off-target effects, and autoimmunity, can be prevented with peptide-based vaccines (Purcell et al., 2007; Skwarczynski and Toth, 2016). Additionally, peptides are capable of self-assembly into ordered supramolecular structures, making them excellent building blocks to form nanofibers, nanovesicles, nanotubes, nanomicelles, and hydrogels (Habibi et al., 2016; Qi et al., 2018). These peptide assemblies can have a multivalent character and present peptides in their native 3D conformation, which is essential for B-cell stimulation. Furthermore, they allow mixing of multiple components with precise stoichiometry (Wen and Collier, 2015). Ultimately, immunogenic, long-lasting, stable, and self-adjuvanted vaccines can be engineered by combining epitopes, antigens, and immunomodulatory moieties within the self-assembled peptide structures (Wen and Collier, 2015).

Besides being exploited as immunostimulatory materials in vaccine development, self-assembled supramolecular peptides are also excellent candidates to serve as carriers for the delivery of immunological factors (Sis and Webber, 2019; Xiao et al., 2019b). The macrostructural features of supramolecular peptide assemblies can be fine-tuned by altering the amino acid sequences. Additionally, bioactive segments can be introduced into the peptides during their self-assembly to design stimuli-responsive and cell- or organ-targeted vaccine delivery vehicles (Sis and Webber, 2019; Xiao et al., 2019a; Lampel, 2020). Moreover, combining immunogenic peptide epitopes with non-immunogenic peptides that form delivery carriers could enhance vaccine efficacy while reducing unwanted side effects (Eskandari et al., 2017).

In this mini review, we first describe the various strategies employed to create self-assembled supramolecular peptides with sophisticated hierarchical nanostructures. Next, their application in subunit vaccine design and delivery for cellular and humoral immunity is highlighted. Finally, we discuss the challenges and clinical translatability of self-assembled peptide-based vaccines, as well as their future perspectives.

DESIGN OF SUPRAMOLECULAR SELF-ASSEMBLED PEPTIDES

Molecular self-assembly is a bottom-up approach for achieving highly ordered and stable nanoscale structures or patterns. This technique is based on the spontaneous assembly of small molecules or nanosized building blocks under thermodynamic equilibrium conditions (Qi et al., 2018). Intermolecular and intramolecular interactions, such as hydrogen bonding, amphiphilic interactions, and aromatic stacking, have been used for supramolecular peptide assembly, allowing the construction of complexes with stratified nanostructures (Lampel, 2020). Specifically, peptides can be designed to exhibit distinctive secondary structures, such as β-sheets, β-hairpins, and α-helices, and these natural motifs can be leveraged to drive a complex hierarchical architecture (Rad-Malekshahi et al., 2015). For instance, β-sheets consisting of alternating hydrophobic and hydrophilic amino acids have been extensively applied in driving self-assembly of peptides into extended fibrillar nanostructures (Moore et al., 2018; Sis and Webber, 2019). Several groups have designed self-assembled nanofibrils from the synthetic amphiphilic peptide RADA16 (RADARADARADARADA) through the β-sheet motifs (**Figure 1A**), in which alternating regions of hydrophobic alanine and hydrophilic arginine/aspartate residues can yield a stable β-sheet-rich structure (Cormier et al., 2013; Lu et al., 2019). Furthermore, the antiparallel orientation of double-layered β-sheets, such as β-hairpins, have shown to generate another secondary structure, which promotes the formation of peptide-based nanofibrous hydrogels under physiological conditions (Worthington et al., 2017). Smith et al. developed a multiphase transitioning, injectable hydrogel through the molecular self-assembly of a peptide-based β-hairpin. Their anastomosis photocage 1 (APC1) peptide, which contains seven lysine residues, was folded into a β-hairpin and rapidly self-assembled into a cross-linked fibrillar hydrogel (Smith et al., 2016). Alternatively, α-helices could also be used to form a highly ordered structure through helical self-assembly, which closely resembles the sophisticated hierarchical coiled coil-type structures of native proteins, such as collagen (Lampel,

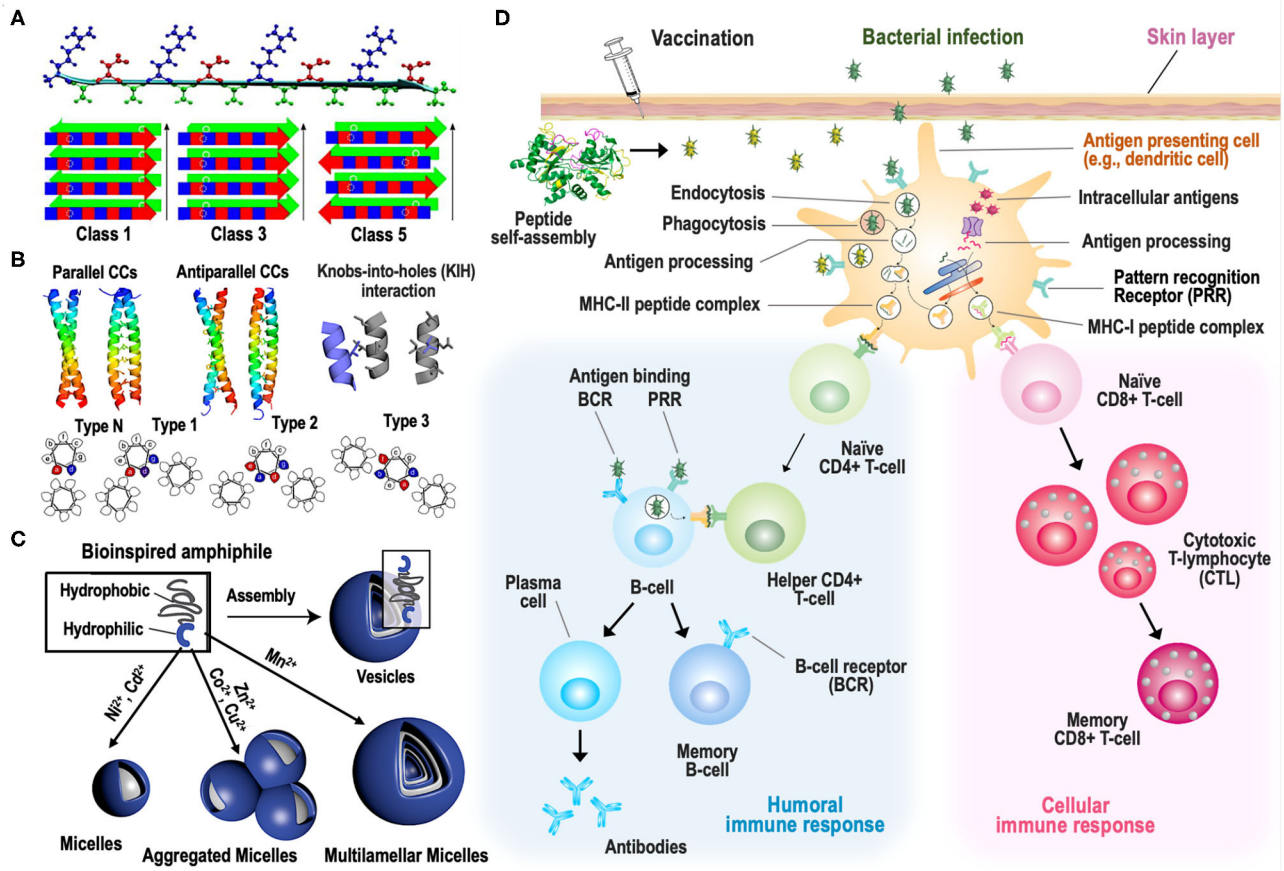

FIGURE 1 | Strategies to induce supramolecular self-assembly of peptides and peptide-based vaccines. **(A)** Formation of β-strands from self-assembling peptide RADA16-I (top) and their arrangement into nanofibers with different symmetry classes arranged into stacks of two β-sheets (bottom). β-sheets are formed by alternating segments of hydrophobic alanine (green) and hydrophilic arginine/aspartate (blue/red) regions (reproduced with permission from Cormier et al., 2013). **(B)** Symmetry (top) and sequence (bottom) of coiled-coils (CCs) made of peptides containing a heptad repeat of hydrophobic (h) and polar (p) residues in a hpphppp pattern. Helical wheels for classical Type-N, and Type-1, Type-2, and Type-3 interfaces are depicted. All are viewed along the α-helices from the N to C termini, labels are for the canonical a–g nomenclature and the teardrop shapes indicate the direction of Cα-Cβ bonds (reproduced with permission from Rhys et al., 2018). **(C)** Effect of different divalent transition metal ions on the morphological transformation of self-assembled PAs, consisting of hexahistidine as a hydrophilic head and oligostyrene as a hydrophobic tail (reproduced from Knight et al., 2018). **(D)** Schematic illustration of immune stimulation by self-assembled peptide-based vaccines. Peptides undergo self-assembly upon intra-muscular or subcutaneous vaccination, after which they can induce humoral and/or cellular immune responses to protect individuals against pathogens. Humoral immune responses arise once B-cells encounter antigens in secondary lymphoid organs, inducing their activation. Mechanistically, B-cell activation occurs upon binding of antigens to the B-cell receptor (BCR), resulting in the internalization of antigens via receptor-mediated endocytosis. These antigens are then processed, and antigenic peptide-loaded MHC II is displayed on the cell surface, allowing CD4+ helper T-cell binding. CD4+ helper T-cells further stimulate B-cells to undergo proliferation, immunoglobulin (Ig) class-switching, and differentiation into antigen-specific antibody-secreting plasma cells and memory B-cells. To induce CTL-mediated cellular immune responses, antigens need to be processed and presented by antigen-presenting cells (APCs), such as dendritic cells and macrophages. APCs take up the antigen by pinocytosis, phagocytosis, and receptor-mediated phagocytosis, cleave the antigen into smaller peptide fragments, and present these peptides on MHC. In the lymph nodes, extracellular antigenic peptides are presented on MHC II to CD4+ T-cells, whereas intracellular proteins, including viral and tumor-associated antigens, are presented on MHC I to CD8+ T-cells. A subset of APCs can also present extracellular antigenic peptides on MHC I in a process known as cross-presentation. Once activated, naïve CD8+ T-cells proliferate into CTLs to mediate antigen-specific cytotoxicity. A fraction of CD8+ T-cells become memory CD8+ T-cells to ensure long-term protection. Upon activation, naïve CD4+ T-cells differentiate into helper T-cells which secrete cytokines to support CTL expansion and survival along with B-cell proliferation and differentiation. Memory B- and T-cells persist in the body for a long time and mount an immediate and efficient antigen-specific immune response upon reinfection with the same pathogen.

2020). Thomson et al. designed supercoiled coil α-helical barrels by self-assembling 5-7 α-helices twisted around each other with cyclic or dihedral symmetry (**Figure 1B**). The peptides used in their study have a canonical hpphppp heptad repeat sequence, in which h and p represent hydrophobic and polar amino acids, respectively (Thomson et al., 2014; Rhys et al., 2018). Di-phenylalanine peptide (FF) is another interesting building block to trigger peptide self-assembly into desirable nanostructures such as nanotubes, nanospheres, and nanoribbons (Habibi et al., 2016). While self-assembly of the FF motif is usually achieved in the form of amyloid-like sheets (Lampel, 2020), Bera et al. interestingly generated a helical

architecture by simply adding one more amino acid (proline) to the FF peptide, forming proline-phenylalanine-phenylalanine (PFF) (Bera et al., 2019).

Additionally, non-peptidic compounds such as alkyls, amino acids, and metal ions have been used to form self-assembled peptide complexes with a wide variety of structures and functionalities (Sis and Webber, 2019). Alkyls, for instance, have been used as a hydrophobic tail to produce peptide amphiphiles (PAs) that undergo self-assembly via hydrophobic shielding (Sis and Webber, 2019). As a result, the nanostructure and other properties of self-assembled PAs can be controlled by switching their hydrophobic components (Qi et al., 2018). Choi et al. proved that the nanostructure of self-assembled amphiphilic Janus peptide dendrimers (JPDs) can be induced via a simple chemical bifurcation. Various JPDs were synthesized by varying the length of their hydrophilic and hydrophobic regions, and their self-assembly resulted in the formation of spherical/cylindrical micelles or bi-layered vesicles (Choi et al., 2019). PAs can also be made by conjugating peptides with functional polymers (Habibi et al., 2016). Chin et al. designed a muscle-inspired anisotropic actuator in the form of a hollow fibrous peptide-based hydrogel, in which VVVAAAEEE peptides were functionalized with a lysine-coupled bromoisobutyryl moiety to enable the grafting of thermo-responsive polymers via atom transfer radical polymerization (Chin et al., 2018). Recent studies also revealed that the nanostructure of self-assembled peptides can be reshaped in a controllable manner by incorporating metal ions (Sis and Webber, 2019). Knight et al. studied the effect of different metal ions on the morphological transformation of self-assembled PAs consisting of hexahistidine as a hydrophilic head and oligostyrene as a hydrophobic tail (**Figure 1C**). Interestingly, the presence of manganese(II) promoted the formation of multilamellar vesicles, while nickel(II) and cadmium(II) gave rise to micelle nanoparticles. In contrast, zinc(II), copper(II), and cobalt(II) led to agglomerated micelles (Knight et al., 2018).

Finally, there has been a growing interest in designing smart nanomaterials that initiate the assembly of molecular building blocks upon application of external stimuli such as enzymes, pH, heat, and light. This strategy can provide additional spatiotemporal control over the formation and structure of supramolecular peptides (Lampel, 2020). For instance, enzyme-instructed self-assembly (EISA) of peptides has recently been applied to allow assembly in complex biological systems (Wang et al., 2019). Li et al. synthesized several dipeptidic precursors, consisting of FF with various stereoisomers, in which N- and C-terminal peptide sequences are linked to 2-(naphthalen-2-yl)acetic acid and 2-(4-(2-aminoethoxy)-4-oxobutanamido)ethane-1-sulfonic acid, respectively. Molecular self-assembly (i.e., EISA) of these peptides is induced by carboxylesterase, which is present inside the cells and in the extracellular space of tissues. Using this approach, intracellular and intercellular peptide self-assembly could be achieved at different rates (Li et al., 2018). Additionally, some stimuli-responsive peptides, such as elastin-like polypeptides (ELPs), exhibit reversible transition behavior upon exposure to specific stimuli (Zhang et al., 2015; Saha et al., 2020). Dreher et al. prepared several ELP block copolymers (with varying molecular weights and block ratios) in a linear AB diblock architecture by homogeneously fusing an N-terminal hydrophilic ELP block to a C-terminal hydrophobic ELP block. They observed that copolymers with suitable diblock ratios are highly water-soluble at normal body temperature (37°C) and can self-assemble into spherical micelles at the tumor temperature (42°C). When the temperature was lowered again, the copolymers showed the inverse transition behavior (Dreher et al., 2008). Hassouneh et al. developed a theoretical model to explain the mechanism for this special reversible transition behavior of the copolymers (Hassouneh et al., 2015).

APPLICATION OF SELF-ASSEMBLED PEPTIDES IN VACCINE DESIGN AND DELIVERY

A wide variety of vaccines have been designed to stimulate the immune system to combat pathogens (e.g., bacteria, viruses) or tumors. In particular, vaccines aim to induce an adaptive immune response that leads to immunological memory, as illustrated in **Figure 1D**. There are two subdivisions of the adaptive immune system: the cell-mediated immune response, which is executed by cytotoxic T lymphocytes (CTLs) that can kill infected or cancerous cells, and the humoral immune response, which is mediated by activated B-cells that produce antibodies to neutralize extracellular pathogens (Molnar and Gair, 2015). Peptide-based vaccines generally require three major components—an antigen, an adjuvant, and a delivery vehicle—to generate efficient adaptive immune responses. When peptides are used as antigens, the conformation of the specific regions recognized by the immune system, known as epitopes, is particularly important for inducing humoral immunity. Specifically, B-cells need to bind epitopes in their native conformation to allow antibody binding. B-cell epitopes usually have α-helical, loop, and β-strand conformations that are generally integrated into vaccines as longer peptides to allow them to adopt their native conformation (Skwarczynski and Toth, 2016; Malonis et al., 2019). When designing vaccines, self-assembly of peptides can be utilized to ensure correct folding of antigenic epitopes. In vaccine applications where antibody affinity and titer are essential, self-assembling peptides that also have inherent CD4+ T-cell epitopes, such as those included in the Coil29 (QARILEADAEILRAYARILEAHAEILRAD) peptide, can be incorporated to induce strong follicular helper T-cell engagement that further promotes B-cell responses (Wu et al., 2020). Similar to CD4+ T-cell stimulation, the peptide sequence is more critical than the epitope conformation itself to induce CTL-mediated cellular immunity. Therefore, shorter peptides can be used to induce T-cell responses, as CD4+ T-cells recognize 12-16 amino acid long peptides presented by MHC II on antigen-presenting cells (APCs), while CD8+ T-cells bind to slightly shorter 8-10 amino acid long peptides displayed by MHC I (Skwarczynski and Toth, 2016; Malonis et al., 2019). Unlike attenuated pathogen-based vaccines, peptide-based vaccines generally incorporate adjuvants to boost the

overall immune response to antigens and mimic the natural "danger signals" which follow infections. The choice of adjuvants depends on several factors such as immunogenicity and toxicity. Several studies have established that the adjuvanticity of self-assembled peptides is mediated via antigen presentation in an ordered and repetitive array that resembles pathogen-associated molecular patterns (PAMPs), resulting in strong immune responses mediated through Toll-like receptor (TLR)-inflammasome signaling pathways via TLR2 and TLR4 activation (Azmi et al., 2014; Negahdaripour et al., 2017; Tandon et al., 2018; Zottig et al., 2020). Additionally, self-assembling peptides may act as adjuvants themselves by forming an antigen depot, directing vaccines to APCs, and ultimately enhancing immune-cell priming (Grenfell et al., 2015; Acar et al., 2017; Negahdaripour et al., 2017).

Self-Assembled Peptide-Based Vaccines for Cellular Immunity

Supramolecular self-assembling peptides can form excellent structures to induce cytotoxic immune responses, which is particularly important for cancer immunotherapy. For this purpose, peptide assemblies can function as a platform for safe and controlled delivery of antigens, adjuvants, immune cells and/or drugs (**Table 1**). For example, Wang et al. utilized a tumor-penetrating peptide Fmoc-KCRGDK-based hydrogel formulation to encapsulate a BRD4 inhibitor, a photothermal agent (indocyanine green), and autologous tumor cells. Upon laser irradiation, the personalized cancer vaccine released tumor-associated antigens. This process promoted DC maturation, T-cell infiltration, the formation of memory immune cells to prevent tumor relapse, and inhibited distant tumors (Wang T. et al., 2018). Interestingly, Xu et al. observed that the configuration and the number of lysine residues in the peptide are critical to enhance CTL response. They described a supramolecular NF-κB-activating nano-adjuvant hydrogel, synthesized by pH-triggered self-assembly of Ada-GFFYGKKK-NH2 peptide, for cancer immunotherapy. According to their findings, nano-adjuvants containing D-configured peptides and 3 lysine residues encapsulated antigens more efficiently through charge-charge interaction than 2 lysine residues, and as a result, generated more robust adaptive and innate immune responses than peptides with L-configuration (Xu et al., 2019). Yang et al. showed that a nanofibrous RADA16 peptide-based hydrogel scaffold encapsulating bone-marrow derived DCs, model antigen ovalbumin (OVA), and anti-PD-1 antibody recruited and stimulated endogenous and exogenous DCs. This process increased DC migration to the lymph nodes, driving a more robust antigen-specific immune response against EG7-OVA tumors (Yang et al., 2018). Furthermore, Wang et al. developed glutathione-responsive nanocomposites by co-assembling a positively charged cell-penetrating CWWRCRCRC peptide with a negatively charged protein such as ovalbumin (OVA) via electrostatic interactions. After being internalized by APCs, intracellular glutathione degraded the disulfide bonds of the peptide, inducing rapid release of the antigen into the cytoplasm, which was then cross-presented to induce potent CD8+ T-cell responses. When compared to free OVA, the peptide-based nanocomposites improved antigen uptake by DCs, promoted DC activation and maturation, and enhanced cellular as well as humoral immune responses (Wang K. et al., 2018). Overall, the use of self-assembled peptides as a delivery vehicle provides multiple benefits, including efficient cell and antigen loading, minimal loss of active components, as well as controlled and targeted release in the lymphoid organs (Zhang, 2017; Lee et al., 2019).

Apart from acting as a delivery vehicle, self-assembling peptides can also serve as an antigen source themselves to induce cellular immunity. For example, Black et al. developed cancer vaccines consisting of self-assembling tumor antigen peptides with enhanced immunogenicity. Conjugating a synthetic lipid tail with two palmitic residues to an OVA-derived peptide containing a CTL epitope initiated the self-assembly of PAs into cylindrical micelles, resulting in multivalent epitope presentation. These micelles were internalized by APCs, likely due to the fusion of their hydrophobic tails with the cell membrane, leading to CTL activation in absence of additional adjuvants. Additionally, these cylindrical micelles act as antigen depots, thereby protecting the peptides from degradation and prolonging antigen exposure to the APCs. Improved *in vivo* protection was observed against OVA-expressing tumor cells after immunization with the diC16-OVA micelles compared to free OVA peptide formulated with incomplete Freund's adjuvant (Black et al., 2012). Xing et al. developed injectable, peptide-based supramolecular hydrogels by co-assembling poly-L-lysine (PLL) and FF dipeptide via an electrostatic coupling. Fmoc-FF/PLL-SH hydrogels have a nanofibrous structure with α-helical conformation which resembles natural fimbrial antigens, thereby acting as an adjuvant. When injected around a tumor, the hydrogels activated T-cell responses and efficiently suppressed tumor growth without the addition of other adjuvants or antigens. In this case, the tumor cells themselves act as the source of antigen to stimulate the immune response (Xing et al., 2017). Self-assembly can also be used to incorporate longer peptides containing multiple epitopes to ensure optimal APC stimulation, increase the magnitude of CTL response, and simultaneously promote helper T-cell activity (Lynn et al., 2020). Overall, peptide-based self-assembly can induce robust cellular immune responses by serving as a durable source of antigen that allows easy uptake and processing by APCs, providing multiple epitopes, and conferring self-adjuvanticity to the vaccine.

Self-Assembled Peptide-Based Vaccines for Humoral Immunity

Robust humoral immune responses are essential to treat infectious diseases. For this purpose, self-assembly designs have included approaches such as flanking the antigen with a self-assembling peptide sequence to display the secondary structure of the antigen, presenting antigens in a highly ordered and repetitive form, and optimizing the distance between repeated epitopes for optimal B-cell receptor (BCR) engagement (Raman et al., 2006; Black et al., 2010; Babapoor et al., 2011; Trent et al., 2015; Skwarczynski et al., 2020). Self-assembling supramolecular

TABLE 1 | Summary of supramolecular peptide-based vaccines for cancer and infectious diseases.

Peptide	Active ingredient	Features	Applications	References
RADA16	Anti-PD-1 + DCs + OVA peptide	β-sheet-rich nanofibrous hydrogel	Delivery system for DC-based vaccine in EG7-OVA tumor model	Yang et al., 2018
$K_2(SL)_6K_2$	STING agonist	Nanofibrous hydrogel with sustainable release properties	Delivery system in MOC_2-E_6E_7 tumor model	Leach et al., 2018
Fmoc-KCRGDK	BRD4 inhibitor + indocyanine green + autologous tumor cells	Micellar hydrogel with tumor penetrating properties	Delivery system for postoperative cancer immunotherapy in 4T1 tumor model	Wang T. et al., 2018
Ac-I3SLKG-NH2	G(IIKK)3I-NH2	MMP-2 mediated enzyme responsive fibrillar hydrogels, sustained and targeted release properties	Delivery system for MMP-2 overexpressing HeLa tumor model	Chen et al., 2017
$OVA_{253-266}$ peptide	$OVA_{253-266}$ peptide conjugated with dialkyl lipid tail and 2 palmitic chains	Cylindrical micelles displaying epitopes at multiple valences with self-adjuvanting properties	Delivery system plus peptide tumor antigen in EG7-OVA tumor model	Black et al., 2012
$OVA_{254-267}$-HBc (Hepatitis B core protein)	$OVA_{254-267}$ peptide	Nanocage with controlled properties and high-density epitope display	Delivery system plus tumor antigen plus adjuvant for B16-OVA-Luc tumor model	Shan et al., 2019
Peptide-MHC/ANXA5	Peptide-MHC (pMHC)	Liposome	Antigen for B16-OVA tumor model	Mao et al., 2018
Ada-GFFYGKKK-NH2	OVA peptide	Nanofibrous hydrogel with NF-κB activating properties	Nano-adjuvant for B16-OVA cancer immunotherapy	Xu et al., 2019
Nap-GFFpY-OMe	OVA peptide	Nanofibrous hydrogel formed by phosphatase enzyme	Vaccine adjuvant for EG7-OVA tumor model	Wang et al., 2016
Q11 (QQKFQFQFEQQ)	Mucin 1 (MUC1) glycopeptide	Nanofibers, β-turn structure with self-adjuvanting properties	Delivery system plus adjuvant for MCF-7 tumor model	Huang et al., 2012
Ac-AAVVLLLW-COOH	$OVA_{250-264}$ + HPV16 $E7_{43-57}$	Nanostructure	TC-1 tumor model	Rad-Malekshahi et al., 2017
Cholesterol-aK-Cha-VAaWTLKAa-LEEKKGNYVVTDH	EGFRvIII + PADRE epitopes	Lipopeptide micelles with self-adjuvanting properties	Cellular and humoral immune response in B16-EGFRvIII tumor model	Chen et al., 2018
Coil29 (QARILEADAEIL RAYARILEAHAEILRAD)	EGFRvIII, PADRE, SIINFEKL, PEPvIII	α-helical coiled-coiled peptide fiber	Induction of CD4+ T-cell, and CD8+ T-cell and B-cell response in mice	Wu et al., 2017
DEAP-DPPA-1	PD-L1 antagonist (^{D}PPA-1) + peptide substrate of MMP-2 + indoleamine-dioxygenase inhibitor (NLG919)	Nanoparticle responding to dual stimuli for targeted delivery and controlled release	B16-F10 tumor model	Cheng et al., 2018
GE11 (EGFR ligand)	Acetylcholinesterase gene + Doxorubicin	Self-assembling peptide nanovesicle	Drug and gene delivery system targeted toward EGFR expressing cancer	Liang et al., 2016
S4-8Q (QAEPDRAHYNIVTFCCKCD conjugated to a 4-arm star polymer)	8Q (HPV-16 E7 epitope)	Dendrimers with self-adjuvanting properties	TC-1 tumor model	Liu et al., 2013; Liu et al., 2015
Nap-GFFY-NMe	DNA encoding gp145	Nanofibrous hydrogel	Strong cellular and humoral immune response for HIV treatment and prevention	Tian et al., 2014
EAK16-II	SL9 (HIV specific CTL epitope) + TL13 (CD4+ T-cell epitope) + R848 (TLR7/8 agonists) + DCs	β-sheet-rich nanofibers	Delivery system for HIV-1 vaccine	Ding et al., 2016
p41	p41 peptide (analog derived from HCV protein NS5A)	α-helical nanocomplexes	HIV and HCV co-inhibition	Zhang et al., 2013
P6HRC1	HRC1 (B-cell epitope from S-protein)	Coiled-coil polypeptide nanoparticles	Coronavirus mediated SARS (severe acute respiratory syndrome) infection	Pimentel et al., 2009
KFE8	EIII (West Nile Virus envelope protein domain)	β-sheet-rich nanofibrous hydrogel with self-adjuvanting properties	West Nile virus vaccine	Friedrich et al., 2016

(Continued)

TABLE 1 | Continued

Peptide	Active ingredient	Features	Applications	References
Pentamer and trimer sequence	PspA and CbpA (CTL epitopes) + PhtD and PiuA (helper T-cell epitopes) + DTD (universal T-helper)	5-stranded + 3-stranded coiled-coils nanoparticle scaffold with self-adjuvanting properties	*Streptococcus pneumoniae* vaccine	Dorosti et al., 2019
J8 B-cell epitope: (SREAKKQVEKAL)	J8 conjugated with dialkyl hydrophobic moiety (diC16)	Cylindrical micelles with self-adjuvanting properties	Group A *Streptococcus pyogenes* vaccine	Trent et al., 2015
MAX1	Inherently antibacterial	β-hairpin-rich hydrogel	Broad spectrum bacterial resistance to gram-positive and gram-negative bacteria	Salick et al., 2007
Fmoc-F_2	Silver nanoparticles	Macroscopic hydrogels	Anti-bacterial wound dressing	Paladini et al., 2013
Phage-VS-LK	Sap2 (VS) + Hsp90 (LK) peptides	Nanofiber	*Candida albicans* detection via ELISA and vaccine	Wang T. et al., 2018
Cholesterol-G3R6TAT	Inherently antimicrobial	Nanoparticles	*Cryptococcus neoformans*-induced mengitis	Wang et al., 2010
Q11	$NANP_3$ (circumsporozoite protein epitope)	β-sheet-rich nanofibers	*P. falciparum* vaccine for malaria	Rudra et al., 2012

peptides can serve as a delivery scaffold to present antigenic peptides, and they can simultaneously possess self-adjuvanting characteristics to induce B-cell responses. For instance, Grenfell et al. exploited RADA4 peptide-based hydrogels that self-assembled into hydrated nanofibers after injection into the tissue to form a gel matrix depot, to deliver a recombinant antigen for the hepatitis B virus. This system elicited enhanced adjuvant-free humoral and cellular responses when compared to the antigen delivered with aluminum hydroxide (alum) and complete Freund's adjuvant. The authors credited the slow release of antigen from the depot to have improved the activation of APCs and prolonged immunostimulation (Grenfell et al., 2015). In a different study, Tian et al. utilized a supramolecular hydrogel-based nanovector comprised of Nap-GFFY-NMe (naphthylacetic acid-modified tetrapeptide GFFY with C-terminal methyl amide group), using an EISA approach to encapsulate a DNA sequence encoding gp145, an envelope glycoprotein of the human immunodeficiency virus (HIV). Alkaline phosphatase triggered self-assembly of the peptide, leading to formation of nanofibrous hydrogels. The strong cellular and humoral immune responses were attributed to the ability of left-handed structure of nanofibers to effectively condense DNA and prevent it from degradation, thus enhancing DNA transfection and gene expression in cells (Tian et al., 2014).

Self-assembling peptides can also be an antigen source to induce humoral immunity. For instance, Kaba et al. utilized a self-assembling peptide-based nanoparticle platform to present repeated immunodominant B-cell circumsporozoite peptide epitope $(DPPPPNPN)_2D$ of the malarial parasite. The polypeptide consisted of two oligomerization domains—a *de novo* trimeric coiled-coil domain and a pentameric coiled-coil domain—which were fused together with flexible diglycine residues. The self-assembled nanoparticles, containing multiple coiled-coil domains, displayed the B-cell peptide epitope in a highly ordered and repetitive array, thereby triggering robust helper T-cell-dependent and long-lasting antibody responses with higher avidity and titer (Kaba et al., 2009). Pimentel et al. utilized a similar polypeptide-based self-assembling nanoparticle platform to display the C-terminal heptad repeat region (HRC) of the SARS-CoV S-protein in its native α-helical trimeric coiled-coil conformation. These nanoparticles not only maintained this conformational integrity, but also provided repetitive presentation of the B-cell epitope and displayed icosahedral symmetry that resembled viral protein capsids. The SARS-CoV vaccine evoked conformation-specific neutralizing antibodies against the B-cell epitope without additional adjuvants (Pimentel et al., 2009). A potent peptide-based vaccine against *Streptococcus pneumoniae* was proposed by Dorosti et al., who incorporated CTL epitopes such as pneumococcal surface protein A (PspA) and choline-binding protein A (CbpA), helper T-cell epitopes such as pneumococcal histidine triad protein D (PhtD) and a lipoprotein from pneumococcal iron ABC transporter (PiuA) and universal helper T-cell epitopes like diphtheria toxoids on a coiled-coil self-assembling interface. The designed vaccine was predicted to exhibit stronger immunogenic responses compared to an analogous epitope-based vaccine (Dorosti et al., 2019). In addition, Rudra et al. developed a peptide-based vaccine to prevent malaria by combining self-assembling β-sheet peptides with epitopes of protozoan parasite *P. falciparum* (Rudra et al., 2012). In another example, Trent et al. designed a self-adjuvanting peptide-based vaccine for group A streptococcus (GAS). When the J8 antigenic peptide of the GAS-M protein is taken out of its native protein environment, its α-helical structure is lost, and as a result, it adopts a random conformation in the solution. The addition of two C16 alkyl chains at the N terminus of the J8 peptide triggered its self-assembly into cylindrical micelles, and reinforced α-helicity of the antigen, which subsequently induced a strong B-cell response in mice. Since the hierarchical micellar structure kept thousands of peptides in close proximity, it conferred potent adjuvanticity while maintaining the native antigen conformation at the injection site. In addition, the micellar structure increased

the local antigen concentration available to immune cells in comparison to free peptide, which quickly diffused away from the injection site (Trent et al., 2015). Taken together, these studies have demonstrated that self-assembled peptides can efficiently induce humoral immune responses through the display of secondary structures, thereby maintaining the conformational integrity of epitopes. Furthermore, these self-assembly platforms offer a highly ordered and multivalent display of relevant antigens, resulting in efficient stimulation and proliferation of B-cells, and their subsequent differentiation into antibody-secreting plasma cells. Inclusion of helper T-cell epitopes further enhances vaccine efficacy by imparting long-lasting B-cell immunity.

CHALLENGES AND FUTURE PERSPECTIVES

Despite the great potential of self-assembled supramolecular peptides for vaccine design and engineering, many challenges still persist. Compared to conventional vaccines containing live-attenuated or inactivated pathogens (viruses, bacteria, etc.), most peptide-based vaccines induce a weak immune response (Malonis et al., 2019). The use of adjuvants can overcome this obstacle, and deepen our understanding of their mechanism of action and their safety (Skwarczynski and Toth, 2016). Additionally, maintaining the stability and efficacy of peptide-based vaccines in complex biological environments remain challenging. For instance, their rapid enzymatic degradation and structural integrity in the body is a major limiting factor (Kim et al., 2019). Self-assembled peptides must exhibit improved stability when interfacing with biological barriers (e.g., pH, enzymes) that are encountered upon administration in tissues (Eskandari et al., 2017). Rational systematic design of the supramolecular peptide structure to include covalent cross-linking—or via improved intermolecular interactions such as hydrogen bonding, π-π stacking, and hydrophobic interactions—may augment their resilience and mechanical stability (Khalily et al., 2015; Li et al., 2019). The development of supramolecular self-assembled peptide-based vaccines is hindered by our limited understanding of the interface between self-assembled nanostructures and immune cells. In-depth investigation of the interactions between the self-assembled structures and the receptors on human immune cells, their uptake by APCs, as well as their effect on DC maturation, B-cell and T-cell priming, and cytokine profile, is needed (Zhao et al., 2017). Challenges exist in translating the ease in design and small-scale synthesis of supramolecular peptides to an industrial scale. Furthermore, advanced engineering of supramolecular assembly (e.g., cell-penetrating peptides) may target intracellular vaccine delivery more precisely, ultimately enhancing antigen uptake, promoting endosomal escape and cross-presentation by APCs, which are critical steps in inducing a robust cellular immune response (Yang et al., 2019). Existing technologies such as machine learning, bioinformatics, and computational modeling can potentially be leveraged for the macromolecular engineering of immunostimulatory peptide assemblies with improved vaccine immunogenicity, efficacy, and safety (Kim et al., 2019). Moving forward, biologically inspired supramolecular peptides, an excellent and sparsely explored class of materials, could be further exploited in designing the next generation of vaccines that are effective, safe, affordable, and accessible to everyone. Despite their importance and great potential, self-assembled peptide-based vaccines do require further investigation and validation prior to regulatory approval and clinical use.

AUTHOR CONTRIBUTIONS

The manuscript was written and edited with contribution from all authors. All authors have given approval to the final version of the manuscript.

FUNDING

SB acknowledges the support from the NSF CAREER award (DMR 1847843). This project was partially funded by the Science and Technology Unit—King Abdulaziz University—Kingdom of Saudi Arabia, award number UE-41-106.

ACKNOWLEDGMENTS

The authors acknowledge and thank the Science and Technology Unit, King Abdulaziz University for the technical support.

REFERENCES

Acar, H., Srivastava, S., Chung, E. J., Schnorenberg, M. R., Barrett, J. C., LaBelle, J. L., et al. (2017). Self-assembling peptide-based building blocks in medical applications. *Adv. Drug Del. Rev.* 110, 65–79. doi: 10.1016/j.addr.2016.08.006

Azmi, F., Ahmad Fuaad, A. A. H., Skwarczynski, M., and Toth, I. (2014). Recent progress in adjuvant discovery for peptide-based subunit vaccines. *Hum. Vaccin. Immunother.* 10, 778–796. doi: 10.4161/hv.27332

Babapoor, S., Neef, T., Mittelholzer, C., Girshick, T., Garmendia, A., Shang, H., et al. (2011). A novel vaccine using nanoparticle platform to present immunogenic M2e against avian influenza infection. *Influenza Res. Treat.* 2011, 1–12. doi: 10.1155/2011/126794

Bencherif, S. A., Sands, R. W., Ali, O. A., Li, W. A., Lewin, S. A., Braschler, T. M., et al. (2015). Injectable cryogel-based whole-cell cancer vaccines. *Nat. Commun.* 6:7556. doi: 10.1038/ncomms8556

Bera, S., Mondal, S., Xue, B., Shimon, L. J., Cao, Y., and Gazit, E. (2019). Rigid helical-like assemblies from a self-aggregating tripeptide. *Nat. Mater.* 18, 503–509. doi: 10.1038/s41563-019-0343-2

Black, M., Trent, A., Kostenko, Y., Lee, J. S., Olive, C., and Tirrell, M. (2012). Self-assembled peptide amphiphile micelles containing a cytotoxic T-Cell epitope promote a protective immune response *in vivo*. *Adv. Mater.* 24, 3845–3849. doi: 10.1002/adma.201200209

Black, M., Trent, A., Tirrell, M., and Olive, C. (2010). Advances in the design and delivery of peptide subunit vaccines with a focus on toll-like receptor agonists. *Expert Rev. Vaccines* 9, 157–173. doi: 10.1586/erv.09.160

Bookstaver, M. L., Tsai, S. J., Bromberg, J. S., and Jewell, C. M. (2018). Improving vaccine and immunotherapy design using biomaterials. *Trends Immunol.* 39, 135–150. doi: 10.1016/j.it.2017.10.002

Chen, C., Zhang, Y., Hou, Z., Cui, X., Zhao, Y., and Xu, H. (2017). Rational design of short peptide-based hydrogels with MMP-2 responsiveness for controlled anticancer peptide delivery. *Biomacromolecules* 18, 3563–3571. doi: 10.1021/acs.biomac.7b00911

Chen, Y., Yuan, F., Jiang, X., Lv, Q., Luo, N., Gong, C., et al. (2018). Discovery of a self-assembling and self-adjuvant lipopeptide as a saccharide-free peptide vaccine targeting EGFRvIII positive cutaneous melanoma. *Biomater. Sci.* 6, 1120–1128. doi: 10.1039/C8BM00017D

Cheng, K., Ding, Y., Zhao, Y., Ye, S., Zhao, X., Zhang, Y., et al. (2018). Sequentially responsive therapeutic peptide assembling nanoparticles for dual-targeted cancer immunotherapy. *Nano Lett.* 18, 3250–3258. doi: 10.1021/acs.nanolett.8b01071

Chiang, C. L.-L., Benencia, F., and Coukos, G. (2010). Whole tumor antigen vaccines. *Semin. Immunol.* 22, 132–143. doi: 10.1016/j.smim.2010.02.004

Chin, S. M., Synatschke, C. V., Liu, S., Nap, R. J., Sather, N. A., Wang, Q., et al. (2018). Covalent-supramolecular hybrid polymers as muscle-inspired anisotropic actuators. *Nat. Commun.* 9:2395. doi: 10.1038/s41467-018-04800-w

Choi, S. J., Kwon, S. H., and Lim, Y. B. (2019). 3D2 Self-assembling janus peptide dendrimers with tailorable supermultivalency. *Adv. Funct. Mater.* 29:1808020. doi: 10.1002/adfm.201808020

Cockburn, I. A., and Seder, R. A. (2018). Malaria prevention: from immunological concepts to effective vaccines and protective antibodies. *Nat. Immunol.* 19, 1199–1211. doi: 10.1038/s41590-018-0228-6

Cormier, A. R., Pang, X., Zimmerman, M. I., Zhou, H.-X., and Paravastu, A. K. (2013). Molecular structure of RADA16-I designer self-assembling peptide nanofibers. *ACS Nano* 7, 7562–7572. doi: 10.1021/nn401562f

Ding, Y., Liu, J., Lu, S., Igweze, J., Xu, W., Kuang, D., et al. (2016). Self-assembling peptide for co-delivery of HIV-1 $CD8^+$ T cells epitope and Toll-like receptor 7/8 agonists R848 to induce maturation of monocyte derived dendritic cell and augment polyfunctional cytotoxic T lymphocyte (CTL) response. *J. Control. Release* 236, 22–30. doi: 10.1016/j.jconrel.2016.06.019

Dorosti, H., Eslami, M., Nezafat, N., Fadaei, F., and Ghasemi, Y. (2019). Designing self-assembled peptide nanovaccine against streptococcus pneumoniae: an *in silico* strategy. *Mol. Cell. Probes* 48:101446. doi: 10.1016/j.mcp.2019.101446

Dreher, M. R., Simnick, A. J., Fischer, K., Smith, R. J., Patel, A., Schmidt, M., et al. (2008). Temperature triggered self-assembly of polypeptides into multivalent spherical micelles. *J. Am. Chem. Soc.* 130, 687–694. doi: 10.1021/ja0764862

Eskandari, S., Guerin, T., Toth, I., and Stephenson, R. J. (2017). Recent advances in self-assembled peptides: Implications for targeted drug delivery and vaccine engineering. *Adv. Drug Del. Rev.* 110, 169–187. doi: 10.1016/j.addr.2016.06.013

Friedrich, B. M., Beasley, D. W. C., and Rudra, J. S. (2016). Supramolecular peptide hydrogel adjuvanted subunit vaccine elicits protective antibody responses against West Nile virus. *Vaccine* 34, 5479–5482. doi: 10.1016/j.vaccine.2016.09.044

Graham, B. S. (2020). Rapid COVID-19 vaccine development. *Science* 368, 945–946. doi: 10.1126/science.abb8923

Grenfell, R. F., Shollenberger, L. M., Samli, E. F., and Harn, D. A. (2015). Vaccine self-assembling immune matrix is a new delivery platform that enhances immune responses to recombinant HBsAg in mice. *Clin. Vaccine Immunol.* 22, 336–343. doi: 10.1128/CVI.00714-14

Habibi, N., Kamaly, N., Memic, A., and Shafiee, H. (2016). Self-assembled peptide-based nanostructures: Smart nanomaterials toward targeted drug delivery. *Nano Today* 11, 41–60. doi: 10.1016/j.nantod.2016.02.004

Hassouneh, W., Zhulina, E. B., Chilkoti, A., and Rubinstein, M. (2015). Elastin-like polypeptide diblock copolymers self-assemble into weak micelles. *Macromolecules* 48, 4183–4195. doi: 10.1021/acs.macromol.5b00431

Huang, Z. H., Shi, L., Ma, J. W., Sun, Z. Y., Cai, H., Chen, Y. X., et al. (2012). A totally synthetic, self-assembling, adjuvant-free MUC1 glycopeptide vaccine for cancer therapy. *J. Am. Chem. Soc.* 134, 8730–8733. doi: 10.1021/ja21 1725s

Kaba, S. A., Brando, C., Guo, Q., Mittelholzer, C., Raman, S., Tropel, D., et al. (2009). A nonadjuvanted polypeptide nanoparticle vaccine confers long-lasting protection against rodent malaria. *J. Immunol.* 183, 7268–7277. doi: 10.4049/jimmunol.0901957

Khalily, M. A., Goktas, M., and Guler, M. O. (2015). Tuning viscoelastic properties of supramolecular peptide gels via dynamic covalent crosslinking. *Org. Biomol. Chem.* 13, 1983–1987. doi: 10.1039/C4OB02217C

Kim, J., Narayana, A., Patel, S., and Sahay, G. (2019). Advances in intracellular delivery through supramolecular self-assembly of oligonucleotides and peptides. *Theranostics* 9:3191. doi: 10.7150/thno.33921

Knight, A. S., Larsson, J., Ren, J. M., Bou Zerdan, R., Seguin, S., Vrahas, R., et al. (2018). Control of amphiphile self-assembly via bioinspired metal ion coordination. *J. Am. Chem. Soc.* 140, 1409–1414. doi: 10.1021/jacs.7b11005

Lampel, A. (2020). Biology-inspired supramolecular peptide systems. *Chem* 6, 1222–1236. doi: 10.1016/j.chempr.2020.03.005

Leach, D. G., Dharmaraj, N., Piotrowski, S. L., Lopez-Silva, T. L., Lei, Y. L., Sikora, A. G., et al. (2018). STINGel: controlled release of a cyclic dinucleotide for enhanced cancer immunotherapy. *Biomaterials* 163, 67–75. doi: 10.1016/j.biomaterials.2018.01.035

Lee, S., Trinh, T. H., Yoo, M., Shin, J., Lee, H., Kim, J., et al. (2019). Self-assembling peptides and their application in the treatment of diseases. *Int. J. Mol. Sci.* 20:5850. doi: 10.3390/ijms20235850

Li, J., Bullara, D., Du, X., He, H., Sofou, S., Kevrekidis, I. G., et al. (2018). Kinetic analysis of nanostructures formed by enzyme-instructed intracellular assemblies against cancer cells. *ACS Nano* 12, 3804–3815. doi: 10.1021/acsnano.8b01016

Li, J., Xing, R., Bai, S., and Yan, X. (2019). Recent advances of self-assembling peptide-based hydrogels for biomedical applications. *Soft Matter.* 15, 1704–1715. doi: 10.1039/C8SM02573H

Liang, X., Shi, B., Wang, K., Fan, M., Jiao, D., Ao, J., et al. (2016). Development of self-assembling peptide nanovesicle with bilayers for enhanced EGFR-targeted drug and gene delivery. *Biomaterials* 82, 194–207. doi: 10.1016/j.biomaterials.2015.12.015

Liu, T. Y., Hussein, W. M., Giddam, A. K., Jia, Z., Reiman, J. M., Zaman, M., et al. (2015). Polyacrylate-based delivery system for self-adjuvanting anticancer peptide vaccine. *J. Med. Chem.* 58, 888–896. doi: 10.1021/jm501514h

Liu, T. Y., Hussein, W. M., Jia, Z., Ziora, Z. M., McMillan, N. A., Monteiro, M. J., et al. (2013). Self-adjuvanting polymer-peptide conjugates as therapeutic vaccine candidates against cervical cancer. *Biomacromolecules* 14, 2798–2806. doi: 10.1021/bm400626w

Lu, L., Armstrong, E. A., Yager, J. Y., and Unsworth, L. D. (2019). sustained release of dexamethasone from sulfobutyl ether β-cyclodextrin modified self-assembling peptide nanoscaffolds in a perinatal rat model of hypoxia–ischemia. *Adv. Healthc. Mater.* 8:1900083. doi: 10.1002/adhm.201900083

Lurie, N., Saville, M., Hatchett, R., and Halton, J. (2020). Developing Covid-19 vaccines at pandemic speed. *N. Engl. J. Med.* 382, 1969–1973. doi: 10.1056/NEJMp2005630

Lynn, G. M., Sedlik, C., Baharom, F., Zhu, Y., Ramirez-Valdez, R. A., Coble, V. L., et al. (2020). Peptide–TLR-7/8a conjugate vaccines chemically programmed for nanoparticle self-assembly enhance CD8 T-cell immunity to tumor antigens. *Nat. Biotechnol.* 38, 320–332. doi: 10.1038/s41587-019-0390-x

Malonis, R. J., Lai, J. R., and Vergnolle, O. (2019). Peptide-based vaccines: current progress and future challenges. *Chem. Rev.* 120, 3210–3229. doi: 10.1021/acs.chemrev.9b00472

Mao, C. P., Peng, S., Yang, A., He, L., Tsai, Y. C., Hung, C. F., et al. (2018). Programmed self-assembly of peptide-major histocompatibility complex for antigen-specific immune modulation. *Proc. Natl. Acad. Sci. U.S.A.* 115, E4032–E4040. doi: 10.1073/pnas.1718434115

Molnar, C., and Gair, J. (2015). *23.2. Adaptive immune response. Concepts of Biology-1st Canadian Edition.* Houston, TX: OpenStax College; Rice University.

Moore, A. N., Silva, T. L. L., Carrejo, N. C., Marmolejo, C. A. O., Li, I.-C., and Hartgerink, J. D. (2018). Nanofibrous peptide hydrogel elicits angiogenesis and neurogenesis without drugs, proteins, or cells. *Biomaterials* 161, 154–163. doi: 10.1016/j.biomaterials.2018.01.033

Negahdaripour, M., Golkar, N., Hajighahramani, N., Kianpour, S., Nezafat, N., and Ghasemi, Y. (2017). Harnessing self-assembled peptide nanoparticles in epitope vaccine design. *Biotechnol. Adv.* 35, 575–596. doi: 10.1016/j.biotechadv.2017.05.002

Paladini, F., Meikle, S. T., Cooper, I. R., Lacey, J., Perugini, V., and Santin, M. (2013). Silver-doped self-assembling di-phenylalanine hydrogels

as wound dressing biomaterials. *J. Mater. Sci. Mater. Med.* 24, 2461–2472. doi: 10.1007/s10856-013-4986-2

Parvizpour, S., Pourseif, M. M., Razmara, J., Rafi, M. A., and Omidi, Y. (2020). Epitope-based vaccine design: a comprehensive overview of bioinformatics approaches. *Drug Discov. Today* 25, 1034–1042. doi: 10.1016/j.drudis.2020.03.006

Pimentel, T. A., Yan, Z., Jeffers, S. A., Holmes, K. V., Hodges, R. S., and Burkhard, P. (2009). Peptide nanoparticles as novel immunogens: design and analysis of a prototypic severe acute respiratory syndrome vaccine. *Chem. Biol. Drug Des.* 73, 53–61. doi: 10.1111/j.1747-0285.2008.00746.x

Piot, P., Larson, H. J., O'Brien, K. L., N'kengasong, J., Ng, E., Sow, S., et al. (2019). Immunization: vital progress, unfinished agenda. *Nature* 575, 119–129. doi: 10.1038/s41586-019-1656-7

Purcell, A. W., McCluskey, J., and Rossjohn, J. (2007). More than one reason to rethink the use of peptides in vaccine design. *Nat. Rev. Drug Discov.* 6, 404–414. doi: 10.1038/nrd2224

Qi, G. B., Gao, Y. J., Wang, L., and Wang, H. (2018). Self-assembled peptide-based nanomaterials for biomedical imaging and therapy. *Adv. Mater.* 30:1703444. doi: 10.1002/adma.201703444

Rad-Malekshahi, M., Fransen, M. F., Krawczyk, M., Mansourian, M., Bourajjaj, M., Chen, J., et al. (2017). Self-assembling peptide epitopes as novel platform for anticancer vaccination. *Mol. Pharm.* 14, 1482–1493. doi: 10.1021/acs.molpharmaceut.6b01003

Rad-Malekshahi, M., Visscher, K. M., Rodrigues, J. P., De Vries, R., Hennink, W. E., Baldus, M., et al. (2015). The supramolecular organization of a peptide-based nanocarrier at high molecular detail. *J. Am. Chem. Soc.* 137, 7775–7784. doi: 10.1021/jacs.5b02919

Raman, S., Machaidze, G., Lustig, A., Aebi, U., and Burkhard, P. (2006). Structure-based design of peptides that self-assemble into regular polyhedral nanoparticles. *Nanomed. Nanotechnol. Biol. Med.* 2, 95–102. doi: 10.1016/j.nano.2006.04.007

Rhys, G. G., Wood, C. W., Lang, E. J., Mulholland, A. J., Brady, R. L., Thomson, A. R., et al. (2018). Maintaining and breaking symmetry in homomeric coiled-coil assemblies. *Nat. Commun.* 9:6391. doi: 10.1038/s41467-018-06391-y

Rudra, J. S., Mishra, S., Chong, A. S., Mitchell, R. A., Nardin, E. H., Nussenzweig, V., et al. (2012). Self-assembled peptide nanofibers raising durable antibody responses against a malaria epitope. *Biomaterials* 33, 6476–6484. doi: 10.1016/j.biomaterials.2012.05.041

Saha, S., Banskota, S., Roberts, S., Kirmani, N., and Chilkoti, A. (2020). Engineering the architecture of elastin-like polypeptides: from unimers to hierarchical self-assembly. *Adv. Ther.* 3:1900164. doi: 10.1002/adtp.201900164

Salick, D. A., Kretsinger, J. K., Pochan, D. J., and Schneider, J. P. (2007). Inherent antibacterial activity of a peptide-based beta-hairpin hydrogel. *J. Am. Chem. Soc.* 129, 14793–14799. doi: 10.1021/ja076300z

Shan, W., Zheng, H., Fu, G., Liu, C., Li, Z., Ye, Y., et al. (2019). Bioengineered nanocage from hbc protein for combination cancer immunotherapy. *Nano Lett.* 19, 1719–1727. doi: 10.1021/acs.nanolett.8b04722

Sis, M. J., and Webber, M. J. (2019). Drug delivery with designed peptide assemblies. *Trends Pharmacol. Sci.* 40, 747–762. doi: 10.1016/j.tips.2019.08.003

Skwarczynski, M., and Toth, I. (2016). Peptide-based synthetic vaccines. *Chem. Sci.* 7, 842–854. doi: 10.1039/C5SC03892H

Skwarczynski, M., Zhao, G., Boer, J. C., Ozberk, V., Azuar, A., Cruz, J. G., et al. (2020). Poly (amino acids) as a potent self-adjuvanting delivery system for peptide-based nanovaccines. *Sci. Adv.* 6:eaax2285. doi: 10.1126/sciadv.aax2285

Smith, D. J., Brat, G. A., Medina, S. H., Tong, D., Huang, Y., Grahammer, J., et al. (2016). A multiphase transitioning peptide hydrogel for suturing ultrasmall vessels. *Nat. Nanotechnol.* 11, 95–102. doi: 10.1038/nnano.2015.238

Tandon, A., Pathak, M., Harioudh, M. K., Ahmad, S., Sayeed, M., Afshan, T., et al. (2018). A TLR4-derived non-cytotoxic, self-assembling peptide functions as a vaccine adjuvant in mice. *J. Biol. Chem.* 293, 19874–19885. doi: 10.1074/jbc.RA118.002768

Thomson, A. R., Wood, C. W., Burton, A. J., Bartlett, G. J., Sessions, R. B., Brady, R. L., et al. (2014). Computational design of water-soluble α-helical barrels. *Science* 346, 485–488. doi: 10.1126/science.1257452

Tian, Y., Wang, H., Liu, Y., Mao, L., Chen, W., Zhu, Z., et al. (2014). A peptide-based nanofibrous hydrogel as a promising DNA nanovector for optimizing the efficacy of HIV vaccine. *Nano Lett.* 14, 1439–1445. doi: 10.1021/nl404560v

Trent, A., Ulery, B. D., Black, M. J., Barrett, J. C., Liang, S., Kostenko, Y., et al. (2015). Peptide amphiphile micelles self-adjuvant group A streptococcal vaccination. *AAPS J.* 17, 380–388. doi: 10.1208/s12248-014-9707-3

Wang, H., Feng, Z., and Xu, B. (2019). Assemblies of peptides in a complex environment and their applications. *Angew. Chem. Int. Ed.* 58, 10423–10432. doi: 10.1002/anie.201814552

Wang, H., Luo, Z., Wang, Y., He, T., Yang, C., Ren, C., et al. (2016). Enzyme-catalyzed formation of supramolecular hydrogels as promising vaccine adjuvants. *Adv. Funct. Mater.* 26, 1822–1829. doi: 10.1002/adfm.201505188

Wang, H., Xu, K., Liu, L., Tan, J. P., Chen, Y., Li, Y., et al. (2010). The efficacy of self-assembled cationic antimicrobial peptide nanoparticles against *Cryptococcus neoformans* for the treatment of meningitis. *Biomaterials* 31, 2874–2881. doi: 10.1016/j.biomaterials.2009.12.042

Wang, K., Yang, Y., Xue, W., and Liu, Z. (2018). Cell penetrating peptide-based redox-sensitive vaccine delivery system for subcutaneous vaccination. *Mol. Pharm.* 15, 975–984. doi: 10.1021/acs.molpharmaceut.7b00905

Wang, T., Wang, D., Yu, H., Feng, B., Zhou, F., Zhang, H., et al. (2018). A cancer vaccine-mediated postoperative immunotherapy for recurrent and metastatic tumors. *Nat. Commun.* 9:1532. doi: 10.1038/s41467-018-03915-4

Wen, Y., and Collier, J. H. (2015). Supramolecular peptide vaccines: tuning adaptive immunity. *Curr. Opin. Immunol.* 35, 73–79. doi: 10.1016/j.coi.2015.06.007

Worthington, P., Langhans, S., and Pochan, D. (2017). β-Hairpin peptide hydrogels for package delivery. *Adv. Drug Del. Rev.* 110, 127–136. doi: 10.1016/j.addr.2017.02.002

Wu, Y., Kelly, S. H., Sanchez-Perez, L., Sampson, J., and Collier, J. H. (2020). Comparative study of α-helical and β-sheet self-assembled peptide nanofiber vaccine platforms: Influence of integrated T-cell epitopes. *Biomater. Sci.* 8 3522–3535. doi: 10.1039/D0BM00521E

Wu, Y., Norberg, P. K., Reap, E. A., Congdon, K. L., Fries, C. N., Kelly, S. H., et al. (2017). A supramolecular vaccine platform based on α-helical peptide nanofibers. *ACS Biomater. Sci. Eng.* 3, 3128–3132. doi: 10.1021/acsbiomaterials.7b00561

Xiao, T., Qi, L., Zhong, W., Lin, C., Wang, R., and Wang, L. (2019a). Stimuli-responsive nanocarriers constructed from pillar [n] arene-based supra-amphiphiles. *Mater. Chem. Front* 3, 1973–1993. doi: 10.1039/C9QM00428A

Xiao, T., Zhong, W., Xu, L., Sun, X.-Q., Hu, X.-Y., and Wang, L. (2019b). Supramolecular vesicles based on pillar [n] arenes: design, construction, and applications. *Org. Biomol. Chem.* 17, 1336–1350. doi: 10.1039/C8OB03095B

Xing, R., Li, S., Zhang, N., Shen, G., MÃhwald, H., and Yan, X. (2017). Self-assembled injectable peptide hydrogels capable of triggering antitumor immune response. *Biomacromolecules* 18, 3514–3523. doi: 10.1021/acs.biomac.7b00787

Xu, Y., Wang, Y., Yang, Q., Liu, Z., Xiao, Z., Le, Z., et al. (2019). A versatile supramolecular nanoadjuvant that activates NF-κB for cancer immunotherapy. *Theranostics* 9:3388. doi: 10.7150/thno.34031

Yang, J., Luo, Y., Shibu, M. A., Toth, I., and Skwarczynskia, M. (2019). Cell-penetrating peptides: Efficient vectors for vaccine delivery. *Curr. Drug Del.* 16, 430–443. doi: 10.2174/1567201816666190123120915

Yang, P., Song, H., Qin, Y., Huang, P., Zhang, C., Kong, D., et al. (2018). Engineering dendritic-cell-based vaccines and PD-1 blockade in self-assembled peptide nanofibrous hydrogel to amplify antitumor T-cell immunity. *Nano Lett.* 18, 4377–4385. doi: 10.1021/acs.nanolett.8b01406

Zhang, J., Mulvenon, A., Makarov, E., Wagoner, J., Knibbe, J., Kim, J. O., et al. (2013). Antiviral peptide nanocomplexes as a potential therapeutic

modality for HIV/HCV co-infection. *Biomaterials* 34, 3846–3857. doi: 10.1016/j.biomaterials.2013.01.026

Zhang, S. (2017). Discovery and design of self-assembling peptides. *Interface Focus* 7:20170028. doi: 10.1098/rsfs.2017.0028

Zhang, Y. N., Avery, R. K., Vallmajo-Martin, Q., Assmann, A., Vegh, A., Memic. A., et al. (2015). A highly elastic and rapidly crosslinkable elastin-Like polypeptide-based hydrogel for biomedical applications. *Adv Funct Mater*. 25, 4814–4826. doi: 10.1002/adfm.201501489

Zhao, G., Chandrudu, S., Skwarczynski, M., and Toth, I. (2017). The application of self-assembled nanostructures in peptide-based subunit vaccine development. *Eur. Polym. J.* 93, 670–681. doi: 10.1016/j.eurpolymj.2017.02.014

Zottig, X., Côté-Cyr, M., Arpin, D., Archambault, D., and Bourgault, S. (2020). Protein supramolecular structures: from self-assembly to nanovaccine design. *Nanomaterials* 10:1008. doi: 10.3390/nano10051008

Conflict of Interest: KB is currently a student at Northeastern University and employed by Moderna Inc. However, Moderna Inc. was not involved in the writing of this review article or the decision to submit it for publication.

The remaining authors declare that the research was conducted in the absence of any commercial or financial relationships that could be construed as a potential conflict of interest.

frontiers in Chemistry

MINI REVIEW
published: 03 November 2020
doi: 10.3389/fchem.2020.585077

Multi-Responsive Silk Fibroin-Based Nanoparticles for Drug Delivery

Ya Ma[1,2], *Brandon S. B. Canup*[3], *Xiaoling Tong*[1], *Fangyin Dai*[1] *and Bo Xiao*[1]*

[1] State Key Laboratory of Silkworm Genome Biology, Key Laboratory of Sericultural Biology and Genetic Breeding, Ministry of Agriculture and Rural Affairs, College of Sericulture, Textile and Biomass Sciences, Southwest University, Chongqing, China, [2] Chongqing Key Laboratory of Soft-Matter Material Chemistry and Function Manufacturing, School of Materials and Energy, Southwest University, Chongqing, China, [3] Department of Chemistry, Georgia State University, Atlanta, GA, United States

Silk fibroin has the merits of biocompatibility, biodegradability, ease of processing, and feasibility of modification, which present it as a promising drug delivery material. This review focuses on the structures of silk fibroin, the controlled transformation of secondary structures, and the formation mechanism of silk fibroin-based nanoparticles (SFNPs). We also discuss the intrinsic multi-responsive, surface functionalization, and transgenic modification of SFNPs for drug delivery.

Keywords: multi-responsibility, drug delivery, silk fibroin, nanoparticle, β-sheet

OPEN ACCESS

Edited by:
Yohann Corvis,
Université de Paris, France

Reviewed by:
Adam Charles Sedgwick,
University of Texas at Austin, United States
Jeffrey Wang,
Western University of Health Sciences, United States

***Correspondence:**
Bo Xiao
bxiao@swu.edu.cn

Specialty section:
This article was submitted to Supramolecular Chemistry, a section of the journal Frontiers in Chemistry

Received: *19 July 2020*
Accepted: *05 October 2020*
Published: *03 November 2020*

Citation:
Ma Y, Canup BSB, Tong X, Dai F and Xiao B (2020) Multi-Responsive Silk Fibroin-Based Nanoparticles for Drug Delivery. Front. Chem. 8:585077. doi: 10.3389/fchem.2020.585077

INTRODUCTION

Drug delivery is required to deliver appropriate amounts of therapeutic agents to the diseased sites to improve the therapeutic effect of drugs and reduce their adverse effects (Tian et al., 2014; Jain, 2020). To achieve these goals, various nanoscale drug delivery systems, including mesoporous silica nanoparticles (NPs), liposomes, and polymeric NPs, have been developed in recent years (Chen H. et al., 2018; Patra et al., 2018). Among them, polymeric NPs have attracted increasing attention due to their numerous advantageous features such as good biocompatibility, desirable biodegradability, and ease of functionalization (Sundar et al., 2010; Merkle, 2015).

In contrast to traditional polymeric NPs, polymeric drug carriers that respond to the external stimuli (e.g., pH, ROS, GSH, enzyme, temperature, and light) by changing their physicochemical properties can maintain the stability of the loaded drugs, prolong the blood circulation time of drugs, realize on-demand drug release in the targeted cells, and reduce the systemic side toxicities (Cheng et al., 2014; Guragain et al., 2015; Fu et al., 2018; Gao et al., 2019). However, many of these stimuli-responsive polymers are synthesized through the integration of multiple functional chemical groups via complex chemical reactions, which involve large amounts of organic solvents and harsh reaction environments, eventually resulting in potential toxicity and high expense (Lei et al., 2017; Bordat et al., 2019; Deng et al., 2020). In recent years, a number of natural polymers, including chitosan, alginate, gelatin, and silk fibroin, have been developed as drug delivery materials. Among them, silk fibroin is an FDA-approved polymer that can be processed into nanoscale particles in the mild environment (Lammel et al., 2011; Kundu et al., 2014; George et al., 2019). For instance, ionic liquid-silk fibroin solutions were prepared and used to fabricate

SFNPs under ultrasounds (Lozano-Pérez et al., 2014). The silk fibroin-based NPs (SFNPs) not only have the merits of excellent biocompatibility and desirable biodegradability, but also show the features of multi-responsive (Maitz et al., 2017; Wongpinyochit et al., 2018; Gou et al., 2019b). In addition, they can efficiently load small-molecule drugs, proteins, and nucleic acids through surface adsorption, physical encapsulation, and chemical coupling, which are able to prevent drug degradation, optimize the drug pharmacokinetics, and increase the cellular uptake amounts of drugs (Zhao et al., 2015).

In this review, we summarize the controlled transformation of the secondary structures, the multiple stimuli-responsive capacities, and the surface/multifunctional modification of SFNPs for drug delivery.

STRUCTURE OF SILK FIBROIN

Primary Structure of Silk Fibroin

Silk fibroin consists of 18 kinds of amino acids, in which Gly is the most abundant amino acid accounting for 43% of all amino acids, followed by Ala (29%) and Ser (12%) (Qi et al., 2017). Silk fibroin is composed of three basic subunits, a heavy chain (H-chain), a light chain (L-chain), and a P25 gene-encoded glycoprotein, whose ratio is 6:6:1. In particular, the H-chain (∼350 kDa) has 12 hydrophobic blocks and 11 hydrophilic blocks, which is the main contributor of β-sheet structures in SFNPs. These hydrophobic β-sheet blocks are constituted of the repeat sequence GAGAGS and are formed on the basis of intramolecular and intermolecular hydrogen bonds (mainly between Gly and Ala), van der Waals force, and hydrophobic interaction, which confer SFNPs with stable 3-dimensional structures (Nguyen et al., 2019; Montalbán et al., 2020; Pham and Tiyaboonchai, 2020). In the context of the L-chain (26 kDa), its primary structure has no amino acid repeat sequence, and it conjugates with the H-chain through a disulfide bond. The main function of the L-chain is to assist with the secretion of the H-chain from the silk gland of silkworm. In addition, the bio-function of P25 glycoprotein (30 kDa) is similar to that of the L-chain.

Secondary Structure of Silk Fibroin

Silk fibroin has two main types of crystal structures, namely Silk I and Silk II. Silk I is a transition state, which contains random coils, α-helical structures, and other amorphous structures. Silk II is composed of antiparallel β-sheet crystal structures, which make silk fibroin insoluble in aqueous solutions (Cebe et al., 2017). In nature, Silk I exists in the silk gland, while Silk II exists in the form of spun silk fiber. Thus, the investigation of the silk spinning mechanism can uncover the influencing factors in the structure transformation process of silk fibroin (Li et al., 2015; Pham et al., 2018b). This information can then be utilized for understanding the formation mechanism of SFNPs.

The formation of SFNPs is based on the structure transformation from Silk I (random coil and α-helical structure) to Silk II (highly ordered β-sheet). Silk fibroin molecules form loose amorphous structures in aqueous solution due to their intrinsic electrostatic repulsion (Zhang et al., 2006). Meanwhile, water tends to couple with these silk fibroin molecules and form a layer of hydration film. Upon the external treatment, β-sheet structures are formed, resulting in the self-assembly of molecular chains and the formation of SFNPs (Mottaghitalab et al., 2015; Zhao et al., 2015).

The self-assembly method has been commonly used to produce SFNPs. It is known that self-assembly, a thermodynamic process, is determined by molecular aggregation, which can be modulated by external environmental factors (Lu et al., 2012; Bai et al., 2013). Under certain external stimulation such as metal ion, low temperature, organic solvent, and ultrasound, the soluble, and irregular Silk I can be transformed into non-soluble Silk II (Hu et al., 2011; Terada et al., 2016). On the other hand, under high concentration of neutral salt and other certain conditions (e.g., acid, ROS, enzyme, and hyperthermia), the β-sheet structures of Silk II undergo a conformational reversion to amorphous structures of Silk I (Wongpinyochit et al., 2018). Therefore, the transformation between the crystal structures of silk fibroin is a complex and multi-factorial regulated process, which is fundamental to the multi-responsive property of SFNPs.

MULTI-STIMULI-RESPONSIVE OF SFNPS

Nanotherapeutics with multi-responsive can achieve spatial and temporal release of drugs in diseased tissues (Qu et al., 2018). Kaplan group was the first to report that SFNPs showed an obvious pH-dependent drug release property. The release rate of doxorubicin (DOX) from SFNPs was significantly increased in the buffer (pH 4.5) in comparison with that in the buffers with the pH values of 7.4 and 6.0. They speculated that the loss of the negative net charges in the buffer (pH 4.5) weakened the electrostatic interaction between silk fibroin molecules and DOX, resulting in the accelerated release of DOX from NPs (Seib et al., 2013). In addition, *Totten et al.*,. studied the DOX release behaviors of PEGylated SFNPs in the acidic buffers with or without lysosomal enzymes. They found that the DOX release rate was significantly increased in the simulated lysosomal fluid (lysosomal enzyme and acidic environment), providing direct evidence of the accelerated release of DOX in the lysosome of tumor cells (Totten et al., 2017). Very recently, our group not only confirmed the pH responsive of SFNPs, but also discovered that they had obvious ROS/GSH/hyperthermia-responsive properties, as shown in **Figure 1**. We further discovered a potential mechanism for their pH/ROS/GSH/hyperthermia-responsive properties. Protons, H_2O_2 molecules, and hyperthermia could gradually destroy the hydrogen bonds in β-sheet structures, and GSH could reduce the internal disulfide bonds into sulfhydryl groups. The treatments with the protons, H_2O_2 molecules, hyperthermia, and GSH loosen the compact structures of SFNPs leading to the acceleration of drug release from these NPs (Gou et al., 2019a, 2020). These results collectively reveal that SFNPs have obvious pH/ROS/GSH/hyperthermia/lysosomal enzyme-responsive properties, which can facilitate the specific drug release in the targeted cells via microenvironmental stimuli.

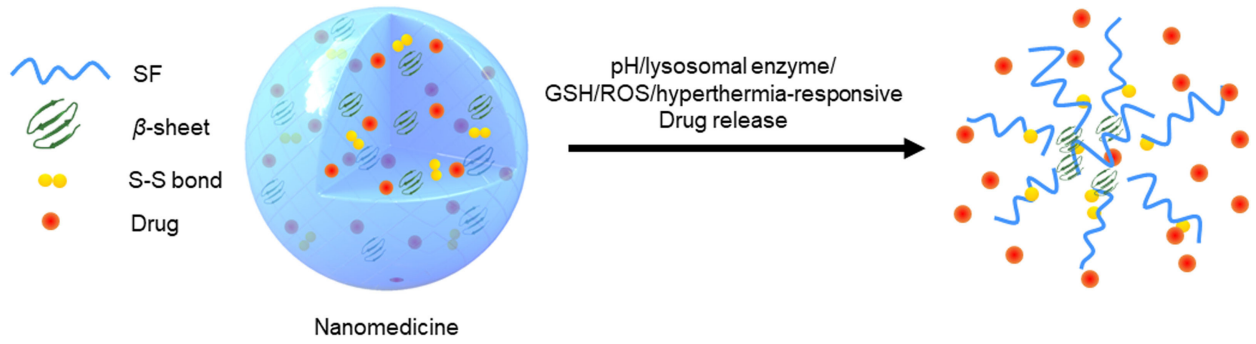

FIGURE 1 | Schematic illustration of multi-responsive properties of SFNPs.

MODIFICATION OF SFNPS

Many chemically active groups such as amino groups, carboxyl groups, and sulfhydryl groups, are present in the backbone of silk fibroin, and these groups are able to be used for chemical modifications, which can endow SFNPs with some advanced functions (e.g., charge reversal, controlled drug release, and targeting property) (Wenk et al., 2011; Chen J. et al., 2018; Pandey et al., 2020).

For instance, to improve the tumor-targeting property, Sun et al. prepared DOX-loaded SFNPs and further functionalized their surface with folic acid (FA) through the chemical reaction between the amino groups of silk fibroin and the carboxyl groups of FA molecules. The obtained FA-DOX-NPs could be specifically internalized by FA receptor-overexpressed tumor cells and release the loaded DOX in a controlled manner. They further found that the surface functionalization of FA significantly improved the chemotherapeutic effect and reduced the potential adverse effects of DOX (Sun et al., 2018). Recently, Pham et al. fabricated a new type of SFNPs by using a reactive carbodiimide (EDC) or polyethyleneimine (PEI). It was found that the hydrodynamic particle sizes of all the developed cross-linked NPs were similar to the traditional SFNPs and their zeta potentials were controllably altered from a negative charge to positive. In addition, the crystallinity of these NPs increased with increasing the amount of EDC or decreasing the PEI content, which can improve drug encapsulation efficiency (Pham et al., 2018a).

Transgenic technology is another promising strategy to produce the modified silk fibroin by inserting or replacing genes in the silkworm genome to generate novel silk fibroin derivatives (Shi et al., 2014; Helfricht et al., 2016). This strategy has attracted increasing attention in recent years, as it can fundamentally alter the primary structure of silk fibroin. Xia et al. adjusted the proportion of elastin in silk fibroin using genetic engineering technology and obtained silk-elastin like proteins (SELPs), which could form NPs *via* self-assembly. The first step was the spontaneous formation of micelles with silk blocks as the core structures, which was driven by hydrogen bonds among silk blocks; the second step was driven by the hydrophobic interactions among elastin blocks, leading to the orderly association of SELP molecules. During the assembly processes, drugs could be encapsulated in the SELP matrix to form NPs (Xia et al., 2011).

CONCLUSIONS

Silk fibroin has become an attractive natural polymer for drug delivery due to its versatile merits such as good biocompatibility, modulated biodegradability, large scale production, easy modification, and self-assembling property. Many approaches can be applied to further the application of silk fibroin as a drug delivery material such as optimization of its primary structures, modification with functional chemical groups, adjusting the self-assembling processes, and controlling the interaction between silk fibroin and the loaded agents. It is also critical to endow them with a diseased site-targeting capacity *via* the conjugation of targeting ligands. Furthermore, the alteration of the contents of hydrophobic β-sheet structures and disulfide bonds is important to improve the responsive capacities of these silk fibroin-based NPs (SFNPs) to acidity, ROS, and GSH, which can facilitate the on-demand release of the loaded drugs from the NPs. Collectively, these SFNPs can be exploited as a promising nanocarrier for drug delivery.

AUTHOR CONTRIBUTIONS

YM wrote the draft of the manuscript. BC, XT, FD, and BX provided suggestions and edited the manuscript. All authors contributed to the article and approved the submitted version.

FUNDING

This research was supported by the National Natural Science Foundation of China (82072060), the Fundamental Research Funds for the Central Universities (XDJK2019TY002), and the Venture and Innovation Support Program for Chongqing Overseas Returnees (cx2018029).

REFERENCES

Bai, S., Liu, S., Zhang, C., Xu, W., Lu, Q., Han, H., et al. (2013). Controllable transition of silk fibroin nanostructures: an insight into *in vitro* silk self-assembly process. *Acta Biomater.* 9, 7806–7813. doi: 10.1016/j.actbio.2013.04.033

Bordat, A., Boissenot, T., Nicolas, J., and Tsapis, N. (2019). Thermoresponsive polymer nanocarriers for biomedical applications. *Adv. Drug Deliv. Rev.* 138, 167–192. doi: 10.1016/j.addr.2018.10.005

Cebe, P., Partlow, B. P., Kaplan, D. L., Wurm, A., Zhuravlev, E., and Schick, C. (2017). Silk I and Silk II studied by fast scanning calorimetry. *Acta Biomater.* 55, 323–332. doi: 10.1016/j.actbio.2017.04.001

Chen, H., Gu, Z., An, H., Chen, C., Chen, J., Cui, R., et al. (2018). Precise nanomedicine for intelligent therapy of cancer. *Sci. China Chem.* 61, 1503–1552. doi: 10.1007/s11426-018-9397-5

Chen, J., Venkatesan, H., and Hu, J. (2018). Chemically modified silk proteins. *Adv. Eng. Mater.* 20:1700961. doi: 10.1002/adem.201700961

Cheng, W., Gu, L., Ren, W., and Liu, Y. (2014). Stimuli-responsive polymers for anti-cancer drug delivery. *Mater. Sci. Eng. C Mater. Biol. Appl.* 45, 600–608. doi: 10.1016/j.msec.2014.05.050

Deng, H., Zhou, Z., Yang, W., Lin, L. S., Wang, S., Niu, G., et al. (2020). Endoplasmic reticulum targeting to amplify immunogenic cell death for cancer immunotherapy. *Nano Lett.* 20, 1928–1933. doi: 10.1021/acs.nanolett.9b05210

Fu, X., Hosta-Rigau, L., Chandrawati, R., and Cui, J. (2018). Multi-stimuli-responsive polymer particles, films, and hydrogels for drug delivery. *Chem* 4, 2084–2107. doi: 10.1016/j.chempr.2018.07.002

Gao, S., Tang, G., Hua, D., Xiong, R., Han, J., Jiang, S., et al. (2019). Stimuli-responsive bio-based polymeric systems and their applications. *J. Mater. Chem. B* 7, 709–729. doi: 10.1039/C8TB02491J

George, A., Shah, P. A., and Shrivastav, P. S. (2019). Natural biodegradable polymers based nano-formulations for drug delivery: a review. *Int. J. Pharm.* 561, 244–264. doi: 10.1016/j.ijpharm.2019.03.011

Gou, S., Huang, Y., Sung, J., Xiao, B., and Merlin, D. (2019a). Silk fibroin-based nanotherapeutics: application in the treatment of colonic diseases. *Nanomedicine* 14, 2373–2378. doi: 10.2217/nnm-2019-0058

Gou, S., Huang, Y., Wan, Y., Ma, Y., Zhou, X., Tong, X., et al. (2019b). Multi-bioresponsive silk fibroin-based nanoparticles with on-demand cytoplasmic drug release capacity for CD44-targeted alleviation of *Ulcerative colitis*. *Biomaterials* 212, 39–54. doi: 10.1016/j.biomaterials.2019.05.012

Gou, S., Yang, J., Ma, Y., Zhang, X., Zu, M., Kang, T., et al. (2020). Multi-responsive nanococktails with programmable targeting capacity for imaging-guided mitochondrial phototherapy combined with chemotherapy. *J. Control. Release* 327, 371–383. doi: 10.1016/j.jconrel.2020.08.014

Guragain, S., Bastakoti, B. P., Malgras, V., Nakashima, K., and Yamauchi, Y. (2015). Multi-stimuli-responsive polymeric materials. *Chemistry* 21, 13164–13174. doi: 10.1002/chem.201501101

Helfricht, N., Doblhofer, E., Duval, J. F. L., Scheibel, T., and Papastavrou, G. (2016). Colloidal properties of recombinant spider silk protein particles. *J. Phys. Chem. C* 120, 18015–18027. doi: 10.1021/acs.jpcc.6b03957

Hu, X., Shmelev, K., Sun, L., Gil, E. S., Park, S. H., Cebe, P., et al. (2011). Regulation of silk material structure by temperature-controlled water vapor annealing. *Biomacromolecules* 12, 1686–1696. doi: 10.1021/bm200062a

Jain, K. K. (2020). An overview of drug delivery systems. *Methods Mol. Biol.* 2059, 1–54. doi: 10.1007/978-1-4939-9798-5_1

Kundu, B., Kurland, N. E., Yadavalli, V. K., and Kundu, S. C. (2014). Isolation and processing of silk proteins for biomedical applications. *Int. J. Biol. Macromol.* 70, 70–77. doi: 10.1016/j.ijbiomac.2014.06.022

Lammel, A., Schwab, M., Hofer, M., Winter, G., and Scheibel, T. (2011). Recombinant spider silk particles as drug delivery vehicles. *Biomaterials* 32, 2233–2240. doi: 10.1016/j.biomaterials.2010.11.060

Lei, Q., Wang, S., Hu, J., Lin, Y., Zhu, C., Rong, L., et al. (2017). Stimuli-responsive "Cluster bomb" for programmed tumor therapy. *ACS Nano* 11, 7201–7214. doi: 10.1021/acsnano.7b03088

Li, A. B., Kluge, J. A., Guziewicz, N. A., Omenetto, F. G., and Kaplan, D. L. (2015). Silk-based stabilization of biomacromolecules. *J. Control. Release* 219, 416–430. doi: 10.1016/j.jconrel.2015.09.037

Lozano-Pérez, A. A., Montalbán, M. G., Aznar-Cervantes, S. D., Cragnolini, F., Cenis, J. L., and Víllora, G. (2014). Production of silk fibroin nanoparticles using ionic liquids and high-power ultrasounds. *J. Appl. Polym. Sci.* 132, 41702. doi: 10.1002/app.41702

Lu, Q., Zhu, H., Zhang, C., Zhang, F., Zhang, B., and Kaplan, D. L. (2012). Silk self-assembly mechanisms and control from thermodynamics to kinetics. *Biomacromolecules* 13, 826–832. doi: 10.1021/bm201731e

Maitz, M. F., Sperling, C., Wongpinyochit, T., Herklotz, M., Werner, C., and Seib, F. P. (2017). Biocompatibility assessment of silk nanoparticles: hemocompatibility and internalization by human blood cells. *Nanomedicine* 13, 2633–2642. doi: 10.1016/j.nano.2017.07.012

Merkle, H. P. (2015). Drug delivery's quest for polymers: where are the frontiers? *Eur. J. Pharm. Biopharm.* 97, 293–303. doi: 10.1016/j.ejpb.2015.04.038

Montalbán, M. G., Chakraborty, S., Peña-García, J., Verli, H., Villora, G., Pérez-Sánchez, H., et al. (2020). Molecular insight into silk fibroin based delivery vehicle for amphiphilic drugs: Synthesis, characterization and molecular dynamics studies. *J. Mol. Liq.* 299:112156. doi: 10.1016/j.molliq.2019.112156

Mottaghitalab, F., Farokhi, M., Shokrgozar, M. A., Atyabi, F., and Hosseinkhani, H. (2015). Silk fibroin nanoparticle as a novel drug delivery system. *J. Control. Release* 206, 161–176. doi: 10.1016/j.jconrel.2015.03.020

Nguyen, T. P., Nguyen, Q. V., Nguyen, V. H., Le, T. H., Huynh, V. Q. N., Vo, D. N., et al. (2019). Silk fibroin-based biomaterials for biomedical applications: a review. *Polymers* 11:1933. doi: 10.3390/polym11121933

Pandey, V., Haider, T., Jain, P., Gupta, P. N., and Soni, V. (2020). Silk as a leading-edge biological macromolecule for improved drug delivery. *J. Drug Deliv. Sci. Tec.* 55:101294. doi: 10.1016/j.jddst.2019.101294

Patra, J. K., Das, G., Fraceto, L. F., Campos, E. V. R., Rodriguez-Torres, M. D. P., et al. (2018). Nano based drug delivery systems: recent developments and future prospects. *J. Nanobiotechnology* 16:71. doi: 10.1186/s12951-018-0392-8

Pham, D. T., Saelim, N., and Tiyaboonchai, W. (2018a). Crosslinked fibroin nanoparticles using EDC or PEI for drug delivery: physicochemical properties, crystallinity and structure. *J. Mater. Sci.* 53, 14087–14103. doi: 10.1007/s10853-018-2635-3

Pham, D. T., Saelim, N., and Tiyaboonchai, W. (2018b). Design of experiments model for the optimization of silk fibroin based nanoparticles. *Int. J. Appl. Pharm.* 10:195. doi: 10.22159/ijap.2018v10i5.28139

Pham, D. T., and Tiyaboonchai, W. (2020). Fibroin nanoparticles: a promising drug delivery system. *Drug Deliv.* 27, 431–448. doi: 10.1080/10717544.2020.1736208

Qi, Y., Wang, H., Wei, K., Yang, Y., Zheng, R., Kim, I. S., et al. (2017). A review of structure construction of silk fibroin biomaterials from single structures to multi-level structures. *Int. J. Mol. Sci.* 18:273. doi: 10.3390/ijms18030237

Qu, J., Wang, Q., Chen, K., Luo, J., Zhou, Q., and Lin, J. (2018). Reduction/temperature/pH multi-stimuli responsive core cross-linked polypeptide hybrid micelles for triggered and intracellular drug release. *Colloids Surf. B Biointerfaces* 170, 373–381. doi: 10.1016/j.colsurfb.2018.06.015

Seib, F. P., Jones, G. T., Rnjak-Kovacina, J., Lin, Y., and Kaplan, D. L. (2013). pH-dependent anticancer drug release from silk nanoparticles. *Adv. Healthc. Mater.* 2, 1606–1611. doi: 10.1002/adhm.201300034

Shi, P., Gustafson, J. A., and Mackay, J. A. (2014). Genetically engineered nanocarriers for drug delivery. *Int. J. Nanomedicine* 9, 1617–1626. doi: 10.2147/IJN.S53886

Sun, N., Lei, R., Xu, J., Kundu, S. C., Cai, Y., Yao, J., et al. (2018). Fabricated porous silk fibroin particles for pH-responsive drug delivery and targeting of tumor cells. *J. Mater. Sci.* 54, 3319–3330. doi: 10.1007/s10853-018-3022-9

Sundar, S., Kundu, J., and Kundu, S. C. (2010). Biopolymeric nanoparticles. *Sci. Technol. Adv. Mater.* 11:014104. doi: 10.1088/1468-6996/11/1/014104

Terada, D., Yokoyama, Y., Hattori, S., Kobayashi, H., and Tamada, Y. (2016). The outermost surface properties of silk fibroin films reflect ethanol-treatment conditions used in biomaterial preparation. *Mater. Sci. Eng. C Mater. Biol. Appl.* 58, 119–126. doi: 10.1016/j.msec.2015.07.041

Tian, Y., Jiang, X., Chen, X., Shao, Z., and Yang, W. (2014). Doxorubicin-loaded magnetic silk fibroin nanoparticles for targeted therapy of

multidrug-resistant cancer. *Adv. Mater.* 26, 7393–7398. doi: 10.1002/adma.201403562

Totten, J. D., Wongpinyochit, T., and Seib, F. P. (2017). Silk nanoparticles: proof of lysosomotropic anticancer drug delivery at single-cell resolution. *J. Drug Target.* 25, 865–872. doi: 10.1080/1061186X.2017.1363212

Wenk, E., Merkle, H. P., and Meinel, L. (2011). Silk fibroin as a vehicle for drug delivery applications. *J. Control. Release* 150, 128–141. doi: 10.1016/j.jconrel.2010.11.007

Wongpinyochit, T., Johnston, B. F., and Seib, F. P. (2018). Degradation behavior of silk nanoparticles—enzyme responsiveness. *ACS Biomater. Sci. Eng.* 4, 942–951. doi: 10.1021/acsbiomaterials.7b01021

Xia, X., Xu, Q., Hu, X., Qin, G., and Kaplan, D. L. (2011). Tunable self-assembly of genetically engineered silk–elastin-like protein polymers. *Biomacromolecules* 12, 3844–3850. doi: 10.1021/bm201165h

Zhang, Y.-Q., Shen, W.-D., Xiang, R.-L., Zhuge, L.-J., Gao, W.-J., and Wang, W.-B. (2006). Formation of silk fibroin nanoparticles in water-miscible organic solvent and their characterization. *J. Nanopart. Res.* 9, 885–900. doi: 10.1007/s11051-006-9162-x

Zhao, Z., Li, Y., and Xie, M. B. (2015). Silk fibroin-based nanoparticles for drug delivery. *Int. J. Mol. Sci.* 16, 4880–4903. doi: 10.3390/ijms16034880

Conflict of Interest: The authors declare that the research was conducted in the absence of any commercial or financial relationships that could be construed as a potential conflict of interest.

Advantages of publishing in Frontiers

OPEN ACCESS
Articles are free to read for greatest visibility and readership

FAST PUBLICATION
Around 90 days from submission to decision

HIGH QUALITY PEER-REVIEW
Rigorous, collaborative, and constructive peer-review

TRANSPARENT PEER-REVIEW
Editors and reviewers acknowledged by name on published articles

Frontiers
Avenue du Tribunal-Fédéral 34
1005 Lausanne | Switzerland

Visit us: www.frontiersin.org
Contact us: info@frontiersin.org | +41 21 510 17 00

REPRODUCIBILITY OF RESEARCH
Support open data and methods to enhance research reproducibility

DIGITAL PUBLISHING
Articles designed for optimal readership across devices

FOLLOW US
@frontiersin

IMPACT METRICS
Advanced article metrics track visibility across digital media

EXTENSIVE PROMOTION
Marketing and promotion of impactful research

LOOP RESEARCH NETWORK
Our network increases your article's readership